Study of the multipolar excitations in cold and hot, deformed and superfluid systems with the method of finite amplitudes

Yann Beaujeault-Taudière

université
PARIS-SACLAY

Study of the multipolar excitations in cold and hot, deformed and superfluid systems with the method of finite amplitudes

Étude des excitations multipolaires dans les noyaux froids et chauds, déformés et superfluides via la méthode des amplitudes finies

Thèse de doctorat de l'université Paris-Saclay

École doctorale n° 576, Particules, Hadrons, Énergie et Noyau : Instrumentation, Imagerie, Cosmos et Simulation (PHENIICS)
Spécialité de doctorat : structure et réactions nucléaires
Unité de recherche : université Paris-Saclay, CEA, Laboratoire Matière sous conditions extrêmes, 91680, Bruyères-le-Châtel, France
Graduate School : Physique. Référent : Faculté des sciences d'Orsay

Thèse présentée et soutenue à Paris-Saclay, le 26 octobre 2021, par

Yann BEAUJEAULT-TAUDIÈRE

Composition du jury

Marcella GRASSO Directrice de recherche, Université Paris-Saclay	Présidente
Dany DAVESNE Professeur, Université Claude Bernard Lyon 1	Rapporteur & examinateur
Robert ROTH Professeur, Université de technologie de Darmstadt	Rapporteur & examinateur
Stéphane GORIELY Chargé de recherche, Université Libre de Bruxelles	Examinateur
Markus KORTELAINEN Professeur assistant, Université de Jyväskylä et Université d'Helsinki	Examinateur
Thomas DUGUET Ingénieur de recherche, CEA Saclay, IRFU	Invité

Direction de la thèse

Denis LACROIX Directeur de recherche, Université Paris-Saclay	Directeur de thèse
Jean-Paul EBRAN Ingénieur de recherche, CEA, DAM, DIF	Co-encadrant

Thèse de doctorat

NNT: 2021UPASP108

université PARIS-SACLAY
ÉCOLE DOCTORALE
Particules, hadrons, énergie et noyau : instrumentation, imagerie, cosmos et simulation (PHENIICS)

Academic summary

Titre : Étude des excitations multipolaires dans les noyaux froids et chauds, déformés et superfluides via la méthode des amplitudes finies

Mots clés : Physique théorique, problème à N corps, modes collectifs, astrophysique nucléaire, transitions de phase

Résumé : La réponse d'un système à une perturbation extérieure est source d'informations précieuses quant à ses propriétés de structure ou aux caractéristiques de l'interaction entre ses constituants. Pour les noyaux atomiques, ces différentes propriétés jouent en particulier un rôle fondamental dans divers scénarios astrophysiques tels que les processus r, s et p. L'une des méthodes les plus directes pour accéder à la réponse d'un système suite à une perturbation extérieure fait appel à la QRPA (quasiparticle random phase approximation), extension au cas des systèmes superfluides de la théorie de la réponse linéaire traitée dans l'approximation de la phase aléatoire. Une reformulation récente des équations lève les limitations qui imposaient de négliger une partie des contributions aux champs ou encore restreignaient la description à des classes spécifiques de corrélations angulaires dans l'état fondamental. Le travail réalisé en thèse a consisté à étendre ce nouveau formalisme au cadre d'un état fondamental s'écrivant comme un mélange statistique de configurations, ouvrant la possibilité d'appliquer la méthode aux systèmes à température finie, et à l'employer avec une interaction entre les nucléons dans le milieu nucléaire dérivant d'une théorie effective à basse énergie de la chromodynamique quantique.

Title: Study of the multipolar excitations in cold and hot, deformed and superfluid systems with the method of finite amplitudes

Keywords: Theoretical physics, many-body problem, collective modes, nuclear astrophysics, phase transitions

Abstract: Studying how a system responds to an external perturbation reveals many features about its structure or the underlying interactions between its constituents. In the case of atomic nuclei, such information plays a prominent role when one aims at understanding how structure properties impact nuclear reactions, e.g. in various astrophysical scenarios such as the r, s and p processes. The quasiparticle random phase approximation (QRPA), i.e. the generalisation to superfluid systems of the linear response theory within the random phase approximation, provides one of the most direct approaches to apprehend how a nucleus behaves under a gentle perturbation. A reformulation of the theory recently lifted some intrinsic limitations that affected it so far, namely the need to neglect some high-order contributions to the fields or the restriction to systems displaying only a specific class of angular correlations in their ground state. The formal work of this thesis involved extending the method to the case of a reference state written as a statistical mixture of different configurations, opening the way to the description of resonances in systems at finite temperature. The formalism is employed with an effective interaction between nucleons deriving from a low-energy effective theory of quantum chromodynamics.

General public summary

Titre : Étude des excitations multipolaires dans les noyaux froids et chauds, déformés et superfluides via la méthode des amplitudes finies

Mots clés : Physique théorique, problème à N corps, modes collectifs, astrophysique nucléaire, transitions de phase

Résumé : La plupart des systèmes quantiques sont composés de plusieurs particules interagissant entre elles. Décrire leur agencement en termes d'énergie, de distribution spatiale, etc, est très compliqué puisque faisant appel à des équations intégro-différentielles couplées. Trouver l'état fondamental du système, c'est-à-dire la configuration la plus stable, nécessite fréquemment le recours à une approximation de "champ moyen", qui néglige certaines corrélations entre les particules pour retenir seulement les plus élémentaires. Lorsque le système interagit avec un environnement extérieur, l'évolution temporelle de ses propriétés est naturellement très complexe, et requiert également des approximations. Souvent, on peut supposer les perturbations induites par le milieu extérieur comme étant de petites vibrations autour de la configuration stable. Cela donne accès à la composante linéaire de la réponse du système ; l'approche est donc valide si cette composante prédomine. Ce problème a été récemment revu afin d'en simplifier la résolution pour un système initialement "froid", c'est-à-dire à température nulle. Le travail réalisé a notamment consisté à étendre ce formalisme au cas où le système est initialement froid ou chaud. Cela a permis de premières applications à l'étude des propriétés de certains phénomènes collectifs dans des conditions extrêmes, telles que celles régnant au sein d'étoiles à neutrons.

Title: Study of the multipolar excitations in cold and hot, deformed and superfluid systems with the method of finite amplitudes

Keywords: Theoretical physics, many-body problem, collective modes, nuclear astrophysics, phase transitions

Abstract: The majority of quantum systems is composed of several particles interacting together. Describing how they organise in terms of spatial distribution, of energy, etc, is highly complicated as it involves coupled integro-differential equations. Finding the ground state of the system, that is, the most stable configuration, often already requires neglecting some correlations between the particles, retaining only the simplest ones. When this ensemble of particles interacts with an environment, the time evolution of its properties is thus very difficult, and calls for similar approximations. In most cases, we may suppose the motion generated by the external perturbation to be small oscillations about the stable configuration. This yields the linear component of the response; the approximation is this valid when this component is the most important one. The mathematical framework of the problem has recently been revisited in order to simplify its resolution for initially "cold" systems, i.e. systems at zero temperature. The work developed in this thesis extends this new formalism to the case of finite temperature, giving access to the response atop cold and hot systems. In particular, this has been employed for the description of some collective phenomena in conditions of extremely high temperature, as can be met in neutron stars.

Contents

Chapter 1

Introduction

The quantum many-body problem is extremely complex, and many phenomena can only be understood by properly treating internal correlations between degrees of freedom beyond the independent particle picture [RS80]. For nuclear physics, such correlations spawn peculiar configurations such as deformation and superfluidity. This already rich phenomenology is spiced up by the occurrence of more exotic configurations such as halo or bubble structures, giant resonances and clusters. A most famous manifestation of the complexity of nuclear systems is certainly the Hoyle state [Hoy54], the clustered excited state of carbon produced during the helium burning phase in stars. Complex phenomena are frequently met in the nuclear chart (figure 1.1) and cannot be treated on the basis of independent particles.

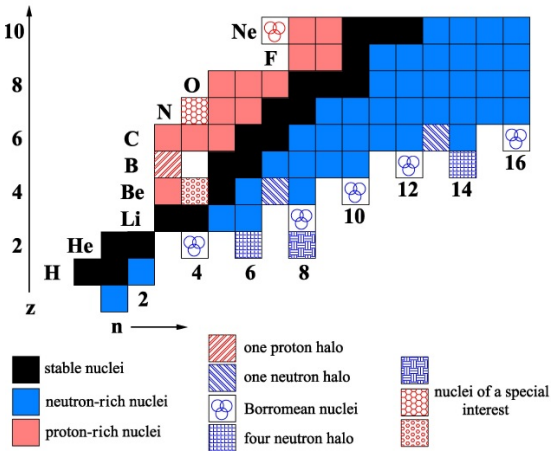

Figure 1.1: Zoom on the nuclear chart for N $\leq$ 16 and Z $\leq$ 10. Courtesy of W. Korten.

The first step of the theoretical description of strongly correlated many-body systems is to identify the pertinent degrees of freedom (d.o.f.) with the help of which the model is constructed.

A possibility is to adopt a macroscopic viewpoint [Rai50; BM53a; BM53b; AI75], interpreting the observed phenomena as collective bosonic excitations of a quantum body. Early attempts at unveiling the connection between collective and independent particle motions were based on experimental observations and chose the collective modes accordingly. As such, the type of such bosons is nearly as vast as the phenomenology of quantum

physics, and proponents of the collective models need to tailor their description to each specific problem, as a price to pay for the crystalline clarity of the model in terms of phenomena at play. Recently, this approach has been reframed in the language of effective field theories (EFTs) [PW14; Coe15; CP15; CP16; PW16], allowing for a systematic improvement of the description of the excitation spectrum and the possibility to quantify theoretical uncertainties. Depending on the contribution of a given class of correlations (pairing, shape, vibrational, etc), an effective theory has to be crafted in terms of adapted symmetry groups and cosets relating them. The low-energy constants entering the effective Hamiltonian must then be adjusted to each system with the help of experimental data.

A completely opposite vision goes by trying to describe all the desired physics on the basis of the interaction between the most microscopic degrees of freedom. In subatomic physics, this is realised into the Standard Model, which aims at describing three of the four known fundamental interactions of nature: the strong, the weak and the electromagnetic interaction. While it can be tempting to delve down this microscopic rabbit hole in the hope of constructing an all-encompassing theory, one is quickly faced with tremendous difficulties when dealing with the theory of the strong interaction, quantum chromodynamics (QCD). Without flaunting a rusty knowledge of QCD, its non-Abelian nature[1] and the covariance criterion force self-interactions among the gluon fields, which results notably in the theory being strongly non-perturbative at low energies. The structure of nuclei is thus hardly predictable from QCD, although recent lattice calculations [IAH07; Aok+12; Kol15] are starting to appear, and will certainly flourish in the future.

To circumvent the enormous difficulties brought by the specificities of QCD, an alternative path is currently being pursued. It aims at maintaining a formal connection to the underlying theory, and anchors on the viewpoint of effective field theories (EFTs) [Wei79], by exploiting a separation of energy scales in the excitation spectrum of quark condensates. The energy cut-off separates which effects are treated explicitly and which ones appear as perturbative corrections [MS16]. At energy scales relevant for nuclear physics, typically a few tens of MeV, the substructure of nucleons in terms of quarks and gluons is not resolved, promoting protons and neutrons to the relevant degrees of freedom of the theory. Still, the strong short-range repulsion between nucleons makes the problem highly non-perturbative. The second difficulty stems from the size of nuclear systems, made of 1 to $\sim$300[2] nucleons. One then has to cope with a non-perturbative finite system, where most often, neither few-body nor statistical techniques can be employed. A challenge of low-energy nuclear physics theory is therefore to obtain a coherent and accurate description of the aforementioned phenomena observed across the nuclear chart, along with their mass, radius, shape, spectroscopic factors, multipolar moments... all the while starting from the interactions between nucleons.

In particular, collective features constitutes an important challenge to a theory based strictly on microscopic ingredients. For vibrational modes, the motion generated by an

[1] The gauge group of QCD is $SU(N_c)$, where N_c is the number of colour charges, and must be equal to three to match the hadron spectrum.

[2] In extreme environments such as neutron stars, clusters comprising a few thousands of nuclei are also predicted; this is still too little to render statistical fluctuations entirely negligible.

external source is generally represented as small amplitude oscillations about a reference state. In that case, the random phase approximation (RPA) and the quasiparticle RPA -its extension including superfluidity- are theoretical tools of choice, as they tackle both individual and collective resonances on the same footing. However, in case of effective interactions rooted in QCD, the complexity of the method hindered its application to systems displaying simultaneously deformation and superfluidity. While spherical systems, both superfluid [HPR11] and not [Paa+06], could be addressed, the study of nuclei exhibiting both superfluidity and deformation remained hitherto out of reach. This thesis goes past this limit by expanding on a novel approach to the QRPA solution [NIY07; AN11], and represents its first application in case the microscopic potential between nucleons derives from a low-energy theory of the strong interaction. In addition, the formalism is extended to include couplings of the systems of interest to external baths. This is done by promoting the density matrix into a statistical operator, and permits the treatment of thermal effects.

The present thesis is organised as follows. Chapter 2 gives the basic formal ingredients of many-body statistical quantum mechanics and linear response theory. The emphasis is put on staying as general as possible, for the methods presented in this thesis are transverse to several branches of physics: condensed matter, molecular and quantum chemistry, and nuclear physics to name a few. General arguments pertaining to thermal phase transition in many-body quantum systems are presented, and schematically illustrated in case of the pairing and shape transitions. The last part of this overture chapter deals with the response of a system to a time-dependent perturbation, where the accent is put on (i) the co-existence of two different points of view to the response theory, (ii) the several formal starting points leading to the equations of interest, and (iii) the linear approximation to the theory, which is only seldom gone beyond in actual calculations.

Chapter 3 details the formalism of the (Quasiparticle) finite amplitude method ((Q)FAM) for statistical ensembles. This formulation allows opening up the inclusion of thermal effects, and is therefore coined the finite temperature QFAM, or FTQFAM[3]. The derivation of the equations of motion is rather simple, however, several critical points require careful examination. The linearisation of the Hamiltonian with respect to first-order fluctuations of the density matrix is studied; it is shown that the fields entering the equations can always be recast in a one-plus-two-body form. As the symmetries of the FTQFAM densities are slightly different from those of the finite temperature Hartree-Fock-Bogoliubov (FTHFB) ones, a detailed analysis is given in the two standard conventions for the Bogoliubov basis. In addition, the connection between the FTQFAM and the more standard finite temperature quasi-particle random phase approximation (FTQRPA) is scrutinised. A few short but nonetheless important points pertaining to the dressing of the one-body propagators occurring self-consistently during the solution of the equations of motion, the elimination of spurious modes, a prescription regarding the centre-of-mass operator, and the identification of instabilities in the response are discussed. The physical effects leading to the broadening of resonances -which cannot be obtained within a linearised response theory, and therefore elude the formalism- are discussed; in particular, the effect of finite temperature is qualitatively pointed out. Finally, selection rules related to

[3] I will however often write "FAM" instead.

the utilisation of the method atop an axially deformed harmonic oscillator basis are given.

In chapter 4, the FTHFB theory is applied to the study of the thermal phase transition in a mid-mass system, namely ^{56}Fe. Although the number of particles is not so large, this study finds an evolution of the order parameters similar to what is expected in the thermodynamic limit. The convergence of a few relevant macroscopic observables with the evolution of the model space and order in the chiral expansion from which the interaction results is analysed. Systematic uncertainties due to the interaction are estimated to about ten percents for all three systems considered.

The core results of this thesis, namely applications of the FTQFAM, are given in chapter 5. The zero temperature, non-superfluid and spherical part of the implementation is benchmarked against existing RPA calculations in ^{16}O. While experimental data show a non-zero limit of the radiative E1+M1 strength functions at energies lower than 5 MeV, such feature does not appear in our results. The strengths are found to be rather insensitive to the temperature, a result along the lines of those obtained by other studies. We obtain however significant thermal enhancements of the dipole strength at approximately 10 MeVs, and a weakening of the low-energy quadrupole resonance when the system is hot. The monopole strengths tend to increase with the temperature, which tentatively signals an enhancement of the compressibility of finite nuclear matter. Lastly, we mention possible effects responsible for the low-energy enhancement of the dipole strengths.

This thesis is concluded by pointing several possible directions of further development of the method.

Chapter 2

Generalities

This chapter provides a very general introduction to the quantum statistical theory of the many-body problem. It contains and discusses the basic formal ingredients on which the work of this thesis relies.

Contents

2.1 Density matrix

The evolution of a quantum state $|\Psi\rangle$ is dictated by the time-dependent Schrödinger equation [Sch26]

$$i\hbar\frac{\mathrm{d}}{\mathrm{d}t}|\Psi\rangle = \underbrace{(H+F)}_{\equiv G}|\Psi\rangle\,, \tag{2.1}$$

where H represents the internal Hamiltonian (i.e., of the isolated system), and F an external perturbation. The time-dependence of the fields is assumed, but not written explicitly. Provided the Hamiltonian $H+F$ is self-adjoint, this is equivalent to the Liouville-von Neumann equation[1]

$$i\hbar\frac{\mathrm{d}}{\mathrm{d}t}D = [H+F, D], \tag{2.2}$$

where $D \equiv |\Psi\rangle\langle\Psi|$ is the density matrix of the system. While H formally encodes all the interaction among the different degrees of freedom, D encodes all of their correlations. For A degrees of freedom, the density matrix can be represented as a tensor containing the one-body, two-body, up to A-body sectors :

$$D = \begin{pmatrix} D^{(1,1)} & D^{(2,1)} & \dots \\ D^{(1,2)} & D^{(2,2)} & \dots \\ \vdots & \vdots & \ddots \end{pmatrix}. \tag{2.3}$$

Naturally, any $A-$body tensor can be written in that manner:

$$H = \begin{pmatrix} H^{(1,1)} & H^{(2,1)} & \dots \\ H^{(1,2)} & H^{(2,2)} & \dots \\ \vdots & \vdots & \ddots \end{pmatrix}; \quad F = \begin{pmatrix} F^{(1,1)} & F^{(2,1)} & \dots \\ F^{(1,2)} & F^{(2,2)} & \dots \\ \vdots & \vdots & \ddots \end{pmatrix}, \tag{2.4}$$

the equation of motion (2.2) can then be recast as a set of coupled equations[2]

$$i\hbar\frac{\mathrm{d}}{\mathrm{d}t}D^{(i,j)} = \sum_k G^{(k,i)}D^{(j,k)} - D^{(k,i)}G^{(j,k)}. \tag{2.5}$$

Each $D^{(i,j)}$ sector has size $C_A^i \times C_A^j$, so that the complete density matrix contains

[1] If the total Hamiltonian were not Hermitian, its left and right eigenfunctions would not be each other's dual; we'd have equations of motion for both the left and right eigenvectors. All the formalism presented here would still apply with this minor change. Alternatively, one can also work in a doubled space and define new operators that are Hermitian, e.g. $H \to \tilde{H} = \begin{pmatrix} 0 & H \\ H^\dagger & 0 \end{pmatrix}$.

[2] I take the convention that the indices (i,j) correspond to matrix elements between j-body bras and i-body kets, in opposition to the usual row-column matrix notation.

$(2^A - 1)^2$ elements. Such an exponential growth of the Hilbert space with the number of particles quickly renders the exact equations of motion (2.1) and (2.2) intractable beyond the few-body cases[3]. In order to tackle a wider range of systems, approximation schemes have to be designed. The conceptually simplest one is to introduce a transformation over the many-body space so as to recast as much of the system's properties as possible onto the few-body densities and discard the high-order terms. The most severe truncation is to retain only one-body degrees of freedom, in which case the Liouville-von Neumann equation reduces to its purely one-body sector:

$$i\hbar \frac{\mathrm{d}}{\mathrm{d}t} D^{(1,1)} = \left[G^{(1,1)}, D^{(1,1)} \right]. \tag{2.6}$$

Nonetheless, such an abrupt restriction is in general not suited for a faithful description: for instance, a genuine Hamiltonian containing a kinetic term and a two-body interaction will be degraded into a free Hamiltonian without further ado. In order to grasp as many correlations as possible within such a reduction, the density matrix is instead optimised by imposing that the energy of the system be a variational minimum with respect to the one-body densities respecting a set of constraints on various observables. This leads to the so-called time-dependent mean-field (TDMF) equations

$$i\hbar \frac{\mathrm{d}}{\mathrm{d}t} R = [G, R], \tag{2.7}$$

with R and G the mean-field density matrix and total mean-field Hamiltonian, respectively. The general framework of the static mean-field theories, along with the specific Hartree-Fock-Bogoliubov (HFB), will be briefly summarised in section 2.4.

2.2 Statistical ensemble

The study of many-body systems requires identifying the thermodynamical quantities of interest. Although all statistical ensembles are equivalent in the thermodynamic limit ($N \to \infty, V \to \infty, N/V = \mathrm{cst}$), this is not the case for systems with a finite number of degrees of freedom, as the relative statistical fluctuations can be of sizeable importance [LL67b, §2]. The case of finite systems therefore demands a careful choice of the statistical ensemble. In this work, we impose that the thermodynamic variables T and μ, respectively corresponding to the temperature and chemical potential of the system, have some fixed value. The second fixes the average particle number. We consider therefore the system as a grand canonical ensemble. This choice permits the theory to incorporate states that do not display the correct number of particles into the description of the system; that is, this ensemble allows including the particle number fluctuations of statistical nature. In addition, we may impose any kind of constraint; typically, geometric/shape constraints may be enforced through the expectation values Q_{LM} of the multipole moments of the density. It is also possible to fix a given value of the total linear or angular momenta P

[3] As a matter of illustration, the current state-of-the-art no-core shell model calculations can reach $A \sim 20$ in the case of atomic nuclei, see e.g. [FN21; Djä+21].

and J by projecting to target values, the former constraint being crucial for the study of self-bound systems such as atomic nuclei, since there is no external potential ensuring the localisation of the total wave function[4]. Consequently, self-bound systems are invariant by translation. As such, any densities that are identical up to a Galilean transformation are equally good reference states. In average, the total wave function is therefore completely delocalised in space. Imposing a zero momentum condition forbids the system to wander inside the coordinate space, thus forcing its localisation. Such shape and momentum constraints allow targeting not only the (hopefully) global minimum of the potential energy surface spanned but any kind of state following the desired constraints[5]. In this work, only centre-of-mass (and eventually deformations) constraints are imposed, hence J will never be forced onto a specific value, although this is allowed by the formalism developed in this thesis. The constraints are imposed by the method of Lagrange multipliers, written λ_{LM} for the multipolar moments and ω_J for the angular momenta. In that case, the constrained states are obtained by minimising the grand potential

$$\Omega = E - TS - \mu N - \sum_{LM} \lambda_{LM} Q_{LM} - \omega_J \sqrt{J(J+1)}. \tag{2.8}$$

The sum encodes the desired shape constraints. Once the (exact) density matrix $\hat{D}$ of the system is known in some basis $\{|n\rangle\}$ fulfilling the closure relation $|n\rangle\langle n| = I$, the calculation of any observable amounts to that of a trace:

$$\left\langle \hat{O} \right\rangle = \langle \Psi | \hat{O} | \Psi \rangle = \sum_n \langle \Psi | \hat{O} | n \rangle \langle n | \Psi \rangle = \sum_n \langle n | \hat{D}\hat{O} | n \rangle = \mathrm{Tr}\Big\{ \hat{D}\hat{O} \Big\}. \tag{2.9}$$

In particular,

$$E = \mathrm{Tr}\Big\{ \hat{D}\hat{H} \Big\}, \tag{2.10}$$

$$N = \mathrm{Tr}\Big\{ \hat{D}\hat{N} \Big\}, \tag{2.11}$$

$$S = \mathrm{Tr}\Big\{ \hat{D} \log \hat{D} \Big\}, \tag{2.12}$$

$$Q_{LM} = \mathrm{Tr}\Big\{ \hat{D}\hat{Q}_{LM} \Big\}. \tag{2.13}$$

Other thermodynamic quantities can be calculated in the usual manner [LL67a, §14] [LL67b, §5] [KG06, 1, A]. The ground state formally writes as the global minimum of (2.8)[6] over the potential (hyper-)surface spanned by the possible eigenvectors (or,

[4] Note however that this full-glory projection is rather costly, as it formally requires integrating over the set of all translated wave functions. Instead, we use the fact that the centre-of-mass motion is decoupled from the motion of the nucleus in its intrinsic frame, which allows correcting the Hamiltonian by a one-plus-two-body term that imposing the zero-momentum condition.

[5] For simplicity, such constrained vacua will be referred to as ground states without distinction, keeping in mind that they may very well not be the vacuum corresponding to the global ground state but those of lowest energy fulfilling some constraints.

[6] For a time-dependent grand potential, the time-dependent ground state is the dense sequence of its ground state at each time, if we assume the adiabatic approximation.

equivalently, density matrices) of the Hilbert space $\mathscr{H}$ (or, equivalently, over the Fock space $\mathscr{F}$)[7]. According to (2.8), the grand potential is a function of observables only (along with their associated Lagrange multipliers), which are themselves functionals of the density matrix per (2.9). As a consequence, the only variational parameters of which the grand potential is an explicit functional are the elements of the density operator, that is, $\Omega = \Omega[\hat{D}]$. It follows that, around the ground state, the variation

$$\begin{aligned}\delta\Omega &= \Omega[\hat{D} + \delta\hat{D}] - \Omega[\hat{D}] \\ &= \mathrm{Tr}\left\{\left(\hat{H} + k_B T(\log \hat{D}) - \mu\hat{N} - \sum_{LM} \lambda_{LM}\hat{Q}_{LM}\right)\delta\hat{D}\right\} = 0. \end{aligned} \tag{2.14}$$

Since $\delta\hat{D}$ represents a virtual variation, i.e. it is not bound to correspond to a physical path, we may choose it as we please. This implies that the term in parentheses is equal to zero[8], providing us with the formal solution

$$\hat{D} = Z^{-1}\mathrm{e}^{-\beta(\hat{H} - \mu\hat{N} - \sum_{LM}\lambda_{LM}\hat{Q}_{LM})}, \quad \beta \equiv (k_B T)^{-1}, \tag{2.15}$$

where $Z = \mathrm{Tr}\left\{\mathrm{e}^{-\beta(\hat{H} - \mu\hat{N} - \sum_{LM}\lambda_{LM}\hat{Q}_{LM})}\right\}$ is the partition function of the system, which ensures $\mathrm{Tr}\left\{\hat{D}\right\} = 1$. Equation (2.15) makes it clear that there exists a bijection between the statistical operator $\hat{D}$ and the number Z: the density operator and the partition functions both encode all the information. Alternatively, in the basis that diagonalises the Hamilton operator, the partition function is simply the sum of the probabilities to find the system in a given many-body configuration (or microstate) C:

$$Z = \sum_C e^{-\beta\mathcal{E}_C} = \sum_C \prod_i z_i^{n_i^C}, \quad z_i \equiv e^{-\beta(\epsilon_i - \mu)}, \tag{2.16}$$

where E_C is the energy of the A-body configuration C, ϵ_i the energy of the individual state i, and n_i^C the occupation number of i within the configuration C. This provides a convenient way of calculating the moments of the occupation numbers distribution:

$$\left\langle n_i^k \right\rangle = \left(z_i \frac{\partial}{\partial z_i}\right)^k \log Z. \tag{2.17}$$

There are therefore two equivalent ways of calculating the diagonal entries of the sta-

[7] This introduces a slight abuse of language in the context of particle-number breaking theories: the ground state is in that case a mixture of states with different particle numbers, so that "the Hilbert space" is to be understood as a direct sum of spaces with different particle numbers, i.e. a Fock space.

[8] As a matter of proof, we may choose the matrix $\delta\hat{D}$ such that all its elements but one are zero: for any given position of the non-zero element, only one element on the diagonal of the product is a priori non-zero. Equation (2.14) then implies that it does, meaning that the corresponding element of the term in parentheses is zero. The only task left is to iterate over the location of the non-zero term.

tistical density matrix: using (2.15), or using (2.17) with $k = 1$. The average occupation numbers are those of a Fermi-Dirac distribution

$$\langle n_i \rangle = \frac{z_i}{1 + z_i}, \tag{2.18}$$

whereas the thermal fluctuation of the particle numbers have variance

$$\sigma_i^2 = \langle n_i^2 \rangle - \langle n_i \rangle^2 = \frac{z_i - z_i^2}{(1 + z_i)^2}. \tag{2.19}$$

Not so surprisingly, the variance (2.19) is maximal for energies close to the temperature, namely $\sigma^2_{\max} = 1/8$ for $E_i = k_B T \ln 3$. That said, the relative thermal fluctuations, $\sigma / \langle n \rangle$, as one could also expect, increase with the energy, as the orbitals are exponentially less occupied.

The solution (2.15) is, as is, not expressed in the basis that diagonalises $\hat{H}$, which makes it impractical for the determination of $\hat{D}$. A most convenient procedure is to explicitly carry on the variations of $\delta\Omega$, after the independent parameters have been identified. This machinery is deployed for the mean-field theories, as presented succinctly in subsection 2.4.2. Whilst the other observables at play in (2.8) are system-independent, the energy requires a thorough analysis of the Hamiltonian, which is done in the next subsection.

2.3 Static Hamiltonian and some general properties

In real life, one may be interested in the response of a system initially in a state of thermodynamic equilibrium (or not) in the absence of external field. Consequently, a first step is to focus on obtaining the isolated eigenstates[9]. The Hamiltonian describing a many-body system writes in the most general form

$$H = T(1) + V(1,2) + W(1,2,3) + \dots, \tag{2.20}$$

where T contains all the one-body terms (typically consisting of the kinetic energy and, for self-bound (resp. externally bound) systems, of a one-body centre-of-mass correction (resp. external potential)), V corresponds to the two-body interactions, and so on. Expliciting the indices of the individual degrees of freedom:

$$H = \sum_i t_i + \frac{1}{2!} \sum_{ij} v_{ij} + \frac{1}{3!} \sum_{ijk} w_{ijk} + \dots, \tag{2.21}$$

or, in second-quantised form in an arbitrary basis spanning the whole one-body Hilbert

[9]Note that the present discussion trivially generalises to time-dependent Hamiltonians, e.g., one could very well study $H(t), E(t)$, etc within the framework presented in this section.

space,

$$H = \sum_{\alpha\beta} t_{\alpha\beta} b^\dagger_\alpha b_\beta + \frac{1}{(2!)^2} \sum_{\alpha\gamma\beta\delta} v_{\alpha\gamma\beta\delta} b^\dagger_\alpha b^\dagger_\gamma b_\delta b_\beta + \frac{1}{(3!)^2} \sum_{\alpha\beta\gamma\delta\epsilon\zeta} w_{\alpha\gamma\epsilon\beta\delta\zeta} b^\dagger_\alpha b^\dagger_\gamma b^\dagger_\epsilon b_\zeta b_\delta b_\beta + \dots, \tag{2.22}$$

where the denominators appearing in (2.21) and (2.22) balance the over-countings due to the sums running over all indices[10].

Although the Hamiltonian describing A particles should in principle involve up to A-body interaction terms, the present work only considers vertices up to the three-body ones. There is no system-independent justification why a many-body system can, either exactly or approximately (but with a good enough accuracy), be described in terms of few-body interactions.

Yet, a few arguments in favour of such low-rank Hamiltonians are the following:

- if the degrees of freedom are approximately independent (i.e., coupled weakly enough), we expect a "natural" hierarchy of the contributions. Loosely speaking, the expectation value $\langle O \rangle = \langle O_{1-\text{body}} \rangle + \langle O_{2-\text{body}} \rangle + \langle O_{3-\text{body}} \rangle + \dots$ of any relevant operator O should obey $\langle O_{i-\text{body}} \rangle \gg \langle O_{(i+1)-\text{body}} \rangle \gg \dots$ for some small i.

- the interaction is not an observable. We therefore have the freedom to transform it the way we fancy[11], with the all-important constraint that all observables are unaffected by said transformation[12]. This is the idea underlying renormalisation group (RG) approaches [GL54a; GL54b; WK74], that have been shown capable of drastically improving the quality of the results obtained with truncated Hamiltonians [Her+17; Her+18; Her20].

- more practically, the matrix representation of a $k-$body operator in a generic basis is a $N^k \times N^k$ object[13], which quickly grows out of the reach of the computational resources a typical physicist has.

In particular, a small coupling constant[14] and the Pauli principle[15] both favour an approximately independent particle picture: while the first one implies a strong hierarchy among the k-body matrix elements, the second tends to disfavour scattering between the particles by reducing the outgoing available phase space. It should nonetheless be noted that small coupling constants do not guarantee the validity of the independent degrees of freedom picture, as combinatorics quickly render the contributions of high rank terms

[10] That is, one could do the substitutions $\frac{1}{k!}\sum_{ij\dots} \to \sum_{i<j<\dots}$ and $\frac{1}{(k!)^2}\sum_{\alpha,\beta,\dots} \to \sum_{\alpha<\beta<\dots}$.

[11] That is, in a way that puts as much weight as possible on the lowest-rank terms.

[12] More precisely, the observables should remain unchanged *if the full initial Hamiltonian is kept.* However, observables obtained from a truncated Hamiltonian *do* depend on the transformation. It is the very purpose of the latter to render the contribution of high-rank terms as little as possible.

[13] This is worse than the combinatorial scaling of the previous section, since for practical applications the wave functions are expanded on a basis which is not the basis spanned by the one-body eigenstates.

[14] As is the case for, e.g., electronic systems.

[15] As is the case for fermionic systems. This includes composite bosons (e.g. Cooper pairs, α particles to name a few) made of fermions, if the bosonic pairs still show substantial interaction.

prevalent[16], see appendix B for an illustration.

When the Hamiltonian (2.22) is truncated at the three-body level, the energy of a (normalised) state $|\Psi\rangle$ writes

$$E[|\Psi\rangle] = \sum_{\alpha\beta} t_{\alpha\beta} \left\langle b_\alpha^\dagger b_\beta \right\rangle + \frac{1}{(2!)^2} \sum_{\alpha\gamma\beta\delta} v_{\alpha\gamma\beta\delta} \left\langle b_\alpha^\dagger b_\gamma^\dagger b_\delta b_\beta \right\rangle + \frac{1}{(3!)^2} \sum_{\alpha\beta\gamma\delta\epsilon\zeta} w_{\alpha\gamma\epsilon\beta\delta\zeta} \left\langle b_\alpha^\dagger b_\gamma^\dagger b_\epsilon^\dagger b_\zeta b_\delta b_\beta \right\rangle , \tag{2.23}$$

where the brackets $\langle . \rangle$ denote the expectation value with respect to $|\Psi\rangle$. As already alluded to, handling two- and higher-body densities is an exceedingly demanding task, which we want to avoid. For our salvation, the Wick theorem lets us recast such many-point correlations functions into products of two-point ones, i.e. one-body densities [FW71, Ch. III.8] [BR86, Ch. IV] [Zee10, Ch. I.A.2].

2.3.1 Wick theorem

The expectation value of strings of creation and annihilation operators can be written as products of one-body densities by applying Wick's theorem [Wic50; ES96] with respect to the yet-to-be-determined ground state $|\Psi\rangle$. The theorem states that any product of ladder operators can be recast as a sum of pairs of such operators. It builds on the use of the normal-ordering of strings of operators, with the elementary contractions of two operators (either creation or annihilation) A_i, A_j defined as

$$\overbrace{A_i A_j} \equiv A_i A_j - :A_i A_j:, \tag{2.24}$$

the dots denoting the normal ordering operation, which places all creation operators to the left. As A_i and A_j can be creation or annihilation operators, there exist four such elementary contractions. Owing to the usual commutation relations for bosons and fermions, three of these contractions vanish, the only remaining one being

$$\overbrace{A_i A_j^\dagger} = \delta_{ij}. \tag{2.25}$$

By induction, arbitrary strings of operators can be recast as a sum of products involving Wick-contracted and normal-ordered terms only. Such combinatorial expansion beams when employed to calculate expectation values atop a reference state which is a vacuum with respect to the annihilation operators. In that case, all strings involving normal-ordered terms vanish, and only the fully contracted term remains. The expectation value of any strings becomes a product of expectation values of pairs of operators, which are tremendously more simple to handle. Since this is only true when the reference state is annihilated by the lowering operators, the measure $\langle . \rangle$ corresponding to taking

[16] Typically, for A degrees of freedom, terms of order $\sim A/2$ become outrageously dominant.

expectation values must be that of independent operators, i.e. be Gaussian[17].

For fermions[18], and after discarding non-fully contracted strings of operators (which amounts to performing a mean-field approximation, as this only retains one-body densities),

$$\left\langle b_\alpha^\dagger b_\beta \right\rangle \equiv \rho_{\beta\alpha} = \delta_{\alpha\beta} - \left\langle b_\beta b_\alpha^\dagger \right\rangle, \tag{2.26}$$

$$\left\langle b_\alpha^\dagger b_\beta^\dagger \right\rangle \equiv \bar{\kappa}_{\beta\alpha}, \tag{2.27}$$

$$\left\langle b_\alpha b_\beta \right\rangle \equiv \kappa_{\alpha\beta}, \tag{2.28}$$

$$\left\langle b_\alpha^\dagger b_\gamma^\dagger b_\delta b_\beta \right\rangle = \rho_{\delta\gamma}\rho_{\beta\alpha} - \rho_{\delta\alpha}\rho_{\beta\gamma} + \bar{\kappa}_{\gamma\alpha}\kappa_{\delta\beta}, \tag{2.29}$$

$$\begin{aligned}\left\langle b_\alpha^\dagger b_\gamma^\dagger b_\epsilon^\dagger b_\zeta b_\delta b_\beta \right\rangle = {} & \rho_{\zeta\epsilon}\rho_{\delta\gamma}\rho_{\beta\alpha} - \rho_{\zeta\gamma}\rho_{\delta\epsilon}\rho_{\beta\alpha} + \rho_{\zeta\alpha}\rho_{\delta\epsilon}\rho_{\beta\gamma} \\ & - \rho_{\zeta\epsilon}\rho_{\delta\alpha}\rho_{\beta\gamma} + \rho_{\zeta\gamma}\rho_{\delta\alpha}\rho_{\beta\epsilon} - \rho_{\zeta\alpha}\rho_{\delta\gamma}\rho_{\beta\epsilon} \\ & + \rho_{\zeta\epsilon}\bar{\kappa}_{\gamma\alpha}\kappa_{\delta\beta} - \rho_{\zeta\gamma}\bar{\kappa}_{\epsilon\alpha}\kappa_{\delta\beta} + \rho_{\zeta\alpha}\bar{\kappa}_{\epsilon\gamma}\kappa_{\delta\beta} \\ & - \rho_{\delta\epsilon}\bar{\kappa}_{\gamma\alpha}\kappa_{\zeta\beta} + \rho_{\delta\gamma}\bar{\kappa}_{\epsilon\alpha}\kappa_{\zeta\beta} - \rho_{\delta\alpha}\bar{\kappa}_{\epsilon\gamma}\kappa_{\zeta\beta} \\ & + \rho_{\beta\epsilon}\bar{\kappa}_{\gamma\alpha}\kappa_{\zeta\delta} - \rho_{\beta\gamma}\bar{\kappa}_{\epsilon\alpha}\kappa_{\zeta\delta} + \rho_{\beta\alpha}\bar{\kappa}_{\epsilon\gamma}\kappa_{\zeta\delta}.\end{aligned} \tag{2.30}$$

More general considerations on the contractions of a string of creation and annihilation operators can be made here, in order to gauge the recording complexity of generic expectation values, and appreciate the relief brought by symmetrising the matrix elements. In the general setting, a string involving $2k$ operators can be contracted in $(2k-1)!!$ different ways. If anomalous contractions are not allowed, only $b^\dagger b$-type strings will result in non-zero contributions, in which case there are $k!$ different contractions. On the other hand, Wick's theorem (along with the use of anti-symmetrised interactions) reduces the number of interactions stemming from a k-body operator to $\lfloor k/2 \rfloor + 1$ if anomalous contractions are allowed, and only 1 if not. This procedure thus reduces the doubly factorial bookkeeping down to a linear one.

2.3.2 Interaction symmetrisation

Depending on the spin of the degrees of freedom, the total many-body wave function is required to be either completely symmetric or antisymmetric under the exchange of any two particles. Introducing the operator P_{ij} that swaps the particles i and j, a fermionic many-body wave function must verify

$$\overbrace{H \underbrace{P_{ij} \left|\Psi\right\rangle}_{-\left|\Psi\right\rangle}}^{-H} = -E \left|\Psi\right\rangle, \tag{2.31}$$

so that the anti-symmetry can be cast into the Hamiltonian, and therefore into the

[17] In the language of path integrals, this means that the Lagrangian must only contain bilinears in the operators (and their derivatives), which strongly suggests the use of mean-field approximations when dealing with many-body problems.

[18] As for bosons, all minus signs would become plusses.

interaction matrix elements. This symmetrisation of the interaction is very useful once the Wick theorem has been applied to the expectation value of H, as it allows transferring the symmetry properties from the densities into the two- and three-body matrix elements. A properly anti-symmetrised interaction matrix elements arises from the following procedure. A generic k-body operator writes, in second-quantised form,

$$\hat{O}_{k-\text{body}} = \frac{1}{(k!)^2} \sum_{\substack{1,\ldots,k \\ 1',\ldots,k'}} u_{1,\ldots,k,1',\ldots,k'} b_1^\dagger \ldots b_k^\dagger b_{k'} \ldots b_{1'}. \tag{2.32}$$

The k-body interaction vertex $u^{(a)}$, anti-symmetrised to the right (i.e.with respect to permutations of the k rightmost operators) can be built from an initial u through

$$\begin{aligned} u^{(a)}_{1,\ldots,k,1',\ldots,k'} &\equiv \sum_{\{\mathcal{P}'\}} (-1)^{\pi_{\mathcal{P}'}} u_{\mathcal{P}'(1,\ldots,k,1',\ldots,k')} \\ &= \Big(1 - \sum_{\substack{i,j \\ \text{all}\neq}} \mathcal{P}'_{ij} + \sum_{\substack{i,j,k \\ \text{all}\neq}} \mathcal{P}'_{ij}\mathcal{P}'_{jk} - \ldots\Big) u_{1,\ldots,k,1',\ldots,k'}, \end{aligned} \tag{2.33}$$

where $\mathcal{P}'$ denotes a permutation of the primed indices, and $\{\mathcal{P}'\}$ the set thereof. The exponent $\pi_{\mathcal{P}'}$ is the parity of the permutation[19]. For instance, the anti-symmetrised fermionic two- and three-body interaction matrix elements read

$$v^{(a)\rho\rho}_{\alpha\gamma\beta\delta} \equiv v_{\alpha\gamma\beta\delta} - v_{\alpha\gamma\delta\beta}, \tag{2.34}$$

$$w^{(a)\rho\rho\rho}_{\alpha\gamma\epsilon\beta\delta\zeta} \equiv w_{\alpha\gamma\epsilon\beta\delta\zeta} - w_{\alpha\beta\epsilon\delta\gamma\zeta} + w_{\epsilon\beta\alpha\delta\gamma\zeta} - w_{\gamma\beta\alpha\delta\epsilon\zeta} + w_{\gamma\beta\epsilon\delta\alpha\zeta} - w_{\epsilon\beta\gamma\delta\alpha\zeta}. \tag{2.35}$$

The anti-symmetrised matrix elements generated by permuting indices to the right are associated to contractions involving only $b^\dagger b$ strings because this amounts to moving annihilation operators only. As for the remaining contractions, the form of the two- and three-body matrix elements can be deduced by noting that the orderings to be involved are, by construction, all the ones that do not contribute in producing the terms (2.34)-(2.35). For a k-body operator, there are $(2k-1)!! - k!$ such types of permutations. Alternatively, one can simply use the Wick-contracted densities (2.29)-(2.30) involving pairing tensors. This yields:

$$v^{(a)\kappa\kappa}_{\alpha\gamma\beta\delta} = v_{\alpha\gamma\beta\delta}, \tag{2.36}$$

$$\begin{aligned} w^{(a)\rho\kappa\kappa}_{\alpha\gamma\epsilon\delta\beta\zeta} &\equiv w_{\alpha\gamma\epsilon\beta\delta\zeta} - w_{\alpha\epsilon\gamma\beta\delta\zeta} + w_{\gamma\epsilon\alpha\beta\delta\zeta} - w_{\alpha\gamma\epsilon\beta\zeta\delta} \\ &+ w_{\alpha\epsilon\gamma\beta\zeta\delta} - w_{\gamma\epsilon\alpha\beta\zeta\delta} + w_{\alpha\gamma\epsilon\delta\zeta\beta} - w_{\alpha\epsilon\gamma\delta\zeta\beta} + w_{\gamma\epsilon\alpha\delta\zeta\beta}. \end{aligned} \tag{2.37}$$

Using anti-symmetrised interactions allows us to recast the 21 different strings into only

[19]Naturally, this procedure can be applied to bosonic operators, with this time no parity (hence no minus signs) involved.

5, transferring the bookkeeping from the densities into the $v_{\alpha\gamma\beta\delta}$ and $w_{\alpha\gamma\epsilon\beta\delta\zeta}$ vertices, which only take up a sign corresponding to the parity of the permutation sequences involved in the elements of (2.29)-(2.30). The joint use of the symmetrisation procedure and Wick's theorem transform the tedious computation of many-body expectation values into a problem of combinatorics involving only one-body densities. Put differently, when the interaction matrix elements have been anti-symmetrised according to (2.34)-(2.37), the strings of densities can be immediately grouped by corresponding powers of ρ's and κ's. The energy (2.23) can then be obtained by teaming up the anti-symmetrisation (2.33) with the Wick-ordered expectation values (2.26)-(2.30):

$$\begin{aligned} E[\rho,\kappa,\bar{\kappa}] = &\sum_{\alpha\beta} t_{\alpha\beta}\rho_{\beta\alpha} \\ &+ \frac{1}{2}\sum_{\alpha\beta\gamma\delta} v^{(a)\rho\rho}_{\alpha\gamma\beta\delta}\rho_{\delta\gamma}\rho_{\beta\alpha} + \frac{1}{4}\sum_{\alpha\gamma\beta\delta} v^{(a)\kappa\kappa}_{\alpha\gamma\beta\delta}\bar{\kappa}_{\gamma\alpha}\kappa_{\beta\delta} \\ &+ \frac{1}{6}\sum_{\alpha\beta\gamma\delta\epsilon\zeta} w^{(a)\rho\rho\rho}_{\alpha\gamma\epsilon\beta\delta\zeta}\rho_{\zeta\epsilon}\rho_{\delta\gamma}\rho_{\beta\alpha} + \frac{1}{4}\sum_{\alpha\beta\gamma\delta\epsilon\zeta} w^{(a)\rho\kappa\kappa}_{\alpha\gamma\epsilon\beta\delta\zeta}\rho_{\zeta\epsilon}\bar{\kappa}_{\gamma\alpha}\kappa_{\beta\delta}. \end{aligned} \tag{2.38}$$

2.4 Mean-field approximations

2.4.1 General setting

Approximating the exact density matrix by its one-body sector amounts to assuming that the eigenstates (not only the ground state) of the A-body system can be written as product states of creation[20] operators on top of the bare vacuum $|-\rangle$, e.g.

$$|\Phi\rangle = \prod_{\lambda} \xi^{\dagger}_{\lambda}|-\rangle\,, \quad \mathbf{card}(\{\lambda\}) = A, \tag{2.39}$$

with the set $\{\xi^{\dagger}\}$ to be determined by minimising the energy under the set of desired constraints. Because the mean-field picture lets us write the eigenstates as products of creation or annihilation operators on top of a vacuum, the ground state is easily identified. At zero temperature, it is simply the product state with the lowest energy. At finite temperature, however, the degrees of freedom have a non-zero probability to scatter towards more energetic orbitals than the lowest ones. It follows in that situation that a product state ansatz is bound to badly fail at providing a faithful description of the structure and dynamics of the system. The ground state density operator must instead be written as a linear combination of the permitted states, that is

$$R(\beta) = \sum_{n} f_n(\beta)\,|n\rangle\langle n| = \sum_{s} \frac{z_s(\beta)}{Z(\beta)} R_s; \quad \beta \equiv (k_B T)^{-1}, \tag{2.40}$$

where the individual states $|n\rangle$ and many-body density matrices R_s associated to pure

[20] or annihilation, in case of the Bogoliubov formalism.

states implicitly depend on the inverse temperature β through the self-consistent solution to the mean-field equation.

The f_n and z_s can be determined by a derivation[21] entirely similar to that of section 2.2:

$$f_n = \frac{1}{e^{\beta E_n} + 1}, \quad z_s = e^{-\beta \mathcal{E}_s}, \quad Z = \sum_s z_s, \tag{2.41}$$

with E_n the energy of the n^{th} one-body eigenstate and $\mathcal{E}_s$ the energy of the s^{th} product state. The fact that the f_n are different from 0 or 1 (except at zero temperature), causes that the thermal density $R(\beta)$ cannot be associated to a pure state, but is rather a statistical mixture of different density operators. The most general (single-reference) finite temperature mean-field transformation, the one of Hartree-Fock-Bogoliubov (HFB), is recapitulated in the next subsection.

2.4.2 Hartree-Fock-Bogoliubov theory

The simplest mean-field theory, the Hartree-Fock approximation, assumes that the optimal creation (resp. annihilation) operators write as linear combinations of the creation (resp. annihilation) operators spanning a basis of the one-body Hilbert space, with the symmetry that only operators of identical time-signature can mix. It is thus by construction unable to account for pairing correlations. In the presence of a pairing interaction among the degrees of freedom, the single-particle states interact even if they do not have the same time signature. While the Bardeen-Cooper-Schrieffer (BCS) theory [Coo56; BCS57a; BCS57b] assumes that only time-reversed partners are explicitly coupled through a pairing field[22], the most general way of constructing the new eigenstates is to express them as a linear combination of all the single particle ones, regardless of their relative quantum numbers. In the same spirit as the BCS theory defines new independent degrees of freedom operators as a mixing of forward- and backward-propagating single particle ones, the HFB transformation [Bog47; Bog58; BTŠ58] defines quasi-particles[23] on top of the HFB vacuum as linear combinations of all possible single-particle states, and is conventionally parametrised as

$$\alpha_\mu = \sum_i U^*_{i\mu} c_i + V^*_{i\mu} c^\dagger_i, \tag{2.42a}$$

$$\alpha^\dagger_\mu = \sum_i V_{i\mu} c_i + U_{i\mu} c^\dagger_i. \tag{2.42b}$$

[21] One could also invoke the "heuristic" argument that $R(\beta)$ being a state built with independent degrees of freedom, the ground state density immediately writes as a linear combination of the independent-particle densities, weighted by their Fermi-Dirac coefficients.

[22] Which is generally a reasonable assumption since these are the pairs of states with maximal spatial overlap.

[23] One can make the distinction between occupied states (quasi-holes, or qh) and unoccupied states (quasi-particles, or qp). While it is customary to refer to both as qp, the discrimination will hopefully be made scrupulously.

The matrices U and V encode the Bogoliubov transformation, and are to be obtained by the minimisation of the mean-field grand potential. The product state of lowest energy is constructed as a vacuum with respect to the newly defined quasi-particle annihilation operators (2.42a)-(2.42b):

$$\alpha_\mu \left|\Phi^{\mathrm{HFB}}\right\rangle = 0 \Rightarrow \left|\Phi^{\mathrm{HFB}}\right\rangle = \prod_\lambda \alpha_\lambda \left|-\right\rangle . \tag{2.43}$$

Special attention should be paid when defining the transformation, as many conventions coexist [DFT84]. The prescription (2.42a)-(2.42b) for the transformations corresponds to the so-called traditional representation of the Bogoliubov transformation. Eventually, the equations for the Russian convention will also be given in section 3.3. The transformation can conveniently be represented in matrix form[24]:

$$\mathcal{B}^\dagger \equiv \begin{pmatrix} U^\dagger & V^\dagger \\ V^T & U^T \end{pmatrix}; \quad \begin{pmatrix} \alpha \\ \alpha^\dagger \end{pmatrix} = \mathcal{B}^\dagger \begin{pmatrix} c \\ c^\dagger \end{pmatrix}, \tag{2.44}$$

defining the Bogoliubov matrix $\mathcal{B}$. The inverse transformation is

$$\begin{pmatrix} c \\ c^\dagger \end{pmatrix} = \mathcal{B} \begin{pmatrix} \alpha \\ \alpha^\dagger \end{pmatrix}; \quad \mathcal{B} = \begin{pmatrix} U & V^* \\ V & U^* \end{pmatrix}; \quad \begin{aligned} c_i &= \sum_\mu U_{\mu i}\alpha_\mu + V^*_{\mu i}\alpha^\dagger_\mu, \\ c^\dagger_i &= \sum_\mu V_{\mu i}\alpha_\mu + U^*_{\mu i}\alpha^\dagger_\mu. \end{aligned} \tag{2.45}$$

Amounting to a mere linear transformation, the passage from the initial basis $\{c^\dagger, c\}$ to the Bogoliubov basis $\{\alpha^\dagger, \alpha\}$ must be achieved through a unitary transformation, i.e., $\mathcal{B}\mathcal{B}^\dagger = I = \mathcal{B}^\dagger\mathcal{B}$. This ensures the preservation of the canonical anti-commutation relations between the Bogoliubov operators:

$$\begin{aligned} \{\alpha_\mu, \alpha^\dagger_\nu\} &= \sum_{ij} U^*_{i\mu}V_{j\nu}\{c_i, c_j\} + U^*_{i\mu}U_{j\nu}\{c_i, c^\dagger_j\} + V^*_{i\mu}V_{j\nu}\{c^\dagger_i, c_j\} + V^*_{i\mu}U_{j\nu}\{c^\dagger_i, c^\dagger_j\} \\ &= \sum_i U^*_{i\mu}U_{i\nu} + V^*_{i\mu}V_{i\nu} = \delta_{\mu\nu}, \end{aligned} \tag{2.46}$$

$$\begin{aligned} \{\alpha_\mu, \alpha_\nu\} &= \sum_{ij} U^*_{i\mu}U_{j\nu}\{c_i, c_j\} + U^*_{i\mu}V_{j\nu}\{c_i, c^\dagger_j\} + V^*_{i\mu}U_{j\nu}\{c^\dagger_i, c_j\} + V^*_{i\mu}V_{j\nu}\{c^\dagger_i, c^\dagger_j\} \\ &= \sum_i U^*_{i\mu}V_{i\nu} + V^*_{i\mu}U_{i\nu} = 0. \end{aligned} \tag{2.47}$$

This unitarity requirement can also be written in matrix form, yielding the two sets of relations

[24] Single-particle operators are not barred to ease the representation; one should see the c's and $c^\dagger$'s as spanning both the time-forward and time-backward states here.

$$\mathcal{B}^\dagger\mathcal{B} = I: \quad U^\dagger U + V^\dagger V = I, \tag{2.48a}$$
$$U^\dagger V^* + V^\dagger U^* = 0, \tag{2.48b}$$
$$V^T U + U^T V = 0, \tag{2.48c}$$
$$V^T V^* + U^T U^* = I, \tag{2.48d}$$

$$\mathcal{B}\mathcal{B}^\dagger = I: \quad UU^\dagger + V^* V^T = I, \tag{2.49a}$$
$$UV^\dagger + V^* U^T = 0, \tag{2.49b}$$
$$VU^\dagger + U^* V^T = 0, \tag{2.49c}$$
$$VV^\dagger + U^* U^T = I. \tag{2.49d}$$

Since the transformation allows the mixing of all the states regardless of their behaviour under symmetry operations (e.g. time reversal, parity, angular momentum, etc), the resulting wave functions do not possess well-defined quantum numbers, and, most notoriously, the product state of lowest energy resulting from the application of the Rayleigh-Ritz method does not conserve the particle number. As an illustration, one has in general a non-zero pairing tensor:

$$\bar{\kappa}_{ij} \equiv \left\langle c_i^\dagger c_j^\dagger \right\rangle = \sum_{\mu\nu} V_{\mu i} V_{\nu j} \left\langle \alpha_\mu \alpha_\nu \right\rangle + V_{\mu i} U_{\nu j}^* \left\langle \alpha_\mu \alpha_\nu^\dagger \right\rangle + U_{\mu i}^* V_{\nu j} \left\langle \alpha_\mu^\dagger \alpha_\nu \right\rangle + U_{\mu i}^* U_{\nu j}^* \left\langle \alpha_\mu^\dagger \alpha_\nu^\dagger \right\rangle . \tag{2.50}$$

Of the four expectation values, only the second and third can survive by virtue of the product state ansatz (2.43). As the independent degrees of freedom of the problem are the quasi-particle operators $\{\alpha, \alpha^\dagger\}$, one has $\left\langle \alpha_\mu \alpha_\nu^\dagger \right\rangle = f_\mu \delta_{\mu\nu}$ and $\left\langle \alpha_\mu^\dagger \alpha_\nu \right\rangle = (1 - \bar{f}_\mu)\delta_{\mu\nu}$. The generalised density (or Valatin) operator, that contains all the one-body density correlations, then writes in its diagonal form

$$\mathcal{R}(\beta) \equiv \begin{pmatrix} \left\langle \alpha^\dagger \alpha \right\rangle & \left\langle \alpha\alpha \right\rangle \\ \left\langle \alpha^\dagger \alpha^\dagger \right\rangle & \left\langle \alpha\alpha^\dagger \right\rangle \end{pmatrix} = \begin{pmatrix} f & \\ & 1 - \bar{f} \end{pmatrix}; \quad \langle . \rangle = \left\langle \Phi^{\mathrm{HFB}} \middle| . \middle| \Phi^{\mathrm{HFB}} \right\rangle , \tag{2.51}$$

f and $\bar{f}$ being the Fermi-Dirac occupations for unbound and bound states, respectively. Naturally, a consequence of the fact that the eigenvalues of the HFB equation come in pair is that $f = \bar{f}$; the distinction is however maintained for bookkeeping purposes. Just like in the BCS theory, the fact that particle-particle and hole-hole correlations can be non-zero forces the doubling of the basis. Equivalently, this necessity can be seen directly from the form of the Bogoliubov transformation (2.42), which mixes creation and annihilation together[25]. Recalling the definitions (2.26)-(2.28) of the elementary contractions with respect to the sought HFB vacuum, the densities in the $c, c^\dagger$ basis write

$$\rho(\beta) = U f U^\dagger + V^*(I - \bar{f})V^T, \tag{2.52a}$$
$$\kappa(\beta) = U f V^\dagger + V^*(I - \bar{f})U^T, \tag{2.52b}$$
$$-\bar{\kappa}(\beta) = V f U^\dagger + U^*(I - \bar{f})V^T, \tag{2.52c}$$
$$I - \bar{\rho}(\beta) = V f V^\dagger + U^*(I - \bar{f})U^T. \tag{2.52d}$$

[25] One may also take the obverse viewpoint, saying that the HF theory is a very peculiar transformation, in which c's and $c^\dagger$'s do not mix so that the density matrix is separable as a direct sum. The often enforced time-reversal symmetry and zero temperature regime then allow discarding half of the generalised density matrix.

The energy writes as in (2.38), with the minimisation of the grand potential to be carried out within the space of one-body densities (2.52). Due to the canonical relations (2.46), not all the variational parameters are independent[26]. This can also be seen straight from (2.52) with the help of (2.48), (2.49):

$$(2.52) \text{ and } f = \bar{f}: \qquad \bar{\rho}(\beta) = \rho^*(\beta), \tag{2.53a}$$
$$\{c, c\} = 0: \qquad \kappa(\beta) = -\kappa^T(\beta), \tag{2.53b}$$
$$\{c^\dagger, c^\dagger\} = 0: \qquad \bar{\kappa}(\beta) = -\bar{\kappa}^T(\beta). \tag{2.53c}$$

In addition, anticipating that the Hamiltonian of the theory is Hermitian[27], one knows that the U and V matrices can be made real, and the eigenvalues come by pairs of opposite sign (hence $\bar{E} = E$, implying in turn $\bar{f} = f$) due to the doubling of the basis. Equipped with this, all densities become real, and can reach finer degrees of symmetries:

$$U, V \text{ real}: \qquad \rho^T(\beta) = \rho(\beta), \tag{2.54a}$$
$$\bar{\rho}^T(\beta) = \bar{\rho}(\beta), \tag{2.54b}$$
$$\bar{\kappa}(\beta) = \kappa(\beta). \tag{2.54c}$$

These symmetries will be reviewed in greater detail in section 3.3. Rather than taking all of $\{\rho, \bar{\rho}, \kappa, \bar{\kappa}\}$, one can thus consider $\{\rho_{ij}, \kappa_{ij}, \bar{\rho}_{ij}, \bar{\kappa}_{ij}\}_{i \leq j}$ as the complete and irreducible[28] set of parameters with respect to which the energy is to be varied. One thus has

$$\delta E = \sum_{i \leq j} \frac{\delta E}{\delta \rho_{ij}} \delta \rho_{ij} + \frac{\delta E}{\delta \bar{\rho}_{ij}} \delta \bar{\rho}_{ij} + \frac{\delta E}{\delta \kappa_{ij}} \delta \kappa_{ij} + \frac{\delta E}{\delta \bar{\kappa}_{ij}} \delta \bar{\kappa}_{ij}. \tag{2.55}$$

Then, on defining the mean and pairing fields according to

$$h_{\nu\mu} \equiv \frac{\delta E}{\delta \rho_{\mu\nu}}, \tag{2.56a}$$
$$\bar{h}_{\nu\mu} \equiv \frac{\delta E}{\delta \bar{\rho}_{\mu\nu}}, \tag{2.56b}$$
$$\Delta_{\mu\nu} \equiv \frac{\delta E}{\delta \bar{\kappa}_{\mu\nu}}, \tag{2.56c}$$
$$\bar{\Delta}_{\mu\nu} \equiv \frac{\delta E}{\delta \kappa_{\mu\nu}}, \tag{2.56d}$$

we may define the generalised Hamilton matrix such that $\delta E = \mathrm{Tr}\{H \delta R\}$: after identifying the diagonal terms of $H\delta R$ with those of (2.55), one obtains

[26] While the corresponding relations between the one-body densities are sometimes determined from the idempotency of the generalised density, at finite temperature the density operator is not longer a single product state, so that this relation does no hold any more. Eventually, the $\mathcal{R}^k(\beta), k \in \mathbb{N}$ form a convex sequence, and have a fixed point only at $T = 0$. The idempotency can only be met in the product states (of which the thermal density is a mixture), not in the thermal density itself.

[27] Which is natural since the system is closed, hence of unitary evolution.

[28] Irreducibility is to be understood within the doubled basis: owing to the relations between barred and non-barred densities, this set still contains redundancies.

$$H = \begin{pmatrix} h & \Delta \\ -\bar{\Delta} & -\bar{h} \end{pmatrix}, \tag{2.57}$$

with the fields deriving from (2.38) writing[29]

$$h_{\alpha\beta} = t_{\alpha\beta} + \sum_{\gamma\delta} v^{(a)\rho\rho}_{\alpha\gamma\beta\delta}\rho_{\delta\gamma} + \frac{1}{2}\sum_{\gamma\delta\epsilon\zeta} w^{(a)\rho\rho\rho}_{\alpha\gamma\epsilon\beta\delta\zeta}\rho_{\zeta\epsilon}\rho_{\delta\gamma} + \frac{1}{4}\sum_{\gamma\delta\epsilon\zeta} w^{(a)\rho\kappa\kappa}_{\alpha\gamma\epsilon\beta\delta\zeta}\bar{\kappa}_{\epsilon\gamma}\kappa_{\delta\zeta}, \tag{2.58a}$$

$$\Delta_{\alpha\gamma} = \frac{1}{2}\sum_{\gamma\delta} v^{(a)\kappa\kappa}_{\alpha\gamma\beta\delta}\kappa_{\beta\delta} + \frac{1}{2}\sum_{\gamma\delta\epsilon\zeta} w^{(a)\rho\kappa\kappa}_{\alpha\gamma\epsilon\beta\delta\zeta}\rho_{\zeta\epsilon}\kappa_{\beta\delta}, \tag{2.58b}$$

$$\bar{\Delta}_{\alpha\gamma} = \frac{1}{2}\sum_{\gamma\delta} v^{(a)\kappa\kappa}_{\alpha\gamma\beta\delta}\bar{\kappa}_{\beta\delta} + \frac{1}{2}\sum_{\gamma\delta\epsilon\zeta} w^{(a)\rho\kappa\kappa}_{\alpha\gamma\epsilon\beta\delta\zeta}\rho_{\zeta\epsilon}\bar{\kappa}_{\beta\delta}, \tag{2.58c}$$

$$\bar{h}_{\alpha\beta} = t_{\alpha\beta} + \sum_{\gamma\delta} v^{(a)\rho\rho}_{\alpha\gamma\beta\delta}\bar{\rho}_{\delta\gamma} + \frac{1}{2}\sum_{\gamma\delta\epsilon\zeta} w^{(a)\rho\rho\rho}_{\alpha\gamma\epsilon\beta\delta\zeta}\bar{\rho}_{\zeta\epsilon}\bar{\rho}_{\delta\gamma} + \frac{1}{4}\sum_{\gamma\delta\epsilon\zeta} w^{(a)\rho\kappa\kappa}_{\alpha\gamma\epsilon\beta\delta\zeta}\bar{\kappa}_{\epsilon\gamma}\kappa_{\delta\zeta}. \tag{2.58d}$$

Due to the hermicity of the HFB Hamiltonian, one has $h^\dagger = h$ and $\Delta^\dagger = -\bar{\Delta}$, in consistency with the symmetries of the generalised density matrix. As a consequence of (2.53a), ones also has $h^* = \bar{h}$, while (2.54c) gives $\bar{\Delta} = \Delta$.

Since the energy is to be varied with certain constraints, one should express these in the doubled basis as well in order to handle a single representation. The expectation values of generic one-body operators $Q = \sum_{ij} Q^\rho_{ij} c_i^\dagger c_j + Q^\kappa_{ij} c_i c_j$ can be written in the doubled basis thanks to the very same procedure, making use of the symmetries (2.53) and (2.54)

$$\mathrm{Tr}\{Q^\rho\rho\} + \mathrm{Tr}\{Q^\kappa\kappa\} = \frac{1}{2}\,\mathrm{Tr}\left\{\begin{pmatrix} Q^\rho & Q^\kappa \\ (Q^\kappa)^T & (-Q^\rho)^* \end{pmatrix}\begin{pmatrix} \rho & \kappa \\ -\bar{\kappa} & I - \bar{\rho} \end{pmatrix}\right\} + \frac{1}{2}\,\mathrm{Tr}\{Q^\rho\}. \tag{2.59}$$

It should be noted that Q^ρ being real and symmetric, using its complex conjugate is entirely conventional and due to using the relation (2.53a). It will be shown in section 3.3 that the only choice consistent with complex matrix elements is to use the scalar transpose of Q^ρ. In our case, where the constraints are imposed solely for the particle numbers and multipolar moments (whose operators only have components in the normal sector), these expressions reduce to the usual block-diagonal ones.

One finds the set of many-body states by minimising the grand potential (2.8), with the additional constraint that the associated density operators $\mathcal{R}_{\text{p.s.}}$ must correspond to product states. This translates into the fact that one can find a set of idempotent density matrices $\{\mathcal{R}_{\text{p.s.}}\}$ solving the equation of motion. However, they only correspond to the possible pure states that can be obtained, and the one of lowest energy identifies with the ground state only in the $T \to 0$ limit. In the $T > 0$ case, the ground state is a mixture of these densities according to (2.15) (or equivalently, in the case of the FTHFB theory,

[29] Note that the indices β and γ are sometimes permuted in order to write $\Delta_{\alpha\beta}$ rather than $\Delta_{\alpha\gamma}$; this is a matter of convention.

using (2.52)). Thus, one only has to solve

$$\delta\left(E-\mu N-\Lambda(\mathcal{R}_{\text{p.s.}}^2-\mathcal{R}_{\text{p.s.}})-\sum_{LM}\lambda_{LM}(Q_{LM}-q_{LM})\right)=0, \tag{2.60}$$

where the indices LM run over the multipole moments we want to constrain to the values q_{LM}. Solving this equation gives the product state of lowest energy, along with the eigenvectors of the constrained Hamiltonian. Recalling the expressions of the expectation values and using (2.59), one obtains by the very same argument as in section 2.2

$$H-\mu N-\Lambda\mathcal{R}_{\text{p.s.}}-\mathcal{R}_{\text{p.s.}}\Lambda+\Lambda-\frac{1}{2}\sum_{LM}\lambda_{LM}Q_{LM}=0. \tag{2.61}$$

This expression can be multiplied by $\mathcal{R}_{\text{p.s.}}$ separately to the left and to the right, the subtraction of these two copies leading to the static HFB equation

$$\left[H-\frac{1}{2}\sum_{LM}\lambda_{LM}Q_{LM},\mathcal{R}_{\text{p.s.}}\right]=0. \tag{2.62}$$

Once this equation has been solved, the thermal state $\mathcal{R}$ can be constructed from the density operator $\mathcal{R}_{\text{p.s.}}$ with the lowest energy using the Fermi-Dirac factors, or equivalently as a weighted sum over the whole set $\{\mathcal{R}_{\text{p.s.}}\}$.

2.5 Thermal phase transitions

Allowing the system to have non-zero temperatures opens a way to several phenomena. Naturally, one might expect from their everyday experience that the changes of a system's temperature can trigger a plethora of effects, the most notable being the occurrence of phase transitions[30]. In the case of interacting quantum systems, thermal scattering of the particles between the possible shells can lead to highly non-trivial rearrangements of the energy spectrum. More specifically, the pair condensate being produced by a (rather weak) interaction between time-reversed partners, the competition between pairing and thermal effects is easily conceived to cause the breakup of pairs when the temperature is increased. In the case of deformation, a restoration of the spherical symmetry is also to be anticipated: a well-pronounced deformation marks that a set of corresponding orbitals is occupied while states of higher energy are not. When the temperature is increased, the nucleons initially sitting on the deformed orbital also have significant probability to occupy all the energetically close states, resulting in an averaging that smoothens the total deformations [BM75][32]. The two following subsections concisely illustrate the two

[30]The complex problem of understanding how phase transitions can occur in finite systems is entirely set aside; the reader may refer to [YL52; LY52], [Mai05][31]and [CG08].

[31]Mind that the r.h.s. of his equation (2) should read $\kappa\prod_{r=1}^{N(V)}\left(1-\frac{z}{z_r}\right)$, without the log.

[32]Likewise, one could also expect a spherical to deformed transition in very small systems.

predicted behaviours.

2.5.1 Collapse of the pairing via thermal excitations

From the expression (2.52b), one sees with the help of (2.49) that the pairing correlations should fade out at high temperatures:

$$\kappa_{ij} = \sum_k V_{ik}^* U_{kj}^T (1 - f_k - \bar{f}_k) \underset{\beta \to 0}{\longrightarrow} 0. \tag{2.63}$$

That said, it leads to a pairing energy that appears smoothly vanishing, whereas it is known that within mean-field theories like HFB and BCS, pairing does not survive beyond a critical temperature T_c at which the transition from the superfluid to the normal phase occurs [BCS57c]. The rapid collapse of the pairing tensor is therefore encoded in the V and U amplitudes. While the sharp transition cannot be inferred directly from (2.69) alone, one can be convinced that, the pairing gap depending on the average occupation of the shells, a much faster collapse than the one predicted by a too quick observation of (2.63) should be expected. In addition, pairing is mostly a surface phenomenon. Albeit this is not easy to see from the Bogoliubov transformation, this is clearer by using the Bloch-Messiah-Zumino (BMZ) decomposition [BM62; Zum62] [RS80, Secs. 7.2, 7.3, App. E1] (and its generalisation [Dob00]):

$$\begin{pmatrix} U^\dagger & V^\dagger \\ V^T & U^T \end{pmatrix} = \begin{pmatrix} C^\dagger & \\ & C^T \end{pmatrix} \underbrace{\begin{pmatrix} \bar{U}^\dagger & \bar{V}^\dagger \\ \bar{V}^\dagger & \bar{U}^\dagger \end{pmatrix}}_{\text{BCS-like}} \underbrace{\begin{pmatrix} D^\dagger & \\ & D^T \end{pmatrix}}_{\text{HF-like}}. \tag{2.64}$$

Since this transformation is well-known, its features are only succinctly recapped here. The first step is a block-diagonal transformation of the single particle operators among themselves, that puts the normal density matrix and pairing tensor in their diagonal form[33]. This defines the so-called canonical basis. In the situation where pairing correlations are not described, this is equivalent to the Hartree-Fock transformation. The Hamiltonian transformed accordingly can thus be written as a collection of two by two matrices:

$$H^{\text{cb}} = \bigoplus_k^N h_k^{\text{cb}} = \bigoplus_k^N \begin{pmatrix} \epsilon_k - \lambda & \Delta_k \\ -\Delta_k & -\epsilon_k + \lambda \end{pmatrix} = \text{diag}(h_1^{\text{cb}}, \dots, h_N^{\text{cb}}), \tag{2.65}$$

each block being diagonalised by a BCS-like transformation with squared amplitudes and eigenvalues

[33] Depending on the ordering of the $\{c^\dagger, c\}$ operators, the pairing tensors can be made either diagonal or anti-diagonal.

$$v_k^2 = \frac{1}{2}\left(1 - \frac{\epsilon_k - \lambda}{\sqrt{(\epsilon_k - \lambda)^2 + \Delta_k^2}}\right), \tag{2.66}$$

$$u_k^2 = \frac{1}{2}\left(1 + \frac{\epsilon_k - \lambda}{\sqrt{(\epsilon_k - \lambda)^2 + \Delta_k^2}}\right), \tag{2.67}$$

$$E_k^{\pm} = \pm\sqrt{(\epsilon_k - \lambda)^2 + \Delta_k^2}. \tag{2.68}$$

This second transformation thus takes the canonical basis to the BCS basis. The third rotation mixes the BCS quasiparticle operators among themselves, leading to the Bogoliubov basis. The BMZ theorem can thus be understood as a decomposition of the full HFB transformation into a series of HF-like and BCS-like transformations, followed by a third one diagonalising the resulting Hamiltonian and density operator simultaneously. As the density matrix is diagonal in the canonical basis, it corresponds to the best independent particle representation of the problem, hence it is convenient for a physical analysis. For the present discussion, we assume that the last transformation is trivial ($C = I$), so that the HFB transformation reduces to the HF-BCS one. In that case, the total energy writes

$$E_{\text{tot}}^{\text{BCS}} = \sum_k (\epsilon_k - \lambda)[v_k^2(1 - f_k) + (1 - v_k^2)f_k] + \Delta_k u_k v_k (2f_k - 1) \equiv E_{\text{normal}}^{\text{BCS}} + E_{\text{pair}}^{\text{BCS}}. \tag{2.69}$$

Remarking that $2u_k v_k = \Delta_k / E_k^{\text{BCS}}$ and eying (2.68), one sees that the effects of pairing are localised around the Fermi surface, which is another argument in favour of a rapid collapse of the pairing with the temperature, since the levels close to the Fermi energy are the most affected by the statistical distribution (2.41). This statement can be made more quantitative by showing [BCS57c; Gor96] that the pairing abruptly vanishes above a critical temperature T_C

$$\Delta(T) = \Delta(0)\left[1 - \left(\frac{T}{T_C}\right)^m\right]^{1/2} \Theta(T_C - T), \tag{2.70}$$

where the zero-temperature pairing gap $\Delta(0)$ is obtained by assuming the pairing interaction to be constant within a small window around the Fermi energy. Typical expected values for the critical temperature are about 0.5-0.6 times $\Delta(0)$.

2.5.2 Spherical symmetry restoration

Like for the pairing transition, the evolution of the deformation with temperature is strongly affected by the energy spectrum and the shape of the corresponding wave function. At low temperature, the overall deformation is that of the lowest energy states. As the temperature increases, several states can be occupied with about similar probabilities, which results in an essentially spherical thermal state. Figure 2.1 considers 100 shells to which are associated Woods-Saxon density profiles, with relative diffusenesses $a_z, a_\perp$ ran-

domly selected between 0.5 and 1.5. The energies are taken equally spaced between 0 and 2 arbitrary units. At zero temperature, the deformation is that of the state of zero energy.

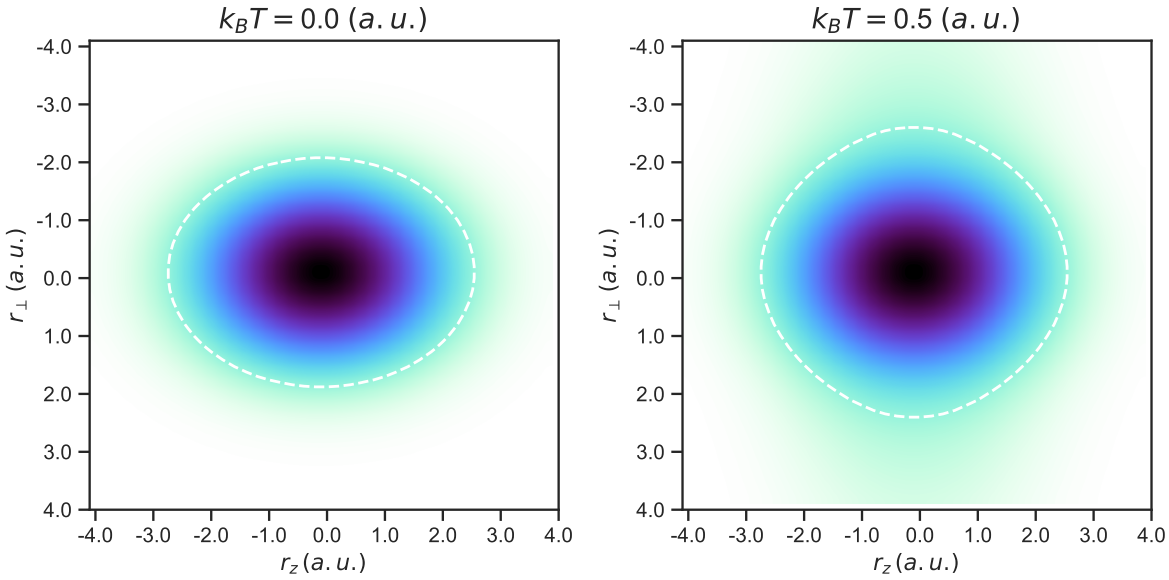

Figure 2.1: Total density at $T = 0$ and $T = 0.5$ a.u. for 100 states with randomly generated prolate ($a_z > a_\perp$) and oblate ($a_z < a_\perp$) deformations. The white dashed contours signal the region where the density reaches 20% of its maximum value and serve as a guide to the eyes. See text for details.

In particular, in large nuclei, the density of states becomes high [Bet36], due to (i) the numerous particles involved, (ii) a deeper confining potential. Within an energy window, there can thus be several states that correspond to quite different deformations due to the abounding possible combinations of quantum numbers. Consequently, even at moderate temperatures, the averaging of the density can be significant, so that we can expect the restoration of spherical symmetry to happen at lower temperature than would be the case for few-body systems. For those, the converse situation is also possible: even if the zero-temperature ground state is spherical, the small number of bound states might not be enough to effectively cause the averaging of the shape towards a spherical density.

2.5.3 Thermal configuration mixing

In the most basic mean-field theories, only the ground state of the system is considered. One should note, however, that the phase transition associated to the passage from a symmetry to another is, in such a single-reference situation, only a very crude representation of what would happen realistically. Indeed, in finite systems, fluctuations in the

order parameters can be of sizeable importance. The corresponding energy surface can be explored to a substantial extent. As a consequence, a more faithful description would involve mixing all the configurations of the surface obtained for a given temperature. Expectation values should therefore be calculated as a doubly averaged quantity: for an operator $\hat{O}$, labelling a point of the energy surface as q,

$$\langle\langle\hat{O}\rangle\rangle = \frac{\int \mathrm{d}q\, e^{-\beta F(q)} \langle\hat{O}\rangle_q}{\int \mathrm{d}q\, e^{-\beta F(q)}}, \tag{2.71}$$

the first averaging being the usual tracing operation, $\langle\hat{O}\rangle_q = \mathrm{Tr}\Big\{\hat{O}\hat{D}(q)\Big\}$, the second the averaging over all configurations at a given temperature, and F the Helmholtz free energy. The results presented in chapters 4-5 only carry out the first averaging. Because the statistical weights of the configuration are exponentially decreasing functions of the inverse temperature, this approximation should be valid only at very low temperatures. In the case of phase transitions, the sharp collapse of the order parameter should not hold any more: close below (or above) the critical temperature, a fraction of the states with significant weight may be in a state fulfilling either symmetry, so that the sharp evolution concerning only the ground state is diluted in the thermal average. In particular, it has been shown in [MER03b; MER03a] that including the thermal averaging smoothens the evolution of the average deformation and pairing a great deal, and also that the discrepancy between the single-reference and fully averaged results indeed increases with the temperature. An interesting alternative is to include the particle number fluctuation directly into the FTHFB equations [DA03; Din06], which is shown to also make the phase transition more gentle in the case of superfluidity.

2.6 Response theory

2.6.1 General aspects and points of view

Collective behaviours are an omnipresent property of strongly correlated systems. In quantum mechanics, all excitations can be represented as picking one or several particle(s) in a given set of states, and placing them back on different orbitals. The overall difference in spin is integer[34], and thus corresponds to bosonic excitations. This bosonic character can only provide an approximate representation for two reasons. First, for fermions, the Pauli principle constrains the permitted transitions, whereas a simple boson picture cannot account for it. Second, the raising and lowering of particles has consequences on the whole structure of the ensemble, since the degrees of freedom interact. Therefore, in interacting theories, the promotion of a degree of freedom from one state to another modifies the levels of all the particles; consequently, a self-consistent theory of collective modes must break this bosonic approximation. When the reference state is obtained via an approximation, e.g. within a mean-field theory, this inclusion of additional correlations

[34] Unless one has the somewhat curious idea of letting bosons transmute into fermions and vice versa, see e.g. [Pol88; Okn14].

changes the reference state, so that the ground state of the system with respect to the excitations is not the mean-field state, but a more correlated one.

The collective features of a quantum system can be studied from two different points of view:

- One may take an "external" (or extrinsic) look and send an external probe onto the system in order to excite the collective eigenmodes that are consistent with the selection rules of the ensemble {probe+system}. This standpoint is commonly formalised as the response theory. As will be shown in subsection 3.4, this view can be related to the "internal" one by extending the linear response into the complex plane and carrying on suitable contour integrations [Som83].

- Conversely, one may adopt an "internal" (or intrinsic) point of view by considering the system as truly isolated, and determine its collective states by diagonalising its full-fledged Hamiltonian, or an approximation thereof. The correspondence with the "external" viewpoint is obtained by calculating the transition probability from an eigenmode to another under the action of a selected probe [RS80, Ch.8][PN66].

The two emblematic formulations of the external and internal perspectives are, respectively, the TDMF and the RPA.

2.6.2 Linear approximation

The linear response theory goes by the assumption that excitations of more than one degree of freedom are largely sub-leading and can therefore be neglected. From the experimental side, this supposes that the probe employed to excite the system is of small enough intensity, and active for a timescale small enough to prevent non-linear effects from building up, for instance through a heating up of the system [Som83]. The validity of the linear regime can thus be experimentally assessed in two different manners:

- by scaling up the intensity I of the probe, e.g. $I \to \lambda I$, with λ some scaling factor,

- by increasing the duration for which the probe is turned on, e.g. $T \to \lambda T$,

the linear response regime resulting in the expectation values of the fluctuations of any observable to scale accordingly, i.e. $\langle \delta O \rangle \to \lambda \langle \delta O \rangle$. In real-life experiments, it is commonly assumed and verified that such non-linear effects are largely sub-leading with respect to statistical fluctuations and device-based sources of non-linear behaviours. From the theory side we can't do wonders, except going beyond the linear approximation and choosing the amplitude of F such that linear terms are dominant. To make the connection with experiment, F can be chosen to match the amplitude of an actual probe. The inclusion of non-linear type of fluctuations is usually realised within second RPA [Da 65; Yan87; GGC10; Gam+16; VGG18], a specific kind of extended RPA theories [LCA98; LCA99; Tse13; Sch+20] where up to two-phonons modes are considered.

While the characteristics of the probe plays a crucial role in the validity of the linear approximation, the initial state of the system is naturally of considerable importance.

If the system is not in a local state of equilibrium, then an arbitrarily small probe can drive it away from its initial state towards a more stable one with an a priori very different structure. Such an instability mathematically translates into a non-semi positive definite Hessian (often called the stability matrix), and therefore into complex eigenvalues. It follows that detecting non-real collective eigenvalues invalidates the linear regime. Two techniques for determining the presence of such instabilities within the formalism developed in this work will be given in subsection 3.8.

2.6.3 Formalisms survey

Given an initial state, collective motion on top of it can be addressed by a plethora of techniques. Non-exhaustively, the equations describing small amplitude fluctuations can be obtained by the following approaches:

- by the equation of motion method on double commutators [Row68; Yan87; Sch+20] [RS80, Sec. 8.4],
- by the Dyson equation and similar methods [Dys49; Nam50; LS50; Sch51; SB51; HM52],
- by diagrammatic techniques [GB57],
- as a linearisation of the time-dependent equations of motion [Noz64, Ch. 2] [RS80, Sec. 8.5] [Som83] or Liouville-von Neumann equations,
- as the small amplitude limit of the full-fledged generator coordinate method (GCM) [JS64; BW68].

Note that these techniques can be used to go beyond the linear approximation, a priori without encountering any critical dead-end, although at the cost of severe complexifications of the formalisms.

Rowe's equation of motion approach re-formulates quantal eigenvalue equations in terms of expectation values identities involving sets of commutators. While they can be derived in a strictly exact manner, the evaluation of the commutators usually requires that approximations be done. For the (Q)RPA, one has to assume the correlated ground state $|\text{(Q)RPA}\rangle$ can be replaced by the mean-field one, $|\text{HF(B)}\rangle$. This amounts to the quasi-boson approximation (QBA), where the excitations are assumed to be of purely bosonic character.

The Dyson equation can be derived from several starting points, e.g. from time-dependent perturbation theory [Dys49] or from a variational principle [Sch51]. In the context of time-dependent oscillations, it can be used to determine the response function of the system, or its linear component, by keeping only the first-order expansion of the time-ordered propagator, as done in subsection 2.6.4.

Diagrammatically, the RPA resums ring-type density correlations only [SHS08; SHB13]. Ladder diagrams are not included, which corresponds to the fact that the basic RPA does

not include short-range correlations. Beyond-RPA theories, such as the self-consistent RPA [Sch+20; DU20a; DU20b] aim at including such polarisation effects by self-consistently correlating the reference state.

As for TDMF-type equations, the linear approximation is easily seen. Since the density fluctuations are expected to be small, only terms linear in the oscillating densities are retained. The generic procedure will be established in chapter 3.

The last point states that the QRPA can be obtained from the GCM. This is perhaps surprising, because the GCM is in practice established as a large amplitude collective motion method over a selected set of few collective coordinates. On the other hand, the QRPA is a small amplitude theory that does not resort to such macroscopic variables. The key to this apparent paradox lies in that the derivation of [JS64] does not specify the coordinates employed in the Hill-Wheeler-Griffith equation. One can thus take them to be a complete set of many-particle many-hole coordinates (mpmh), which reduce in the small amplitudes limit to a 1p1h (or 2qp when superfluidity is included) expansion. Conversely, one can consider a set of collective coordinates -and their canonical conjugates- sufficiently large and rich to approach the exact motion of the system. The small amplitude limit then selects the 1p1h or 2qp components of these fluctuations, leading to the QRPA. The standard implementations of the QRPA and the GCM thus go along two different directions: the first belongs to the class of approaches building up correlations in terms of mpmh excitations on top of a single reference state, whereas the second targets a resummation of the correlations through an approach where no excitations on top of the multiple reference states are considered explicitly. In this formulation as well, the QBA is performed.

A general observation is that in their simplest formulation, all of these approaches perform the QBA, be it somewhat implicitly. While this is essentially an ad-hoc approximation (although the mean-field picture strongly suggests it should be good), its successes, be it within quantum chemistry, atomic or nuclear physics, can be taken as a justification to its approximate validity. That said, the formal mapping of the fermions pairs operators to bosonic ones is a well-studied problem. The map can be expressed as a series in the boson operators, two common prescriptions being of the Belyaev-Zelevinksii [BZ62] and of the Marumori [MYT64] types. This procedure is discussed in detail in [RS80, Ch.9], [AYG81; BC92], and references therein. In passing, it can be remarked that this bosonisation approach constitutes the foundation of models of interacting bosons [AI75; AI76; AI78; AI81].

Independently of these considerations, the general formalism of the linear response theory is reviewed in the next subsection, and will serve as a basis to establish the connection between the FAM amplitudes and the eigenproperties of the system under scrutiny.

2.6.4 Elements of formalism

The solution to the Schrödinger equation (2.1) is formally given by the time-ordered exponential [FW71, Secs. 3.6, 3.8] [BR86] [Sak85, Sec 5.5] ($\hbar$ will be set equal to one past

this equation)

$$U(t,t_0) = T\exp\left\{-\frac{i}{\hbar}\int_{t_0}^{t} dt_1 F(t_1)\right\}$$
$$\sim I - \frac{i}{\hbar}\int_{t_0}^{t} dt_1 F(t_1) - \mathcal{O}\left(\frac{1}{\hbar^2}\int_{t_1}^{t} dt_1 \int_{t_0}^{t_1} dt_2 F(t_1)F(t_2)\right). \tag{2.72}$$

In this equation, t_0 corresponds to the time at which the external probe F is switched on, i.e., the evolution is free for $t < t_0$. Keeping only the first order of the expansion constitutes the linear response approximation. In that setting, the expectation value of some operator $\hat{O}$ with respect to the perturbed state is

$$\left\langle \hat{O}(t)\right\rangle = \langle \mathrm{HFB}|U^\dagger(t,t_0)O(t)U(t,t_0)|\mathrm{HFB}\rangle$$
$$\sim \langle \mathrm{HFB}|O(t)|\mathrm{HFB}\rangle + i\langle \mathrm{HFB}|\int_{t_0}^{t} d\tau [F_H(\tau), O_H(t)]|\mathrm{HFB}\rangle \tag{2.73}$$
$$= \mathrm{Tr}\{O(t)D_0\} + i\,\mathrm{Tr}\left\{\int_{t_0}^{t} d\tau [O_H(t), F_H(\tau)]D_0\right\} \equiv \left\langle \hat{O}(t)\right\rangle_0 + \left\langle \delta\hat{O}(t)\right\rangle, \tag{2.74}$$

with the correlated part $\left\langle \delta\hat{O}(t)\right\rangle$ becoming, after inserting two complete sets of unperturbed eigenstates $\{|\mu\rangle\}, \{|\nu\rangle\}$, using $D_0 = Z^{-1}\sum_\lambda e^{-\beta\mathcal{E}_\lambda}|\lambda\rangle\langle\lambda|$ and the cyclic property of the trace

$$\left\langle \delta\hat{O}(t)\right\rangle = iZ^{-1}\sum_{\mu\nu} e^{-\beta\mathcal{E}_\nu}\int_{t_0}^{t} d\tau \Big\{ \langle\nu|O(t)|\mu\rangle\ \langle\mu|F(\tau)|\nu\rangle\, e^{i\Omega_\mu^\nu(t-\tau)}$$
$$- \langle\nu|F(\tau)|\mu\rangle\ \langle\mu|O(t)|\nu\rangle\, e^{-i\Omega_\mu^\nu(t-\tau)}\Big\}, \tag{2.75}$$

with the shorthand definition $\Omega_\mu^\nu \equiv \mathcal{E}_\nu - \mathcal{E}_\mu$. If F is chosen as a one-body operator, Ω_μ^ν becomes a sum or difference of quasiparticles energies E_μ, E_ν. Moreover, when considering a one-body operator, e.g. $F(\tau) = \sum_{cd} F_{cd}(\tau)c_c^\dagger c_d$, and the density oscillations (so that $\hat{O} = \sum_{ab} O_{ab}c_b^\dagger c_a$ has no time dependence[35]), the density fluctuations are given by the convolution product

$$\delta\rho_{ab}(t) = \int_{t_0}^{t} d\tau \sum_{\gamma\delta} \mathfrak{R}^\rho_{abcd}(t-\tau)F_{cd}(\tau) \tag{2.76}$$
$$\mathfrak{R}^\rho_{abcd}(t-\tau) \equiv iZ^{-1}\sum_{\mu\nu} e^{-\beta E_\nu}\Big\{ \langle\nu|c_b^\dagger c_a|\mu\rangle\ \langle\mu|c_c^\dagger c_d|\nu\rangle\, e^{+i\Omega_\mu^\nu(t-\tau)}$$
$$- \langle\nu|c_c^\dagger c_d|\mu\rangle\ \langle\mu|c_b^\dagger c_a|\nu\rangle\, e^{-i\Omega_\mu^\nu(t-\tau)}\Big\}\theta(t-\tau), \tag{2.77}$$

[35] In the present case of densities, $O_{ab} = 1$.

with the step function $\theta(t-\tau)$ to ensure a causal response (i.e. $\mathfrak{R}(t-\tau)=0$ for $t<\tau$). The object $\mathfrak{R}$ is commonly named the response function[36]. Equation (2.76) can be handled by inserting an exponential damping prior to taking its Fourier transform. This amounts to assuming the interaction is switched off adiabatically, so that it vanishes at large times. The convolution integral is then replaced by the matrix product

$$\delta\rho(\omega) = \mathfrak{R}^{\rho}(\omega)F(\omega), \tag{2.78}$$

where

$$\mathfrak{R}^{\rho}_{abcd}(\omega) = Z^{-1}\sum_{\mu\nu} e^{-\beta E_\nu}\left(\frac{\langle\nu|c_b^\dagger c_a|\mu\rangle\ \langle\mu|c_c^\dagger c_d|\nu\rangle}{\Omega_\mu^\nu+\omega+i\gamma} - \frac{\langle\nu|c_c^\dagger c_d|\mu\rangle\ \langle\mu|c_b^\dagger c_a|\nu\rangle}{\Omega_\mu^\nu-\omega-i\gamma}\right), \tag{2.79}$$

which makes it clear that the introduction of the damping has the same effect as tilting the excitation frequency into the complex plane, i.e. $\omega\to\omega+i\gamma\equiv\omega_\gamma$. This result is essentially the Umezawa-Kamefuchi-Källén-Lehmann spectral representation [UK51; Käl52; Leh54], and can also typically be obtained from Green's functions theory (for a pedagogical introduction see [BC17] and references therein, see also [Som20] for a more practical overview). It is useful to remark that this result has been obtained in a non-perturbative way, and thus entirely encodes the linear component of the two-point (i.e. one-body) response of the system. Additionally, it shows that the response function can be determined from the knowledge of the static structure only. Finally, within the one-body sector, the only approximation results from using as a reference the mean-field state. Had we used the exact ground state instead of the HFB, (2.79) would be the exact linear, one-body response function of the system. In case superfluidity is included, one can derive an equation of the form (2.78) for each type of density, and we can write

$$\delta R(\omega) = \mathfrak{R}(\omega)F(\omega), \tag{2.80}$$

where $\delta R(\omega)$ is to be understood as the vector $(\delta\rho,\delta\kappa,\delta\bar{\kappa},\delta\bar{\rho})$. The extensions of this derivation to both $2k$-point expectation values and N^{th} order in the expansion (2.72) are given in appendix D.

As can be seen from (2.78) and (2.80), if the operator F representing the probe is real (meaning that the norm of the probe's wave function is conserved through time evolution – more precisely, a unitary evolution translates in the hermicity of the corresponding operator, which imply that it can be made to have real entries only–), then the imaginary part of the response function determines the dissipative component of the density fluctuations. In that setting, the imaginary part of the oscillating density δR is therefore the relevant quantity to characterise the resonances of the system.

[36] Attention should be paid, however, since the response function can also refer to the strength function $S(F,\omega_\gamma)$.

In particular, the transition rate $\Gamma(\omega)$ for an excitation of frequency ω writes, from second-order perturbation theory [Dir27][Sak85, Sec. 5.6]

$$\Gamma(\omega) = \frac{2\pi}{\hbar} \underbrace{Z^{-1} \sum_{\mu\nu} |\langle\nu|F|\mu\rangle|^2 e^{-\beta E_\mu} \delta(\omega - \Omega_\mu^\nu)}_{\equiv S(F,\omega)} = -\frac{2}{\hbar} \operatorname{Im} \operatorname{Tr}\{F^\dagger \delta R(\omega)\}. \tag{2.81}$$

In consistency with the introduction of the damping frequency γ, the strength function $S(F, \omega_\gamma)$ becomes

$$S(F, \omega_\gamma) = Z^{-1} \sum_{\mu\nu} e^{-\beta E_\mu} \left(\frac{|\langle\nu|F|\mu\rangle|^2}{\Omega_\mu^\nu - \omega_\gamma} + \frac{|\langle\mu|F|\nu\rangle|^2}{\Omega_\mu^\nu + \omega_\gamma} \right), \tag{2.82}$$

the imaginary part of which exhibits a Lorentzian smearing of full width at half maximum 2γ. Thus, introducing the complex frequency results in a spreading of the resonances. The relevance of using a finite value for γ will be addressed in section 3.9. The complex-valued function $S(F, \omega_\gamma)$ thus defined can be recast as the non-smeared function $S(F, \omega)$ by writing the denominators as the sum of their principal values and Dirac distributions, then using l'Hospital's rule.

It can be shown without much trouble [PN66, p. 132] that the competition between $\Gamma(\omega)$ and $\Gamma(-\omega)$ follows the principle of detailed balance

$$\frac{\Gamma(\omega)}{\Gamma(-\omega)} = e^{\beta\omega}. \tag{2.83}$$

In particular, this translates the fact that the decay rate $\Gamma(-\omega)$ must vanish when the temperature goes to zero: de-excitations are not possible since the system is assumed to be in a ground state.

Due to the probabilistic nature of the transition between states, it is also convenient to consider the probability distribution for the system to jump from a state $|\mu\rangle$ to a state $|\nu\rangle$ under the action of the operator F and be left with an energy ω. This microscopic probability writes

$$p(F, \omega, \mu, \nu) \equiv \delta(\omega - \Omega_\mu^\nu) |\langle\nu|F|\mu\rangle|^2 \frac{e^{-\beta E_\mu}}{Z}. \tag{2.84}$$

The statistical weight is included in the definition, since the states $|\mu\rangle$ implicitly depend on the temperature (and therefore, not including the weight could be confusing as somewhat concealing this fact). As an aside, it makes the definition of the moments more natural. The macroscopic probability that a transition occurs is obtained by summing over all possible initial and final states. One can then obtain the moments of this distribution as

$$m_k \equiv \int \mathrm{d}\omega \sum_{\mu\nu} \omega^k p(F,\omega,\mu,\nu) = Z^{-1} \sum_{\mu\nu} (\Omega_\mu^\nu)^k e^{-\beta E_\mu} |\langle\nu|F|\mu\rangle|^2. \tag{2.85}$$

In case of "external" point of view theories like the linear response formalism [Som83] and the FAM, only the complex strength $S(F,\omega_\gamma)$ can be calculated. The exact moments can be recovered by applying Cauchy's integral theorem to (2.82) around a contour $\mathcal{C}$ circling all the positive energy eigenmodes:

$$m_k = \frac{1}{2i\pi} \oint_{\mathcal{C}} \mathrm{d}\omega_\gamma \omega_\gamma^k S(F,\omega_\gamma). \tag{2.86}$$

This complex-energy formulation of the sum rules has been successfully applied within the context of the FAM [Hin+15] at zero temperature, and (2.86) is valid at $T \geq 0$.

The present approach to the linear response theory involves calculating the response function. Being a four-indices object, this task is often very involved. In order to connect the derivation of this section to the QRPA form of the theory, we follow [Som83], and put the linear response equation under the following form:

$$\left[\begin{pmatrix} \tilde{C} & \tilde{a} & \tilde{b} & \tilde{D} \\ \tilde{a}^\dagger & \tilde{A} & \tilde{B} & \tilde{b}^T \\ \tilde{b}^\dagger & \tilde{B}^* & \tilde{A}^* & \tilde{a}^T \\ \tilde{D}^* & \tilde{b}^* & \tilde{a}^* & \tilde{C}^* \end{pmatrix} - \omega_\gamma \begin{pmatrix} 1 & & & \\ & 1 & & \\ & & -1 & \\ & & & -1 \end{pmatrix} \right] \begin{pmatrix} \tilde{W} \\ \tilde{X} \\ \tilde{Y} \\ \tilde{Z} \end{pmatrix} = \begin{pmatrix} \tilde{F}^{11} \\ \tilde{F}^{20} \\ \tilde{F}^{02} \\ \tilde{F}'^{11} \end{pmatrix}, \tag{2.87}$$

which can be reduced to the FTQRPA when the external operator F is set to zero and the frequency of the probe ω are replaced by eigenfrequencies Ω of the isolated system. While we have in mind the prescription of [Som83] for the definition of the QRPA sub-matrices, the definition of [VM84] can also be employed. The choice of [Som83] leads to a Hermitian matrix, and thus more straightforwardly to the eigenmodes [Sch19, Ch. 7.4].

Equation (2.87) involving two qp excitations, the matrices A, B, C, D and a, b are represented by four indices tensors, where one index tags one quasi-particle state. In the linear response formulation, finding the W, X, Y, Z amplitudes (2.87) amounts to solving a four-indices equation for each operator F and excitation frequency ω. The QRPA version is not much more appealing: albeit only one equation has to be solved, it is an eigenvalue equation over the same very large configuration space. Both methods consider the matrix elements of the interaction as basic building blocks of the problem. Roughly speaking, the finite amplitude method replaces the costly handling of these matrix elements by the fields constructed from them, turning the question of determining the density response into a set of one-body problems.

As will be shown in the next section, the FAM is very close to the TDMF approach for the description of collective modes. Very quickly, TDMF techniques proceed as follows:

- pick an excitation operator $F(t)$;
- apply it to the system as a boost;
- solve the TDMF equations with sufficient accuracy;
- eventually, take the Fourier transform of $\langle F(t) \rangle$ to obtain the strength function.

One may then wonder what can be the advantages of the FAM. The FAM equations can be solved for a small (typically, ~ 100) number of frequencies for a given operator. On the opposite side, TDMF approaches follow the propagation in the time domain. Basic signal processing considerations (namely the Nyquist-Shannon theorem, or equivalently Heisenberg's uncertainty relation) tell us that the number of time values must be at least twice the largest frequency of the signal (typical responses can reach ~ 50 MeV), while the energy resolution is inversely proportional to the total propagation time. Thus, describing low-energy modes with good resolution requires substantially more time steps than higher energy ones, up to the point where typical TDHF calculations require about a thousand points or more. In the FAM, as the grid spacing in the frequency domain is at the discretion of the user, one can freely adapt the energy range of interest and the corresponding resolution. The detailed formalism of the FAM, including several technical points, is the subject of the next chapter.

Chapter 3

Finite Amplitude Method

This chapter details the formalism employed and developed during this thesis. Several formal properties of the equations are derived and discussed.

Contents

3.1 Derivation

The usual derivations of the FAM equation of motion start from either the TDHF equations [NIY07; INY09a; Sto+11; Lia+13] or from the TDHFB ones [Nik+13; Ney+20]. One can however start from the full-fledged Liouville-von Neumann equation (2.2), which reduces to TDMF in the case of a mean-field approximation. The derivation presented follows this route, thus proceeding in a different order than usual: the time-dependent equation of motion is first obtained, then reduced to the linearised mean-field approximation. Note that these derivations could also be carried out for the (quasi-)particle operators instead of the density matrix, as done in [AN11]. For convenience, let us split the matrices into their static and time-dependent components, writing $O(t) = O_0 + \delta O(t)$ (and recalling that $G(0) = H(0)$):

$$0 = \sum_k G_0^{(k,i)} D_0^{(j,k)} - D_0^{(k,i)} G_0^{(j,k)}, \tag{3.1}$$

$$\begin{aligned} i\hbar \frac{\mathrm{d}}{\mathrm{d}t} \delta D^{(i,j)}(t) = &\sum_k \left\{ G_0^{(k,i)} \delta D^{(j,k)} - \delta D^{(k,i)} G_0^{(j,k)} + \delta G^{(k,i)} D_0^{(j,k)} - D_0^{(k,i)} \delta G^{(j,k)} \right\} \\ &+ \sum_k \left\{ \delta G^{(k,i)} \delta D^{(j,k)} - \delta D^{(k,i)} \delta G^{(j,k)} \right\}. \end{aligned} \tag{3.2}$$

The first equation corresponds to the static solution, whereas the second describes time-dependent fluctuations. Since we want to study the response of the system as a function of the probe's energy, it is more convenient to take the Fourier transform of (3.2),

$$\begin{aligned} \hbar\omega \delta D^{(i,j)}(\omega) = &\sum_k \left\{ G_0^{(k,i)} \delta D^{(j,k)}(\omega) - \delta D^{(k,i)}(\omega) G_0^{(j,k)} + \delta G^{(k,i)}(\omega) D_0^{(j,k)} - D_0^{(k,i)} \delta G^{(j,k)}(\omega) \right\} \\ &+ \sum_k \left\{ \left(\delta G^{(k,i)} * \delta D^{(j,k)} \right)(\omega) - \left(\delta D^{(k,i)} * \delta G^{(j,k)} \right)(\omega) \right\}, \end{aligned} \tag{3.3}$$

where $*$ denotes the convolution product.

In the present work, we make the small amplitude approximation, that is, the hypothesis that all the fluctuations are of much smaller amplitude than the corresponding static quantities. Thus, only terms that are linear in the fluctuations are kept. In addition, owing to the mean-field approximation, only the $(1,1)$ sectors of the many-body tensors are treated. In that case, the response of the system verifies the equation

$$\hbar\omega \delta D^{(1,1)}(\omega) = \left[G_0^{(1,1)}, \delta D^{(1,1)}(\omega) \right] + \left[\delta G^{(1,1)}(\omega), D_0^{(1,1)} \right]. \tag{3.4}$$

With the specific notations introduced for the FTHFB approximation, $D_0^{(1,1)} = \mathcal{R}_0$, $G_0^{(1,1)} = \mathcal{H}_0$, $\delta D^{(1,1)} = \delta\mathcal{R}$ and $\delta G^{(1,1)} = \delta\mathcal{H} + \mathcal{F}$, leading to

$$\hbar\omega \delta\mathcal{R}(\omega) = [\mathcal{H}_0, \delta\mathcal{R}(\omega)] + [\delta\mathcal{H}(\omega) + \mathcal{F}(\omega), \mathcal{R}_0]. \tag{3.5}$$

The static matrices write in the quasiparticle basis

$$\mathcal{R}_0 = \begin{pmatrix} f & \\ & 1-\bar{f} \end{pmatrix}; \quad \mathcal{H}_0 = \begin{pmatrix} E & \\ & -\bar{E} \end{pmatrix}, \tag{3.6}$$

whereas the oscillating fields are parametrised as

$$\delta\mathcal{R}(\omega) = \begin{pmatrix} W & X \\ Y & Z \end{pmatrix}; \quad \delta\mathcal{H}(\omega) = \begin{pmatrix} H^{11} & H^{20} \\ H^{02} & H'^{11} \end{pmatrix}; \quad \mathcal{F}(\omega) = \begin{pmatrix} F^{11} & F^{20} \\ F^{02} & F'^{11} \end{pmatrix}. \tag{3.7}$$

Plugging these expressions back into (3.4) leads, after solving for $\delta\mathcal{R}$, to

$$X_{\mu\nu}(T) = -\frac{H^{20}_{\mu\nu} + F^{20}_{\mu\nu}}{E_\mu + \bar{E}_\nu - \omega_\gamma}(1 - \bar{f}_\nu - f_\mu), \tag{3.8a}$$

$$Y_{\mu\nu}(T) = -\frac{H^{02}_{\mu\nu} + F^{02}_{\mu\nu}}{\bar{E}_\mu + E_\nu + \omega_\gamma}(1 - \bar{f}_\mu - f_\nu), \tag{3.8b}$$

$$W_{\mu\nu}(T) = -\frac{H^{11}_{\mu\nu} + F^{11}_{\mu\nu}}{E_\mu - E_\nu - \omega_\gamma}(f_\nu - f_\mu), \tag{3.8c}$$

$$Z_{\mu\nu}(T) = -\frac{H'^{11}_{\mu\nu} + F'^{11}_{\mu\nu}}{\bar{E}_\mu - \bar{E}_\nu + \omega_\gamma}(\bar{f}_\nu - \bar{f}_\mu), \tag{3.8d}$$

which reduce at $T = 0$ to only two equations:

$$X_{\mu\nu} = -\frac{H^{20}_{\mu\nu} + F^{20}_{\mu\nu}}{E_\mu + \bar{E}_\nu - \omega_\gamma} \tag{3.9a}$$

$$Y_{\mu\nu} = -\frac{H^{02}_{\mu\nu} + F^{02}_{\mu\nu}}{\bar{E}_\mu + E_\nu + \omega_\gamma}. \tag{3.9b}$$

In this derivation, the coefficients f_k have been thought of as Fermi-Dirac factors coming from the finite temperature. However, as their specific expressions are not needed throughout the calculations, equations (3.8) can also be employed when the f_k stem from a different mechanism than thermal excitations. In particular, it reduces to the zero-temperature expressions within the QFAM on top of the equal-filling approximation to the HFB theory for nuclei with odd number of protons and/or neutrons [Ney+20]. Naturally, the equal-filling QFAM could also be extended to finite temperature, with this time the coefficients f_k encoding for both the Fermi-Dirac distribution and the fact that a state is blocked.

Since the QFAM equations involve first order poles on the real axis, the frequency ω must be tilted into the complex plane: $\omega \to \omega_\gamma = \omega + i\gamma$. The corresponding strength function writes as the expectation value of the response function with respect to the perturbed ground state:

$$S(F,\omega_\gamma) = \langle F^\dagger \Re F \rangle = \mathrm{Tr}\{\mathcal{F}^\dagger \delta\mathcal{R}\} = \mathrm{Tr}\Big\{F^{11\dagger}W + F^{02\dagger}Y + F^{20\dagger}X + F'^{11\dagger}Z\Big\}, \quad (3.10)$$

the imaginary part of which gives the smeared transition rate

$$\frac{\mathrm{d}B(F,\omega)}{\mathrm{d}\omega} = -\frac{1}{\pi}\,\mathrm{Im}\{\mathrm{Tr}\{\mathcal{F}^\dagger \delta\mathcal{R}\}\}. \quad (3.11)$$

The continuation of the excitation frequency into the complex plane introduces a Lorentzian smearing into the strength distribution:

$$\frac{\mathrm{d}B(F,\omega)}{\mathrm{d}\omega} = \frac{\gamma}{\pi}\sum_{\mu\nu} e^{-\beta E_\mu}\left(\frac{|\langle\nu|F|\mu\rangle|^2}{(\Omega_\mu^\nu-\omega)^2+\gamma^2} - \frac{|\langle\mu|F|\nu\rangle|^2}{(\Omega_\mu^\nu+\omega)^2+\gamma^2}\right). \quad (3.12)$$

As a consequence, the introduction of the imaginary frequency $i\gamma$ here serves two purposes: (i) it regularises the otherwise divergent expressions (3.8), and (ii) it artificially gives a width $\Gamma = 2\gamma$ to the resonances of the response function, and as such, can emulate a part of their physical width that the theory is not able to account for.

Regardless of the physical considerations in terms of symmetries, temperature, parity of the particle number, etc, the procedure to solve the FAM equation can be summarised in the diagram of figure 3.1.

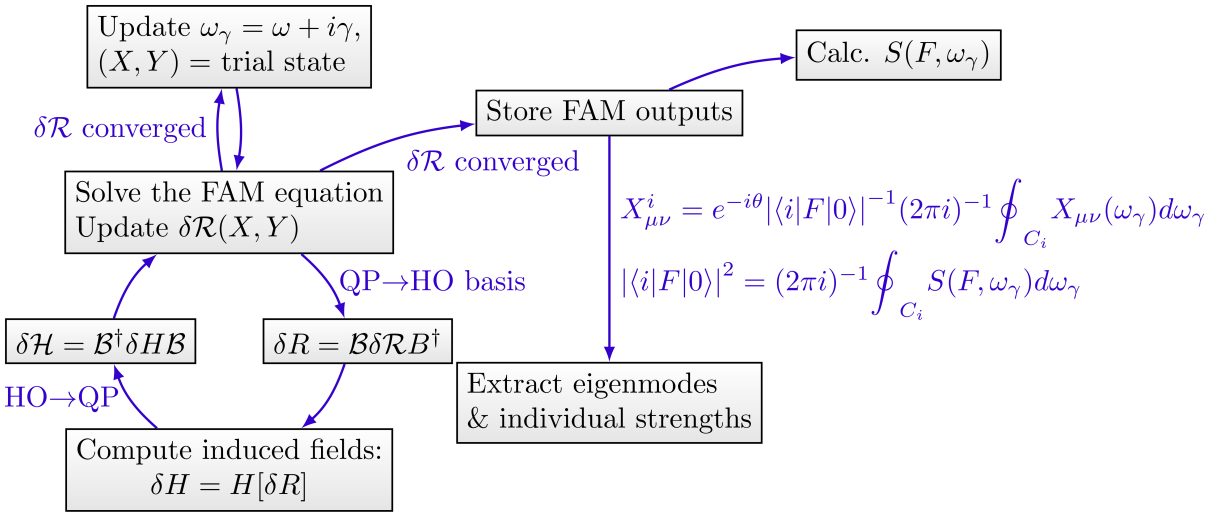

Figure 3.1: Algorithm employed for the self-consistent solution of (3.8).

The procedure goes by picking an operator F with complex frequency ω_γ, before calculating the transition fields and density self-consistently. The transformations between computational and static quasiparticle bases are easily carried out. Once convergence has been reached, the transition densities can be stored, and serve to calculate the strength function. It will be shown in subsection 3.4 that these densities can be related to the

QRPA eigenvectors. The most complicated and time-consuming bit is the calculation of the fields[1], which can only be done in the computational basis. The cornerstone of the FAM lies in the ability to calculate the linearised field $\delta\mathcal{H}$ facilely. Because the structure of the associated fields is different from that of the static Hamiltonian, an in-depth presentation is given in the next sections.

3.2 Linearisation of the fields

Formally, the transition fields are the first order derivatives of the mean-field:

$$\delta h = \lim_{\eta\to 0}(h[R+\eta\delta R] - h[R])/\eta, \tag{3.13}$$

$$\delta\Delta = \lim_{\eta\to 0}(\Delta[R+\eta\delta R] - \Delta[R])/\eta, \tag{3.14}$$

$$\delta\bar{\Delta} = \lim_{\eta\to 0}(\bar{\Delta}[R+\eta\delta R] - \bar{\Delta}[R])/\eta, \tag{3.15}$$

$$\delta\bar{h} = \lim_{\eta\to 0}(\bar{h}[R+\eta\delta R] - \bar{h}[R])/\eta. \tag{3.16}$$

Two different ways of obtaining these are discussed below.

3.2.1 Implicit linearisation

In the original formulation of the FAM [NIY07] the fields are linearised by assuming that they are at least once-differentiable functions of the density matrices in a small region about the static solution. Eventually, one can make the stronger assumption that they can be differentiated more than once, and obtain the usual finite difference formulae:

$$H[D_0 \pm \eta\delta D] \equiv H_\pm = \sum_{k=0} \frac{(\pm\eta\delta D)^k}{k!} H_0^{(k)}, \tag{3.17}$$

so that the even and odd derivatives can be zeroed out by adding or subtracting the forward and backward expansions:

$$H_+ + H_- = 2\sum_{k=0} \frac{(\eta\delta D)^{2k}}{(2k)!} H_0^{(2k)}, \tag{3.18}$$

$$H_+ - H_- = 2\sum_{k=0} \frac{(\eta\delta D)^{2k+1}}{(2k+1)!} H_0^{(2k+1)}. \tag{3.19}$$

In particular, the first order derivative writes, using (3.17),

$$\delta H = H^{(1)} = \frac{H_+ - H_0}{\eta} + \underset{\eta\to 0}{\mathcal{O}}(\eta), \tag{3.20}$$

[1] But still, at a cost comparable with that of a HFB calculation

whilst using both the backward and forward expansions (3.19) gives the more accurate

$$\delta H = H^{(1)} = \frac{H_+ - H_-}{2\eta} + \underset{\eta\to 0}{\mathcal{O}}(\eta^2). \tag{3.21}$$

In practice however, calculating H is quite demanding, so that the less accurate but twice faster first-order expression is employed in [NIY07; INY09a; Sto+11; Nik+13; Lia+13; AN11][2], while care is taken that η is chosen appropriately. Regarding the use of higher-order formulae, this not only increases the number of calculations to be realised numerically, but also rests on the assumption that the potential energy surface does not possess any discontinuity in the neighbourhood explored by using the small parameter η. The first point is only a dull matter of computational efficiency. The second, however, is critical from a physical perspective, where discontinuities may very well happen, e.g. in the case of phase transitions. All in all, sticking to a first-order, two points forward (3.20) or centred (3.21) scheme seems to be the soundest choice.

This explicit finite-difference scheme, while relatively simple, suffers from the fact that the small expansion parameter η cannot be estimated a priori, so that practical calculations must always resort to an ad-hoc value for it. The finite-difference technique has been shown to be stable over about three orders of magnitude (typically $\eta \sim 10^{-5}$ to 10^{-8}), regardless of the fact that η is fixed [Sto+11; AN11; Lia+13] or adjusted with respect to the entries of the density fluctuations matrix in the quasi-particle basis [NIY07; INY09a]. However, this introduces an additional parameter to be adjusted. This drawback can be circumvented by the explicit linearisation.

3.2.2 Explicit linearisation

An appealing alternative is to explicitly linearise the fields with respect to first-order fluctuations of the density [KHN15; OKH16; SL17]. All non-linear terms are then fully omitted. This procedure is particularly suited for ab initio theories, where we enjoy the fact that the fields write as polynomials of the normal and anomalous densities[3]. A field h (normal or pairing) produced by anti-symmetrised many-body interactions can be written, with full generality and sloppiness,

$$h = \sum_{k=1} v^{(k)}(\underbrace{\rho\dots\rho}_{q \text{ times}}\underbrace{\kappa\dots\kappa}_{q' \text{ times}}), \quad q + q' = k - 1, \tag{3.22}$$

so that its derivatives with respect to the densities are easy to calculate:

[2]It is to be noted that this article does not solve the FAM equations, but rather uses the FAM to construct the QRPA matrix.

[3]The application of the method to energy density functionals involving non-integer powers of the densities (and more generally, to any kind of functional) poses no formal problem, although it requires a more attentive handling of the linearised fields in practical implementations.

$$\begin{aligned}\delta h &\sim \sum_{k=1} v^{(k)} \delta(\underbrace{\rho \dots \rho}_{q \text{ times}} \underbrace{\kappa \dots \kappa}_{q' \text{ times}}) = \sum_{k=1} v^{(k)} (q \rho^{q-1} \kappa^{q'} \delta\rho + q' \rho^{q} \kappa^{q'-1} \delta\kappa) \\ &\equiv \sum_{k=1} \tilde{v}^{(k)}_{\rho} \delta\rho + \tilde{v}^{(k)}_{\kappa} \delta\kappa, \end{aligned} \tag{3.23}$$

where the first equality comes from the (anti-)symmetry of the interaction vertices with respect to swapping the particles.

Therefore, no matter how complicated the interaction, the fluctuation δh can always be calculated as coming from a collection of two-body effective interactions, after all the contractions with respect to the static densities have been performed. Absorbing the constant factor falling when differentiating the fields, one can further group the effective vertices together, so that any k-body interaction can be represented exactly by either one or three effective interactions, once the pre-contractions have been carried out.

With these considerations and the symmetries of the static densities (2.53)(2.54), one can write down the expressions for the linearised fields arising from a three-body Hamiltonian:

$$\delta h_{\alpha\beta} = \sum_{\gamma\delta} v^{(a)\rho\rho}_{\alpha\gamma\beta\delta} \delta\rho_{\delta\gamma} + \sum_{\gamma\delta\epsilon\zeta} w^{(a)\rho\rho\rho}_{\alpha\gamma\epsilon\beta\delta\zeta} \rho_{\zeta\epsilon} \delta\rho_{\delta\gamma} + \frac{1}{4} \sum_{\gamma\delta\epsilon\zeta} w^{(a)\rho\kappa\kappa}_{\alpha\gamma\epsilon\beta\delta\zeta} (\bar{\kappa}_{\epsilon\gamma} \delta\kappa_{\delta\zeta} + \kappa_{\delta\zeta} \delta\bar{\kappa}_{\epsilon\gamma}), \tag{3.24}$$

$$\delta \Delta_{\alpha\gamma} = \frac{1}{2} \sum_{\beta\delta} v^{(a)\kappa\kappa}_{\alpha\gamma\beta\delta} \delta\kappa_{\beta\bar{\delta}} + \frac{1}{2} \sum_{\beta\delta\epsilon\zeta} w^{(a)\rho\kappa\kappa}_{\alpha\gamma\epsilon\beta\delta\zeta} (\rho_{\zeta\epsilon} \delta\kappa_{\beta\delta} + \delta\rho_{\zeta\epsilon} \kappa_{\beta\delta}), \tag{3.25}$$

$$\delta \bar{\Delta}_{\alpha\gamma} = \frac{1}{2} \sum_{\beta\delta} v^{(a)\kappa\kappa}_{\alpha\gamma\beta\delta} \delta\bar{\kappa}_{\beta\bar{\delta}} + \frac{1}{2} \sum_{\beta\delta\epsilon\zeta} w^{(a)\rho\kappa\kappa}_{\alpha\gamma\epsilon\beta\delta\zeta} (\rho_{\zeta\epsilon} \delta\bar{\kappa}_{\beta\delta} + \delta\rho_{\zeta\epsilon} \bar{\kappa}_{\beta\delta}), \tag{3.26}$$

$$\delta \bar{h}_{\alpha\beta} = \sum_{\gamma\delta} v^{(a)\rho\rho}_{\alpha\gamma\beta\delta} \delta\bar{\rho}_{\delta\gamma} + \sum_{\gamma\delta\epsilon\zeta} w^{(a)\rho\rho\rho}_{\alpha\gamma\epsilon\beta\delta\zeta} \bar{\rho}_{\zeta\epsilon} \delta\bar{\rho}_{\delta\gamma} + \frac{1}{4} \sum_{\gamma\delta\epsilon\zeta} w^{(a)\rho\kappa\kappa}_{\alpha\gamma\epsilon\beta\delta\zeta} (\bar{\kappa}_{\epsilon\gamma} \delta\kappa_{\delta\zeta} + \kappa_{\delta\zeta} \delta\bar{\kappa}_{\epsilon\gamma}). \tag{3.27}$$

These expressions can be recast in a way that makes apparent the possibility to carry out the FAM as a problem involving only two-body effective interactions:

$$\begin{aligned}\delta h_{\alpha\beta} = &\sum_{\gamma\delta} \left(v^{(a)\rho\rho}_{\alpha\gamma\beta\delta} + \sum_{\epsilon\zeta} w^{(a)\rho\rho\rho}_{\alpha\gamma\epsilon\beta\delta\zeta} \rho_{\zeta\epsilon} \right) \delta\rho_{\delta\gamma} \\ &+ \frac{1}{4} \sum_{\delta\zeta} \left(\sum_{\gamma\epsilon} w^{(a)\rho\kappa\kappa}_{\alpha\gamma\epsilon\beta\delta\zeta} \bar{\kappa}_{\epsilon\gamma} \right) \delta\kappa_{\delta\zeta} + \frac{1}{4} \sum_{\gamma\epsilon} \left(\sum_{\delta\zeta} w^{(a)\rho\kappa\kappa}_{\alpha\gamma\epsilon\beta\delta\zeta} \kappa_{\delta\zeta} \right) \delta\bar{\kappa}_{\epsilon\gamma}, \end{aligned} \tag{3.28}$$

$$\delta \Delta_{\alpha\gamma} = \frac{1}{2} \sum_{\beta\delta} v^{(a)\kappa\kappa}_{\alpha\gamma\beta\delta} \delta\kappa_{\beta\bar{\delta}} + \frac{1}{2} \sum_{\beta\delta} \left(\sum_{\epsilon\zeta} w^{(a)\rho\kappa\kappa}_{\alpha\gamma\epsilon\beta\delta\zeta} \rho_{\zeta\epsilon} \right) \delta\kappa_{\beta\delta} + \frac{1}{2} \sum_{\beta\delta} \left(\sum_{\epsilon\zeta} w^{(a)\rho\kappa\kappa}_{\alpha\gamma\epsilon\beta\delta\zeta} \kappa_{\beta\delta} \right) \delta\rho_{\zeta\epsilon}, \tag{3.29}$$

$$\delta\bar{\Delta}_{\alpha\gamma} = \frac{1}{2}\sum_{\beta\delta} v^{(a)\kappa\kappa}_{\alpha\gamma\beta\delta}\delta\bar{\kappa}_{\beta\bar{\delta}} + \frac{1}{2}\sum_{\beta\delta}\left(\sum_{\epsilon\zeta} w^{(a)\rho\kappa\kappa}_{\alpha\gamma\epsilon\beta\delta\zeta}\rho_{\zeta\epsilon}\right)\delta\bar{\kappa}_{\beta\delta} + \frac{1}{2}\sum_{\epsilon\zeta}\left(\sum_{\beta\delta} w^{(a)\rho\kappa\kappa}_{\alpha\gamma\epsilon\beta\delta\zeta}\bar{\kappa}_{\beta\delta}\right)\delta\rho_{\zeta\epsilon}, \tag{3.30}$$

$$\begin{aligned}\delta\bar{h}_{\alpha\beta} = &\sum_{\gamma\delta}\left(v^{(a)\rho\rho}_{\alpha\gamma\beta\delta} + \sum_{\epsilon\zeta} w^{(a)\rho\rho\rho}_{\alpha\gamma\epsilon\beta\delta\zeta}\bar{\rho}_{\zeta\epsilon}\right)\delta\bar{\rho}_{\delta\gamma} \\ &+ \frac{1}{4}\sum_{\delta\zeta}\left(\sum_{\gamma\epsilon} w^{(a)\rho\kappa\kappa}_{\alpha\gamma\epsilon\beta\delta\zeta}\bar{\kappa}_{\epsilon\gamma}\right)\delta\kappa_{\delta\zeta} + \frac{1}{4}\sum_{\gamma\epsilon}\left(\sum_{\delta\zeta} w^{(a)\rho\kappa\kappa}_{\alpha\gamma\epsilon\beta\delta\zeta}\kappa_{\delta\zeta}\right)\delta\bar{\kappa}_{\epsilon\gamma}.\end{aligned} \tag{3.31}$$

Due to the small amplitude limit, the fields can now be evaluated directly from the transition densities after carrying out their explicit linearisation, so that we can write $\delta H = H[\delta R]$ as in the static case.

3.3 Symmetries of the QFAM and HFB equations

As mentioned in section 2.4.2, the symmetries of the HFB equations depend on the chosen parametrisation for the Bogoliubov matrix. Some of them directly stem from the fact that the Hamiltonian is Hermitian. In the FAM, this symmetry is no longer present due to the analytic continuation of the transition amplitudes. This section recapitulates the symmetries of the HFB operators, and present the remaining symmetries of the FAM objects. For completeness, the equations are given in both the Russian and the traditional representations. The useful notations and symmetries are given as:

Traditional

$$\mathcal{B} = \begin{pmatrix} U & V^* \\ V & U^* \end{pmatrix}, \tag{3.32}$$

$$R = \begin{pmatrix} \rho & +\kappa \\ -\bar{\kappa} & I-\bar{\rho} \end{pmatrix}, \tag{3.33}$$

$$H = \begin{pmatrix} h & +\Delta \\ -\bar{\Delta} & -\bar{h} \end{pmatrix}, \tag{3.34}$$

Russian

$$\mathcal{B} = \begin{pmatrix} U & -V \\ V & U \end{pmatrix}, \tag{3.35}$$

$$R = \begin{pmatrix} \rho & \tilde{\rho} \\ \bar{\tilde{\rho}} & I-\bar{\rho} \end{pmatrix}, \tag{3.36}$$

$$H = \begin{pmatrix} h & \tilde{h} \\ \bar{\tilde{h}} & -\bar{h} \end{pmatrix}, \tag{3.37}$$

$$\rho(\beta) = UfU^\dagger + V^*(I-\bar{f})V^T, \tag{3.38a}$$
$$\kappa(\beta) = UfV^\dagger + V^*(I-\bar{f})U^T, \tag{3.38b}$$
$$-\bar{\kappa}(\beta) = VfU^\dagger + U^*(I-\bar{f})V^T, \tag{3.38c}$$
$$I-\bar{\rho}(\beta) = VfV^\dagger + U^*(I-\bar{f})U^T, \tag{3.38d}$$

$$\rho(\beta) = UfU^\dagger + V(I-\bar{f})V^\dagger, \tag{3.39a}$$
$$\tilde{\rho}(\beta) = UfV^\dagger - V(I-\bar{f})U^\dagger, \tag{3.39b}$$
$$\bar{\tilde{\rho}}(\beta) = VfU^\dagger - U(I-\bar{f})V^\dagger, \tag{3.39c}$$
$$I-\bar{\rho}(\beta) = VfV^\dagger + U(I-\bar{f})U^\dagger. \tag{3.39d}$$

The anti-commutation relations imply the skew-symmetry of both pairing tensors in both representations:

$$\kappa = -\kappa^T \tag{3.40a}$$
$$\bar{\kappa} = -\bar{\kappa}^T \tag{3.40b}$$

$$\tilde{\rho} = -\tilde{\rho}^T \tag{3.41a}$$
$$\bar{\tilde{\rho}} = -\bar{\tilde{\rho}}^T, \tag{3.41b}$$

while the unitarity of the Bogoliubov transformation along with $f = \bar{f}$ yield

$$\bar{\rho} = \rho^* = \rho^T \tag{3.42a}$$
$$\bar{\kappa} = \kappa \tag{3.42b}$$

$$\bar{\rho} = \rho = \rho^\dagger \tag{3.43a}$$
$$\bar{\tilde{\rho}} = \tilde{\rho}^\dagger \tag{3.43b}$$

At the FAM level, one has the following expressions:

$$\delta R = \begin{pmatrix} \delta\rho & \delta\kappa \\ -\delta\bar{\kappa} & -\delta\bar{\rho} \end{pmatrix} \text{ with } \begin{cases} \delta\rho = UWU^\dagger + V^*YU^\dagger + UXV^T + V^*ZV^T & (3.44a) \\ \delta\kappa = UWV^\dagger + V^*YV^\dagger + UXU^T + V^*ZU^T & (3.44b) \\ -\delta\bar{\kappa} = VWU^\dagger + U^*YU^\dagger + VXV^T + U^*ZV^T & (3.44c) \\ -\delta\bar{\rho} = VWV^\dagger + U^*YV^\dagger + VXU^T + U^*ZU^T & (3.44d) \end{cases}$$

$$\delta\mathcal{H} = \begin{pmatrix} H^{11} & H^{20} \\ H^{02} & H'^{11} \end{pmatrix} \text{ with } \begin{cases} H^{11} = +U^\dagger\delta hU - V^\dagger\delta\bar{\Delta}U + U^\dagger\delta\Delta V - V^\dagger\delta\bar{h}V & (3.45a) \\ H^{20} = +U^\dagger\delta hV^* - V^\dagger\delta\bar{\Delta}V^* + U^\dagger\delta\Delta U^* - V^\dagger\delta\bar{h}U^* & (3.45b) \\ H^{02} = +V^T\delta hU - U^T\delta\bar{\Delta}U + V^T\delta\Delta V - U^T\delta\bar{h}V & (3.45c) \\ H'^{11} = +V^T\delta hV^* - U^T\delta\bar{\Delta}V^* + V^T\delta\Delta U^* - U^T\delta\bar{h}U^* & (3.45d) \end{cases}$$

$$\delta R = \begin{pmatrix} \delta\rho & -\delta\kappa \\ -\delta\bar{\kappa} & -\delta\bar{\rho} \end{pmatrix} \text{ with } \begin{cases} \delta\rho = UWU^\dagger - VYU^\dagger - UXV^\dagger + VZV^\dagger & (3.46a) \\ \delta\tilde{\rho} = UWV^\dagger - VYV^\dagger + UXU^\dagger - VZU^\dagger & (3.46b) \\ \delta\bar{\tilde{\rho}} = VWU^\dagger + UYU^\dagger + VXV^\dagger - UZV^\dagger & (3.46c) \\ -\delta\bar{\rho} = VWV^\dagger + UYV^\dagger + VXU^\dagger + UZU^\dagger & (3.46d) \end{cases}$$

$$\delta\mathcal{H} = \begin{pmatrix} H^{11} & H^{20} \\ H^{02} & H'^{11} \end{pmatrix} \text{ with } \begin{cases} H^{11} = +U^\dagger\delta hU + V^\dagger\delta\bar{\tilde{h}}U + U^\dagger\delta\tilde{h}V - V^\dagger\delta\bar{h}V & (3.47a) \\ H^{20} = -U^\dagger\delta hV - V^\dagger\delta\bar{\tilde{h}}V + U^\dagger\delta\tilde{h}U - V^\dagger\delta\bar{h}U & (3.47b) \\ H^{02} = -V^\dagger\delta hU + U^\dagger\delta\bar{\tilde{h}}U - V^\dagger\delta\tilde{h}V - U^\dagger\delta\bar{h}V & (3.47c) \\ H'^{11} = +V^\dagger\delta hV - U^\dagger\delta\bar{\tilde{h}}V - V^\dagger\delta\tilde{h}U - U^\dagger\delta\bar{h}U. & (3.47d) \end{cases}$$

3.3.1 Density matrices

We'd like to identify under which conditions the QFAM equations are invariant under time-reversal symmetry: if both the ground state and the external operator are, we expect that the symmetry is preserved by the QFAM. In particular, the RPA does preserve the symmetry for even-even nuclei and a perturbation $F(t) = F(-t)$, hence the QFAM should also under the same conditions.

Symmetries of $\delta\rho$

In both the Russian and the traditional convention, the ground state normal density is real, hence (3.42a)-(3.43a) can be grouped as $\bar{\rho} = \rho = \rho^* = \rho^T$. As for $\delta\rho$, the imaginary part makes it impossible to verify all of these relations simultaneously; the correct one must be identified with the help of (3.44) and (3.46). In both representations, the HFB Hamiltonian is Hermitian, thus the eigenvectors $\{(U, V)\}$ can be made real [4], whereas the complex frequency $\omega_\gamma = \omega + i\gamma$ implies the following:

- $X \neq X^\dagger; X \neq X^*$
- $Y \neq Y^\dagger; Y \neq Y^*$.

The only possibilities left are $X \propto X^T$ and $Y \propto Y^T$, which tell us that the relation

$$\delta\rho = \delta\bar{\rho}^T \tag{3.48}$$

is the only correct one when complex matrices are involved. From there, we deduce:

$$X = -X^T, \tag{3.49a}$$
$$Y = -Y^T, \tag{3.49b}$$

$$X = X^T, \tag{3.50a}$$
$$Y = Y^T. \tag{3.50b}$$

As for W and Z, inspecting (3.46a)-(3.46d) and (3.44a)-(3.44d) tells us that W should be related to Z. With the help of (3.48), we get to the same relation in both conventions:

$$W = -Z^T. \tag{3.51}$$

Symmetries of $\delta\kappa$ and $\delta\bar{\kappa}$

The symmetries of the pairing tensors still holds at the QFAM level: from (3.46b)-(3.46c) & (3.44b)-(3.44c) and the symmetries of U, V, X, Y, W, Z, one obtains that

$$\delta\kappa = -\delta\kappa^T, \tag{3.52a}$$
$$\delta\bar{\kappa} = -\delta\bar{\kappa}^T, \tag{3.52b}$$

$$\delta\kappa = +\delta\kappa^T, \tag{3.53a}$$
$$\delta\bar{\kappa} = +\delta\bar{\kappa}^T. \tag{3.53b}$$

The static pairing tensors being related through (3.40a) or (3.41a), we may expect similar relations to hold in the dynamic case. Since the U, V matrices can be made real, the Hermitian conjugation can be replaced by a transpose. Yet, having an explicit link between $\delta\kappa$ and $\delta\bar{\kappa}$ as for the static case would require that X and Y are related, which is not possible since X has poles on $\mathbb{R}^+$ while those of Y lie on $\mathbb{R}^-$. Even in the case $X = Y = 0$, one can quickly show using (3.44)-(3.46) that no connection can be established between $\delta\kappa$ and $\delta\bar{\kappa}$, for it would be incompatible with the relation (3.51).

[4] Note that this requirement is not necessary in the traditional representation (transpositions and conjugations balance each other out nicely), while it is mandatory in the mixed one in order to carry on the present derivations

3.3.2 Dynamical fields

In order that the amplitudes verify their symmetry relations, one must have, from their expressions (3.8):

Traditional

- $H^{11} + F^{11} = -(H'^{11} + F'^{11})^T$
- $H^{20} + F^{20} = -(H^{20} + F^{20})^T$
- $H^{02} + F^{02} = -(H^{02} + F^{02})^T$

Russian

- $H^{11} + F^{11} = -(H'^{11} + F'^{11})^T$
- $H^{20} + F^{20} = (H^{20} + F^{20})^T$
- $H^{02} + F^{02} = (H^{02} + F^{02})^T$.

External perturbation

At the very first iteration, $\delta H = 0$, so that the structure of the FAM amplitudes is entirely determined by that of F. The conditions thus translate into a set of symmetries that the external operator $\mathcal{F}$ must fulfil. The symmetries of the response $\delta\mathcal{H}$ will be checked in a second step. Writing the perturbation in the doubled single-particle basis via $\mathcal{F} = \mathcal{B}^\dagger F \mathcal{B}$ leads to

$$F^{11} = U^\dagger f^{11} U + V^\dagger f^{02} U + U^\dagger f^{20} V + V^\dagger f'^{11} V, \tag{3.54a}$$
$$F^{20} = U^\dagger f^{11} V^* + V^\dagger f^{02} V^* + U^\dagger f^{20} U^* + V^\dagger f'^{11} U^*, \tag{3.54b}$$
$$F^{02} = V^T f^{11} U + U^T f^{02} U + V^T f^{20} V + U^T f'^{11} V, \tag{3.54c}$$
$$F'^{11} = V^T f^{11} V^* + U^T f^{02} V^* + V^T f^{20} U^* + U^T f'^{11} U^*, \tag{3.54d}$$

$$F^{11} = U^\dagger f^{11} U + V^\dagger f^{02} U + U^\dagger f^{20} V + V^\dagger f'^{11} V, \tag{3.55a}$$
$$F^{20} = -U^\dagger f^{11} V - V^\dagger f^{02} V + U^\dagger f^{20} U + V^\dagger f'^{11} U, \tag{3.55b}$$
$$F^{02} = -V^\dagger f^{11} U + U^\dagger f^{02} U - V^\dagger f^{20} V + U^\dagger f'^{11} V, \tag{3.55c}$$
$$F'^{11} = V^\dagger f^{11} V - U^\dagger f^{02} V - V^\dagger f^{20} U + U^\dagger f'^{11} U. \tag{3.55d}$$

Requiring consistency with the constraints derived from (3.8) results in

$$f^{11} = -(f'^{11})^T, \tag{3.56}$$

$$f^{20} = -(f^{20})^T, \tag{3.57a}$$
$$f^{02} = -(f^{02})^T, \tag{3.57b}$$

$$f^{20} = (f^{20})^T, \tag{3.58a}$$
$$f^{02} = (f^{02})^T. \tag{3.58b}$$

Internal fields

By the very same procedure, inspecting (3.45) and (3.47) lead to the following conditions:

Traditional	Russian
• $\delta h = \delta\bar{h}^T$	• $\delta h = \delta\bar{h}^T$
• $\delta\Delta = -\delta\Delta^T$	• $\delta\tilde{h} = \delta\tilde{h}^T$
• $\delta\bar{\Delta} = -\delta\bar{\Delta}^T$	• $\delta\bar{\tilde{h}} = \delta\bar{\tilde{h}}^T$

The fulfilment of these constraints is verified in detail in the following page for the traditional convention. In case of the Russian convention, these requirements can only be met at the two-body level, as an undesired consequence of the static pairing tensors being skew-symmetric ((3.41)) whereas the time-dependent are symmetric ((3.53))[5]. The normal and anomalous fields are thus inspected in the traditional representation only. They rely on the fact that the two- and three-body interactions are invariant under time-reversal ($\mathcal{T}$), symmetric under swapping the labels of two particles $i\,\&\,j$ ($\mathcal{S}(i,j)$), and antisymmetric under particle exchange. Renaming of the dummy indices will be shown as well.

Normal fields

The three sums contributing to

$$\delta h_{\alpha\beta} = \delta h^{(2)}_{\alpha\beta} + \delta h^{(3)\rho}_{\alpha\beta} + \delta h^{(3)\kappa}_{\alpha\beta} \tag{3.59}$$

write

$$\begin{aligned}
\delta h^{(2)}_{\alpha\beta} &= \sum_{\gamma\delta} v^{(a)\rho\rho}_{\alpha\gamma\beta\delta}\delta\rho_{\delta\gamma} \overset{\mathcal{T}}{=} \sum_{\gamma\delta} v^{(a)\rho\rho}_{\bar{\delta}\bar{\beta}\bar{\gamma}\bar{\alpha}}\delta\rho_{\delta\gamma} \overset{\mathcal{S}(1,2)}{=} \sum_{\gamma\delta} v^{(a)\rho\rho}_{\bar{\beta}\bar{\delta}\bar{\alpha}\bar{\gamma}}\delta\rho_{\delta\gamma} \\
&\overset{(3.48)}{=} \sum_{\gamma\delta} v^{(a)\rho\rho}_{\bar{\beta}\bar{\delta}\bar{\alpha}\bar{\gamma}}\delta\bar{\rho}_{\bar{\gamma}\bar{\delta}} \overset{\gamma\leftrightarrow\delta}{=} \sum_{\gamma\delta} v^{(a)\rho\rho}_{\bar{\beta}\bar{\gamma}\bar{\alpha}\bar{\delta}}\delta\bar{\rho}_{\bar{\delta}\bar{\gamma}} = \delta\bar{h}^{(2)}_{\bar{\beta}\bar{\alpha}},
\end{aligned} \tag{3.60a}$$

$$\begin{aligned}
\delta h^{(3)\rho}_{\alpha\beta} &= \sum_{\gamma\delta\epsilon\zeta} w^{(a)\rho\rho\rho}_{\alpha\gamma\epsilon\beta\delta\zeta}\rho_{\zeta\epsilon}\delta\rho_{\delta\gamma} \overset{\mathcal{T}}{=} \sum_{\gamma\delta\epsilon\zeta} w^{(a)\rho\rho\rho}_{\bar{\zeta}\bar{\delta}\bar{\beta}\bar{\epsilon}\bar{\gamma}\bar{\alpha}}\rho_{\zeta\epsilon}\delta\rho_{\delta\gamma} \overset{\mathcal{S}(1,3)}{=} \sum_{\gamma\delta\epsilon\zeta} w^{(a)\rho\rho\rho}_{\bar{\beta}\bar{\delta}\bar{\zeta}\bar{\alpha}\bar{\gamma}\bar{\epsilon}}\rho_{\zeta\epsilon}\delta\rho_{\delta\gamma} \\
&\overset{(3.48)}{=} \sum_{\gamma\delta\epsilon\zeta} w^{(a)\rho\rho\rho}_{\bar{\beta}\bar{\delta}\bar{\zeta}\bar{\alpha}\bar{\gamma}\bar{\epsilon}}\bar{\rho}_{\bar{\epsilon}\bar{\zeta}}\delta\bar{\rho}_{\bar{\gamma}\bar{\delta}} \overset{\substack{\gamma\leftrightarrow\delta\\ \epsilon\leftrightarrow\zeta}}{=} \sum_{\gamma\delta\epsilon\zeta} w^{(a)\rho\rho\rho}_{\bar{\beta}\bar{\gamma}\bar{\epsilon}\bar{\alpha}\bar{\delta}\bar{\zeta}}\bar{\rho}_{\bar{\zeta}\bar{\epsilon}}\delta\bar{\rho}_{\bar{\delta}\bar{\gamma}} = \delta\bar{h}^{(3)\rho}_{\bar{\beta}\bar{\alpha}},
\end{aligned} \tag{3.60b}$$

$$\delta h^{(3)\kappa}_{\alpha\beta} = \sum_{\gamma\delta\epsilon\zeta} w^{(a)\rho\kappa\kappa}_{\alpha\gamma\epsilon\beta\delta\zeta}(\kappa_{\delta\zeta}\delta\bar{\kappa}_{\epsilon\gamma} + \delta\kappa_{\delta\zeta}\bar{\kappa}_{\epsilon\gamma}) \overset{\mathcal{T}}{=} \sum_{\gamma\delta\epsilon\zeta} w^{(a)\rho\kappa\kappa}_{\bar{\zeta}\bar{\delta}\bar{\beta}\bar{\epsilon}\bar{\gamma}\bar{\alpha}}(\kappa_{\delta\zeta}\delta\bar{\kappa}_{\epsilon\gamma} + \delta\kappa_{\delta\zeta}\bar{\kappa}_{\epsilon\gamma})$$

[5] One can however remark that the components of the pairing tensor being typically much smaller (say of order 1) than those of the normal density (which are, say, of order 0), these contributions with incorrect properties should be of order 3 for the normal field (versus 1 for the two-body component and 2 for the $\delta\rho$-dependent three-body), and of order 2 for the anomalous fields. The symmetry-breaking contribution thus comes at next to leading order, so to speak.

$$\overset{\mathcal{S}(1,3)}{=} \sum_{\gamma\delta\epsilon\zeta} w^{(a)\rho\kappa\kappa}_{\bar{\beta}\bar{\delta}\bar{\zeta}\bar{\alpha}\bar{\gamma}\bar{\epsilon}} (\kappa_{\delta\zeta}\delta\bar{\kappa}_{\epsilon\gamma} + \delta\kappa_{\delta\zeta}\bar{\kappa}_{\epsilon\gamma}) \overset{\substack{\gamma\leftrightarrow\delta \\ \epsilon\leftrightarrow\zeta}}{=} \sum_{\gamma\delta\epsilon\zeta} w^{(a)\rho\kappa\kappa}_{\bar{\beta}\bar{\gamma}\bar{\epsilon}\bar{\alpha}\bar{\delta}\bar{\zeta}} (\kappa_{\gamma\epsilon}\delta\bar{\kappa}_{\zeta\delta} + \delta\bar{\kappa}_{\gamma\epsilon}\kappa_{\zeta\delta})$$
$$\overset{\substack{(3.40) \\ (3.52)}}{=} \sum_{\gamma\delta\epsilon\zeta} w^{(a)\rho\kappa\kappa}_{\bar{\beta}\bar{\gamma}\bar{\epsilon}\bar{\alpha}\bar{\delta}\bar{\zeta}} (\kappa_{\epsilon\gamma}\delta\bar{\kappa}_{\delta\zeta} + \delta\bar{\kappa}_{\epsilon\gamma}\kappa_{\delta\zeta}) = \delta\bar{h}^{(3)\kappa}_{\bar{\beta}\bar{\alpha}}. \tag{3.60c}$$

This shows the desired symmetry property of the normal fields, namely $\delta h = \delta\bar{h}^T$.

Anomalous fields

In the anomalous contractions, the indices associated to ρ matrices can be made to run only over the time-normal sector, due to the relation $\bar{\rho} = \rho^T$. More generally, the bars can be dropped if one keeps in mind that their position should be consistent with the indices of the interaction matrix elements and the definitions (2.27)(2.28) of the elementary contractions. In particular, note that one can only swap particles in the interaction matrix elements, but non-dummy indices cannot be exchanged if they correspond to particles propagating in opposite time directions[6]. With these lightweight notations, one has:

$$\delta\Delta_{\alpha\gamma} = \delta\Delta^{(2)}_{\alpha\gamma} + \delta\Delta^{(3)\rho}_{\alpha\gamma} + \delta\Delta^{(3)\kappa}_{\alpha\gamma}, \tag{3.61}$$

with

$$\delta\Delta^{(2)}_{\alpha\gamma} = \frac{1}{2}\sum_{\beta\delta} v^{(a)\kappa\kappa}_{\alpha\gamma\beta\delta}\delta\kappa_{\beta\delta} \overset{\mathcal{S}(1,2)}{=} \frac{1}{2}\sum_{\beta\delta} v^{(a)\kappa\kappa}_{\gamma\alpha\delta\beta}\delta\kappa_{\beta\delta} \overset{\beta\leftrightarrow\delta}{=} \frac{1}{2}\sum_{\beta\delta} v^{(a)\kappa\kappa}_{\gamma\alpha\beta\delta}\delta\kappa_{\delta\beta}$$
$$\overset{(3.52a)}{=} -\sum_{\beta\delta} v^{(a)\kappa\kappa}_{\gamma\alpha\beta\delta}\delta\kappa_{\beta\delta} = -\delta\Delta^{(2)}_{\gamma\alpha}, \tag{3.62a}$$

$$\delta\Delta^{(3)\rho}_{\alpha\gamma} = \frac{1}{2}\sum_{\beta\delta\epsilon\zeta} w^{(a)\rho\kappa\kappa}_{\alpha\gamma\epsilon\beta\delta\zeta}\delta\rho_{\zeta\epsilon}\kappa_{\beta\delta} \overset{\mathcal{S}(1,2)}{=} \frac{1}{2}\sum_{\beta\delta\epsilon\zeta} w^{(a)\rho\kappa\kappa}_{\gamma\alpha\epsilon\delta\beta\zeta}\delta\rho_{\zeta\epsilon}\kappa_{\beta\delta} \overset{\beta\leftrightarrow\delta}{=} \frac{1}{2}\sum_{\beta\delta\epsilon\zeta} w^{(a)\rho\kappa\kappa}_{\gamma\alpha\epsilon\beta\delta\zeta}\delta\rho_{\zeta\epsilon}\kappa_{\delta\beta}$$
$$\overset{(3.40a)}{=} -\frac{1}{2}\sum_{\beta\delta\epsilon\zeta} w^{(a)\rho\kappa\kappa}_{\gamma\alpha\epsilon\beta\delta\zeta}\delta\rho_{\zeta\epsilon}\kappa_{\beta\delta} = -\delta\Delta^{(3)\rho}_{\gamma\alpha}, \tag{3.62b}$$

$$\delta\Delta^{(3)\kappa}_{\alpha\gamma} = \frac{1}{2}\sum_{\beta\delta\epsilon\zeta} w^{(a)\rho\kappa\kappa}_{\alpha\gamma\epsilon\beta\delta\zeta}\rho_{\zeta\epsilon}\delta\kappa_{\beta\delta} \overset{\mathcal{S}(1,2)}{=} \frac{1}{2}\sum_{\beta\delta\epsilon\zeta} w^{(a)\rho\kappa\kappa}_{\gamma\alpha\epsilon\delta\beta\zeta}\rho_{\zeta\epsilon}\delta\kappa_{\beta\delta} \overset{\beta\leftrightarrow\delta}{=} \frac{1}{2}\sum_{\beta\delta\epsilon\zeta} w^{(a)\rho\kappa\kappa}_{\gamma\alpha\epsilon\beta\delta\zeta}\rho_{\zeta\epsilon}\delta\kappa_{\delta\beta}$$
$$\overset{(3.52a)}{=} -\frac{1}{2}\sum_{\beta\delta\epsilon\zeta} w^{(a)\rho\kappa\kappa}_{\gamma\alpha\epsilon\beta\delta\zeta}\rho_{\zeta\epsilon}\delta\kappa_{\beta\delta} = -\delta\Delta^{(3)\kappa}_{\gamma\alpha}, \tag{3.62c}$$

and using the very same sequence of operations yields identical relations for $\delta\bar{\Delta}$. Thus, one has the claimed properties $\delta\Delta = -\delta\Delta^T$ and $\delta\bar{\Delta} = -\delta\bar{\Delta}^T$.

[6] In mathematical terms, $v^{\kappa\kappa}_{\alpha\gamma\beta\delta} = v^{\kappa\kappa}_{\gamma\alpha\delta\beta}$ but $v^{\kappa\kappa}_{\alpha\gamma\beta\delta} \neq -v^{\kappa\kappa}_{\gamma\alpha\beta\delta}$, and similar remarks for the three-body terms.

3.4 Connection with the QRPA

In the QFAM formulation of the linear response theory, an excitation operator F is needed in order to calculate the strength function. The QFAM therefore belongs to the "external point of view" theories. As mentioned in subsection 2.6.1, the "internal" vision (as realised by the QRPA theory), characterised by the knowledge of the collective eigenstates, can be recovered through integration along aptly chosen contours in the complex plane. This section generalises the work of [HKN13], showing the link between the QFAM and the QRPA at finite temperature.

As discussed in section 2.6, the eigenmodes of a quantum system can be studied from two different points of view. The usual setting of the QRPA involves diagonalising the Hamiltonian, giving as a result the eigenvectors and eigenvalues. Since it does not call for an external probe, it can be labelled as an "internal point of view" description. Conversely, the FAM explicitly demands a probe in the form of the operator F, it is thus an "external" approach. The extension of the excitation frequency ω into the complex plane and the occurrence of first order poles both in the FAM equations (3.8) and strength function (3.10) clearly hints that a contour integration should make the link between the FAM and the QRPA.

3.4.1 Eigenvectors and transition amplitudes

The zero temperature QRPA equation writes

$$\begin{pmatrix} A & B \\ B^* & A^* \end{pmatrix} \begin{pmatrix} X \\ Y \end{pmatrix} = \Omega \begin{pmatrix} 1 & \\ & -1 \end{pmatrix} \begin{pmatrix} X \\ Y \end{pmatrix}, \tag{3.63}$$

where Ω is the diagonal matrix containing all the (positive and negative) eigenvalues. Due to the eigenvalues occurring in pairs, this equation can be doubled[7]:

$$\begin{pmatrix} A & B \\ B^* & A^* \end{pmatrix} \begin{pmatrix} X & \lambda \\ Y & \mu \end{pmatrix} = \begin{pmatrix} 1 & \\ & -1 \end{pmatrix} \begin{pmatrix} X & \lambda \\ Y & \mu \end{pmatrix} \begin{pmatrix} \Omega & \\ & -\Omega \end{pmatrix}. \tag{3.64}$$

The matrices λ, μ are the solutions of

$$\begin{cases} AX + BY = \Omega X \\ B^*Y + A^*X = -\Omega Y \\ A\lambda + B\mu = -\Omega\lambda \\ B^*\lambda + A^*\mu = \Omega\mu, \end{cases} \tag{3.65}$$

that is, after identifying the two last equations with the two firsts, $\lambda = Y^*$ and $\mu = X^*$. The procedure is exactly the same at finite temperature: one starts with the QRPA equation [Som83]

[7] The eigenvalues matrix occurring to the right of the eigenvectors one comes from identifying the "doubled" vectors as the negative Ω solutions.

$$\tilde{\mathcal{S}}\tilde{\mathcal{X}} = \begin{pmatrix} \tilde{C} & \tilde{a} & \tilde{b} & \tilde{D} \\ \tilde{a}^\dagger & \tilde{A} & \tilde{B} & \tilde{b}^T \\ \tilde{b}^\dagger & \tilde{B}^* & \tilde{A}^* & \tilde{a}^T \\ \tilde{D}^* & \tilde{b}^* & \tilde{a}^* & \tilde{C}^* \end{pmatrix} \begin{pmatrix} \tilde{W} \\ \tilde{X} \\ \tilde{Y} \\ \tilde{Z} \end{pmatrix} = \Omega \begin{pmatrix} \tilde{W} \\ \tilde{X} \\ \tilde{Y} \\ \tilde{Z} \end{pmatrix}, \tag{3.66}$$

and extends the matrix $\tilde{\mathcal{X}}$ to be of size $4N \times 4N$. Because we want that only the core remains when taking the $T \to 0$ limit, the "known" vectors must come at the centre:

$$\tilde{\mathcal{X}} \to \tilde{\mathcal{X}}' = \begin{pmatrix} i & \tilde{W} & q & m \\ j & \tilde{X} & \tilde{Y}^* & n \\ k & \tilde{Y} & \tilde{X}^* & o \\ l & \tilde{Z} & r & p \end{pmatrix}. \tag{3.67}$$

The missing entries can be found by matching the system $\tilde{\mathcal{S}}\tilde{\mathcal{X}}' = \tilde{\mathcal{N}}\tilde{\mathcal{X}}'\tilde{\mathcal{O}}$, which is quite pedestrian although not difficult. Much more efficiently, one remarks that the third column corresponds to the negative eigenvalues, so that $q = \tilde{Z}^*$ and $r = \tilde{W}^*$ in analogy with (3.65). Because the outermost columns must correspond to positive and negative eigenvalues likewise, they are simply the duplicates of the central ones. When calculating the response function, one should be careful in dividing by a factor two to compensate for the doubling of the matrix elements. Hence,

$$\tilde{\mathcal{X}}' = \begin{pmatrix} \tilde{W} & \tilde{W} & \tilde{Z}^* & \tilde{Z}^* \\ \tilde{X} & \tilde{X} & \tilde{Y}^* & \tilde{Y}^* \\ \tilde{Y} & \tilde{Y} & \tilde{X}^* & \tilde{X}^* \\ \tilde{Z} & \tilde{Z} & \tilde{W}^* & \tilde{W}^* \end{pmatrix}. \tag{3.68}$$

In the following, $\tilde{\mathcal{X}}$ will denote the linear response vector, while $\tilde{\mathcal{X}}'$ will be its extension into a 4×4 tensor. The linear response equation can be written [Som83]

$$[\tilde{\mathcal{S}} - \omega_\gamma \mathcal{N}]\tilde{\mathcal{X}} = \left[\begin{pmatrix} \tilde{C} & \tilde{a} & \tilde{b} & \tilde{D} \\ \tilde{a}^\dagger & \tilde{A} & \tilde{B} & \tilde{b}^T \\ \tilde{b}^\dagger & \tilde{B}^* & \tilde{A}^* & \tilde{a}^T \\ \tilde{D}^* & \tilde{b}^* & \tilde{a}^* & \tilde{C}^* \end{pmatrix} - \omega_\gamma \begin{pmatrix} 1 & & & \\ & 1 & & \\ & & -1 & \\ & & & -1 \end{pmatrix} \right] \begin{pmatrix} \tilde{W} \\ \tilde{X} \\ \tilde{Y} \\ \tilde{Z} \end{pmatrix} = \begin{pmatrix} \tilde{F}^{11} \\ \tilde{F}^{20} \\ \tilde{F}^{02} \\ \tilde{F}'^{11} \end{pmatrix} = \tilde{\mathcal{F}}, \tag{3.69}$$

from which one gets the expression for the linear response vectors (the factor two balances the double counting):

$$\begin{aligned} \tilde{\mathcal{X}}(\omega_\gamma) &= (\tilde{\mathcal{S}} - \omega_\gamma \mathcal{N})^{-1} \tilde{\mathcal{F}} \\ &\equiv 2R(\omega_\gamma)\tilde{\mathcal{F}}. \end{aligned} \tag{3.70}$$

The equation defines the response function as the matrix relating the external field to the induced oscillation of the system. On the other hand, the QRPA equation is easily seen to generalise as

$$\tilde{\mathcal{S}}\tilde{\mathcal{X}}' = \mathcal{N}\tilde{\mathcal{X}}'\mathcal{O}, \tag{3.71}$$

where $\mathcal{N} = \mathrm{diag}(1, 1, -1, -1)$ is the metric and $\mathcal{O} = \mathrm{diag}(\Omega_1, \ldots, \Omega_N, -\Omega_1, \ldots, -\Omega_N)$ is the matrix of eigenvalues. The orthonormalisation condition corresponds to[8]

$$\tilde{\mathcal{X}}'^{\dagger}\mathcal{N}\tilde{\mathcal{X}}' = \mathcal{N}. \tag{3.72}$$

Eq. (3.71) yields

$$\tilde{\mathcal{S}} = \mathcal{N}\tilde{\mathcal{X}}'\mathcal{O}\tilde{\mathcal{X}}'^{-1}, \tag{3.73}$$

which, inserted in (3.70), produces

$$\begin{aligned}\tilde{\mathcal{X}}(\omega_\gamma) &= (\mathcal{N}\tilde{\mathcal{X}}'\mathcal{O}\tilde{\mathcal{X}}'^{-1} - \omega_\gamma\mathcal{N})^{-1}\tilde{\mathcal{F}} \\ &= (\mathcal{N}\tilde{\mathcal{X}}'\mathcal{O}\tilde{\mathcal{X}}'^{-1} - \omega_\gamma\mathcal{N}\tilde{\mathcal{X}}'\tilde{\mathcal{X}}'^{-1})^{-1}\tilde{\mathcal{F}} \\ &= \tilde{\mathcal{X}}'(\mathcal{O} - \omega_\gamma\mathcal{I})^{-1}\tilde{\mathcal{X}}'^{-1}\mathcal{N}\tilde{\mathcal{F}}. \end{aligned} \tag{3.74}$$

Then, (3.72) gives[9]

$$\mathcal{N}\tilde{\mathcal{X}}' = \left(\tilde{\mathcal{X}}'^{\dagger}\right)^{-1}\mathcal{N} \Rightarrow \tilde{\mathcal{X}}'^{-1}\mathcal{N} = \mathcal{N}\tilde{\mathcal{X}}'^{\dagger}, \tag{3.75}$$

therefore

$$\tilde{\mathcal{X}}(\omega_\gamma) = \tilde{\mathcal{X}}'(\mathcal{O} - \omega_\gamma\mathcal{I})^{-1}\mathcal{N}\tilde{\mathcal{X}}'^{\dagger}\tilde{\mathcal{F}}, \tag{3.76}$$

showing the link between the linear response amplitudes (on the left-hand side) and the QRPA ones (on the right-hand side). The thermal response function (3.70) can now be calculated after remembering the necessary 1/2 factor:

$$R(\omega_\gamma) = \frac{1}{2}\tilde{\mathcal{X}}'(\mathcal{O} - \omega_\gamma\mathcal{I})^{-1}\mathcal{N}\tilde{\mathcal{X}}'^{\dagger} \tag{3.77a}$$

[8]Note: this condition differs from the one of Hinohara [HKN13] but is the same as Sommermann [Som83]. While both are correct at zero temperature, the former is not valid for the thermal regime, as it gives, e.g., $W^\dagger W - Z^* Z^T$ instead of $W^\dagger W + X^\dagger X - Y^* Y^T - Z^* Z^T$.

[9]The orthonormalisation of [HKN13] gives the same equation.

$$
\begin{aligned}
&= \frac{1}{2}\tilde{\mathcal{X}}' \begin{pmatrix} \frac{1}{\Omega-\omega_\gamma} & & & \\ & \frac{1}{\Omega-\omega_\gamma} & & \\ & & \frac{1}{\Omega+\omega_\gamma} & \\ & & & \frac{1}{\Omega+\omega_\gamma} \end{pmatrix} \begin{pmatrix} \tilde{W}^\dagger & \tilde{X}^\dagger & \tilde{Y}^\dagger & \tilde{Z}^\dagger \\ \tilde{W}^\dagger & \tilde{X}^\dagger & \tilde{Y}^\dagger & \tilde{Z}^\dagger \\ \tilde{Z}^T & \tilde{Y}^T & \tilde{X}^T & \tilde{W}^T \\ \tilde{Z}^T & \tilde{Y}^T & \tilde{X}^T & \tilde{W}^T \end{pmatrix} \\
&= \frac{1}{2} \begin{pmatrix} \tilde{W} & \tilde{W} & \tilde{Z}^* & \tilde{Z}^* \\ \tilde{X} & \tilde{X} & \tilde{Y}^* & \tilde{Y}^* \\ \tilde{Y} & \tilde{Y} & \tilde{X}^* & \tilde{X}^* \\ \tilde{Z} & \tilde{Z} & \tilde{W}^* & \tilde{W}^* \end{pmatrix} \begin{pmatrix} \frac{\tilde{W}^\dagger}{\Omega-\omega_\gamma} & \frac{\tilde{X}^\dagger}{\Omega-\omega_\gamma} & \frac{\tilde{Y}^\dagger}{\Omega-\omega_\gamma} & \frac{\tilde{Z}^\dagger}{\Omega-\omega_\gamma} \\ \frac{\tilde{W}^\dagger}{\Omega-\omega_\gamma} & \frac{\tilde{X}^\dagger}{\Omega-\omega_\gamma} & \frac{\tilde{Y}^\dagger}{\Omega-\omega_\gamma} & \frac{\tilde{Z}^\dagger}{\Omega-\omega_\gamma} \\ \frac{\tilde{Z}^T}{\Omega+\omega_\gamma} & \frac{\tilde{Y}^T}{\Omega+\omega_\gamma} & \frac{\tilde{X}^T}{\Omega+\omega_\gamma} & \frac{\tilde{W}^T}{\Omega+\omega_\gamma} \\ \frac{\tilde{Z}^T}{\Omega+\omega_\gamma} & \frac{\tilde{Y}^T}{\Omega+\omega_\gamma} & \frac{\tilde{X}^T}{\Omega+\omega_\gamma} & \frac{\tilde{W}^T}{\Omega+\omega_\gamma} \end{pmatrix} \\
&\equiv \begin{pmatrix} R_{11} & R_{12} & R_{13} & R_{14} \\ R_{21} & R_{22} & R_{23} & R_{24} \\ R_{31} & R_{32} & R_{33} & R_{34} \\ R_{41} & R_{42} & R_{43} & R_{44} \end{pmatrix}. \qquad (3.77b)
\end{aligned}
$$

The collection of blocks involved in (3.77b) are the matrices

$$R_{11} = \sum_i \frac{\tilde{W}^i \tilde{W}^{i,\dagger}}{\Omega_i - \omega_\gamma} + \frac{\tilde{Z}^{i,*} \tilde{Z}^{i,T}}{\Omega_i + \omega_\gamma}, \qquad (3.78a)$$

$$R_{12} = \sum_i \frac{\tilde{W}^i \tilde{X}^{i,\dagger}}{\Omega_i - \omega_\gamma} + \frac{\tilde{Z}^{i,*} \tilde{Y}^{i,T}}{\Omega_i + \omega_\gamma}, \qquad (3.78b)$$

$$R_{13} = \sum_i \frac{\tilde{W}^i \tilde{Y}^{i,\dagger}}{\Omega_i - \omega_\gamma} + \frac{\tilde{Z}^{i,*} \tilde{X}^{i,T}}{\Omega_i + \omega_\gamma}, \qquad (3.78c)$$

$$R_{14} = \sum_i \frac{\tilde{W}^i \tilde{Z}^{i,\dagger}}{\Omega_i - \omega_\gamma} + \frac{\tilde{Z}^{i,*} \tilde{W}^{i,T}}{\Omega_i + \omega_\gamma}, \qquad (3.78d)$$

$$R_{21} = \sum_i \frac{\tilde{X}^i \tilde{W}^{i,\dagger}}{\Omega_i - \omega_\gamma} + \frac{\tilde{Y}^{i,*} \tilde{Z}^{i,T}}{\Omega_i + \omega_\gamma}, \qquad (3.78e)$$

$$R_{22} = \sum_i \frac{\tilde{X}^i \tilde{X}^{i,\dagger}}{\Omega_i - \omega_\gamma} + \frac{\tilde{Y}^{i,*} \tilde{Y}^{i,T}}{\Omega_i + \omega_\gamma}, \qquad (3.78f)$$

$$R_{23} = \sum_i \frac{\tilde{X}^i \tilde{Y}^{i,\dagger}}{\Omega_i - \omega_\gamma} + \frac{\tilde{Y}^{i,*} \tilde{X}^{i,T}}{\Omega_i + \omega_\gamma}, \qquad (3.78g)$$

$$R_{24} = \sum_i \frac{\tilde{X}^i \tilde{Z}^{i,\dagger}}{\Omega_i - \omega_\gamma} + \frac{\tilde{Y}^{i,*} \tilde{W}^{i,T}}{\Omega_i + \omega_\gamma}, \qquad (3.78h)$$

$$R_{31} = \sum_i \frac{\tilde{Y}^i \tilde{W}^{i,\dagger}}{\Omega_i - \omega_\gamma} + \frac{\tilde{X}^{i,*} \tilde{Z}^{i,T}}{\Omega_i + \omega_\gamma}, \qquad (3.78i)$$

$$R_{32} = \sum_i \frac{\tilde{Y}^i \tilde{X}^{i,\dagger}}{\Omega_i - \omega_\gamma} + \frac{\tilde{X}^{i,*} \tilde{Y}^{i,T}}{\Omega_i + \omega_\gamma}, \qquad (3.78j)$$

$$R_{33} = \sum_i \frac{\tilde{Y}^i \tilde{Y}^{i,\dagger}}{\Omega_i - \omega_\gamma} + \frac{\tilde{X}^{i,*} \tilde{X}^{i,T}}{\Omega_i + \omega_\gamma}, \qquad (3.78k)$$

$$R_{34} = \sum_i \frac{\tilde{Y}^i \tilde{Z}^{i,\dagger}}{\Omega_i - \omega_\gamma} + \frac{\tilde{X}^{i,*} \tilde{W}^{i,T}}{\Omega_i + \omega_\gamma}, \tag{3.78l}$$

$$R_{41} = \sum_i \frac{\tilde{Z}^i \tilde{W}^{i,\dagger}}{\Omega_i - \omega_\gamma} + \frac{\tilde{W}^{i,*} \tilde{Z}^{i,T}}{\Omega_i + \omega_\gamma}, \tag{3.78m}$$

$$R_{42} = \sum_i \frac{\tilde{Z}^i \tilde{X}^{i,\dagger}}{\Omega_i - \omega_\gamma} + \frac{\tilde{W}^{i,*} \tilde{Y}^{i,T}}{\Omega_i + \omega_\gamma}, \tag{3.78n}$$

$$R_{43} = \sum_i \frac{\tilde{Z}^i \tilde{Y}^{i,\dagger}}{\Omega_i - \omega_\gamma} + \frac{\tilde{W}^{i,*} \tilde{X}^{i,T}}{\Omega_i + \omega_\gamma}, \tag{3.78o}$$

$$R_{44} = \sum_i \frac{\tilde{Z}^i \tilde{Z}^{i,\dagger}}{\Omega_i - \omega_\gamma} + \frac{\tilde{W}^{i,*} \tilde{W}^{i,T}}{\Omega_i + \omega_\gamma}. \tag{3.78p}$$

One can recover the elements indexed by the four indices (μ, ν, μ', ν') of each block by substitutions of the form $\tilde{W}^i \tilde{W}^{i,T} \to \tilde{W}^i_{\mu\nu} \tilde{W}^{i,\dagger}_{\mu'\nu'}$.

All of that mess can be conveniently written by defining the forward and backward responses:

$$R(\omega_\gamma) = R^+(\omega_\gamma) + R^-(\omega_\gamma), \tag{3.79}$$

$$R^+(\omega_\gamma) = \sum_i \frac{1}{\Omega_i - \omega_\gamma} \begin{pmatrix} \tilde{W}^i \tilde{W}^{i,T} & \tilde{W}^i \tilde{X}^{i,T} & \tilde{W}^i \tilde{Y}^{i,T} & \tilde{W}^i \tilde{Z}^{i,T} \\ \tilde{X}^i \tilde{W}^{i,T} & \tilde{X}^i \tilde{X}^{i,T} & \tilde{X}^i \tilde{Y}^{i,T} & \tilde{X}^i \tilde{Z}^{i,T} \\ \tilde{Y}^i \tilde{W}^{i,T} & \tilde{Y}^i \tilde{X}^{i,T} & \tilde{Y}^i \tilde{Y}^{i,T} & \tilde{Y}^i \tilde{Z}^{i,T} \\ \tilde{Z}^i \tilde{W}^{i,T} & \tilde{Z}^i \tilde{X}^{i,T} & \tilde{Z}^i \tilde{Y}^{i,T} & \tilde{Z}^i \tilde{Z}^{i,T} \end{pmatrix}, \tag{3.80}$$

$$R^-(\omega_\gamma) = \sum_i \frac{1}{\Omega_i + \omega_\gamma} \begin{pmatrix} \tilde{Z}^{i,*} \tilde{Z}^{i,T} & \tilde{Z}^{i,*} \tilde{Y}^{i,T} & \tilde{Z}^{i,*} \tilde{X}^{i,T} & \tilde{Z}^{i,*} \tilde{W}^{i,T} \\ \tilde{Y}^{i,*} \tilde{Z}^{i,T} & \tilde{Y}^{i,*} \tilde{Y}^{i,T} & \tilde{Y}^{i,*} \tilde{X}^{i,T} & \tilde{Y}^{i,*} \tilde{W}^{i,T} \\ \tilde{X}^{i,*} \tilde{Z}^{i,T} & \tilde{X}^{i,*} \tilde{Y}^{i,T} & \tilde{X}^{i,*} \tilde{X}^{i,T} & \tilde{X}^{i,*} \tilde{W}^{i,T} \\ \tilde{W}^{i,*} \tilde{Z}^{i,T} & \tilde{W}^{i,*} \tilde{Y}^{i,T} & \tilde{W}^{i,*} \tilde{X}^{i,T} & \tilde{W}^{i,*} \tilde{W}^{i,T} \end{pmatrix}. \tag{3.81}$$

Thus,

$$\begin{aligned} \tilde{\mathcal{X}}(\omega_\gamma) =& R(\omega_\gamma) \mathcal{F} \\ =& \sum_i \frac{1}{\Omega_i - \omega_\gamma} \begin{bmatrix} \tilde{W}^{i,*} \left(\tilde{W}^{i,\dagger} F^{11} + \tilde{X}^{i,\dagger} F^{20} + \tilde{Y}^{i,\dagger} F^{02} + \tilde{Z}^{i,\dagger} F'^{11} \right) \\ \tilde{X}^{i,*} \left(\tilde{W}^{i,\dagger} F^{11} + \tilde{X}^{i,\dagger} F^{20} + \tilde{Y}^{i,\dagger} F^{02} + \tilde{Z}^{i,\dagger} F'^{11} \right) \\ \tilde{Y}^{i,*} \left(\tilde{W}^{i,\dagger} F^{11} + \tilde{X}^{i,\dagger} F^{20} + \tilde{Y}^{i,\dagger} F^{02} + \tilde{Z}^{i,\dagger} F'^{11} \right) \\ \tilde{Z}^{i,*} \left(\tilde{W}^{i,\dagger} F^{11} + \tilde{X}^{i,\dagger} F^{20} + \tilde{Y}^{i,\dagger} F^{02} + \tilde{Z}^{i,\dagger} F'^{11} \right) \end{bmatrix} \end{aligned} \tag{3.82}$$

$$+\sum_i \frac{1}{\Omega_i+\omega_\gamma}\begin{bmatrix} \tilde{Z}^*\left(\tilde{Z}^{i,T}F^{11}+\tilde{Y}^{i,T}F^{20}+\tilde{X}^{i,T}F^{02}+\tilde{W}^{i,T}F'^{11}\right)\\ \tilde{Y}^*\left(\tilde{Z}^{i,T}F^{11}+\tilde{Y}^{i,T}F^{20}+\tilde{X}^{i,T}F^{02}+\tilde{W}^{i,T}F'^{11}\right)\\ \tilde{X}^*\left(\tilde{Z}^{i,T}F^{11}+\tilde{Y}^{i,T}F^{20}+\tilde{X}^{i,T}F^{02}+\tilde{W}^{i,T}F'^{11}\right)\\ \tilde{W}^*\left(\tilde{Z}^{i,T}F^{11}+\tilde{Y}^{i,T}F^{20}+\tilde{X}^{i,T}F^{02}+\tilde{W}^{i,T}F'^{11}\right)\end{bmatrix}.$$

The forward component $R^+(\omega_\gamma)$ involves the QRPA amplitudes $\langle i|\mathcal{F}|0\rangle$ as is:

$$\begin{aligned}\langle i|\mathcal{F}|0\rangle &= \langle\Phi_{\text{HFB}}|[\mathcal{Q}_i,\mathcal{F}]|\Phi_{\text{HFB}}\rangle = \langle\Phi_{\text{HFB}}|\mathcal{Q}_i\mathcal{F}|\Phi_{\text{HFB}}\rangle\\ &= \text{Tr}\{\mathcal{F}\mathcal{Q}_i\} = \text{Tr}\Big\{\tilde{W}^{i,\dagger}F^{11}+\tilde{Y}^{i,\dagger}F^{02}+\tilde{X}^{i,\dagger}F^{20}+\tilde{Z}^{i,\dagger}F'^{11}\Big\},\end{aligned} \tag{3.83}$$

where the excitation operator $\hat{Q}_i^\dagger = \frac{1}{2}\sum_{\mu\nu} X^i_{\mu\nu}\alpha^\dagger_\mu\alpha^\dagger_\nu + Y^i_{\mu\nu}\alpha_\mu\alpha_\nu + W^i_{\mu\nu}\alpha_\mu\alpha^\dagger_\nu + Z^i_{\mu\nu}\alpha^\dagger_\mu\alpha_\nu$. Strangely, $R^-(\omega_\gamma)$ does not involve any amplitude: the three remaining ones are[10]

$$\begin{aligned}\langle 0|\mathcal{F}|i\rangle &= \langle\Phi_{\text{HFB}}|\Big[\mathcal{F},\mathcal{Q}_i^\dagger\Big]|\Phi_{\text{HFB}}\rangle = \langle\Phi_{\text{HFB}}|\mathcal{F}\mathcal{Q}_i^\dagger|\Phi_{\text{HFB}}\rangle\\ &= \text{Tr}\Big\{\mathcal{F}\mathcal{Q}_i^\dagger\Big\} = \text{Tr}\Big\{F^{11}\tilde{W}^i+F^{20}\tilde{Y}^i+F^{02}\tilde{X}^i+F'^{11}\tilde{Z}^i\Big\},\end{aligned} \tag{3.84}$$

$$\begin{aligned}\langle 0|\mathcal{F}^\dagger|i\rangle &= \langle\Phi_{\text{HFB}}|\Big[\mathcal{F}^\dagger,\mathcal{Q}_i^\dagger\Big]|\Phi_{\text{HFB}}\rangle = \langle\Phi_{\text{HFB}}|\mathcal{F}^\dagger\mathcal{Q}_i^\dagger|\Phi_{\text{HFB}}\rangle\\ &= \text{Tr}\Big\{\mathcal{F}^\dagger\mathcal{Q}_i^\dagger\Big\} = \text{Tr}\Big\{(F^{11})^\dagger\tilde{W}^i+(F^{02})^\dagger\tilde{Y}^i+(F^{20})^\dagger\tilde{X}^i+(F'^{11})^\dagger\tilde{Z}^i\Big\},\end{aligned} \tag{3.85}$$

$$\begin{aligned}\langle i|\mathcal{F}^\dagger|0\rangle &= \langle\Phi_{\text{HFB}}|\big[\mathcal{Q}_i,\mathcal{F}^\dagger\big]|\Phi_{\text{HFB}}\rangle = \langle\Phi_{\text{HFB}}|\mathcal{Q}_i\mathcal{F}^\dagger|\Phi_{\text{HFB}}\rangle\\ &= \text{Tr}\big\{\mathcal{Q}_i\mathcal{F}^\dagger\big\} = \text{Tr}\Big\{\tilde{W}^{i,\dagger}(F^{11})^\dagger+\tilde{X}^{i,\dagger}(F^{20})^\dagger+\tilde{Y}^{i,\dagger}(F^{02})^\dagger+\tilde{Z}^{i,\dagger}(F'^{11})^\dagger\Big\}.\end{aligned} \tag{3.86}$$

Lacking a better notation, let's define the "anti-diagonal swap" of $\mathcal{F}^T$ as $\mathcal{F}^S$:

$$\mathcal{F}^S \equiv \begin{pmatrix}(F'^{11})^T & (F^{20})^T\\ (F^{02})^T & (F^{11})^T\end{pmatrix} = \begin{pmatrix}0&1\\1&0\end{pmatrix}\mathcal{F}^T\begin{pmatrix}0&1\\1&0\end{pmatrix}. \tag{3.87}$$

One has

$$\langle 0|\mathcal{F}^S|i\rangle = \langle\Phi_{\text{HFB}}|\Big[\mathcal{F}^S,\mathcal{Q}_i^\dagger\Big]|\Phi_{\text{HFB}}\rangle = \langle\Phi_{\text{HFB}}|\mathcal{F}^S\mathcal{Q}_i^\dagger|\Phi_{\text{HFB}}\rangle \tag{3.88}$$

$$= \text{Tr}\Big\{\mathcal{F}^S\mathcal{Q}_i^\dagger\Big\} = \text{Tr}\Big\{(F'^{11})^T\tilde{W}^i+(F^{20})^T\tilde{Y}^i+(F^{02})^T\tilde{X}^i+(F^{11})^T\tilde{Z}^i\Big\} \tag{3.89}$$

$$= \text{Tr}\Big\{(\tilde{W}^i)^T(F'^{11})+\tilde{X}^\dagger(F^{02})+\tilde{Y}^\dagger(F^{20})+\tilde{Z}^\dagger(F^{11})\Big\}, \tag{3.90}$$

the last line being a consequence of the identity $\text{Tr}\{A^TB^T\} = \text{Tr}\{BA\}$. In the $T=0$ limit and for $\mathcal{F}$ Hermitian, one recovers $\langle 0|\mathcal{F}^S|i\rangle = \langle 0|\mathcal{F}|i\rangle^* = \langle 0|\mathcal{F}|i\rangle$ as in [HKN13]. With this newly defined operator,

[10] These four amplitudes evidently reduce to two when $\mathcal{F} = \mathcal{F}^\dagger$.

$$\tilde{W}_{\mu\nu}(\omega_\gamma) = -\sum_i \left\{ \frac{\tilde{W}^i_{\mu\nu} \langle i|\mathcal{F}|0\rangle}{\Omega_i - \omega_\gamma} + \frac{\tilde{Z}^{i*}_{\mu\nu} \langle 0|\mathcal{F}^S|i\rangle}{\Omega_i + \omega_\gamma} \right\}, \tag{3.91a}$$

$$\tilde{X}_{\mu\nu}(\omega_\gamma) = -\sum_i \left\{ \frac{\tilde{X}^i_{\mu\nu} \langle i|\mathcal{F}|0\rangle}{\Omega_i - \omega_\gamma} + \frac{\tilde{Y}^{i*}_{\mu\nu} \langle 0|\mathcal{F}^S|i\rangle}{\Omega_i + \omega_\gamma} \right\}, \tag{3.91b}$$

$$\tilde{Y}_{\mu\nu}(\omega_\gamma) = -\sum_i \left\{ \frac{\tilde{Y}^i_{\mu\nu} \langle i|\mathcal{F}|0\rangle}{\Omega_i - \omega_\gamma} + \frac{\tilde{X}^{i*}_{\mu\nu} \langle 0|\mathcal{F}^S|i\rangle}{\Omega_i + \omega_\gamma} \right\}, \tag{3.91c}$$

$$\tilde{Z}_{\mu\nu}(\omega_\gamma) = -\sum_i \left\{ \frac{\tilde{Z}^i_{\mu\nu} \langle i|\mathcal{F}|0\rangle}{\Omega_i - \omega_\gamma} + \frac{\tilde{W}^{i*}_{\mu\nu} \langle 0|\mathcal{F}^S|i\rangle}{\Omega_i + \omega_\gamma} \right\}. \tag{3.91d}$$

From Cauchy's integral theorem, one sees that integrating those equations around a contour $\mathcal{C}$ enclosing any number of poles yields

$$\frac{1}{2i\pi} \oint_{\mathcal{C}} \tilde{W}_{\mu\nu}(\omega_\gamma) \mathrm{d}\omega_\gamma = \sum_i \tilde{W}^i_{\mu\nu} \langle i|\mathcal{F}|0\rangle , \tag{3.92a}$$

$$\frac{1}{2i\pi} \oint_{\mathcal{C}} \tilde{X}_{\mu\nu}(\omega_\gamma) \mathrm{d}\omega_\gamma = \sum_i \tilde{X}^i_{\mu\nu} \langle i|\mathcal{F}|0\rangle , \tag{3.92b}$$

$$\frac{1}{2i\pi} \oint_{\mathcal{C}} \tilde{Y}_{\mu\nu}(\omega_\gamma) \mathrm{d}\omega_\gamma = \sum_i \tilde{Y}^i_{\mu\nu} \langle i|\mathcal{F}|0\rangle , \tag{3.92c}$$

$$\frac{1}{2i\pi} \oint_{\mathcal{C}} \tilde{Z}_{\mu\nu}(\omega_\gamma) \mathrm{d}\omega_\gamma = \sum_i \tilde{Z}^i_{\mu\nu} \langle i|\mathcal{F}|0\rangle , \tag{3.92d}$$

In the fortunate event where the contour circles exactly one pole, these reduce to the expression of the eigenmatrices in terms of the FAM ones:

$$\frac{1}{2i\pi} \oint_{C_i} \tilde{W}_{\mu\nu}(\omega_\gamma) \mathrm{d}\omega_\gamma = \tilde{W}^i_{\mu\nu} \langle i|\mathcal{F}|0\rangle , \tag{3.93a}$$

$$\frac{1}{2i\pi} \oint_{C_i} \tilde{X}_{\mu\nu}(\omega_\gamma) \mathrm{d}\omega_\gamma = \tilde{X}^i_{\mu\nu} \langle i|\mathcal{F}|0\rangle , \tag{3.93b}$$

$$\frac{1}{2i\pi} \oint_{C_i} \tilde{Y}_{\mu\nu}(\omega_\gamma) \mathrm{d}\omega_\gamma = \tilde{Y}^i_{\mu\nu} \langle i|\mathcal{F}|0\rangle , \tag{3.93c}$$

$$\frac{1}{2i\pi} \oint_{C_i} \tilde{Z}_{\mu\nu}(\omega_\gamma) \mathrm{d}\omega_\gamma = \tilde{Z}^i_{\mu\nu} \langle i|\mathcal{F}|0\rangle , \tag{3.93d}$$

The QRPA amplitudes can then be found once the associated matrix elements $\langle i|\mathcal{F}|0\rangle$ are obtained. The requirement (3.72) that the eigenstates be orthonormal with respect to the metric $\mathcal{N} = \mathrm{diag}(1, 1, -1, -1)$ translates as

$$\delta_{ii'} = \langle i'|\mathcal{N}|i\rangle = \langle 0|\mathcal{Q}_{i'}\mathcal{N}\mathcal{Q}_i^\dagger|0\rangle\,; \quad \mathcal{Q}_i^\dagger = \begin{pmatrix} \tilde{W}^i \\ \tilde{X}^i \\ \tilde{Y}^i \\ \tilde{Z}^i \end{pmatrix}. \tag{3.94}$$

To make the indices match with the rest of the derivations (and most of the literature), it's more convenient to explicitly stack the vectors, i.e. go back to the matrix notation:

$$\delta_{ii'} = \langle i'|\mathcal{N}|i\rangle = \mathrm{Tr}\Big\{\mathcal{Q}_{i'}\mathcal{N}\mathcal{Q}_i^\dagger\Big\}; \quad \mathcal{Q}_i^\dagger = \begin{pmatrix} \tilde{W}^i & \tilde{X}^i \\ \tilde{Y}^i & \tilde{Z}^i \end{pmatrix}, \mathcal{N} = \begin{pmatrix} 1 & \\ & -1 \end{pmatrix} \tag{3.95}$$

$$= \mathrm{Tr}\Big\{\tilde{W}^{i',\dagger}\tilde{W}^i + \tilde{X}^{i',\dagger}\tilde{X}^i - \tilde{Y}^{i',\dagger}\tilde{Y}^i - \tilde{Z}^{i',\dagger}\tilde{Z}^i\Big\} \tag{3.96}$$

$$= \sum_{\mu\nu} \tilde{W}^{i'*}_{\mu\nu}\tilde{W}^i_{\mu\nu} + \tilde{X}^{i'*}_{\mu\nu}\tilde{X}^i_{\mu\nu} - \tilde{Y}^{i'*}_{\mu\nu}\tilde{Y}^i_{\mu\nu} - \tilde{Z}^{i'*}_{\mu\nu}\tilde{Z}^i_{\mu\nu}. \tag{3.97}$$

It follows that the transition probability from the ground state to the i^{th} excited state writes

$$|\langle i|\mathcal{F}|0\rangle|^2 = \frac{1}{4\pi^2}\sum_{\mu\nu}\Bigg\{\left|\oint_{C_i}\tilde{W}_{\mu\nu}(\omega_\gamma)\mathrm{d}\omega_\gamma\right|^2 + \left|\oint_{C_i}\tilde{X}_{\mu\nu}(\omega_\gamma)\mathrm{d}\omega_\gamma\right|^2 - \left|\oint_{C_i}\tilde{Y}_{\mu\nu}(\omega_\gamma)\mathrm{d}\omega_\gamma\right|^2 - \left|\oint_{C_i}\tilde{Z}_{\mu\nu}(\omega_\gamma)\mathrm{d}\omega_\gamma\right|^2\Bigg\}. \tag{3.98}$$

(Remark that the contribution of the W and Z amplitudes should cancel each other exactly, by (3.51)). Eq. (3.98) can be paired up with (3.93) to give forth the QRPA amplitudes:

$$\tilde{W}^{i'}_{\mu\nu} = \frac{e^{-i\theta}}{|\langle i'|\mathcal{F}|0\rangle|}\frac{1}{2i\pi}\oint_{C_{i'}}\tilde{W}_{\mu\nu}(\omega_\gamma)\mathrm{d}\omega_\gamma \tag{3.99a}$$

$$\tilde{X}^{i'}_{\mu\nu} = \frac{e^{-i\theta}}{|\langle i'|\mathcal{F}|0\rangle|}\frac{1}{2i\pi}\oint_{C_{i'}}\tilde{X}_{\mu\nu}(\omega_\gamma)\mathrm{d}\omega_\gamma \tag{3.99b}$$

$$\tilde{Y}^{i'}_{\mu\nu} = \frac{e^{-i\theta}}{|\langle i'|\mathcal{F}|0\rangle|}\frac{1}{2i\pi}\oint_{C_{i'}}\tilde{Y}_{\mu\nu}(\omega_\gamma)\mathrm{d}\omega_\gamma \tag{3.99c}$$

$$\tilde{Z}^{i'}_{\mu\nu} = \frac{e^{-i\theta}}{|\langle i'|\mathcal{F}|0\rangle|}\frac{1}{2i\pi}\oint_{C_{i'}}\tilde{Z}_{\mu\nu}(\omega_\gamma)\mathrm{d}\omega_\gamma, \tag{3.99d}$$

where the phase $e^{+i\theta} = \langle i|\mathcal{F}|0\rangle / |\langle i|\mathcal{F}|0\rangle|$ cannot be determined, but can be chosen arbitrarily since it is common to all the eigenvectors[11]. Because the thermal factor of the

[11]Note that in practical calculations, one may choose it so that all the discrete amplitudes are real, since the eigenvectors of a positive definite matrix can be made real simultaneously.

QRPA and QFAM amplitudes are the same, all these equations (and most importantly, (3.93), (3.98) and (3.99)) also hold when removing the tildes.

3.4.2 Eigenvalues

Line by line, and after multiplying either by $\sigma_{\mu\nu} \equiv \sqrt{f_\nu - f_\mu}$ or by $\eta_{\mu\nu} \equiv \sqrt{1 - f_\mu - f_\nu}$, (3.69) leads to

$$\sigma_{\mu\nu} \sum_{\mu'<\nu'} (\tilde{C}_{\mu\nu\mu'\nu'} - \omega_\gamma \delta_{\mu\mu'}\delta_{\nu\nu'})\tilde{W}_{\mu'\nu'} + \tilde{a}_{\mu\nu\mu'\nu'}\tilde{X}_{\mu'\nu'} + \tilde{b}_{\mu\nu\mu'\nu'}\tilde{Y}_{\mu'\nu'} + \tilde{D}_{\mu\nu\mu'\nu'}\tilde{Z}_{\mu'\nu'} = -\sigma_{\mu\nu}^2 F_{\mu\nu}^{11} \tag{3.100}$$

$$\eta_{\mu\nu} \sum_{\mu'<\nu'} \tilde{a}^\dagger_{\mu\nu\mu'\nu'}\tilde{W}_{\mu'\nu'} + (\tilde{A}_{\mu\nu\mu'\nu'} - \omega_\gamma \delta_{\mu\mu'}\delta_{\nu\nu'})\tilde{X}_{\mu'\nu'} + \tilde{B}_{\mu\nu\mu'\nu'}\tilde{Y}_{\mu'\nu'} + \tilde{b}^T_{\mu\nu\mu'\nu'}\tilde{Z}_{\mu'\nu'} = -\eta_{\mu\nu}^2 F_{\mu\nu}^{20} \tag{3.101}$$

$$\eta_{\mu\nu} \sum_{\mu'<\nu'} \tilde{b}^\dagger_{\mu\nu\mu'\nu'}\tilde{W}_{\mu'\nu'} + \tilde{B}^*_{\mu\nu\mu'\nu'}\tilde{X}_{\mu'\nu'} + (\tilde{A}^*_{\mu\nu\mu'\nu'} + \omega_\gamma \delta_{\mu\mu'}\delta_{\nu\nu'})\tilde{Y}_{\mu'\nu'} + \tilde{a}^T_{\mu\nu\mu'\nu'}\tilde{Z}_{\mu'\nu'} = -\eta_{\mu\nu}^2 F_{\mu\nu}^{02} \tag{3.102}$$

$$\sigma_{\mu\nu} \sum_{\mu'<\nu'} \tilde{D}^*_{\mu\nu\mu'\nu'}\tilde{W}_{\mu'\nu'} + \tilde{b}^*_{\mu\nu\mu'\nu'}\tilde{X}_{\mu'\nu'} + \tilde{a}^*_{\mu\nu\mu'\nu'}\tilde{Y}_{\mu'\nu'} + (\tilde{C}^*_{\mu\nu\mu'\nu'} + \omega_\gamma \delta_{\mu\mu'}\delta_{\nu\nu'})\tilde{Z}_{\mu'\nu'} = -\sigma_{\mu\nu}^2 F'^{11}_{\mu\nu}. \tag{3.103}$$

On the other hand, the QFAM equations read[12]

$$(E_\mu - E_\nu - \omega_\gamma)W_{\mu\nu}(\omega_\gamma) + H^{11}_{\mu\nu}(f_\nu - f_\mu) = -F^{11}_{\mu\nu}(f_\nu - f_\mu) = -\sigma^2_{\mu\nu}F^{11}_{\mu\nu} \tag{3.104}$$

$$(E_\mu + \bar{E}_\nu - \omega_\gamma)X_{\mu\nu}(\omega_\gamma) + H^{20}_{\mu\nu}(1 - f_\mu - \bar{f}_\nu) = -F^{20}_{\mu\nu}(1 - f_\mu - \bar{f}_\nu) = -\eta^2_{\mu\bar{\nu}}F^{20}_{\mu\nu} \tag{3.105}$$

$$(\bar{E}_\mu + E_\nu + \omega_\gamma)Y_{\mu\nu}(\omega_\gamma) + H^{02}_{\mu\nu}(1 - \bar{f}_\mu - f_\nu) = -F^{02}_{\mu\nu}(1 - \bar{f}_\mu - f_\nu) = -\eta^2_{\bar{\mu}\nu}F^{02}_{\mu\nu} \tag{3.106}$$

$$(\bar{E}_\mu - \bar{E}_\nu + \omega_\gamma)Z_{\mu\nu}(\omega_\gamma) + H'^{11}_{\mu\nu}(\bar{f}_\nu - \bar{f}_\mu) = -F'^{11}_{\mu\nu}(\bar{f}_\nu - \bar{f}_\mu) = -\sigma^2_{\bar{\mu}\bar{\nu}}F'^{11}_{\mu\nu}, \tag{3.107}$$

so that (the dependence of the fields and amplitudes on ω_γ has been omitted for legibility)

$$H^{11}_{\mu\nu} = \sigma^{-1}_{\mu\nu} \sum_{\mu'<\nu'} \Bigg[\left(\tilde{C}_{\mu\nu\mu'\nu'} - \left(\omega_\gamma + \frac{E_\mu - E_\nu - \omega_\gamma}{\sigma^2_{\mu\nu}} \right) \delta_{\mu\mu'}\delta_{\nu\nu'} \right) \tilde{W}_{\mu'\nu'} + \tilde{a}_{\mu\nu\mu'\nu'}\tilde{X}_{\mu'\nu'} + \tilde{b}_{\mu\nu\mu'\nu'}\tilde{Y}_{\mu'\nu'} + \tilde{D}_{\mu\nu\mu'\nu'}\tilde{Z}_{\mu'\nu'} \Bigg] \tag{3.108a}$$

$$H^{20}_{\mu\nu} = \eta^{-1}_{\mu\bar{\nu}} \sum_{\mu'<\nu'} \Bigg[\tilde{a}^\dagger_{\mu\nu\mu'\nu'}\tilde{W}_{\mu'\nu'} + \left(\tilde{A}_{\mu\nu\mu'\nu'} - \left(\omega_\gamma + \frac{E_\mu + \bar{E}_\nu - \omega_\gamma}{\eta^2_{\mu\bar{\nu}}} \right) \delta_{\mu\mu'}\delta_{\nu\nu'} \right) \tilde{X}_{\mu'\nu'}$$

[12] The bars correspond to matrix elements in the $\langle \mathrm{HFB}|\alpha\alpha^\dagger|\mathrm{HFB}\rangle$ sector; they are equal to their $\alpha^\dagger\alpha$ partners owing to the eigenvalues of the HFB equation coming by pairs of opposite sign. We have $\bar{E} = E$ and $\bar{f} = f$, but conserve the bars for bookkeeping.

$$+ \tilde{B}_{\mu\nu\mu'\nu'}\tilde{Y}_{\mu'\nu'} + \tilde{b}^{T}_{\mu\nu\mu'\nu'}\tilde{Z}_{\mu'\nu'}\Bigg] \tag{3.108b}$$

$$H^{02}_{\mu\nu} = \eta^{-1}_{\bar{\mu}\bar{\nu}} \sum_{\mu'<\nu'} \Bigg[\tilde{b}^{\dagger}_{\mu\nu\mu'\nu'}\tilde{W}_{\mu'\nu'} + \tilde{B}^{*}_{\mu\nu\mu'\nu'}\tilde{X}_{\mu'\nu'}$$
$$+ \left(\tilde{A}^{*}_{\mu\nu\mu'\nu'} + \left(\omega_\gamma - \frac{\bar{E}_\mu + E_\nu + \omega_\gamma}{\eta^2_{\bar{\mu}\nu}}\right)\delta_{\mu\mu'}\delta_{\nu\nu'}\right)\tilde{Y}_{\mu'\nu'} + \tilde{a}^{T}_{\mu\nu\mu'\nu'}\tilde{Z}_{\mu'\nu'}\Bigg] \tag{3.108c}$$

$$H'^{11}_{\mu\nu} = \sigma^{-1}_{\bar{\mu}\bar{\nu}} \sum_{\mu'<\nu'} \Bigg[\tilde{D}^{*}_{\mu\nu\mu'\nu'}\tilde{W}_{\mu'\nu'} + \tilde{b}^{*}_{\mu\nu\mu'\nu'}\tilde{X}_{\mu'\nu'}$$
$$+ \tilde{a}^{*}_{\mu\nu\mu'\nu'}\tilde{Y}_{\mu'\nu'} + \left(\tilde{C}^{*}_{\mu\nu\mu'\nu'} + \left(\omega_\gamma - \frac{\bar{E}_\mu - \bar{E}_\nu + \omega_\gamma}{\sigma^2_{\bar{\mu}\bar{\nu}}}\right)\delta_{\mu\mu'}\delta_{\nu\nu'}\right)\tilde{Z}_{\mu'\nu'}\Bigg]. \tag{3.108d}$$

These equations show that the FAM one-body fields can be directly linked to the QRPA two-body tensors and one-body eigenvectors. What's more, as these expressions explicitly involve the frequency of the perturbation, they provide a closed set of expression for the eigenfrequencies. Indeed, integrating (anti-clockwise) each of them around a contour $\mathcal{C}$ circling one or more poles, we obtain with the help of (3.93) and the QRPA equation (3.66)

$$\oint_{\mathcal{C}} H^{11}_{\mu\nu}(\omega_\gamma)\mathrm{d}\omega_\gamma = \sum_{i'}\oint_{C_{i'}} H^{11}_{\mu\nu}(\omega_\gamma)\mathrm{d}\omega_\gamma = 2i\pi\sigma_{\mu\nu}\sum_{i'}\langle i'|\mathcal{F}|0\rangle\,\tilde{W}^{i'}_{\mu\nu}(\Omega_{i'} - (E_\mu - E_\nu)) \tag{3.109a}$$

$$\oint_{\mathcal{C}} H^{20}_{\mu\nu}(\omega_\gamma)\mathrm{d}\omega_\gamma = \sum_{i'}\oint_{C_{i'}} H^{20}_{\mu\nu}(\omega_\gamma)\mathrm{d}\omega_\gamma = 2i\pi\eta_{\mu\bar{\nu}}\sum_{i'}\langle i'|\mathcal{F}|0\rangle\,\tilde{X}^{i'}_{\mu\nu}(\Omega_{i'} - (E_\mu + \bar{E}_\nu)) \tag{3.109b}$$

$$\oint_{\mathcal{C}} H^{02}_{\mu\nu}(\omega_\gamma)\mathrm{d}\omega_\gamma = \sum_{i'}\oint_{C_{i'}} H^{02}_{\mu\nu}(\omega_\gamma)\mathrm{d}\omega_\gamma = 2i\pi\eta_{\bar{\mu}\nu}\sum_{i'}\langle i'|\mathcal{F}|0\rangle\,\tilde{Y}^{i'}_{\mu\nu}(-\Omega_{i'} - (\bar{E}_\mu + E_\nu)) \tag{3.109c}$$

$$\oint_{\mathcal{C}} H'^{11}_{\mu\nu}(\omega_\gamma)\mathrm{d}\omega_\gamma = \sum_{i'}\oint_{C_{i'}} H'^{11}_{\mu\nu}(\omega_\gamma)\mathrm{d}\omega_\gamma = 2i\pi\sigma_{\bar{\mu}\bar{\nu}}\sum_{i'}\langle i'|\mathcal{F}|0\rangle\,\tilde{Z}^{i'}_{\mu\nu}(-\Omega_{i'} - (\bar{E}_\mu - \bar{E}_\nu)). \tag{3.109d}$$

When the contour $\mathcal{C}$ goes around only one pole (collective or not), these expressions reduce in the zero temperature limit to eqs. (25a)-(25b) of [HKN13]. Each pair (μ,ν) of indices gives four different expressions for the frequency. However, these involve dividing by the matrix elements and amplitudes, yet both may be small. It would be great if the sum of the eigenvalues could be calculated without needing to identify all the poles. This is sadly not possible, due to the presence of the transition matrix elements. Our last resort is to manage to locate the poles individually: in that case, the sum over i' contains only one term, and each frequency can be calculated by inverting (3.109). Due to the aforementioned potentially small denominators, it is safer to recast these equations as

$$2i\pi \langle i'|\mathcal{F}|0\rangle \sigma_{\mu\nu}\tilde{W}^{i'}_{\mu\nu}\Omega_{i'} = (E_\mu - E_\nu)2i\pi \langle i'|\mathcal{F}|0\rangle \sigma_{\mu\nu}\tilde{W}^{i'}_{\mu\nu} + \oint_{C_i} H^{11}_{\mu\nu}(\omega_\gamma)\mathrm{d}\omega_\gamma \tag{3.110a}$$

$$2i\pi \langle i'|\mathcal{F}|0\rangle \eta_{\mu\bar{\nu}}\tilde{X}^{i'}_{\mu\nu}\Omega_{i'} = (E_\mu + \bar{E}_\nu)2i\pi \langle i'|\mathcal{F}|0\rangle \eta_{\mu\bar{\nu}}\tilde{X}^{i'}_{\mu\nu} + \oint_{C_i} H^{20}_{\mu\nu}(\omega_\gamma)\mathrm{d}\omega_\gamma \tag{3.110b}$$

$$-2i\pi \langle i'|\mathcal{F}|0\rangle \eta_{\bar{\mu}\nu}\tilde{Y}^{i'}_{\mu\nu}\Omega_{i'} = (\bar{E}_\mu + E_\nu)2i\pi \langle i'|\mathcal{F}|0\rangle \eta_{\bar{\mu}\nu}\tilde{Y}^{i'}_{\mu\nu} + \oint_{C_i} H^{02}_{\mu\nu}(\omega_\gamma)\mathrm{d}\omega_\gamma \tag{3.110c}$$

$$-2i\pi \langle i'|\mathcal{F}|0\rangle \sigma_{\bar{\mu}\bar{\nu}}\tilde{Z}^{i'}_{\mu\nu}\Omega_{i'} = (\bar{E}_\mu - \bar{E}_\nu)2i\pi \langle i'|\mathcal{F}|0\rangle \sigma_{\bar{\mu}\bar{\nu}}\tilde{Z}^{i'}_{\mu\nu} + \oint_{C_i} H'^{11}_{\mu\nu}(\omega_\gamma)\mathrm{d}\omega_\gamma \tag{3.110d}$$

and use (3.93) to obtain

$$\tilde{W}^{i'}_{\mu\nu}\Omega_{i'} = \frac{1}{\langle i'|\mathcal{F}|0\rangle}\oint_{C_i}\left[(E_\mu - E_\nu)\tilde{W}_{\mu\nu}(\omega_\gamma) + \sigma^{-1}_{\mu\nu}H^{11}_{\mu\nu}(\omega_\gamma)\right]\mathrm{d}\omega_\gamma \tag{3.111a}$$

$$\tilde{X}^{i'}_{\mu\nu}\Omega_{i'} = \frac{1}{\langle i'|\mathcal{F}|0\rangle}\oint_{C_i}\left[(E_\mu + \bar{E}_\nu)\tilde{X}_{\mu\nu}(\omega_\gamma) + \eta^{-1}_{\mu\bar{\nu}}H^{20}_{\mu\nu}(\omega_\gamma)\right]\mathrm{d}\omega_\gamma \tag{3.111b}$$

$$-\tilde{Y}^{i'}_{\mu\nu}\Omega_{i'} = \frac{1}{\langle i'|\mathcal{F}|0\rangle}\oint_{C_i}\left[(\bar{E}_\mu + E_\nu)\tilde{Y}_{\mu\nu}(\omega_\gamma) + \eta^{-1}_{\bar{\mu}\nu}H^{02}_{\mu\nu}(\omega_\gamma)\right]\mathrm{d}\omega_\gamma \tag{3.111c}$$

$$-\tilde{Z}^{i'}_{\mu\nu}\Omega_{i'} = \frac{1}{\langle i'|\mathcal{F}|0\rangle}\oint_{C_i}\left[(\bar{E}_\mu - \bar{E}_\nu)\tilde{Z}_{\mu\nu}(\omega_\gamma) + \sigma^{-1}_{\bar{\mu}\bar{\nu}}H'^{11}_{\mu\nu}(\omega_\gamma)\right]\mathrm{d}\omega_\gamma. \tag{3.111d}$$

With the help of the normalisation condition, we then have

$$\begin{aligned}
\Omega_i^2 &= \sum_{\mu<\nu}\Omega_i^2(|\tilde{W}^i_{\mu\nu}|^2 + |\tilde{X}^i_{\mu\nu}|^2 - |\tilde{Y}^i_{\mu\nu}|^2 - |\tilde{Z}^i_{\mu\nu}|^2) \\
&= \frac{1}{4\pi^2|\langle i|\mathcal{F}|0\rangle|^2}\sum_{\mu<\nu}\left\{\left|\oint_{C_i}\left[(E_\mu - E_\nu)\tilde{W}_{\mu\nu}(\omega_\gamma) + \sigma^{-1}_{\bar{\mu}\nu}H^{11}_{\mu\nu}(\omega_\gamma)\right]\mathrm{d}\omega_\gamma\right|^2\right. \\
&+\left|\oint_{C_i}\left[(\bar{E}_\mu + E_\nu)\tilde{X}_{\mu\nu}(\omega_\gamma) + \eta^{-1}_{\mu\nu}H^{20}_{\mu\nu}(\omega_\gamma)\right]\mathrm{d}\omega_\gamma\right|^2 \\
&-\left|\oint_{C_i}\left[(E_\mu + \bar{E}_\nu)\tilde{Y}_{\mu\nu}(\omega_\gamma) + \eta^{-1}_{\mu\bar{\nu}}H^{02}_{\mu\nu}(\omega_\gamma)\right]\mathrm{d}\omega_\gamma\right|^2 \\
&\left.-\left|\oint_{C_i}\left[(\bar{E}_\mu - \bar{E}_\nu)\tilde{Z}_{\mu\nu}(\omega_\gamma) + \sigma^{-1}_{\bar{\mu}\bar{\nu}}H'^{11}_{\mu\nu}(\omega_\gamma)\right]\mathrm{d}\omega_\gamma\right|^2\right\},
\end{aligned} \tag{3.112}$$

which allows us to calculate the energy Ω_i once we have found a contour selecting this frequency only.

3.4.3 Eigenvalues and transition amplitudes from the moments

As shown in 2.6.4, integrating the smeared strength in the whole positive ω complex half-plane gives the moments of the strength distribution. More precisely, if a contour $\mathcal{C}$ goes

around some poles $\{\Omega_{\mu\nu}\}$ of the strength function, one can obtain from (2.82), (2.85) and (2.86) that

$$m_k(\mathcal{C}) = \frac{1}{2i\pi}\oint_{\mathcal{C}} \mathrm{d}\omega_\gamma \omega_\gamma^k S(F,\omega_\gamma) = Z^{-1}\sum_{\Omega_{\mu\nu}\in\mathcal{C}} \Omega_{\mu\nu}^k e^{-\beta E_\mu}|\langle\nu|F|\mu\rangle|^2. \tag{3.113}$$

In a situation where only one pole is enclosed by $\mathcal{C}$ (noted C_i for the occasion),

$$m_0(C_i) = Z^{-1}e^{-\beta E_\mu}|\langle\nu|F|\mu\rangle|^2, \tag{3.114a}$$

$$\frac{m_{k+k'}(C_i)}{m_k(C_i)} = \Omega_{\mu\nu}^{k'}, \quad \forall\, k,k' \in \mathbb{Z}. \tag{3.114b}$$

Thus, if one is only interested in the thermal matrix elements (3.114a) and/or eigenvalues (3.114b), only two partial moments of the strength need to be calculated.

3.4.4 Summary

Finally, the equations allowing the calculation of different interesting quantities are given here:

- eigenvectors: (3.99),
- eigenvalues: (3.112), (3.114b).

As of obtaining the transition matrix elements, there are two possibilities[13] [HKN13]:

- by a contour integral of the FAM amplitudes (3.98),
- the thermally weighted squared matrix element can be found by (3.114a).

Note that only the latter is physically meaningful at $T > 0$, since it properly encodes the statistical distribution of the initial state. Following [HKN13] again, we remark that in case the chosen contour contains more than one pole, (3.112) and (3.114b) must give different results: the first contains interferences between the enclosed modes due to squaring the matrix elements, whereas the second equation does not. This can in practice be employed to determine whether the contour loops around a single pole or more than one.

Similarly, the integral (3.98) contains interferences. On the other hand, (3.114a) does not. The two techniques can thus be tested against each other, to discriminate the occurrence of more than one pole. One could also think of using (3.99) to calculate (3.83), but the value of matrix element depends on the choice of the technique, hence it does contain contaminations or does not, depending on the technique. It should be remarked that this cross-validation is only possible at $T = 0$, unless the partition function and energies $\{E_\mu\}$ of the many-body microstates are calculated as well.

[13] Calculating the trace (3.83) is not possible since the matrix element is needed to obtain the FAM amplitudes from (3.99).

3.5 Self-consistent dressing

At first glance, the propagators seem to always be the HFB ones. This turns out not to be the case when the dynamical fields are included, as they will implicitly dress the propagators by self-consistently including RPA correlations. This can be illustrated by inspecting a simple two-level system (representing for instance a two-level system with two particles, in the presence of an oscillating electromagnetic field):

$$H_0 = \begin{pmatrix} \epsilon & \\ & -\epsilon \end{pmatrix}; \quad R_0 = \begin{pmatrix} 1 & \\ & 1 \end{pmatrix}; \quad F = \begin{pmatrix} & f \\ f & \end{pmatrix}; \quad \delta H = \begin{pmatrix} & vx \\ vy & \end{pmatrix}; \quad \delta R = \begin{pmatrix} & x \\ y & \end{pmatrix}. \tag{3.115}$$

Here, H_0 and R_0 are the unperturbed Hamiltonian and density matrix, F is the external field, δH and δR are the residual interaction and density fluctuations. The FAM equations read

$$x = -\frac{f + vx}{2\epsilon - \omega} \tag{3.116}$$

$$y = -\frac{f + vy}{2\epsilon + \omega}. \tag{3.117}$$

Solving for the amplitudes x and y yields first-order poles at $\omega = \pm(2\epsilon + v)$, which shows that the poles are shifted due to the residual interaction. Note that the $2\epsilon + v$ residual is reminiscent of the entries of the QRPA matrix $A_{\mu\nu\mu'\nu'} = (E_\mu + E_\nu)\delta_{\mu\mu'}\delta_{\nu\nu'} + V_{\mu\nu\mu'\nu'}$: if the two-body interaction is diagonal in the two-body basis, the energy shifts are trivially obtained due to their $\delta_{\mu\mu'}\delta_{\nu\nu'}$ character.

3.6 Nambu-Goldstone modes

3.6.1 Equations of motion for the NG modes

Nambu-Goldstone (NG) modes correspond to zero-energy excitations restoring spontaneously broken symmetries [Nam60; Gol61; GSW62]. For a system described by the Hamiltonian H, the density matrix solves the Liouville-von Neumann equation

$$i\dot{D} = [H, D]. \tag{3.118}$$

Likewise, we have for mean-field theories

$$i\dot{\mathcal{R}} = [\mathcal{H}, \mathcal{R}] \qquad \text{HFB}, \tag{3.119}$$

$$i\dot{\rho} = [h, \rho] \qquad \text{HF}. \tag{3.120}$$

Since these have the same form as (3.118), the results of this subsection transpose to the mean-field theories with no problem. For some arbitrary Hermitian operator P corresponding to a transformation of magnitude α, the symmetry transformation of an

operator A is written as

$$A \to \tilde{A} = e^{i\alpha P} A e^{-i\alpha^* P^\dagger} = e^{i\alpha P} A e^{-i\alpha P}. \tag{3.121}$$

Spontaneous symmetry breaking occurs when H is invariant under the symmetry transformation S (that is, $[H, S] = 0$, or equivalently, $\tilde{H} = H$), but the density matrix is not. The Liouville equation remains unchanged by the transformation:

$$\begin{aligned} i\tilde{\dot{D}} = \widetilde{[H, D]} &= e^{i\alpha P}[H, D]e^{-i\alpha P} = e^{i\alpha P} H e^{-i\alpha P} e^{i\alpha P} D e^{-i\alpha P} - H \leftrightarrow D \\ &= \left[\tilde{H}, \tilde{D}\right]. \end{aligned} \tag{3.122}$$

The derivative of the transformed density matrix is

$$\begin{aligned} \dot{\tilde{D}} &= \frac{\mathrm{d}}{\mathrm{d}t}\left(e^{i\alpha P} D e^{-i\alpha P}\right) \\ &= i(\dot{\alpha}P + \alpha\dot{P})e^{i\alpha P} D e^{-i\alpha P} + e^{i\alpha P}\dot{D}e^{-i\alpha P} - ie^{i\alpha P} D(\dot{\alpha}P + \alpha\dot{P})e^{-i\alpha P} \\ &= \tilde{\dot{D}} + i\left((\dot{\alpha}P + \alpha\dot{P})e^{i\alpha P} D e^{-i\alpha P} - e^{i\alpha P} D(\dot{\alpha}P + \alpha\dot{P})e^{-i\alpha P}\right) \\ &= \tilde{\dot{D}} + i\dot{\alpha}\left[P, \tilde{D}\right] + i\alpha\left[\dot{P}, e^{i\alpha P} D\right]e^{-i\alpha P}. \end{aligned} \tag{3.123}$$

If α and P are both independent of time, one finds that[14]

$$\dot{\tilde{D}} = \tilde{\dot{D}}, \tag{3.124}$$

yielding

$$i\dot{\tilde{D}} = \left[H, \tilde{D}\right] \tag{3.125}$$

after recalling that P and H commute, hence $\tilde{H} = H$. Therefore, any solution of the Liouville-von Neumann equation transformed according to a continuous symmetry of the system is also a solution of the equation of motion.

3.6.2 NG modes removal

Since the transformed density matrices verify the transformed Liouville-von Neumann equation for the same Hamiltonian, they describe an equivalent state. The eigenvalues are therefore identical to those of the original state. The resulting Nambu-Goldstone modes relate elements of this manifold of states differing by zero-energy excitations through the application of the exponential map associated to the algebra describing the symmetry

[14] Which could have been seen by the following argument: if the generator of the transformation does not depend on time, the order between the transformation and the derivation does not matter, i.e. $\forall A, \left[\frac{\mathrm{d}}{\mathrm{d}t}, P\right]A = \dot{P}A + P\dot{A} - P\dot{A} = 0$.

operator.

One can measure the difference between two equivalent operators (in that case, density matrices) through the definition

$$\begin{aligned}\Delta D_P \equiv (\tilde{D}_P - D) &= e^{i\alpha P} D e^{-i\alpha P} - D \\ &\sim i\alpha[P, D]\end{aligned} \tag{3.126}$$

from which, regardless of the magnitude α of the transformation, one defines

$$\delta D_P \equiv \alpha^{-1} \Delta D_P \sim i[P, D]. \tag{3.127}$$

It is no big deal to show that δD_P is Hermitian if so does D (and being the ground state density matrix, it does) and P[15]:

$$\delta D_P^\dagger = \alpha^{-1} \Delta D_P^\dagger = \alpha^{-1} \left(e^{i\alpha P} D^\dagger e^{-i\alpha P} - D^\dagger \right) = \delta D_P. \tag{3.128}$$

This forbids one to use the normalisation condition for the density fluctuations (3.72), since it requires these to be non-Hermitian (the hermicity of $\tilde{Q}_i \equiv Q_i \mathcal{N}^{1/2}$ follows from that of Q_i and $\mathcal{N}$):

$$\delta_{ii'} = \langle i'|\mathcal{N}|i\rangle = \langle 0|Q_{i'}\mathcal{N}Q_i^\dagger|0\rangle = \langle 0|\tilde{Q}_{i'}\tilde{Q}_i^\dagger|0\rangle = \langle 0|\left[\tilde{Q}_{i'}, \tilde{Q}_i^\dagger\right]|0\rangle = \mathrm{Tr}\left\{ \left[\tilde{Q}_{i'}, \tilde{Q}_i^\dagger\right] R_0 \right\}. \tag{3.129}$$

Therefore, these modes cannot be separated from the physical ones using this orthogonality relation. Instead, we assume that the spurious densities contribute linearly to the calculated density:

$$\delta D_{\mathrm{calc}} = \delta D_{\mathrm{phys}} + \delta D_{\mathrm{spurious}} = \delta D_{\mathrm{phys}} + \sum_P \lambda_P \delta D_P + \sum_R \lambda_R \delta D_R, \tag{3.130}$$

which is reasonable since the density fluctuations are expected to be small, hence couplings between NG modes and non-spurious ones should be second order terms. The orthogonality of the spurious densities with the non-contaminated one, $\langle \delta D_{\mathrm{phys}} \delta D_{P,R} \rangle = 0$, can be recast under a commutator form:

$$\begin{aligned}\langle [\delta D_{\mathrm{phys}}, \delta D_P] \rangle = 0 &= \left\langle \left[\delta D_{\mathrm{calc}} - \sum_R \lambda_R \delta D_R, \delta D_P \right] \right\rangle \\ &= \langle [\delta D_{\mathrm{calc}}, \delta D_P] \rangle - \sum_R \lambda_R \langle [\delta D_R, \delta D_P] \rangle ,\end{aligned} \tag{3.131}$$

[15] This is also immediate from the first order expression in (3.127).

$$\begin{aligned}\langle[\delta D_{\text{phys}}, \delta D_R]\rangle = 0 &= \left\langle \left[\delta D_{\text{calc}} - \sum_P \lambda_P \delta D_P, \delta D_R \right] \right\rangle \\ &= \langle[\delta D_{\text{calc}}, \delta D_R]\rangle - \sum_P \lambda_P \langle[\delta D_P, \delta D_R]\rangle . \end{aligned} \tag{3.132}$$

All the quantities in that last equation can be calculated from static operators and the computed transition density. One finds

$$\lambda_R = \frac{\langle[\delta D_{\text{calc}}, \delta D_P]\rangle}{\langle[\delta D_R, \delta D_P]\rangle}, \tag{3.133}$$

$$\lambda_P = \frac{\langle[\delta D_{\text{calc}}, \delta D_R]\rangle}{\langle[\delta D_P, \delta D_R]\rangle}, \tag{3.134}$$

which yield the final expression

$$\begin{aligned}\delta D_{\text{phys}} &= \delta D_{\text{calc}} - \frac{\langle[\delta D_{\text{calc}}, \delta D_R]\rangle}{\langle[\delta D_P, \delta D_R]\rangle} i[P, D] - \frac{\langle[\delta D_{\text{calc}}, \delta D_P]\rangle}{\langle[\delta D_R, \delta D_P]\rangle} i[R, D] \\ &= \delta D_{\text{calc}} - \frac{\langle[\delta D_{\text{calc}}, [R, D]]\rangle}{\langle[[P, D], [R, D]]\rangle}[P, D] - \frac{\langle[\delta D_{\text{calc}}, [P, D]]\rangle}{\langle[[R, D], [P, D]]\rangle}[R, D]. \end{aligned} \tag{3.135}$$

If there is more than one pair of operators that generate spurious modes, this subtraction can be applied iteratively, provided the generators of the transformations commute.

In practise, the direction of symmetry breaking is entirely determined by the external operator $\hat{Q}$: if it does not break a symmetry S, there will be no induced spurious density in the direction in which S is broken. Therefore, the number of broken generators depends on the choice of $\hat{Q}$. For instance, an operator of which the projection K along the $r_\perp$ axis is zero cannot reach spurious states generated by rotation in the $\perp$ direction (in other words, it does not break $S_\perp$), so that one only has to subtract $\{\delta D_{r_z}, \delta D_{p_z}\}$ from the calculated density. Conversely, an operator depending only on the radial distance $r_\perp$ does not break S_z but only $S_\perp$.

3.7 Centre of mass

As mentioned in section 2.2, the centre of mass of a system that is not bound by an external field must be fixed by imposing explicitly that the total linear momentum vanishes:

$$\mathbf{P} = \sum_i^A \mathbf{p}_i = \mathbf{0}, \tag{3.136}$$

which is equivalent to

$$0 = \frac{\mathbf{P}^2}{2M} = \sum_i^A \frac{\mathbf{p}_i^2}{2M} + \sum_{i\neq j}^A \frac{\mathbf{p}_i.\mathbf{p}_j}{2M}, \tag{3.137}$$

M being the total mass. In the following, we assume that all masses are identical[16]. At the one-body level, one can simply subtract from each particle's kinetic energy the average kinetic energy of the translation-invariant system:

$$T = \frac{\mathbf{p}^2}{2m} \to \left(1 - \frac{1}{A}\right) \frac{\mathbf{p}^2}{2m}, \tag{3.138}$$

while an additional two-body interaction appears:

$$v_{\text{c.o.m}} = -\frac{\mathbf{p}_i.\mathbf{p}_j}{2Am}. \tag{3.139}$$

This understanding of the centre of mass contribution is only valid when the particle number A can take a single value. Indeed, mathematical correctness commands to write the intrinsic momentum at the operator level. Is has been shown in detail [HR09] that two identical (at the operator level) representations of the kinetic operator may lead to different normal and anomalous fields. This possible discrepancy has been tracked down to idempotency of the generalised density matrix, owing to which the ρ and κ densities are related. The rest of this section summarises the findings of [HR09], and shows that the same conclusion hold for the linearised fields entering the FAM.

The kinetic operator can take the form either of a one-plus-two-body operator:

$$\hat{T}_{\text{int}}^{(a)} = \hat{T}_{\text{lab}} - \hat{T}_{\text{c.o.m}} = \left(I - \hat{A}^{-1}\right) \sum_i \frac{\mathbf{p}_i^2}{2m} - \frac{\hat{A}^{-1}}{2m} \sum_{i\neq j} \mathbf{p}_i.\mathbf{p}_j, \tag{3.140}$$

or a purely two-body term, corresponding to the relative kinetic energy of each pair:

$$\hat{T}_{\text{int}}^{(b)} = \hat{A}^{-1} \sum_{i<j} \frac{(\mathbf{p}_i - \mathbf{p}_j)^2}{2m}. \tag{3.141}$$

While these two expressions are formally equivalent, the second leads to an ambiguity regarding whether the variation of the kinetic energy contributions in the normal or pairing channel. It can be shown [HR09] that a specific prescription has to be taken to enforce the equality of the normal and pairing fields derived from either (3.140) or (3.141). In such case, since $h^{(a)} = h^{(b)}$ and $\Delta^{(a)} = \Delta^{(b)}$, the explicitly linearised terms entering the FAM equation are identical as well with either choice (a) or (b). Conversely, the conclusion of

[16] If one has different types of degrees of freedom (e.g. two for protons and neutrons), as many copies of (3.137) -and the forthcoming equations- should be considered, since having one species with non-zero linear momentum would signify it can drift away from the total origin of the coordinate frame. The fact identical particles are grouped together stems from their indistinguishability.

[HR09] is expected to hold at the FAM level as well: when no prescription is taken, (a) and (b) should lead to identical fields if and only if the total wave function is an eigenstate of the particle number operator. The rest of this section proves this statement. For the expressions of the static mean-field, we refer the reader to [HR09] (Eqs. 23 and 31, 25 and 32) once more. In the FAM, the first iteration can be initialised with $\delta h = \delta\Delta = 0$[17], hence the very first trial $\delta\rho$ and $\delta\kappa$ are the same with both ways of calculating the fields. It is thus sufficient to examine whether the different fields given by (a) and (b) lead to identical expressions once linearised. One finds

$$\delta h^{(a)}_{kk'} = \sum_{qq'} \left\{ \left(v_{kqk'q'} - \frac{1}{\langle\hat{A}\rangle m} \langle kq|p_1.p_2|k'q'\rangle \right) \delta\rho_{q'q} \right\}, \tag{3.142}$$

and

$$\begin{aligned} \delta h^{(b)}_{kk'} = &\sum_{qq'} \left\{ \left(v_{kqk'q'} + \frac{2}{\langle\hat{A}\rangle m} \langle kq|q^2_{12}|k'q'\rangle \right) \delta\rho_{q'q} \right\} \\ &+ \frac{1}{\langle\hat{A}\rangle} \sum_q \left(t_{kq}\delta\rho_{qk'} + t_{qk'}\delta\rho_{kq} \right). \end{aligned} \tag{3.143}$$

The difference $\mathrm{d}h_{kk'} \equiv \delta h^{(b)}_{kk'} - \delta h^{(a)}_{kk'}$ is

$$\begin{aligned} \mathrm{d}h_{kk'} = &\frac{1}{\langle\hat{A}\rangle m} \sum_{qq'} \langle kq|(2q^2_{12} + p_1.p_2)|k'q'\rangle \, \delta\rho_{q'q} \\ &+ \frac{1}{\langle\hat{A}\rangle} \sum_q \left(t_{kq}\delta\rho_{qk'} + t_{qk'}\delta\rho_{kq} \right). \end{aligned} \tag{3.144}$$

Using the identity

$$\frac{2}{m} \langle kq|q^2_{12}|k'q'\rangle = t_{kk'}\delta_{qq'} - t_{kq'}\delta_{qk'} + t_{qq'}\delta_{kk'} - t_{qk'}\delta_{kq'} - \frac{1}{m} \langle kq|p_1.p_2|k'q'\rangle, \tag{3.145}$$

we get

$$\begin{aligned} \mathrm{d}h_{kk'} = &\frac{1}{\langle\hat{A}\rangle} \sum_{qq'} \Big[(t_{kk'}\delta_{qq'} - t_{kq'}\delta_{qk'} + t_{qq'}\delta_{kk'} - t_{qk'}\delta_{kq'} \\ &- \frac{1}{m} \langle kq|p_1.p_2|k'q'\rangle) + \frac{1}{m} \langle kq|p_1.p_2|k'q'\rangle \Big] \delta\rho_{q'q} \\ &+ \frac{1}{\langle\hat{A}\rangle} \sum_q \left(t_{kq}\delta\rho_{qk'} + t_{qk'}\delta\rho_{kq} \right) \end{aligned}$$

[17] And the same for the barred fields.

$$
\begin{aligned}
&= \frac{1}{\langle \hat{A} \rangle} \left[t_{kk'} \sum_q \delta\rho_{qq} - \sum_{q'} t_{kq'} \delta\rho_{q'k'} + \sum_{qq'} t_{qq'} \delta_{kk'} \delta\rho_{q'q} - \sum_q t_{qk'} \delta\rho_{kq} \right] \\
&+ \frac{1}{\langle \hat{A} \rangle} \sum_q \left(t_{kq} \delta\rho_{qk'} + t_{qk'} \delta\rho_{kq} \right) \\
&= \frac{1}{\langle \hat{A} \rangle} \left[t_{kk'} \sum_q \delta\rho_{qq} + \delta_{kk'} \sum_{qq'} t_{qq'} \delta\rho_{q'q} \right] \\
&= \frac{1}{\langle \hat{A} \rangle} \left[t_{kk'} \operatorname{Tr}\{\delta\rho\} + \delta_{kk'} \operatorname{Tr}\{T\delta\rho\}. \right]
\end{aligned} \tag{3.146}
$$

In the cases where the excitation couples elements having different angular momenta projections (AMP), both traces vanish[18]. There can thus be no difference in the results obtained with these two prescription as far as these excitation modes are concerned. As for AMP non-conserving transitions, the first trace vanishes only for particle-number dispersion-less theories[19]. Indeed,

$$
\begin{aligned}
\operatorname{Tr}\{\delta\rho\} &\overset{(3.44a)}{=} \operatorname{Tr}\left\{ UWU^\dagger + V^* Y U^\dagger + U X V^T + V^* Z V^T \right\} \\
&\underset{(2.48b)}{\overset{(2.48a)}{=}} \operatorname{Tr}\left\{ V^T U (X - Y) + W - 2 V^\dagger V W \right\};
\end{aligned} \tag{3.147}
$$

the second and third terms vanish at zero temperature, since $W = 0$ in this limit. The first term involves $V^T U$, which quite resembles the pairing tensor. Yet, the presence of X does not allow applying the cyclic property. Instead, one can invert block-wise the Bogoliubov matrix to show that $U \propto U^\dagger$ and $V \propto V^\dagger$. The transformation being encoded in a real matrix, one immediately deduces $\operatorname{Tr}\{\delta\rho\} = 0$ at zero temperature and for a vanishin

The second part, however, is apparently not zero. It results in the normal fields being "shifted":

$$
\delta h^{(b)} = \delta h^{(a)} + \alpha I, \quad \alpha = \langle \hat{A} \rangle^{-1} \operatorname{Tr}\{T\delta\rho\}. \tag{3.148}
$$

It follows that the generalised Hamiltonian becomes

$$
\delta H^{(b)} = \delta H^{(a)} + \alpha \begin{pmatrix} I & \\ & -I \end{pmatrix}. \tag{3.149}
$$

The shift transforms into the Bogoliubov basis as

$$
\begin{pmatrix} \mathrm{d}H^{(11)} & \mathrm{d}H^{(20)} \\ \mathrm{d}H^{(02)} & \mathrm{d}H^{('11)} \end{pmatrix}_\rho = \mathrm{d}\mathcal{H}_\rho = \alpha \begin{pmatrix} U^\dagger & V^\dagger \\ -V^\dagger & U^\dagger \end{pmatrix} \begin{pmatrix} I & \\ & -I \end{pmatrix} \begin{pmatrix} U & -V \\ V & U \end{pmatrix}
$$

[18] Provided the matrix representation of the operators is consistently ordered, i.e. the basis states come in the same order column-wise (from left to right) and row-wise (from top to bottom).

[19] The cyclic property of the trace and the tracelessness of W -see (3.8c)- are employed)

$$
\begin{aligned}
&= \alpha \begin{pmatrix} U^\dagger U - V^\dagger V & -U^\dagger V - V^\dagger U \\ -V^\dagger U - U^\dagger V & V^\dagger V - U^\dagger U \end{pmatrix} \\
&= \alpha \begin{pmatrix} \rho + \bar{\rho} - I & \kappa + \bar{\kappa} \\ \kappa + \bar{\kappa} & I - \rho - \bar{\rho} \end{pmatrix} . \qquad (3.150)
\end{aligned}
$$

Unfortunately, the shift results in non-zero changes in the perturbed fields. One may note, however, that at the Hartree-Fock approximation, the (20) and (02) blocks remain unchanged. At $T = 0$, the diagonal blocks (11) and ($'11$) do not contribute to any observable, as can be seen from (3.9) and (3.10). Altogether, we find that versions (a) and (b) of the centre of mass correction yield identical observables within the FAM. This is consistent with the result obtained in [HR09] for the static fields. It has been numerically checked that the two prescriptions yield the same strengths functions (up to machine precision) for the double magic nucleus ^{16}O at $T = 0$ for IS monopole, IV dipole and IS quadrupole excitations.

If the system is either thermally excited and/or superfluid, the above derivations show that the two representations (3.140)-(3.141) do not lead to identical fields if one is not careful. In that case, the simplest choice is to adopt the kinetic operator (3.140), which does not require a specific prescription.

Finally, the pairing fields need not be examined, since the consistency is valid only for non-superfluid systems. For completeness, the difference between the two pairing fields writes, in the very same manner,

$$
\begin{aligned}
\mathrm{d}\Delta_{kk'} &\equiv \delta\Delta^{(b)}_{kk'} - \delta\Delta^{(a)}_{kk'} \\
&= \frac{1}{\langle\hat{A}\rangle} \sum_q \left[t_{kq}\delta\kappa_{qk'} + t^*_{qk'}\delta\kappa_{kq} \right] \\
&+ \frac{1}{\langle\hat{A}\rangle} \sum_{qq'} \left[t_{kq}\delta_{k'q'} - t_{kq'}\delta_{qk'} + t_{k'q'}\delta_{kq} - t_{k'k'}\delta_{kq'} \right] \delta\kappa_{qq'} \\
&= \frac{1}{\langle\hat{A}\rangle} \sum_q \left[t_{kq}\delta\kappa_{qk'} + t^*_{qk'}\delta\kappa_{kq} \right] \\
&+ \frac{1}{\langle\hat{A}\rangle} \sum_q \left[t_{kq}\delta\kappa_{qk'} - t_{kq}\delta\kappa_{k'q} + t_{k'q}\delta\kappa_{kq} - t_{k'k'}\delta\kappa_{qk} \right] \\
&= \frac{2}{\langle\hat{A}\rangle} \sum_q \left[t_{kq}\delta\kappa_{qk'} + t^*_{qk'}\delta\kappa_{kq} \right] - \frac{1}{\langle\hat{A}\rangle} \sum_q \left[t_{kq}\delta\kappa_{k'q} + t_{k'k'}\delta\kappa_{qk} \right] . \qquad (3.151)
\end{aligned}
$$

Bonus: Coordinate space centre of mass correction

The zero-momentum condition writes

$$
\mathbf{0} = \mathbf{K} = \sum_i^A \mathbf{k} \Leftrightarrow \frac{\mathbf{K}^2}{2Am} = \frac{1}{2Am} \left(\sum_i \mathbf{k}_i^2 + \sum_{i \neq j} \mathbf{k}_i . \mathbf{k}_j \right) , \qquad (3.152)
$$

viz., the correction has the same form as in a basis. This is evident, as (3.137) makes no reference to a particular basis whatsoever: the coordinate basis is simply a special one, where the basis "functions" are Dirac and form a mesh. The one-body contribution can simply be subtracted, while the two-body is most easily calculated by Fourier transforming the wave functions:

$$-\langle a|\frac{\mathbf{k}_a.\mathbf{k}_b}{2Am}|b\rangle = -\int \mathrm{d}\mathbf{k}_1\mathrm{d}\mathbf{k}_2\tilde{\Phi}^*_a(\mathbf{k}_1)\frac{\mathbf{k}_a.\mathbf{k}_b}{2Am}\tilde{\Phi}_b(\mathbf{k}_2), \tag{3.153}$$

which seems rather involved for such a simple field. Among the infinitely many choices for the grid, it is smart to choose one such that multidimensional integrals like (3.153) can be carried out analytically. The obvious and standard choice is to employ a Cartesian mesh, for which the eigenfunctions are those of a particle in a box, that is, plane waves. Behold! The integrals in (3.153) suddenly become easy.

3.8 Unstable modes

Although the FAM formalism can always (why not?) be applied to obtain the linear response of a system to some given perturbation, the linear regime is expected only when the system undergoes small oscillations around the reference state. This means for instance that the approach must fail when applied on top of a reference state which is unstable with respect to the perturbation. As is known[20], instabilities in the RPA response lead to imaginary eigenvalues. Complex QRPA eigenvalues thus constitute clear indicators of the breakdown of the linear approximation[21]. This section examines how and when it is possible, from FAM calculations, to detect such poles that characterise the collapse of the method's validity.

Method 1: sum rules

The sum rules can be obtained [Hin+15] (see also (2.6.4)) by contour integration around the $\mathrm{Re}(\omega) > 0$ half-plane. When performed around a contour $\mathcal{C}$ that does not circle all the poles of the strength function, one may define the partial sum rules as

$$m_k(\mathcal{C}) = \frac{1}{2i\pi}\oint_{\mathcal{C}} \mathrm{d}\omega_\gamma \omega_\gamma^k S(F,\omega_\gamma) = Z^{-1}\sum_{\Omega^\nu_\mu\in\mathcal{C}} (\Omega^\nu_\mu)^k e^{-\beta E_\mu}|\langle\nu|F|\mu\rangle|^2. \tag{3.154}$$

In particular,

[20] This can be checked in the simple case of a 2×2 RPA matrix $\begin{pmatrix} a & b \\ -b^* & -a^* \end{pmatrix}$, which bears minus signs as opposed to (2.87) to account for the metric, and thus deal with an eigenvalue equation instead of a generalised one. It is a bit more involved to show that the stability of the ground state is related to the positive-definiteness of the RPA matrix (2.87), this time with plus signs only.

[21] But the converse is not true: having real eigenvalues only by no means imply that the linear response is a "good" approximation.

$$m_1(\mathcal{C}) = Z^{-1} \sum_{\Omega_\mu^\nu \in \mathcal{C}} \Omega_\mu^\nu e^{-\beta E_\mu} |\langle \nu|F|\mu\rangle|^2. \tag{3.155}$$

Thus, the partial sum rules can be employed to check if any unstable mode is present within a given contour $\mathcal{C}$. Provided unstable eigenvalues do not come in conjugate pairs, the existence of such values can be characterised by a non-zero imaginary part of the m_1 sum rule. If they do come in pair (and with transition matrix elements of identical norm for the pair), as is the case with the RPA theory, a contour $\mathcal{C}$ going around all the poles in the positive ω half-plane will always result in real moments m_k. As such, an all-encompassing contour cannot be employed to detect complex-energy modes. This downside is sidestepped by a simple ruse: rather than calculating the total sum rules, one restricts the contour to one looping around the $\Gamma \geq 0$ axis.

Method 2: sign of S

Another means of identifying the presence of complex energy eigenvalues comes from the strength function: writing $\Omega_\mu^\nu = \Omega_q + i\Gamma_q$, $e^{-\beta E_\mu}|\langle \nu|F|\mu\rangle|^2 = M_q^2$ and $e^{-\beta E_\mu}|\langle \mu|F|\nu\rangle|^2 = M_{-q}^2$,

$$\mathrm{Im}\{S(F,\omega_\gamma)\} = -\gamma \sum_{q>0} \left(\mathscr{M}_q^2 - \mathscr{M}_{-q}^2\right) + \sum_{q>0} \Gamma_q \left(\mathscr{M}_q^2 + \mathscr{M}_{-q}^2\right) \tag{3.156}$$

$$\mathscr{M}_q^2 \equiv \frac{M_q^2}{(\Omega_q - \omega)^2 + (\Gamma_q - \gamma)^2}; \quad \mathscr{M}_{-q}^2 \equiv \frac{M_{-q}^2}{(\Omega_q + \omega)^2 + (\Gamma_q + \gamma)^2}. \tag{3.157}$$

When no complex-energy eigenmodes is present, the imaginary part of the strength is always negative. Conversely, if the frequencies Γ_q are large enough, (3.156) becomes positive. Hence, a positive imaginary part of S always implies the instability of the system with respect to the perturbation. Equation (3.156) can be used to give the following bounds:

$$\Gamma_{\min} < \gamma \frac{\sum_{q>0} \mathscr{M}_q^2 - \mathscr{M}_{-q}^2}{\sum_{q>0} \mathscr{M}_q^2 + \mathscr{M}_{-q}^2} \quad \mathrm{Im}\{S(F,\omega_\gamma)\} < 0, \tag{3.158}$$

$$\Gamma_{\max} > \gamma \frac{\sum_{q>0} \mathscr{M}_q^2 - \mathscr{M}_{-q}^2}{\sum_{q>0} \mathscr{M}_q^2 + \mathscr{M}_{-q}^2} \quad \mathrm{Im}\{S(F,\omega_\gamma)\} > 0. \tag{3.159}$$

More drastically, the strength is non-zero on the imaginary axes only when instabilities are present.

$$\mathrm{Im}\{S(F,\omega_\gamma = i\gamma)\} = 0 \Leftrightarrow \gamma \sum_{q>0} \left(\mathscr{M}_q^2 - \mathscr{M}_{-q}^2\right) = \sum_{q>0} \Gamma_q \left(\mathscr{M}_q^2 + \mathscr{M}_{-q}^2\right). \tag{3.160}$$

This is shown in two steps. First, because the eigenvalues come in pair, Eq. (3.156)

becomes

$$\mathrm{Im}\{S(F,\omega_\gamma = i\gamma)\} = -\gamma \sum_{q>0} \frac{M_q^2 - M_{-q}^2}{\Omega_q^2 + \gamma^2}, \quad \text{if } \Gamma_q = 0 \text{ for all } q. \tag{3.161}$$

For a Hermitian probe, $F = F^\dagger$, implying the matrix elements M_q^2 and M_{-q}^2 are equal. Having no complex eigenvalues thus causes (3.161) to be equal to zero for imaginary excitation frequencies. Second, assuming there is at least one $\Gamma_q \neq 0$ (and $F = F^\dagger$ for consistency with the previous equation), there exist frequencies such that $\gamma \ll \Omega_q^2 + \Gamma_q^2$. Expanding the denominators to second order and keeping terms up to γ^3, one obtains by imposing $\mathrm{Im}\{S\} = 0$ on the imaginary axis

$$-\gamma \sum_{\substack{q>0 \\ \Gamma_q \neq 0}} \frac{M_q^2}{(\Omega_q^2 + \Gamma_q^2)^2}(\gamma^2 - 2\gamma\Gamma_q) = \sum_{\substack{q>0 \\ \Gamma_q \neq 0}} \frac{M_q^2}{\Omega_q^2 + \Gamma_q^2} \left(1 + \gamma^2 \frac{1 + 4\Gamma_q^2}{(\Omega_q^2 + \Gamma_q^2)^3}\right). \tag{3.162}$$

Being a polynomial in γ, in only has a finite number of roots. Finding $\mathrm{Im}\{S\} = 0$ along the imaginary axis thus gives a proof of the stability of the ground state with respect to the perturbation.

3.9 Resonance broadening

The linear approximation at the heart of the theory implies that the excited states, regardless of their collective or individual character, do not couple to each other. As such, the theory is not able to give a width to the strength obtained from the eigenmodes. However, experimental measurements show that the resonances do possess a generally sizeable width. Besides those introduced by the measurement apparatus, the phenomena responsible for the broadening of the response spectra can be separated in two categories:

- On the one hand, several effects are due to the many-body character of the systems we look at. Namely, we typically distinguish three phenomena [HW01, Ch. 1]:
  - The coupling to excitations of richer nature, i.e. 2p2h/4qp, and higher. To these is associated a spreading width Γ^s;
  - The coupling between collective and individual states, causing the fragmentation of the resonance through the opening of several decay channels. It is characterised by the so-called Landau damping, of width Γ^L;
  - The coupling to continuum states, to which can be associated an escape width Γ^e. It is generally assumed to be much weaker than the two others for stable systems. However, in systems containing few nucleons and/or close to instability, coupling to continuum can be of sizeable importance.
- A Doppler broadening due to the thermal motion of the particles. While this effect is often overlooked, it gives a significant contribution to the spectral width at temperatures relevant for astrophysical processes. Figure 3.2 gives the relative thermal

broadening for a non-relativistic macroscopic gas at thermal equilibrium. For temperatures of a few MeV, the broadening can be of about $1-5\%$ of a resonance's energy. This effect is more pronounced for light nuclei.

The non-thermal effects result in a Lorentzian smearing, which is accidentally modelled by the parameter γ. On the other hand, thermal effects not only enhance the Lorentzian smearing (because the strength becomes more fragmented), but also produce a Gaussian broadening. Even by staying at the linear response approximation, offering the possibility for the system to have a non-zero temperature adds a macroscopic degree of freedom. For atomic nuclei, the relative Doppler broadening starts to be of a few per cents for $k_BT \sim 1$ MeV, as can be seen in figure 3.2. Using macroscopic estimations, the thermal width of a giant resonance in a system of A nucleons evolves as $A^{-1/2}$, and is thus a relatively moderate function of the mass. Temperatures relevant for neutron stars physics are of the order of $\sim 1-2$ MeV [Pot10; Lat15], for which the thermal broadening of a giant resonance in ^{56}Fe is of a few hundreds of keV to about half a MeV. Since at finite temperature, the response function is in general quite fragmented due to several excitation channels opening, such Doppler broadening might contribute in sizable extents to the total width of the strengths, which at zero temperature are generally of about 5 MeV.

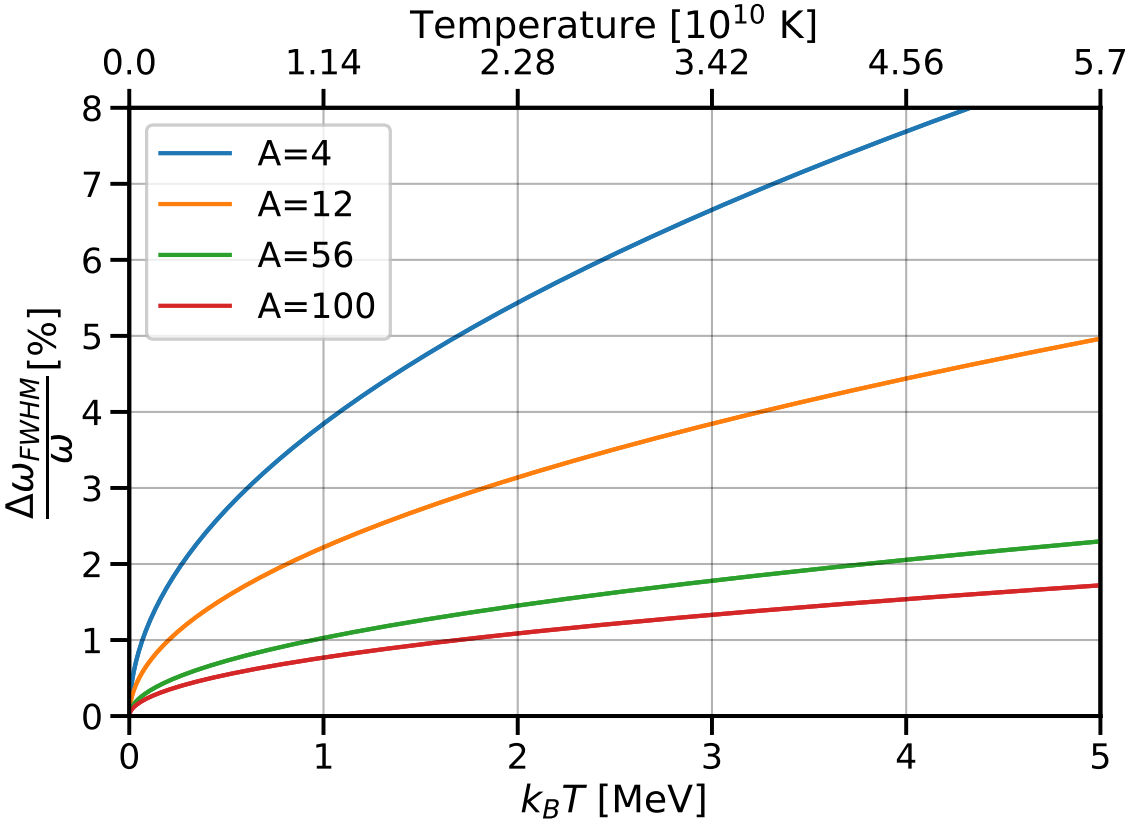

Figure 3.2: Evolution of the relative thermal width of spectral lines as a function of the temperature and atomic mass.

In the case of neutron stars, the interaction of the nuclei with their environment could play a considerable role [Peñ+11; KMC00; KMC01], so that this model of isolated nuclei is by no means expected to be valid in presence of extremely high magnetic fields. Additionally, it assumes all nuclei are perfectly thermalised, which may very well not be the case in realistic situations, e.g. in the case of newly formed neutron stars, whose temperature drops by five to six orders of magnitude within a few years [Pot10; Lat15], although pairing correlations [For+10], electronic collisions and interaction with photons can significantly accelerate the cooling. Finally, since the structure of the nuclei is strongly affected by their temperature, thermal effects cannot be faithfully represented by the overly simplistic form of a Gaussian spreading of the zero-temperature spectral function: strictly speaking, the effect of the temperature on nuclei in a macroscopic body should be accounted for by drawing T from their temperature distribution, then summing their responses altogether to obtain the properly weighted average:

$$S(F,\omega_\gamma,T_{\text{bath}}) = \int \mathrm{d}T p(T_{\text{nucl}} = T \mid T_{\text{bath}}) S(F,\omega_\gamma,T), \tag{3.163}$$

$p(T_{\text{nucl}} = T \mid T_{\text{bath}})$ being the probability of finding a nucleus with temperature T within a bath at temperature T_{bath}[22].

For crude estimations of the thermal broadening of a particular resonance mode and nucleus, one can use the macroscopic formulae of [Cho97]. In particular, these tell us that the thermal broadening should be the most important in case of iso-vector quadrupole oscillations. As for low-lying resonances, which in general are of single-particle character, the effect of temperature is expected to be much stronger, since the participant orbitals are those with energy close to the Fermi energy.

3.10 QFAM in harmonic oscillator basis: selection rules

3.10.1 From the external probe

A convenient approach to the treatment of collective excitations is to study the response of the system to a probe of well-defined multipolarity. Indeed, a given multipolarity comes along with its associated selection rules, so that one can, owing to the linear approximation, decompose the total response of the system to any kind of perturbation as a sum over the different projections of the angular momentum:

$$F(\omega) = \sum_{\substack{J,K \\ K \text{ all} \neq}} c_{JK}(\omega) Q_{JK} \rightsquigarrow S(F,\omega) = \sum_{\substack{J,K \\ K \text{ all} \neq}} c_{JK}(\omega) S(Q_{JK},\omega). \tag{3.164}$$

This translates into the fact that for a given J, the different $K = -J, -J+1, \ldots, J$ can

[22] If the ensemble {nuclei+bath} is in statistical equilibrium and the nuclei form a gaseous state, one has $p(T_{\text{nucl}} = T \mid T_{\text{bath}})$ equal to the Maxwell-Boltzmann distribution.

be studied separately.

A typical means of exciting a system is through an electromagnetic (EM) probe. The structure of the corresponding EM operators Q_{JK} must follow that of the basis employed for the expansion of the wave functions, in order to assure the decoupling (3.164) of the excitations. In this work, the computational basis is that of an axially symmetric harmonic oscillator, of which the states can be assigned well-defined quantum numbers[23]. A multipolar excitation can thus be characterised in this basis by three numbers:

- its quantum number J, characterising the transfer of total angular momentum;
- its quantum number K, characterising the change in the projection of $\vec{J}$ along the symmetry axis;
- its quantum number S, characterising the change of spin, and therefore the electric ($S = 0$) or magnetic ($S = \pm 1$) character of the excitation.

In practice, the axial basis can be arranged such that its vectors are grouped by their value of the quantum number $\Omega = m + \sigma$, corresponding to the projection of the total angular momentum (orbital m + spin σ) on the symmetry axis. The structure of the Q_{JK} operator then becomes block-diagonal in K:

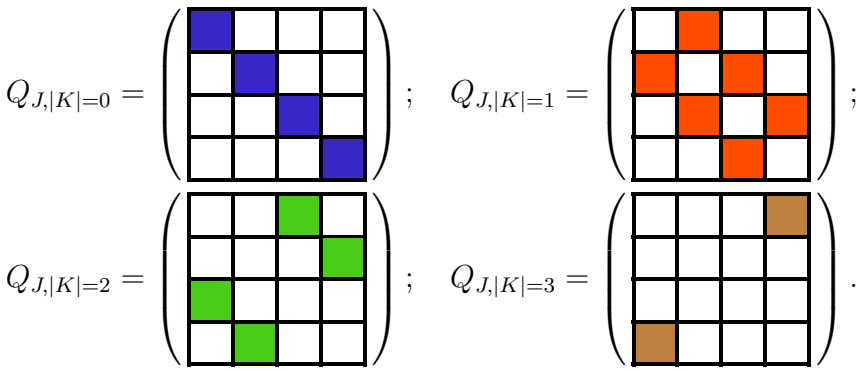

3.10.2 From the interaction

The interaction is taken to be a scalar in the both two-body and three-body Ω, τ, π spaces; that is, it does not change the overall angular momentum projection, isospin and parity. The conservation of angular momentum and parity result from the isotropy of space. In parallel, since the gauge bosons carrying the strong interaction, the gluons, have no electric charge, the residual interaction cannot change the total isospin of the particles it acts on. This implies that the following selection rules are always verified by the matrix elements $v_{\alpha\gamma\beta\delta}$ and $w_{\alpha\gamma\epsilon\beta\delta\zeta}$ of the interaction[24]

[23] The axial harmonic oscillator basis is presented in a bit more details in appendix E.

[24] Note that the rules in the anomalous sectors are given with the convention $v_{\alpha\beta\gamma\delta}$ and $w_{\alpha\beta\epsilon\gamma\delta\zeta}$. For the convention (used throughout this document) of keeping the same ordering for both sectors, the selection rules are those of the normal case.

Normal sectors

$$\Omega_\alpha + \Omega_\gamma = \Omega_\beta + \Omega_\delta \quad (3.165)$$
$$\tau_\alpha + \tau_\gamma = \tau_\beta + \tau_\delta \quad (3.166)$$
$$\pi_\alpha + \pi_\gamma = \pi_\beta + \pi_\delta. \quad (3.167)$$

Anomalous sectors

$$\Omega_\alpha + \Omega_\beta = \Omega_\gamma + \Omega_\delta \quad (3.168)$$
$$\tau_\alpha + \tau_\beta = \tau_\gamma + \tau_\delta \quad (3.169)$$
$$\pi_\alpha + \pi_\beta = \pi_\gamma + \pi_\delta. \quad (3.170)$$

Normal sectors

$$\Omega_\alpha + \Omega_\gamma + \Omega_\epsilon = \Omega_\beta + \Omega_\delta + \Omega_\zeta \quad (3.171)$$
$$\tau_\alpha + \tau_\gamma + \tau_\epsilon = \tau_\beta + \tau_\delta + \tau_\zeta \quad (3.172)$$
$$\pi_\alpha + \pi_\gamma + \pi_\epsilon = \pi_\beta + \pi_\delta + \pi_\zeta. \quad (3.173)$$

Anomalous sectors

$$\Omega_\alpha + \Omega_\beta + \Omega_\epsilon = \Omega_\gamma + \Omega_\delta + \Omega_\zeta \quad (3.174)$$
$$\tau_\alpha + \tau_\beta + \tau_\epsilon = \tau_\gamma + \tau_\delta + \tau_\zeta \quad (3.175)$$
$$\pi_\alpha + \pi_\beta + \pi_\epsilon = \pi_\gamma + \pi_\delta + \pi_\zeta. \quad (3.176)$$

This leads to some relationships between the structure of the density matrix and the fields. If we define K such that $\Omega_\delta = \Omega_\gamma + K$ (resp. $\Omega_\delta = \Omega_\beta + K$) in the normal (resp. anomalous) sector, (3.165) (resp. (3.168)) implies $\Omega_\alpha = \Omega_\beta + K$ (resp. $\Omega_\alpha = \Omega_\gamma + K$). Therefore, if the density matrix contains coupling between elements differing by K, so do the h and Δ fields. The isospin and parity being both invariant under time-reversal, the selections rules (3.166)-(3.167) & (3.169)-(3.170) are also valid in the time-reversed sectors with no sign to be introduced. In addition, the invariance of quantum mechanics under time-reversal implies that the inter-nucleons interactions are invariant under this symmetry. Finally, the interaction must be the same if all the initial and final states are swapped consistently, as the indices labelling the states are evidently dummy. These two last properties come in handy when calculating the fields, and are for instance put to work in the derivations of (3.60) and (3.62).

3.10.3 Quantum numbers of the oscillations

In usual mean-field calculations, the matrices representing the many-body interactions can be brought to a form that is block-diagonal in the conserved quantum numbers[25]. The densities are mandated to have the same structure, and thus, so do the fields. The situation is slightly richer when a probe is included, since it is allowed to excurse outside the symmetry imposed to the unperturbed Hamiltonian, for which $K = 0$. It is easily verified[26] that the fields constructed by contracting the two- and three-body interactions with the off-diagonal densities have the same quantum number K. Then, the FAM amplitudes (3.8) always display the same structure as the operator $\mathcal{F}(\omega)$. Finally, transforming back to single-particle basis leads to transition densities non-zero only when they connect states with difference of the angular momentum projection of K. Altogether, the structure of the external operator propagates to all of the FAM densities and fields.

[25] This can be achieved simply by arranging the basis vectors appropriately.
[26] Sketching the operation as a block-wise product of two matrices does the trick.

Chapter 4

Application to thermal phase transitions

This chapter presents a succinct study of phase transitions triggered by temperature. Although these phenomena are usually studied in heavy nuclei, which exhibit properties closer to the thermodynamic limit, the work of this chapter is centered around the mid-mass system ^{56}Fe. The characteristic features of the phase transition can be well reproduced. The results are in good qualitative agreement with those observed in heavy systems.

Contents

4.1 Signatures of phase transitions

Colloquially, a phase transition is defined by the sudden and drastic change in the structure of the system. This is often realised by the different phases possessing different symmetries [Lan37][LL67b, Ch. 14]. Formally, the phase transition is identified with a discontinuity in a derivative of the free energy F. The modern classification labels phase transitions as discontinuous or continuous, depending on whether the entropy

$$S = -\left(\frac{\partial F}{\partial T}\right)_{N,V} \tag{4.1}$$

shows a discontinuity or not. The derivatives of the free energy are to be taken with respect to the parameter that is varied, namely the temperature in the present case. As the transition corresponds to an abrupt modification of the system's properties across the different phases, at least one macroscopic observable must undergo identical changes. There exists therefore a quantity characterising, loosely speaking, the extent to which the high-symmetry phase is broken down to the low-symmetry one. These are the so-called order parameters. An intuitive example is the shape phase transition in finite systems. An axially deformed phase breaks $SO(3)$ down to $SU(2)$, and is identified by a non-zero quadrupole moment β_{20}. The transition from a spherical to a deformed phase therefore occurs as soon as β_{20} departs from zero. The high-energy phase typically has higher symmetry than the low-energy one. This can be understood by arguing that at large energy, the degrees of freedom can explore a wider part of the parameter space, washing out the effects of the small region corresponding to a particular subgroup of the overall symmetry group of the high-energy phase. The situation is similar for the pairing transition, which breaks the particle number symmetry at low energy; the pairs break up as the temperature is increased, effectively restoring the $U(1)$ symmetry.

A somewhat more rigorous definition is that different phase of the system are characterised by different symmetries or topologies, that are identified with the expectation values of symmetry operators, which commute with the Hamiltonian in one phase but not in another. This translates in an order parameter acquiring a non-zero expectation value, that can be used as a gauge of the extent to which the symmetry is broken. For instance, a superconducting phase involves a non-zero pair creation gap, whereas a normal phase corresponds to disfavoured pair condensation. The corresponding order parameter is the pairing gap, or equivalently the pairing energy. Likewise, a deformed ground state is not invariant under rotations, and thus exhibits one or more non-zero expectation values of multipolar moments.

In this chapter, we study the shape phase transition of the deformed nucleus ^{56}Fe. The lighter ^{46}Ti and ^{44}Ti display a step-like collapse of the deformation, and are therefore discarded for this thermodynamically inclined analysis. Iron is found to exhibit an oblate shape. The evolution of the appropriate order parameter, namely the quadrupole deformation β_{20}, is studied as a function of the temperature. This allows to identify the critical temperature T_C and observe the behaviour of thermodynamical parameters deriving from the free energy. The convergence with respect to numerical parameters of the axial har-

monic oscillator basis is studied, as well as the convergence as different orders in the chiral interaction are included.

4.2 Motivation for studying ^{56}Fe

A fine understanding of nuclear structure and reactions is required if one desires to accurately describe the giant resonances, and by such the origin and abundances of chemical elements [Bur+57]. The whole nucleosynthesis can schematically be split into two parts, corresponding to the formation of light to mid-mass nuclei, and the generation of heavier ones. From the appearance of light nuclei through the cooling down of the early universe, a gravitational collapse of protostellar clouds (composed of hydrogen in atomic or molecular form, helium and, to a lesser extent, of nuclei up to carbon) may trigger thermonuclear fusion, and hence the genesis of stars. High pressure and temperature cause nuclear reactions to abound. Illustratively, the combustion of hydrogen towards heavier nuclei is a series of energetically favoured processes, up to iron and nickel. During the late stages of stellar nucleosynthesis, the earlier-formed silicon nuclei capture alpha particles towards ^{56}Ni [Cla68, Ch. 7]. This nucleus undergoes beta-decay towards ^{56}Co, which also converts one of its protons to form ^{56}Fe. Having one of the highest fractional binding energies of the whole nuclide chart [Few95], the chain stops here. This explains the abundance of iron in the universe [Cla68; LPG09; AG20] and its role as a starting point for the formation of heavier nuclei through the s-process [Hil78; MC90; CT04] that occurs during the late life of stars with about one to eight solar masses [Boo06]. Knowing of the rates at which these reactions occur is key to faithful prediction of nucleosynthetic processes. The status of this iron isotope as both an accumulation point of the silicon burning stage and a starting point for the nucleosynthesis of heavier elements calls for an in-depth understanding of the structure of its ground and excited states. The present chapter analyses and discusses the effects of coupling to a thermal bath on the bulk properties of ^{56}Fe.

4.3 Results

4.3.1 Foreword: mean-field and expectations from ab initio interactions

In case of a microscopic theory, the exact, many-body Schrödinger must in principle be solved. However, its exponentially increasing dimension with the number of degrees of freedom often makes such an approach a daunting task. As an alternative, we resort to a Hartree-Fock-Bogoliubov mean field theory, including superfluidity (see subsection 2.4.2). Furthermore, we allow the breaking of the rotational $SO(3)$ symmetry down to an axial ($SU(2)$) one, as a means of grasping additional correlations at a mild cost by letting the system explore a landscape of lesser symmetry. While breaking symmetries may seem curious for finite systems, this approach can be phenomenologically justified. For deformation, several types of quantum systems (atoms, molecules and nuclei alike) do exhibit rotational bands, that can only exist in non-spherical bodies. In case of pairing interactions, the odd-even staggering effect signals an increase of binding energy for systems possessing even numbers of nucleons. This suggested the possibility of pairing in atomic

nuclei early on [BMP58]. It is important to note that on average, symmetries are preserved in finite systems: while frameworks allowing for their breaking are allowed and motivated by empirical facts, the story must be complemented by a symmetry-restoration step in order to obtain eigenstates exhibiting the same symmetries as the Hamiltonian. Additional correlations beyond the single-reference mean-field can be obtained by including mpmh correlations in a perturbative manner [Tic+16; Tic+18; TRD20] or not [DS15; Qiu+19; BD21], and carrying a projection onto the desired symmetries.

On the other side, interactions derived from an effective theory become less reliable as the size of the system increases. Indeed, in order to maintain the connection to QCD, the low-energy constants must be adjusted on few-body data, and as such, the quality of the predictions degrades with increasing masses by lack of four-body (and higher) terms. The derivation and production of high-rank interactions is a highly involved endeavour [Her+13; Hup+13; Rot+14]. Extending the reach of ab initio methods to higher masses is a task currently being undertaken [Som+14; Her20]. It should be pointed out that the ab-initio interactions are known for providing differential quantities (e.g. nucleonic separation energies) in better agreement with experiment than the integrated values such as the total binding energies. Still, neither can rival the results obtained with phenomenological interactions, that are adjusted over the whole nuclear chart, and thus yield more accurate results on average.

The results presented in this thesis thus rest on the arguable balance of tackling mid-mass systems. On the one hand, mean field approximations are not well-suited for light systems, where the contribution from individual particles with respect to the bulk can be non-negligible. Alternatively, the use of ab initio interactions, adjusted on few-body data, becomes questionable for large numbers of particles, at least when using a simple HFB framework. Despite this apparent flaw, we can stress two points. First, the relevant quantities for the study of temperature on FTHFB results are calculated as differences or differentials, we can thus expect a correct quantitative behaviour even if the ground state energy is shifted from the experimental values. In case of the FTFAM, simple particle-hole type excitations over a ground state are considered. The energy differences between single-particle states being in general overestimated, we can expect the strengths function obtained in the next chapter to overestimate the excitation energies, although the qualitative behaviour should be correct. On the other hand, the self-consistent solution of the FAM equation incorporates collective correlations, and as such contribute in correcting the quasiparticle self-energies. Second, the improvement of "raw" FTHFB results is still possible by any of the previously mentioned techniques (provided they are formalised for non-zero temperatures). Although our results on binding energies, radii, or deformations are no match for those given by phenomenological interactions, they remain relevant as first steps towards the extension of usual mean-field-and-beyond techniques to the finite temperature regime within an ab initio setting.

4.3.2 Convergence with model space parameters and chiral order

The calculations performed here depend on several parameters: the frequency $\hbar\Omega$ of the harmonic oscillator employed to construct the basis functions, the number of single-particle basis functions (characterised by the integer e_{max}), the relative length of the oscillator in the radial and axial directions[1], and the order in the chiral expansion, to name the most important. The axial and radial oscillator frequencies could be optimised simultaneously, but are always taken to be equal. The three first are essentially numerical parameters to be optimised in order to obtain the lowest energy, whereas the latter has a clear physical meaning and will be discussed in a following section.

The oscillator frequency controls the stiffness of the basis functions: a large (resp. small) frequency corresponds to narrow (resp. spread out) wave functions. In the $\hbar\Omega \to 0$ limit, the wave functions become those of plane waves, for which achieving localisation can sensibly be conceived to be more difficult than when using a non-zero frequency. On the other hand, the $\hbar\Omega \to \infty$ translates into basis function sharply localised around the centre of the coordinate frame, so that the system can only be much more localised than its ground state shape within an otherwise identical model space. These two extreme cases should thus lead to ground state energies far above the minimum of $E(\hbar\Omega)$. A reasonable choice for $\hbar\Omega$ can be to have resulting eigenfunctions with a spatial extent close to the expected (e.g. estimated from a hard-sphere formula) radius of the nucleus, although the dependence of the radius on the shell structure makes this guess usually land off the optimal value. Taking $\hbar\Omega$ according to a liquid drop formula, $\hbar\Omega \propto A^{-1/3}$, can nonetheless provide a starting point for scanning a range of oscillator frequencies.

On the opposite side, increasing the size of the model space must unambiguously lead to lower ground state energies, all other parameters being equal. The $e_{max} \to \infty$ is obviously unreachable, as it would require infinitely many basis functions. Since the energy is expected to converge smoothly with the size of the model space, one can instead study the convergence by carrying calculations with a set of different values of e_{max}. It should be noted that the energy is the only quantity for which this monotonous convergence is guaranteed, by the variational principle underlying the resolution of the equations of motion.

Interpolations in oscillator frequency

Assuming the shell structure of the nucleus under study is relatively independent of $\hbar\Omega$, one can presume that the energy does not vary too abruptly with the oscillator frequency about the optimal value. It is thus reasonable to suppose the energy to be a quadratic function of $\hbar\Omega$ when close to the best frequency. This can be used to interpolate numerically the optimal oscillator frequency, and obtain the corresponding energy, or an estimate thereof, straight from the polynomial regression.

[1] Because Ω is the geometric mean of the oscillator frequencies in the two directions, one can either take their ratio and Ω as the parameters of the basis, or the two oscillator lengths, both choices being strictly equivalent.

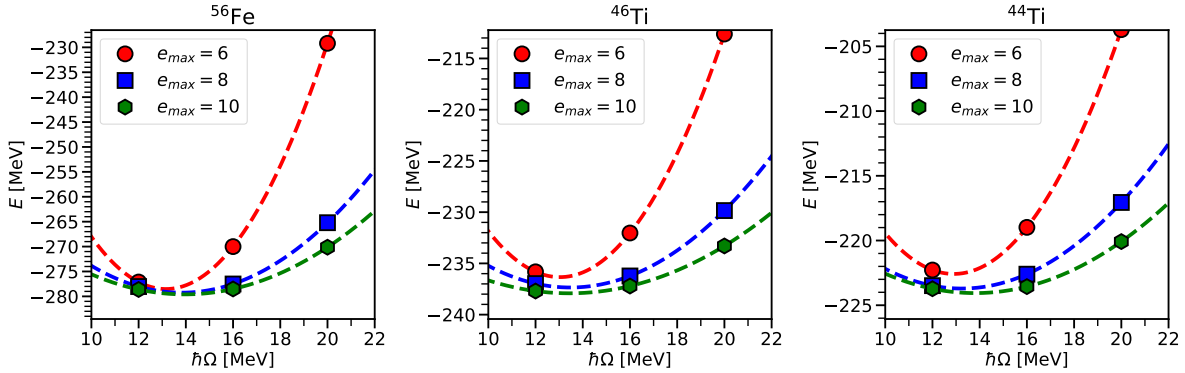

Figure 4.1: Ground state energies as a function of the oscillator frequencies at $e_{max} = 6, 8, 10$ with $e_{3max} = 14$.

Figure 4.1 summarises the ground states obtained for three different values of $\hbar\Omega$, for all three nuclei considered. Different values e_{max} of the single-particle model space are employed, and we use the N^{3}LO interaction. The calculated energies are interpolated with a quadratic polynomial in order to identify the supposedly optimal oscillator frequencies, along with the corresponding energies. The results are given in table 4.1. While a more in-depth study of the convergence with the oscillator frequency would require more values of $\hbar\Omega$, in order to employ supplement the extrapolated values with statistical uncertainties[2]. Interactions matrix elements with different frequencies than the ones presented here were not available at the time these calculations were carried; we therefore restrict to the three given values. Owing to the energies being very close to their interpolated optimal value and the fact the corresponding frequencies lie within the studied ones, we can be confident that the interpolated energies are very close to the true minimal ones.

Nucleus	$\hbar\Omega$ (best) [MeV]	E [MeV]	$\hbar\Omega$ (interp.) [MeV]	E (interp.) [MeV]	diff (%)	$E_{exp.}$ [MeV]
^{56}Fe	12	-278.62	14.0	-279.60	0.35	-492.26
^{46}Ti	12	-237.30	13.4	-237.70	0.17	-398.19
^{44}Ti	12	-223.72	13.8	-224.01	0.15	-375.47

Table 4.1: Lowest ground state energies obtained within the set $\hbar\Omega = (12, 16, 20)$ for $(e_{max}, e_{3max}) = (10, 14)$. The interpolated optimal values are also given; the last column is the relative difference between E and E(interp.), calculated as $(E(\text{interp.}) - E)/E(\text{interp.})$. The last column gives the experimental binding energies from the NuDat database [Bro08].

One observes that the energy is less sensitive to the frequency as the number of basis states increases, as a larger number of basis functions is more flexible in accommodating a less suitable choice of $\hbar\Omega$. In the limit of an infinite-dimensional model space, the frequency should be irrelevant; the energy should be identical for all frequencies. Although the model spaces are not so large, a very good convergence of the energies is achieved, especially when the oscillator frequency is close to its optimal value. As already mentioned in the foreword, ab initio interaction are unable to reproduce the experimental binding

[2]These are of course determined by the used fitting function, which is itself conditioned by the dependence of the energy on the oscillator frequency (and dimension of the model space). To the best of my knowledge, no such formula has been derived for schematic models.

energies when only a single mean field is employed, as can be seen from the rightmost column.

Although for all nuclei, the energy varies in less than 5% among the three frequencies employed at $e_{max} = 10$, this does not guarantee the convergence of all observables. The ground state quadrupole deformations and radii are displayed in figures 4.2-4.3 in order to verify whether these quantities vary in similar magnitude. While all three observable depend on the nucleonic densities, it can be anticipated that they do not vary to similar extents with the spatial extension of the basis functions. The energy is a spatial integral involving the local parts of the densities and mean-fields. Since these typically resemble each other (the density is higher in the regions where the potential is higher in absolute value), an overall quite reasonable variation of the energy with the basis frequency can be expected. Conversely, the quadrupole moment is more directly sensitive to the density distribution, as the corresponding operator, Q_{20}, is not a functional of the densities. Changing the stiffness of the basis functions should have large consequences on the overall shape of the system, resulting in deformations more strongly dependent on $\hbar\Omega$ that the energy is. Finally, since the spatial matter density does not take particularly exotic shapes, but is instead rather constant (at around the saturation density $\rho_0 = 0.16$ fm^{-3}), we can presume the point-particle radii to vary fairly less than the deformations.

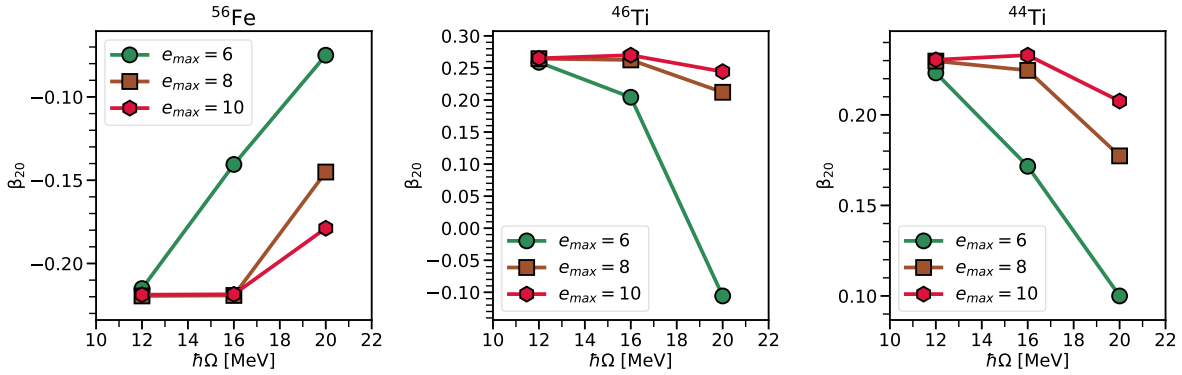

Figure 4.2: Same as figure 4.1 for the quadrupole moments.

The quadrupole moments are found to exhibit a strong dependence on the frequency of the basis. At $e_{max} = 8$, their values at $\hbar\Omega = 20$ MeV are 20-40% off the $\hbar\Omega = 12$ results, while the larger basis $e_{max} = 10$ diminishes the discrepancies roughly by a factor of two. Although the energy also displays non-negligible dependence on the oscillator frequency, the β_{20} observable varies in much greater amounts. This hints that the study of deformation-dependent observables (e.g. inertial masses, rotational and vibrational spectra) requires a careful verification that the numerical parameters of the model space are optimised, even in cases where the energy does not vary too much. On the other hand, at $e_{max} = 10$, the radii of all three nuclei are observed to vary within a few percents only, showing relative variations of the same order as the energies. Note that the trend in the evolution of β_{20} and R with $\hbar\Omega$ can be understood on the basis that larger oscillator frequencies correspond to more squeezed basis functions, which yields smaller deformations

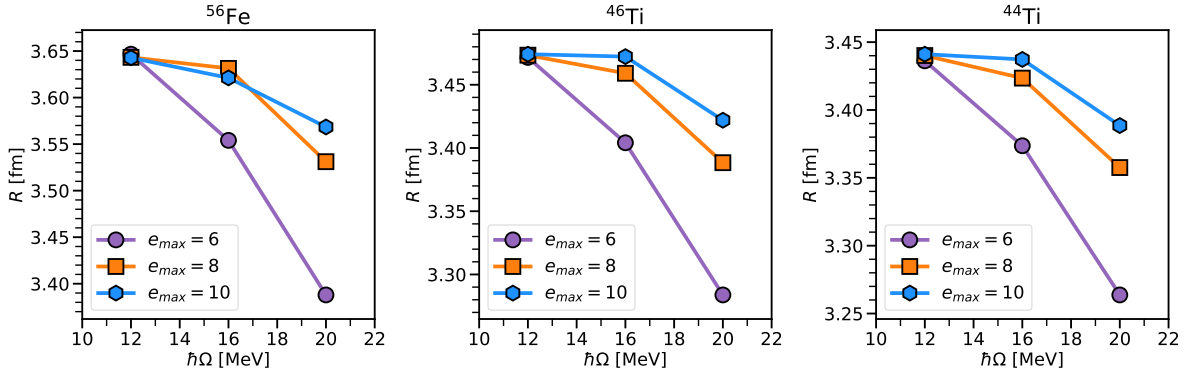

Figure 4.3: Same as figure 4.1 for the point-particle radii.

and radii.

It appears that for all three nuclei, the optimal oscillator frequency among the available ones is $\hbar\Omega = 12$. The seemingly good agreement between the results obtained with the different values of e_{max} suggests that the convergence with the dimension of the model space is well-reached; this point is discussed in the next subsection.

Extrapolations in basis size

Owing to the variational principle, the energy is guaranteed to always decrease when the size of the basis employed for expanding the solution of the equations of motion is increased. This is not true for other observables[3]. In addition, within a given set of basis functions (harmonic oscillator, plane waves, etc), one typically selects the ones that correspond to the lowest eigenvalues of the Hamiltonian defining the basis. Thus, increasing the size of the model space adds functions of increasing eigenvalues, hence the corrections to the energy should get smaller when the model space becomes larger. In practise, the energy difference between finite and infinite basis size is found to be well-approximated by a decreasing exponential [MVS09; VBG09; Tic+19; Sán+20], see also [Lüs86; FMP14; Dum+18] for a complete and rigorously derived formula.

Tables 4.2, 4.3 and 4.4 gather the energies, quadrupole moments and radii for the three nuclei, at $e_{max} = 8, 10$. The three-body space is truncated at $e_{3max} = 14$. The relative differences between the two values of e_{max} are also given. Prior to analysing the discrepancy between our $e_{max} = 8$ and $e_{max} = 10$ results, it is worth mentioning that:

i) The ground state energies strongly differ from the experimental measurements, due to ab initio interactions not being able to incorporate strongly collective correlations in the single mean-field reference approximation, as a result of being adjusted on few-body data[4],

[3] For instance, the convergence of other quantities sometimes resembles exponentially damped oscillations; extrapolating on these bears little meaning in general and is quite dubious.

[4] and therefore, not resuming implicitly these correlations like EDFs do.

ii) No experimental data for the ground state deformations being available, we resort to comparing with the available EDF predictions of [BN20] and [HG07], and observe a mismatch of the β_{20} values between EDF and ab initio results for ^{56}Fe, and between all three calculations for ^{44}Ti. Besides the fact that such masses touch on the verge of the current ab initio interaction's reach (at least within a single-reference HFB approach), we note that ^{56}Fe posses both oblate and prolate minima, the oblate being lower in our calculations. On the other hand, the softness of ^{44}Ti, especially towards the prolate deformations, explains why we find such different quadrupole moment.

	E [MeV]	β_{20}	R [fm]
$e_{max} = 8$	-277.51	-0.2192	3.6313
$e_{max} = 10$	-278.62	-0.2187	3.6427
diff. (%)	0.40	0.20	0.31

	E [MeV]	β_{20}	R [fm]
DD-PC1	-489.63	0.24	3.6931
D1S	-488.84	0.20	x

Table 4.2: Selected ground state observables for ^{56}Fe at $e_{max} = 8$ and 10 (left), and fully converged EDF results for a relativistic (DD-PC1) and a non-relativistic (D1S) functional (right). The three-body space is truncated at $e_{3max} = 14$. The relative difference on an observable X is calculated as $|X(e_{max} = 10) - X(e_{max} = 8)/X(e_{max} = 10)|$, and is rounded up to two decimal places. The experimental charge radius is $R_{ch}^{exp} = 3.7377 \pm 0.0016$ fm [AM13].

	E [MeV]	β_{20}	R [fm]
$e_{max} = 8$	-236.92	0.2625	3.4591
$e_{max} = 10$	-237.30	0.2650	3.4742
diff. (%)	0.16	0.94	0.43

	E [MeV]	β_{20}	R [fm]
DD-PC1	-397.11	0.24	3.5040
D1S	-396.04	0.20	x

Table 4.3: Same as table 4.2 for ^{46}Ti. The experimental charge radius is $R_{ch}^{exp} = 3.6070 \pm 0.0022$ fm [AM13].

	E [MeV]	β_{20}	R [fm]
$e_{max} = 8$	-223.49	0.2329	3.4234
$e_{max} = 10$	-223.72	0.2304	3.4411
diff. (%)	0.11	1.10	0.51

	E [MeV]	β_{20}	R [fm]
DD-PC1	-373.60	0.15	3.4478
D1S	-372.97	0.00	x

Table 4.4: Same as table 4.2 for ^{44}Ti. The experimental charge radius is $R_{ch}^{exp} = 3.6115 \pm 0.0051$ fm [AM13].

For all three systems, the macroscopic observables are quite well converged with respect to the basis sizes we use. This however holds only close to the optimal frequencies; see figures 4.1, 4.2, 4.3 where the discrepancy between $e_{max} = 8$ and $e_{max} = 10$ reaches much higher levels for $\hbar\Omega = 20$. The fact all three observables are converged within roughly one percent or less is a first hint that the model space $(e_{max}, e_{3max}) = (10, 14)$ with $\hbar\Omega = 14$ is large enough to describe the structure of the system. One can go a small step further,

by applying the aforementioned extrapolation to apprehend the $e_{max} \to \infty$ limit. The energies are fitted with

$$E(e_{max}, \hbar\Omega) = E_\infty(\hbar\Omega) + A(\hbar\Omega) \exp^{-b(\hbar\Omega)e_{max}}, \tag{4.2}$$

and, for a given nucleus, we call the best extrapolated value the energy $\min_{\hbar\Omega=12,16,20} E_\infty(\hbar\Omega)$.

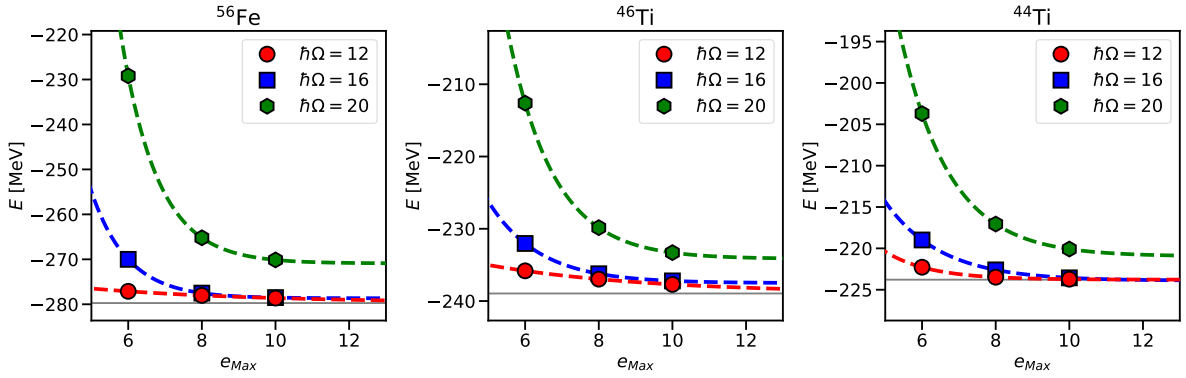

Figure 4.4: Evolution of the ground state energies with e_{max}. The dashed lines represent the fitted curves, and the grey lines denote the best extrapolated values. The model space used has $e_{3max} = 14$.

	^{56}Fe	^{46}Ti	^{44}Ti
$E(e_{max} = 10)$	-278.62	-237.30	-223.72
E_∞	-279.73	-238.95	-223.78
diff. (%)	0.40	0.69	0.03

Table 4.5: Values and relative differences between the energies obtained at $e_{max} = 10$ and their extrapolation. The results are given for $\hbar\Omega = 12$ MeV. The differences are calculated as $(E_\infty - E(e_{max} = 10))/E_\infty$.

The corresponding values are given in figure 4.4, and the relative differences are listed in table 4.5. In all nuclei, the extrapolated values are astonishingly close to the finite-basis results, which testifies once more that the convergence is well-attained. This conclusion is consistent with the results of [Tic+19; Hop+21], that use the same potentials, regulator and SRG evolution, with a slightly different adjustment of the coupling constants. However, the obtention of different extrapolated values when using different frequencies signals that the extrapolation (4.2) does not exactly hold; it is rather a convenient and simple tool to gauge the convergence with e_{max}, and can only be given a meaningful meaning when associated with covariances.

Convergence in the chiral expansion

The two previous parameters, while bearing a more or less pronounced physical meaning, can be classified as principally numerical. On the completely opposite side, how many

orders are included in the chiral expansion is entirely physical, and the convergence of the expansion with the order of the expansion and classes of diagrams included can be used as a tool to gauge the quality of the interaction [MS16]. The present work uses a novel family of pionful [EKM15; Bin+18; Hüt+20] interactions containing all two- and three-body nucleon-nucleon interactions up to next-to-next-to-next-to-leading order (N^3LO). A similarity renormalisation group (SRG) procedure is applied to the interaction, in order to recast four-body and higher terms into the two- and three-body matrix elements. The comparison of the N^3LO results with the ones obtained by restricting the expansion to lower orders allows for a systematic assessment of the systematical errors associated to the truncation of the chiral expansion. The error on an observable at a given order is calculated as in [EKM15; Bin+18; Hüt+20]. The leading-order (LO) interaction being of poor quality, it is not included in the calculations; all LO observables are attributed the value zero. As we were not provided with the NLO interactions at $\hbar\Omega = 12$ MeV, the convergence with the chiral order in both this chapter and chapter 5 is studied at $\hbar\Omega = 16$ MeV, for which the ground state energies are at worst 0.2% higher.

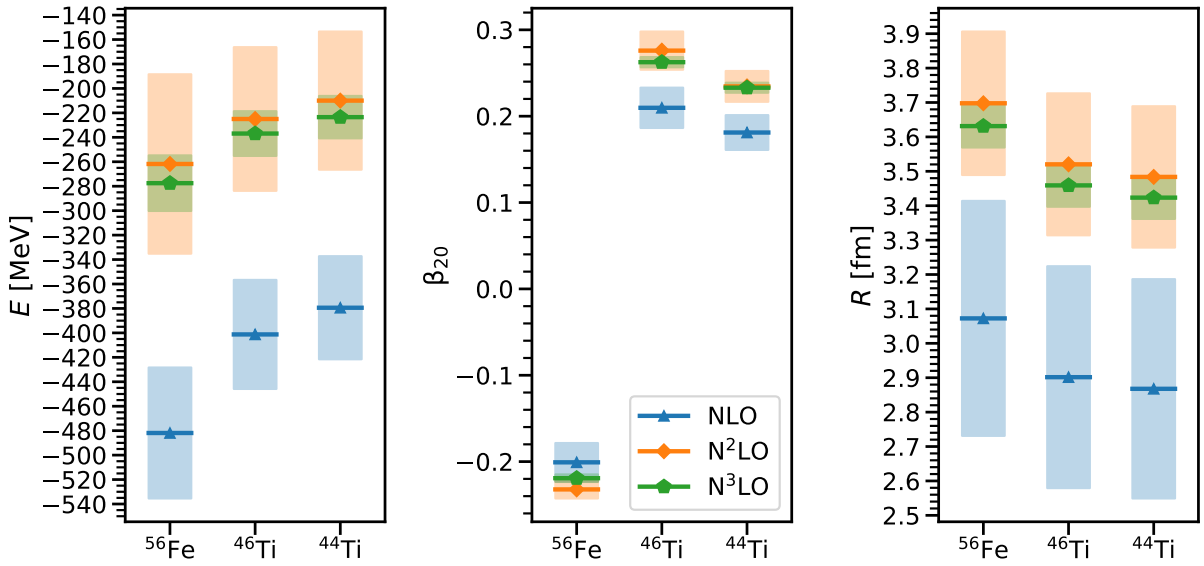

Figure 4.5: Ground state energies, quadrupole moments and radii at NLO, N^2LO and N^3LO for ^{56}Fe, ^{46}Ti and ^{44}Ti at zero temperature. The model space is $(e_{max}, e_{3max}) = (10, 14)$ and $\hbar\Omega = 16$ MeV.

Figure 4.5 shows the ground state energies, deformation order parameter and radii obtained for all three orders of the chiral interaction. For all observables, the N^2LO and N^3LO values lie almost always within each other's uncertainties range. More quantitatively, we find the systematic uncertainty at N^3LO to be of about 8% for the energy, and 2% for the quadrupole moments and radii; this for all three nuclei. This indicates that the interaction is starting to yield converged results with respect to the chiral order, at least at zero temperature. This observation will be put to the test when non-zero temperatures are enforced.

4.3.3 Shape transition in ^{56}Fe

At zero temperature, the vast majority of atomic nuclei are found by experiment [Nis+17; Gaf+13; Yan+04; Yan+03; Iwa+01; Mot+95; Orr+91; Dét+83; Dét+79] and theory [Möl+16; Möl+95; BBH06; HG07; RB11] to have a deformed ground state shape, quadrupole deformations being particularly frequent. When the temperature is increased, the nucleons distribute over all the possible shells, which results in the individual properties of each one being washed out. In particular, the shape of the system is thus expected to be driven back to sphericity when the temperature is high enough. As the order parameters associated to deformations are the expectation values of the multipole moments β_{LM}, their return to zero signals the restoration of spherical symmetry. The shape transitions in atomic nuclei have been studied theoretically already forty years ago [Mor73; Goo86; Goo90], albeit initially with simplified models. More recent calculations [MER03b; MER03a; Hil+12; RA15; ZN17; KN20] were able to used more advanced Hamiltonians or phenomenological (both covariant and non-relativistic) interactions and larger model spaces. In all studies, deformation is found to exhibit the same trend of a quick collapse when temperature increases. The findings of this chapter are essentially along the same lines, namely a second-order continuous shape transition, with a critical temperature of roughly 2 MeV. It can also be remarked that shape and pairing are principally driven by the occupations of open shells, and therefore are mainly surface phenomena with an important sensitivity to temperature. It is thus natural to expect a large degree of similarity in the evolution of pairing and deformation with temperature.

If the mean-field theory is able to satisfactorily describe the ground state of the system, then an independent particle picture should provide a qualitatively faithful representation of it. Under such circumstances, the thermodynamic properties should depend on temperature in a manner qualitatively similar to the case of a free fermion gas (FFG). These dependencies can be recovered quickly by remembering that the energy of a free gas is proportional to the temperature, and a first-order development of the Fermi-Dirac distribution around the chemical potential[5] shows that the energy window where thermal excitations are active has a width proportional to the temperature too. The thermal excitation energy $E^*(T) \equiv E(T) - E(0)$, defined as the difference between the energy of the ground state at temperature T and at zero temperature, is then expected to be proportional to T^2. The entropy and specific heat, respectively related to the first and second derivatives of the free energy $F \equiv E - TS$, are then both linear in T, except possibly at the phase transition temperature where the specific heat is found to be discontinuous[6]. More quantitative results can be found following the derivations of [LL67b, §57]: taking into account that we here have two different species -Z protons and N neutrons-, the excitation energy, entropy and heat capacity of the gas write

$$E^*_{\mathrm{FFG}}(T) = \frac{1}{2}\left(\frac{\pi}{3}\right)^{2/3}\frac{m}{\hbar^2}T^2\left(N\rho_{\mathrm{n}}^{-2/3} + Z\rho_{\mathrm{p}}^{-2/3}\right), \tag{4.3}$$

$$S_{\mathrm{FFG}}(T) = \left(\frac{\pi}{3}\right)^{2/3}\frac{m}{\hbar^2}T\left(N\rho_{\mathrm{n}}^{-2/3} + Z\rho_{\mathrm{p}}^{-2/3}\right), \tag{4.4}$$

[5] Because this is the region where the effect of temperature is the most important.
[6] Making this shape transition of second order in the Ehrenfest classification.

$$C_{\mathrm{FFG}}(T) = S_{\mathrm{FFG}}(T). \tag{4.5}$$

In all numerical calculations, we take for the FFG $\rho_{\mathrm{n}} = \rho_{\mathrm{p}} = \rho_0/2$, with the saturation density $\rho_0 = 0.16$ fm^{-3}; the same mass $m = 939$ MeV/c^2 is used for protons and neutrons. Finally, the evolution of the deformation in thermal mid-mass and heavy nuclei can be understood on the basis of Landau's theory of continuous phase transitions [Lan37].

A shape phase transition is observed in finite temperature calculations of the ground state of the mid-mass nuclei ^{56}Fe. The coordinate-space density of the ground state at different temperatures is given in figure 4.6, to help visualising the restoration of spherical symmetry. The $T = 0$ and $T = 1$ MeV densities are almost identical, while the deformation is much less pronounced at $T = 2$ MeV already. The spherical symmetry is fully restored at $T = 3$ MeV. As mentioned in section 2.5, no thermal averaging is carried out, so that the symmetry restoration occurs sharply at a critical temperature T_c.

Figure 4.7 shows the excitation energy as a function of temperature, obtained with the NLO, N^{2}LO and N^{3}LO orders of the chiral interaction. Calculations are performed at $\hbar\Omega = 16$ MeV, $(\mathrm{e}_{\max}, \mathrm{e}_{3\max}) = (8, 14)$. The excitation energies exhibit the quadratic dependence estimated from the schematic model of independent fermions, and the nucleus is found to be bound up to $T = 8.6$ MeV with the N^{3}LO interaction. The very good agreement between the two last orders seems to indicate that the convergence of the zero-temperature observables, usually reached with the third and fourth orders in the chiral expansion, also holds at finite temperature. This can be taken as a strong indication that the quality of these interactions is about the same for both occupied and unoccupied orbitals of the zero-temperature nucleus. The same conclusion can be drawn from figure 4.8, where the total entropy is represented. The excellent agreement among the two last orders clearly signals the onset of convergence.

The entropy is found to globally display the expected linear dependence, except at very small temperatures where thermal excitations occur with negligible probabilities. This deviation from the Fermi gas-like behaviour occurs predominantly at low temperature because this is the region where the structure effects, in particular the shell gaps, are most sensitive to the individual properties of each orbital. At low temperatures, the entropy (and thus, the free energy, and all thermodynamical variables) is for the largest part determined by the states close to the Fermi energy[7]. The low-temperature regime should thus be the region where the deviations from a Fermi liquid model are the most important. As a side remark, the fact the free energy is, for finite systems, mostly a surface quantity at low temperature, and grows to become a bulk quantity at high temperature, could be used as a means of determining the degree of agreement between different interactions while using only macroscopic observables.

The static quadrupole moment β_{20}(T) is shown on figure 4.9. The discrepancy between N^{2}LO and N^{3}LO is slightly more pronounced away from the phase transition, albeit remaining of less than 5%. Including the systematic errors according to the for-

[7] To be more precise, by those with energy E such that $\beta E < 1$, owing to the rapid fall-off of the Fermi distribution away from $E = 0$.

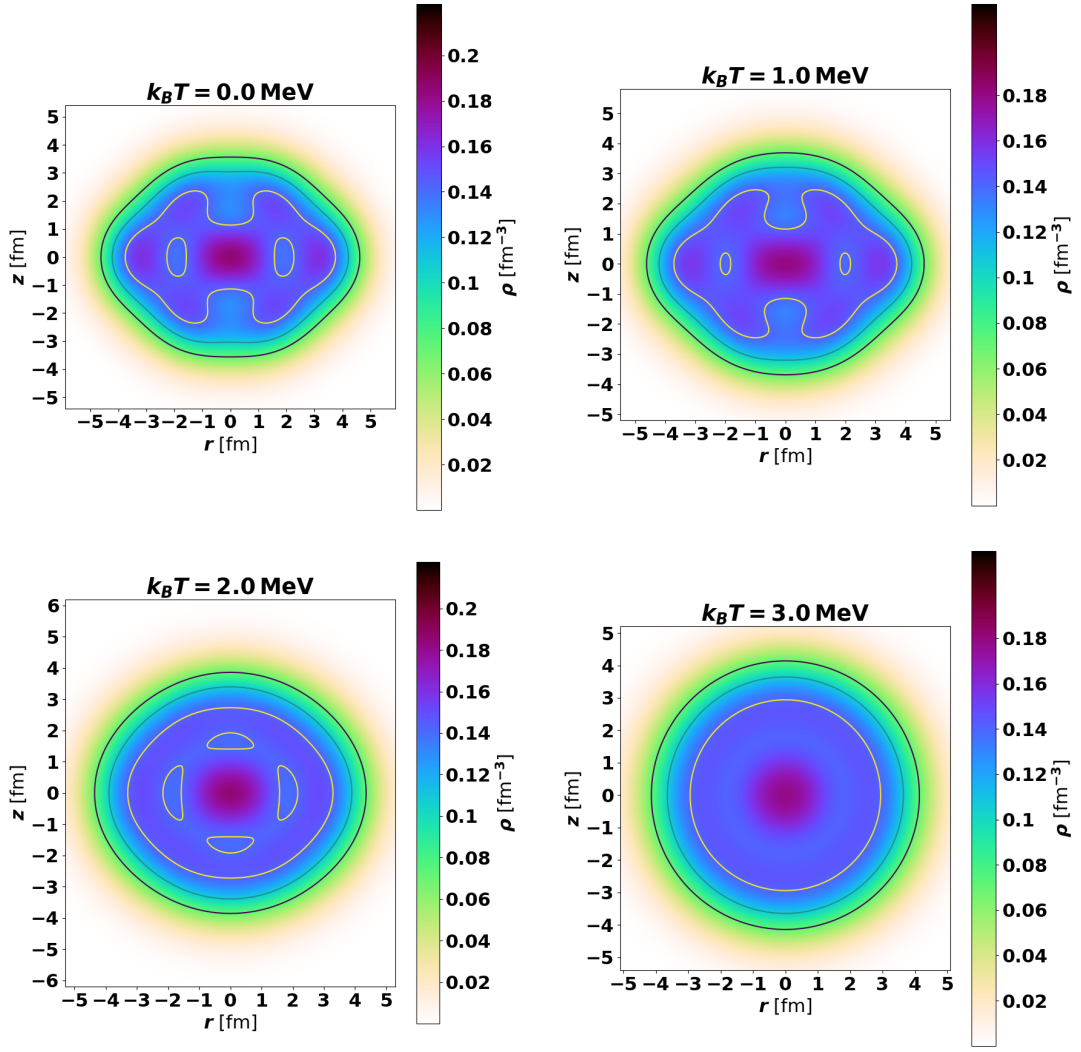

Figure 4.6: Total (protons+neutrons) ground state densities of ^{56}Fe for four temperatures. The calculations are made at $(e_{max}, e_{3max}) = (8, 14), \hbar\Omega = 12$ MeV, with the N^{3}LO interaction. The black, blue and yellow contours signal the iso-density surfaces, where $\rho = 0.08, 0.12$ and 0.16 fm^{-3}, respectively.

mulae of [EKM15; Bin+18; Hüt+20], the critical temperature at N^{3}LO is found to be $T_c = 2.46 \pm 0.23$ MeV. The large uncertainty is due to the NLO prediction at around 4.5 MeV; the N^{2}LO and N^{3}LO values differ in only 80 keV. The deformation showing significant variations over the span of a few MeV, it can be concluded that realistic predictions of astrophysical processes involving iron in high-temperature environments should significantly cannot be made using information about the zero-temperature structure only. This statement is even to be given more credit by the fact we do not mix different configurations according to their statistical weight (see (2.71)). Remarking that the modification of the observables once the thermal averaging is carried out can be qualitatively understood with statistical arguments only, we can expect to observe similar changes in $\beta_{20}(T)$ as the ones found in [MER03b; MER03a], namely a steeper decrease of the deformation below the critical temperature than found with a single-thermal state calculation, and a more

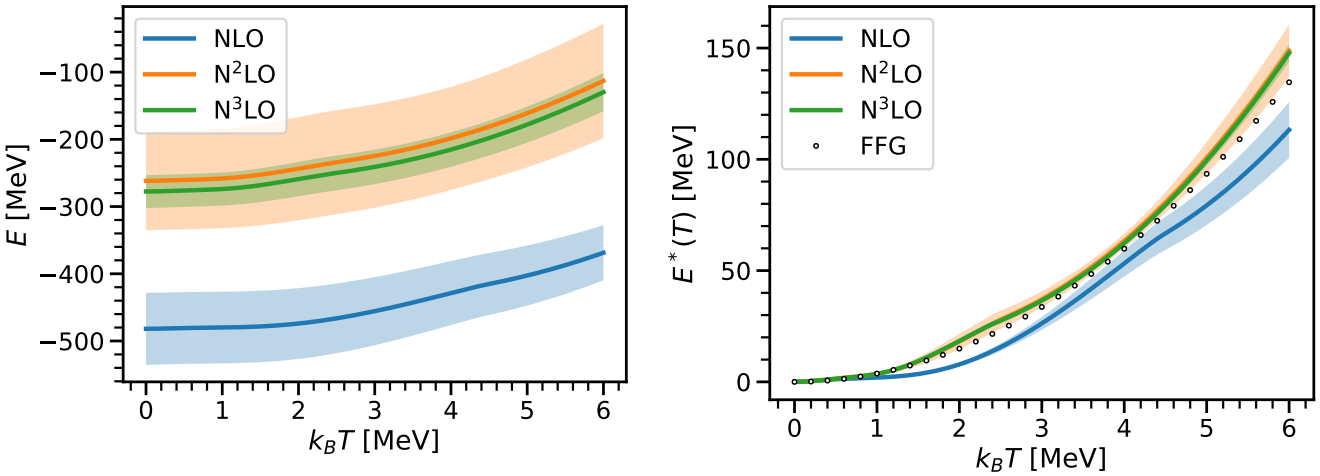

Figure 4.7: Ground state energy (left) and excitation energy (right) as a function of temperature in ^{56}Fe. The excitation energy of a two-components free fermion gas of protons and neutrons at saturation density is also represented as circles placed every 0.2 MeV.

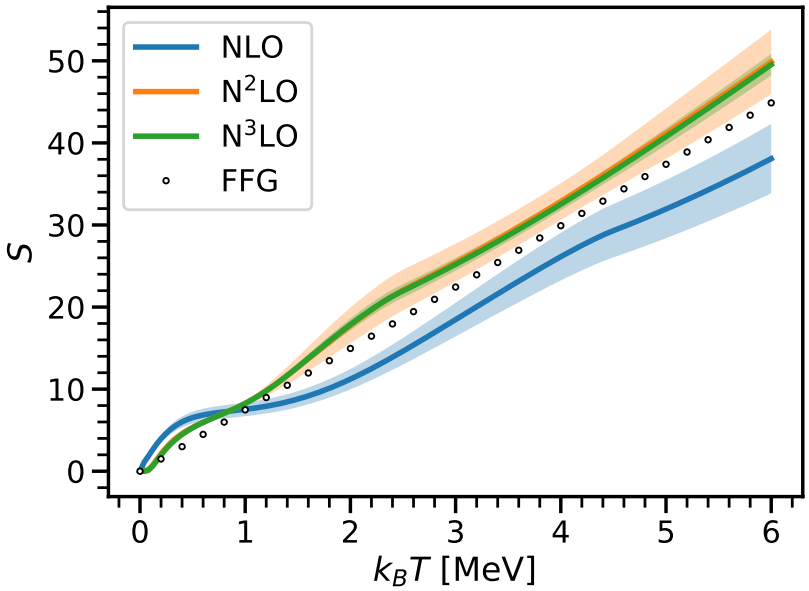

Figure 4.8: Same as figure 4.7 for the total entropy.

gentle return to sphericity beyond.

The energy and entropy being continuous functions of the temperature across the phase transition, so is the free energy. However, the specific heat, related to the second derivative of F and defined as

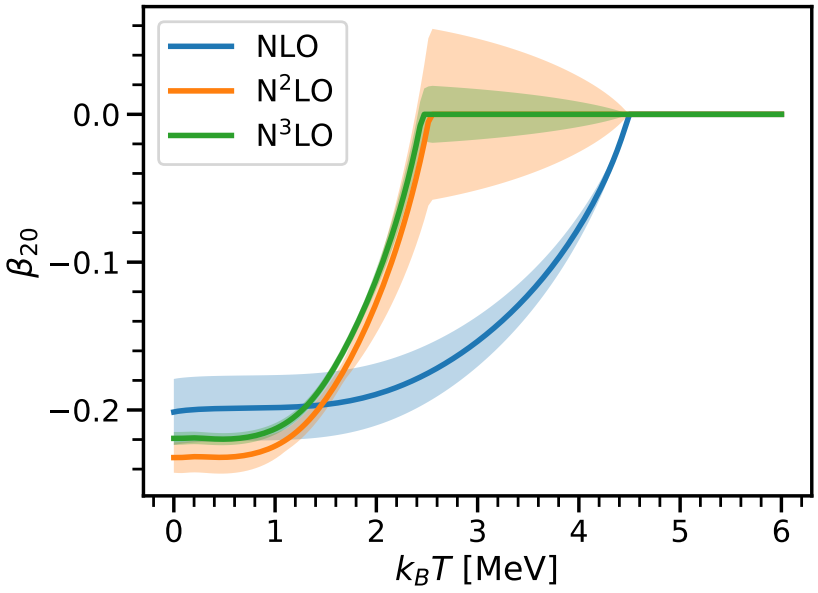

Figure 4.9: Static quadrupole moment as a function of the temperature.

$$C_v \equiv T\frac{\partial S}{\partial T}, \tag{4.6}$$

steeply decreases at the critical temperature. Although not as sharp as to unambiguously signal a discontinuity, a sudden drop of C_v has been observed for heavier systems in the work of [MER03b; MER03a; RA15; ZN17; KN20]. The same discontinuity has also been observed in superfluid systems at the superfluid to normal phases critical temperature [Egi+85; GLS13; Li+15]. The fact that the heat capacity decreases at the phase transition temperature can be understood informally as follows. Below T_c, the system is deformed. The spectrum thus comprises eigenstates that can be mapped to the eigenfunction of harmonic oscillators with different deformations. In a given energy interval, one can thus find states associated to deformation in either an axial or a radial direction[8]. A slight amount of energy added to the system by increasing T can then be dissipated easily by letting the nucleons rearrange themselves over the nearby states. These having different deformation causes the β_{LM} moments to decrease. However, when spherical symmetry is restored ($\beta_{LM} = 0$ for all $L > 0, M$), axial and radial states become identical, hence the density of states suddenly drops by a factor of roughly two. Energy dissipation is therefore less efficient, so that the heat capacity reduces[9]. Finally, the heat capacity C_v (figure 4.10) starts increasing again past T_c, since, as for the $T < T_c$ regime, heating up the system causes the nucleons to occupy more states in significant amounts, which in turn eases dissipative processes.

[8] Or any direction in the three-dimensional coordinate space, if considering triaxial deformations.

[9] In a less visual manner, this argument can also be made by arguing that a state with lesser symmetry requires more quantum numbers, which is easily understood to cause a higher level density provided the energy gap between states is of the same order of magnitude among the corresponding quantum numbers.

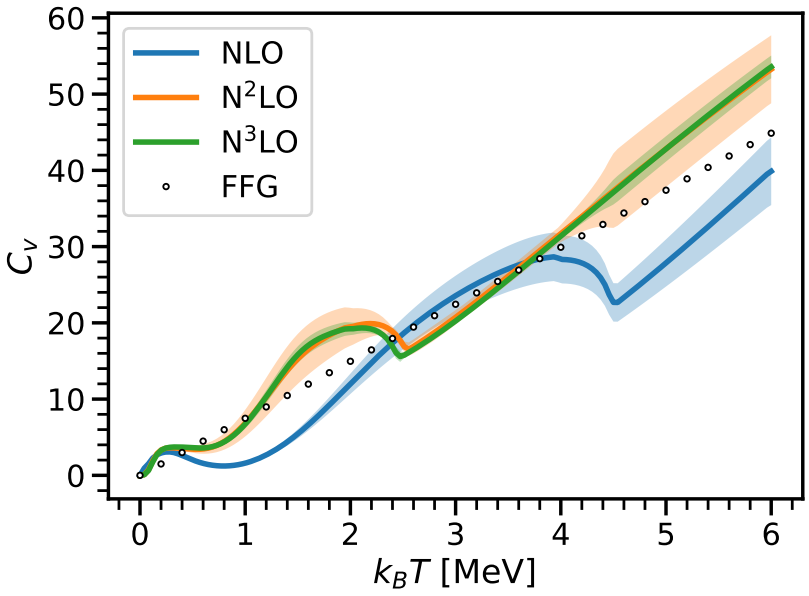

Figure 4.10: Same as figure 4.7 for the heat capacity. The derivatives are calculated using finite differences, for temperatures equally spaced of 0.01 MeV.

As a final remark, the energy, deformations and radii being bulk observables, they are not so much sensitive to the details of the spectrum. At zero temperature, the good agreement between the last two orders can only be taken as an indicator that the interaction yields converged values for thermodynamic observables that are not driven by a specific region of the spectrum. The maintaining of a good agreement between these different orders at finite temperatures and for all the studied quantities allows more ambitious statements. The fact that the N^{2}LO and N^{3}LO results (not looking at the error bars, to discard the poorly-converged NLO results from the discussion) remain almost identical over the whole $T = 0 - 6$ MeV range brings the conclusion that these two interactions not only give converged bulk quantities at $T = 0$, but also at finite temperature, and thus remain of identical quality for the study of hot nuclei.

Chapter 5

Application to giant resonances

In this chapter, the finite amplitude method is put into operation to study giant resonances in the mid-mass nuclei ^{56}Fe, ^{46}Ti and ^{44}Ti. A strong dependence of the isovector dipole strength on the temperature is observed, characterised by a downwards shift of the resonance centroid when the systems are heated up. The chapter starts by comparing the FAM results to the standard RPA in the case of ^{16}O, which, being spherical and non-superfluid, is currently within the reach of ab-initio RPA. As should be, the dependence of the results on the parameters studied for the ground states calculations is also scrutinised.

Contents

The richness of collective features arising in quantum systems reveals the complex interplay between their microscopic constituents. In strongly correlated systems, excited states can be highly different from the ones built from simple particle-hole excitations on top of the ground state, owing to the self-consistent rearrangement occurring when one (or several) particle(s) is (are) moved from an orbital to another. From a physical perspective, the apparition of such collective resonances under the action of an external field can be understood from a self-consistent field picture. For simplicity, assume the system of interest to be at equilibrium, that is, static in its ground state. Then, apply a polarising field. This triggers the motion of each particle, so that the overall field oscillates along. Since the degrees of freedom interact, the motion of each one (or, equivalently, of the total field) affects the others'. These interferences can be one either side of the two extreme situations, i.e., destructive or constructive. The first case corresponds to an overall cancellation of the oscillations, while the second results in a coherent oscillation of the surface at a single frequency. Thus, the emergence of collective modes in complex systems can be seen as a consequence of non-linear interferences. In nuclear physics, the eigenstates of a system under a time-dependent field range from rather "simple" individual oscillations to excitations of the whole nuclear surface, passing through somehow more exotic oscillations of nuclear clusters (typically by groups of α-particles) [ITH68; SHI72; Ito+14]. From the dynamical viewpoint, nuclear collisions can give rise to several outcomes, depending on the kinetic energies and impact parameter of the participant nuclei. A fine understanding of the structure of such resonances, in terms of degree of collectivity, evolution of correlations with temperature, etc, is of paramount importance to accurately describe capture and decay processes, and as such, predict nucleosynthetic reactions in astrophysical sites. Indeed, the formation of heavy elements in astrophysical environments typically happens through the capture of neutrons, followed by β^- decays to attain stable nuclei. Such environments also comprise extreme electromagnetic fields, that can strongly influence the structural properties of the nuclei. Knowing a nucleus' behaviour under the action of electromagnetic fields, or of adding or removing particles, thus gives keys to understanding the chemical elements' abundances.

Among others, the so-called giant resonances correspond to coherent excitations of the system as a whole, and find their name in the large associated cross-sections. Experimentally, their occurrence in atomic nuclei at excitation energies typically twice or thrice greater than the typical nucleon separation energy signals the collective nature of these modes.

As a test-bench system for the applications of the FTQFAM machinery, we focus on the mid-mass ^{56}Fe nucleus. Being a starting point for the stellar nucleosynthesis of heavier elements, understanding its structure properties, among which the energies of its collective resonances, is thus highly important for the study of such astrophysical processes. In particular, experiments have found an up-bend [Voi+04; Voi+06] in the low-energy part of the de-excitations strength functions for this nucleus, a feature also present in ^{46}Ti and ^{44}Ti. Although the FAM describes the reverse process of excitation from the ground state, emission and absorption can be related within the Brink-Axel (BA) hypothesis [Bri55; Axe62]. This assumption states that these two processes are oblivious to the detailed structure (in terms of absolute energies, spin, parity) of the initial and

final states, but only depend on the energy of the emitted or absorbed photons. The BA hypothesis has been demonstrated to be consistent within experimental uncertainties for ^{56}Fe [Voi+06; Lar+17; Jon+18], ^{46}Ti [Gut+11] and ^{44}Ti [Lar+12].

While these peaks are attributed to dipole excitations, their electric or magnetic nature is yet unclear [Gor+19]. Although the FTQFAM and FTQRPA are capable of producing strength functions for these modes [Paa+09; Yük+14; Yük+17; LW18; WL19; Yük+19; LW19; LRW20; Yük+20; Rav+20; LR21], phenomenological corrections are usually applied to improve the agreement with experimental data whenever the strength functions serve as input ingredients for reaction models. This is due to the non-linear effects mentioned in section 3.9. An approximate account may be supplied by a Fermi liquid correction, which gives the smearing width a quadratic temperature dependence [Bru+08; Yan+19]. Additionally, accounting for the Doppler broadening might be important for macroscopic nuclear matter, e.g. in stellar bodies. All such corrections could be applied in the calculations of this chapter, but are not, so as to render the comparison between the strength functions obtained at different temperatures more transparent.

In this chapter, we therefore study basic electric multipole excitations, and centre our attention on the astrophysically relevant ^{56}Fe, ^{46}Ti, ^{44}Ti nuclei. A first part is however dedicated to the benchmark results of the FAM against a spherical HF-RPA solution.

5.1 Benchmark against standard RPA

As discussed in chapter 3, the FAM and RPA should yield identical strength functions. In this first section, the implementation of the FAM is validated against RPA calculations for the doubly-magic nucleus ^{16}O. This serves as a benchmark of the FAM for non-superfluid nuclei only; ab initio matrix QRPA calculations including the three-body terms are not yet feasible. The implementation of the FAM is agnostic to the employed basis, in the sense that one can incorporate a FAM module on top of a static code without ever using any explicit property of the computational basis; such task is left to the static code up to adequate (and tricky) modifications. Figure 5.1 displays the FAM strength function, along with the one obtained from RPA matrix elements with a Lorentzian smearing, as in (2.82). In these figures and the rest of the document, we use the compact notation $S_{JK} \equiv -\pi^{-1}\,\mathrm{Im}\{S(Q_{JK},\omega_\gamma)\}$.

For all three multipolarities, the RPA and FAM results agree up to four decimal places at worst, which corresponds to the number of digits of the RPA matrix elements in the data files. This set of calculations confirms the correctness of the FAM implementation.

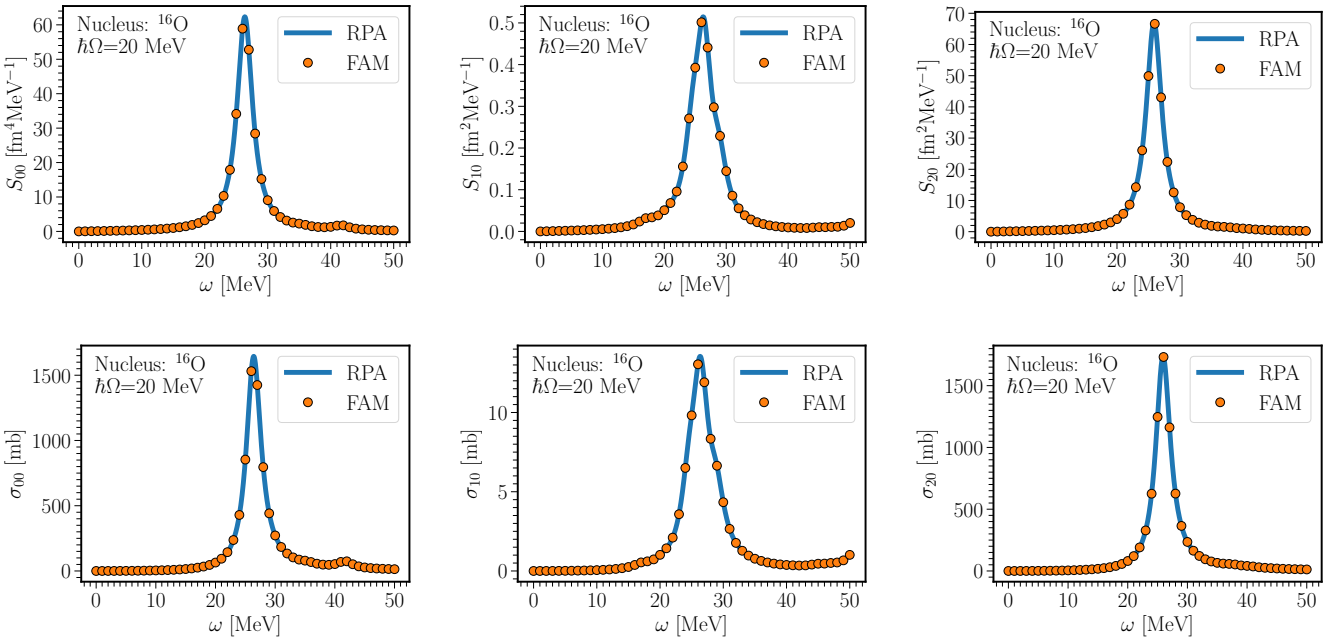

Figure 5.1: RPA and FAM strength functions (top) and photoemission cross-sections (bottom). The calculations are performed with a smearing width $\gamma = 1.5$ MeV and $(\mathrm{e_{max}}, \mathrm{e_{3max}}) = (6, 14)$, at an oscillator frequency $\hbar\Omega = 20$ MeV.

5.2 Convergence aspects

Although comparing the strength functions altogether gives an appreciable idea of the convergence of the results, it can also be relevant to employ integrated quantities in order to obtain a general estimation of the degree of agreement among the sets of parameters. Clearly, the moments m_k (2.85) play the fine role here. These can possibly be employed to compute the mean excitation energy and resonance width, respectively defined as[1]

$$\langle E \rangle \equiv \frac{m_1}{m_0}, \tag{5.1a}$$

$$\Gamma \equiv \sqrt{\langle E^2 \rangle - \langle E \rangle^2} = \sqrt{\frac{m_2}{m_0} - \left(\frac{m_1}{m_0}\right)^2}. \tag{5.1b}$$

The definitions of these quantities always involve the normalisation by m_0, i.e. the integral of the strength, which in passing compensates for possibly different pre-factors to the multipole operators among different conventions.

The same convergence-checking routine as for the ground state observables can be applied for the strengths. For simplicity, the study is conducted for ^{56}Fe only; the results are qualitatively identical for the titanium isotopes. Because the strengths are built on

[1] From the physical side, these quantities really make sense only when the spectrum shows a single dominant resonance.

the ground states, we expect the differences in the results obtained with different parameters and chiral orders to be magnified with respect to those observed in chapter 4. It is important to realise that the discrepancies can be evaluated in two manners, depending on whether we want to focus on integrated quantities or on the difference at a given frequency. I thus define the errors on an integrated quantity X calculated at a parameter q as

$$\Delta^{(1)}X^{[q]} \equiv \max_{q'\in\{q\}}\left(\int_0^\infty d\omega Q(q,q')\left|X^{[q]}(\omega) - X^{[q']}(\omega)\right|\right), \tag{5.2}$$

$$\Delta^{(2)}X^{[q]} \equiv \int_0^\infty d\omega \max_{q'\in\{q\}}\left(Q(q,q')\left|X^{[q]}(\omega) - X^{[q']}(\omega)\right|\right). \tag{5.3}$$

In these definitions, the integrand ω is typically the energy, and for the specific purpose of the section, it corresponds to the frequency of the probe F. The set $\{q\}$ represents the set of parameters we can vary: in our case, it is either the set of oscillator frequencies, of the size of single-particle basis, or of the chiral orders. The quantity $X^{[q']}(\omega)$ is the strength function calculated with the parameter q' and at excitation frequency ω, and the particular value q is the parameter with respect to which the error is calculated. The factor $Q(q')$ gives a weight to each difference, and should be motivated by physical sense. Equation (5.2) corresponds to comparing the integrated quantities, whereas (5.3) integrates the function defined by the largest error at each ω, and thus we have $\Delta^{(2)} > \Delta^{(1)}$. This is easier to see with loose notations:

$$\Delta^{(1)}X \sim \max\left(\left|\int \mathrm{d}\omega x_1(\omega)\right|, \left|\int \mathrm{d}\omega x_2(\omega)\right|, \dots\right) \tag{5.4}$$

$$\Delta^{(2)}X \sim \int \mathrm{d}\omega \max\left(|x_1(\omega)|, |x_2(\omega)|, \dots\right). \tag{5.5}$$

To illustrate, we may take X as the set of eigenvalues of the HFB equation, weighted by the density function. In that case (omitting the q, q' exponents for clarity),

$$\omega \to E, \tag{5.6}$$

$$X \to E_i \frac{1}{e^{\beta E_i}+1}\delta(E_i - E), \tag{5.7}$$

$$Q \to 1, \tag{5.8}$$

and the definition (5.2) corresponds to adding the absolute value of the differences for each single particle eigenvalue (weighted by its occupation number),

$$\Delta^{(1)}E^{[q]} = \max_{q'\in\{q\}}\sum_i \left|\frac{E_i^{[q]}}{e^{E_i^{[q]}}+1} - \frac{E_i^{[q']}}{e^{E_i^{[q]}}+1}\right|. \tag{5.9}$$

Errors thus pile up, and the values obtained with different parameters q' are compared

afterwards. Conversely, (5.3) always takes the worst of all:

$$\Delta^{(2)}E^{[q]} = \sum_i \max_{q'\in\{q\}} \left| \frac{E_i^{[q]}}{e^{E_i^{[q]}}+1} - \frac{E_i^{[q']}}{e^{E_i^{[q]}}+1} \right|. \tag{5.10}$$

The studies of [EKM15; Bin+18; Hüt+20] use a formula derived from (5.2), where q is the N^{3}LO, q' are the lower orders, and Q is a power of 1/3. To obtain meaningful comparisons, we must adopt a formula compatible with (5.2). The simplest way being to calculate the m_k moments (and if need be, derive the values of (5.1) accordingly), errors are defined as

$$\Delta m_k^{[q]}(F) \equiv \max_{q'\in\{q\}} \left(Q(q,q') \left| m_k^{[q]}(F) - m_k^{[q']}(F) \right| \right), \tag{5.11}$$

and we take the $Q(q,q')$ identically to the prescription of [EKM15; Bin+18; Hüt+20] in case q, q' are chiral orders, and equal to one otherwise. Note that comparing the strengths at a given frequency can also provide quality information, and is in particular much more connected to what is measured experimentally, namely a number of counts as a function of an energy. Whenever it is relevant for the discussion, the strength functions will be presented with their error bars.

5.2.1 With the oscillator frequency

We saw in subsection 4.3.2 that all macroscopic observables bore a non-negligible dependence on the frequency $\hbar\Omega$ of the harmonic oscillator basis. Larger variations, but on the same order of magnitude, should be expected for the strength functions and derived quantities. Such affirmations are verified on figure 5.2, where the isoscalar monopole (ISM), isovector dipole (IVD) and isoscalar quadrupole (ISQ) electric responses of iron at three temperatures are given.

On the qualitative aspects, the results obtained at all three values of the oscillator stiffness are altogether consistent. The monopole operator visibly has the most pronounced $\hbar\Omega$-dependence. A more quantitative view is given in figures 5.3-5.4-5.5, which review the variations of the moments with the oscillator frequencies, for all three types of perturbation. In most cases, the moments undergo variations of a few percents in case of the IVD and ISQ excitations, but eventually reach 20-30% for the monopole mode. The mean excitation energies, being calculated as the ratio of m_1 and m_0, exhibit a dependence roughly equal to the sum of the variations of these two moments. This translates in 25% relative difference between the $\hbar\Omega = 20$ and $\hbar\Omega = 12$ MeV in case of the monopole operator, and about 9% (resp. 3%) for the dipole (resp. quadrupole). Except for the strongly frequency-dependent S_{00} response, the variations are of the same order as those observed for the energy and radii in the static HFB calculations. Overall, the quality of the results obtained with suboptimal frequencies is deteriorated as compared with the static case. In the particular case of the monopole mode, the large error calls for a precise adjustment of $\hbar\Omega$ at the HFB level. In all cases, the variations do not suffer great changes

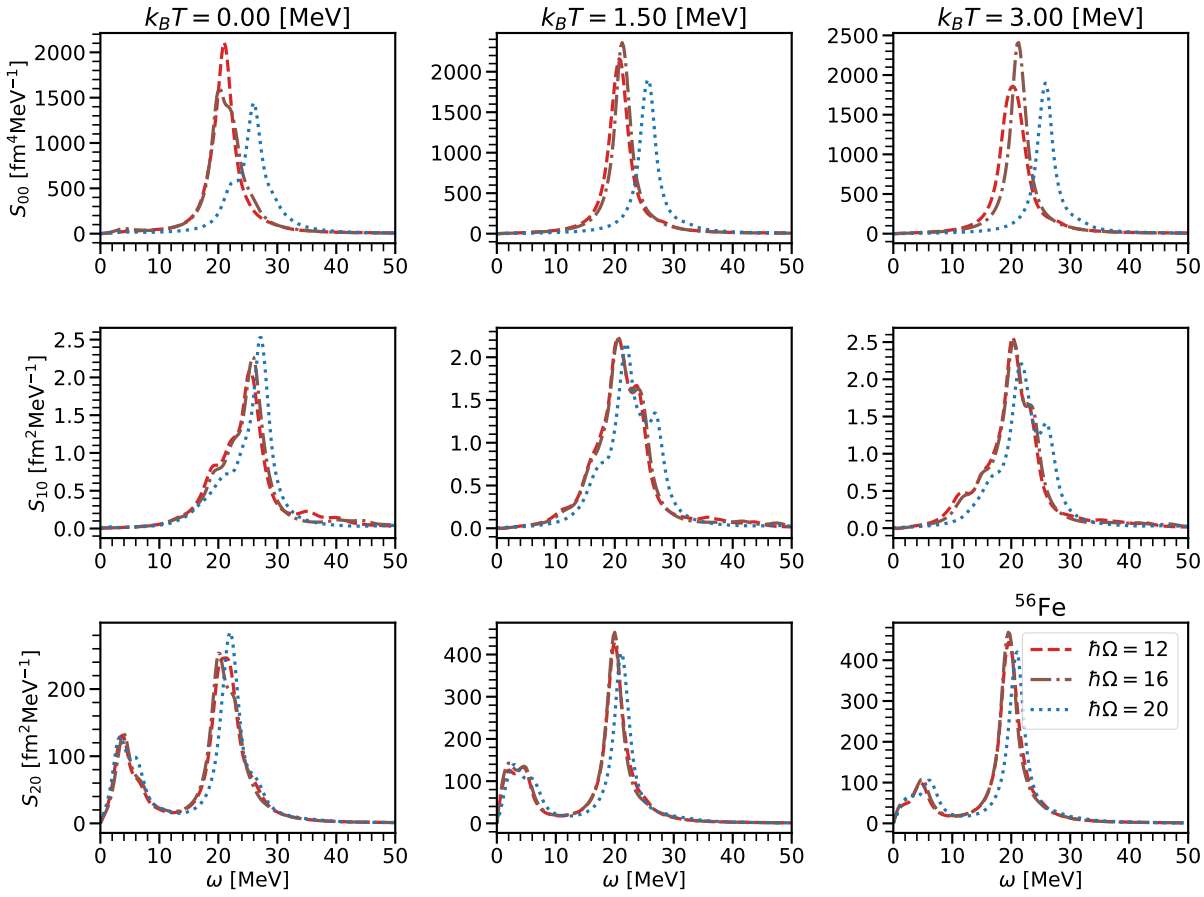

Figure 5.2: Electric multipole responses of ^{56}Fe at different oscillator frequencies. The calculations are done at $(e_{max}, e_{3max}) = (10, 14)$, with $\gamma = 1.5$ MeV. We show the IS monopole (top), IV dipole (middle) and IS quadrupole (bottom) responses, for three different temperatures: $T = 0$ (left), $T = 1.5$ (middle) and $T = 3$ MeV (right).

when the system is hot.

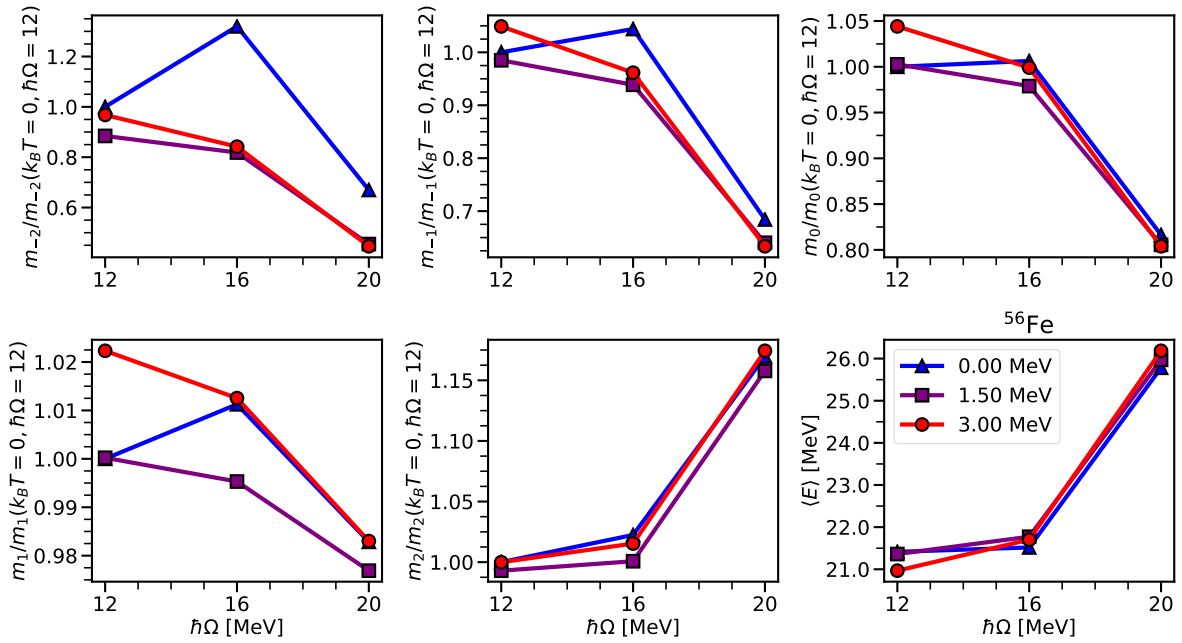

Figure 5.3: Normalised moments of the Q_{00} strength function for ^{56}Fe. The normalisation is applied with respect to the $k_BT = 0$ MeV, $\hbar\Omega = 12$ MeV values. The bottom-right subplot represents the mean excitation energy calculated as in (5.1a). The calculations are performed with the model space $(e_{max}, e_{3max}) = (10, 14)$ and use a smearing $\gamma = 1.5$ MeV.

As for the mean energy of the resonances, we find it to be almost independent of the temperature for the monopole operator, and to change in approximately one MeV for the quadrupole excitation. For the former, this can be interpreted by the compressibility of nuclear matter undergoing only small changes with the temperature. In the Q_{20} case, $\langle E \rangle$ is lowest at $k_BT = 1.5$ MeV, because deformation is still present, and excitations are facilitated by the finite temperature. Beyond T_c, $\langle E \rangle$ increases past its zero-temperature value, as a consequence of the restoration of spherical symmetry. Conversely, the giant dipole resonance shows a strong $T-$ dependence, dropping from several MeVs within the temperature range scanned. This is mainly due to the low-ω part of the strengths, which is more sensitive to temperature. In case of the S_{10} strength, which visibly undergoes the largest variations via the onset of low-energy resonances at around 10 MeV (and to a lesser extent, smaller resonances beyond 30 MeV), the differences between the observables calculated using $\hbar\Omega = 12$ MeV and $\hbar\Omega = 20$ MeV grow to ten percents. Finally, at a given frequency and in all cases, the ratios between the strengths can grow several orders of magnitudes. This stems from the fact that the single-particle energies are slightly different between the set of parameters, which result in the energy of the peaks being shifted. The sharp increase of the strength around the resonances aggravates this difference. This observation shows the importance of comparing more meaningful quantities, namely integrated ones.

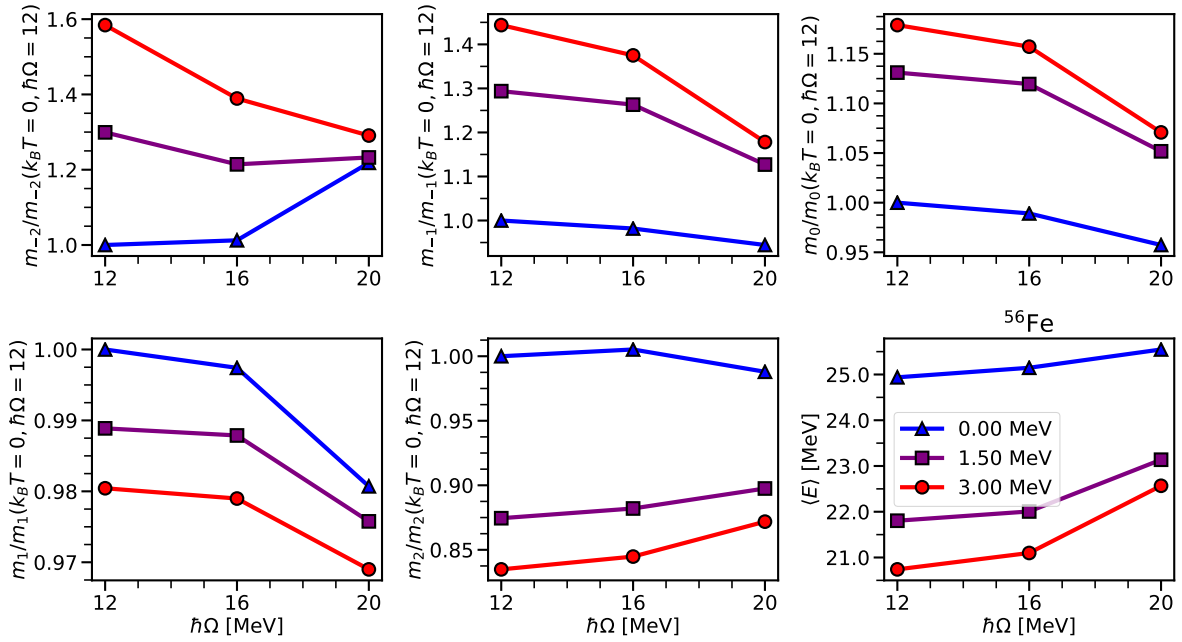

Figure 5.4: Same as figure 5.3 for the Q_{10} mode.

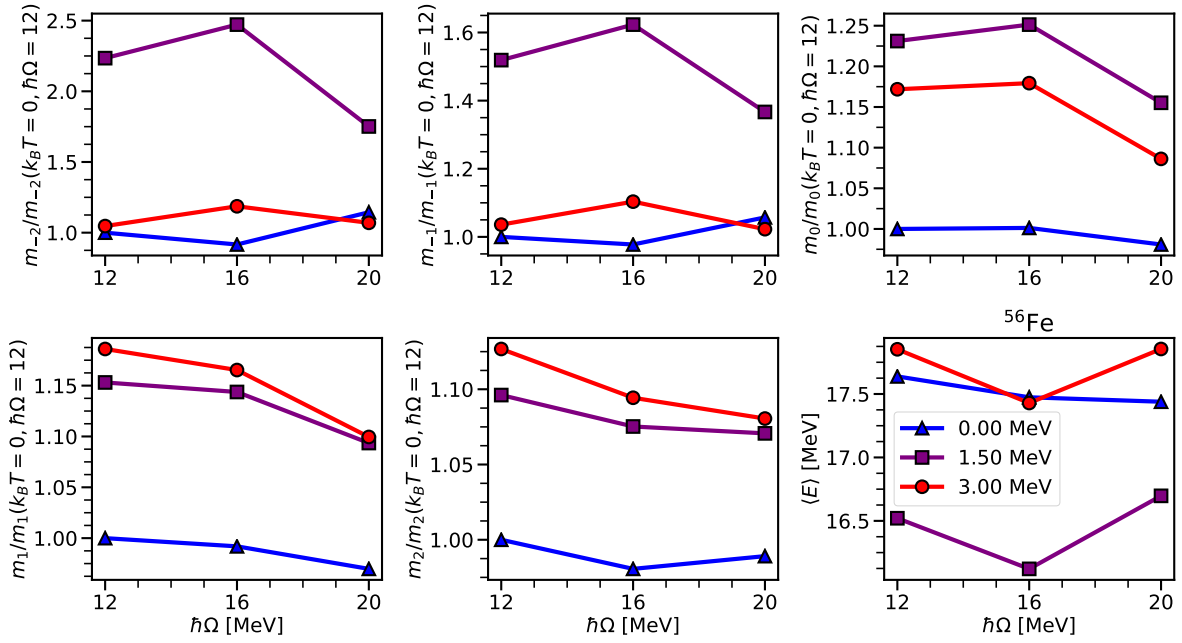

Figure 5.5: Same as figure 5.3 for the Q_{20} mode.

Globally, the errors resulting from non-optimal choices of $\hbar\Omega$ are several times larger than for the ground state properties. On average, we obtain 2-10% difference in either the m_k or the quantities (5.1) calculated from these, while in extremal cases the discrepancies reach 20 to 30%. This illustrates the importance of employing a well-chosen frequency.

Unless great caution has been taken in determining the one giving the lowest ground state energy, the predicted moments vary strongly. This harsh conclusion can however be balanced by the observation that the overall shape of the strengths remains similar across the choices of $\hbar\Omega$, and we still obtain very close moments whenever the frequency is sufficiently close to its optimal value.

5.2.2 With the basis size

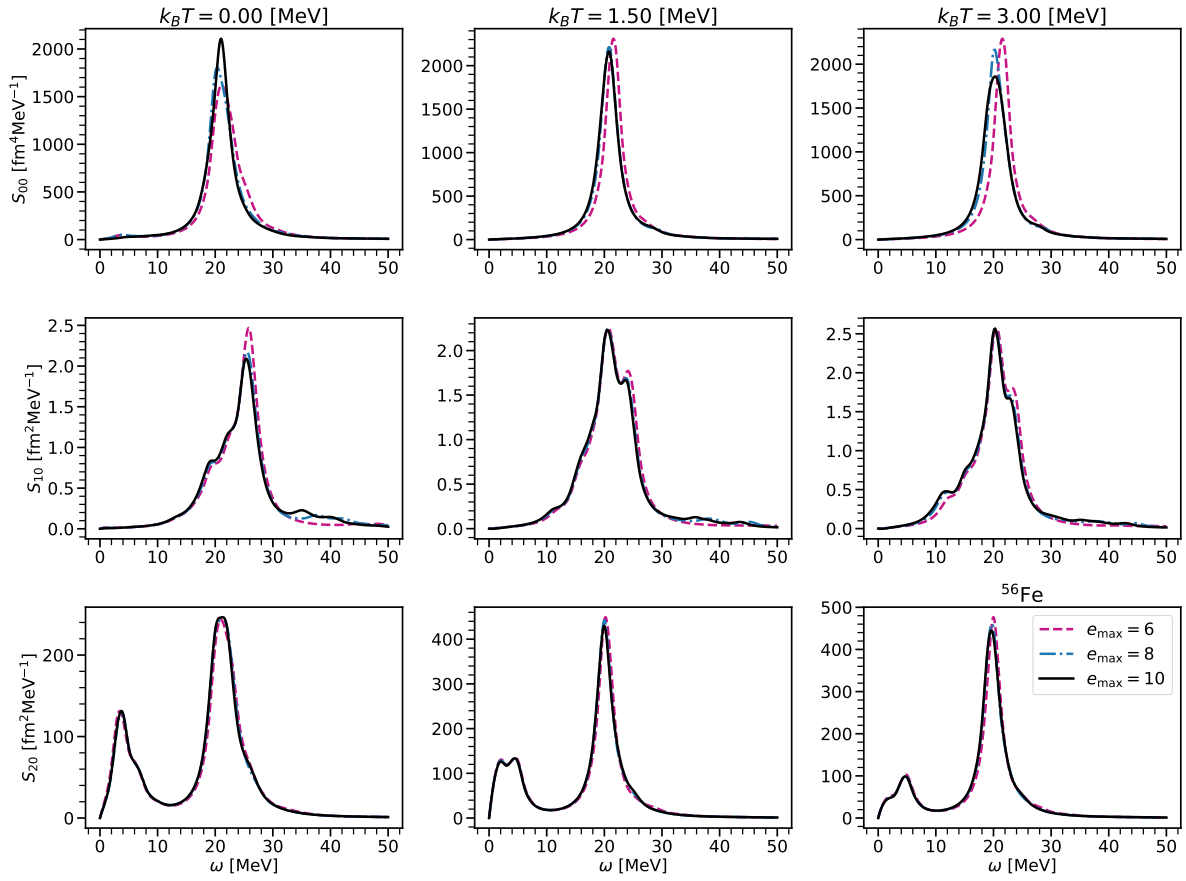

Figure 5.6: Multipole responses of ^{56}Fe at $e_{max} = 6$ (dashed), $e_{max} = 8$ (dash-dotted) and $e_{max} = 10$ (full). All calculations use a model space of $e_{3max} = 14$ and $\hbar\Omega = 12$ MeV; the smearing width $\gamma = 1.5$ MeV.

In subsection 4.3.2, a good convergence of the bulk quantities with the size of the single-particle space was found. The corrections brought by increasing the parameter e_{max} from 8 to 10 were of about one percent. In figure 5.6, we show the strength functions obtained at the three values of e_{max} used throughout this chapter. We place the model space in its optimal frequency, $\hbar\Omega = 12$ MeV, and fold the strength function with $\gamma = 1.5$ MeV.

In all cases, the difference between $e_{max} = 8$ and $e_{max} = 10$ is faint. For the dipole and quadrupole modes, it rarely goes beyond 3% for all m_k with k ranging from -3 to 3, and remains less than 6%. The disagreement is on average slightly higher for

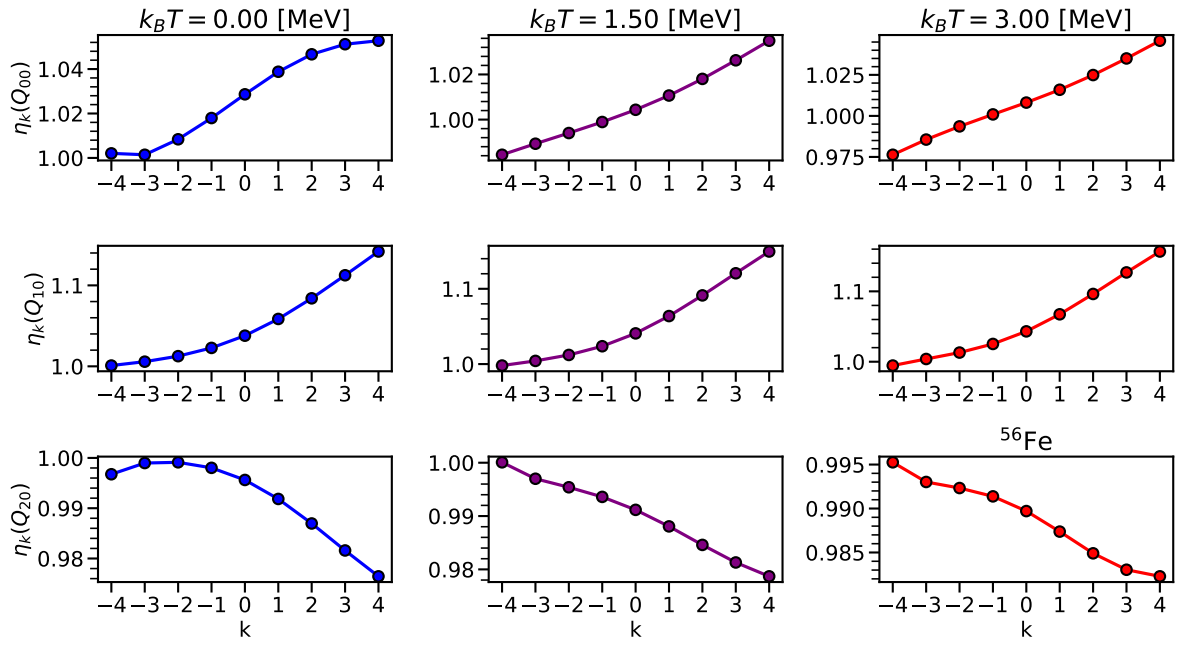

Figure 5.7: Ratios between the moments calculated at $e_{max} = 8$ and $e_{max} = 10$. The definition $\eta_k \equiv m_k(e_{max} = 8)/m_k(e_{max} = 10)$ serves as a shorthand. The calculations are carried out with $\hbar\Omega = 12$ MeV, $e_{3max} = 14$, and the smoothing $\gamma = 1.5$ MeV.

the monopole mode, albeit remaining under 6% as well. The good convergence of the strengths, concluded by visual inspection of figure 5.6, can be given a more numerical flavour by representing the ratios between the moments calculated within different model spaces. These are traced in figure 5.7 in the case of ^{56}Fe. The moments are calculated by direct integration along the $\mathbb{R}^+$ axis. As always, the results for $^{46-44}$Ti follow the same trends and are in the same ranges. The increase of the errors with larger k originates from the different strengths being marginally different at high energy (cf. (3.113))). As for $k < 0$ moments, which are more sensitive to the low-ω strength, the ratios η_k are always close to one. This is due to the low-energy part of the strength converging faster with the size of the model space than the high-energy region, since the latter requires more energetic quasiparticles, and therefore larger basis sizes. The dust settles down in the same path as for subsection 5.2.1: the error due to finite values of e_{max} is substantially higher than it was for the HFB calculations, but can be considered kept under reasonable ranges.

5.2.3 With the chiral expansion

We saw in subsection 4.3.2 that using the second to fourth chiral orders lets us establish error bars on the observables, yielding around 10% uncertainty on the three analysed ground state quantities. Moreover, the preservation of such uncertainties when the temperature is increased let use anticipate that the convergence in the chiral order remains valid at non-zero temperatures.

As the interactions are pre-processed through a normal-ordering, we verify that the

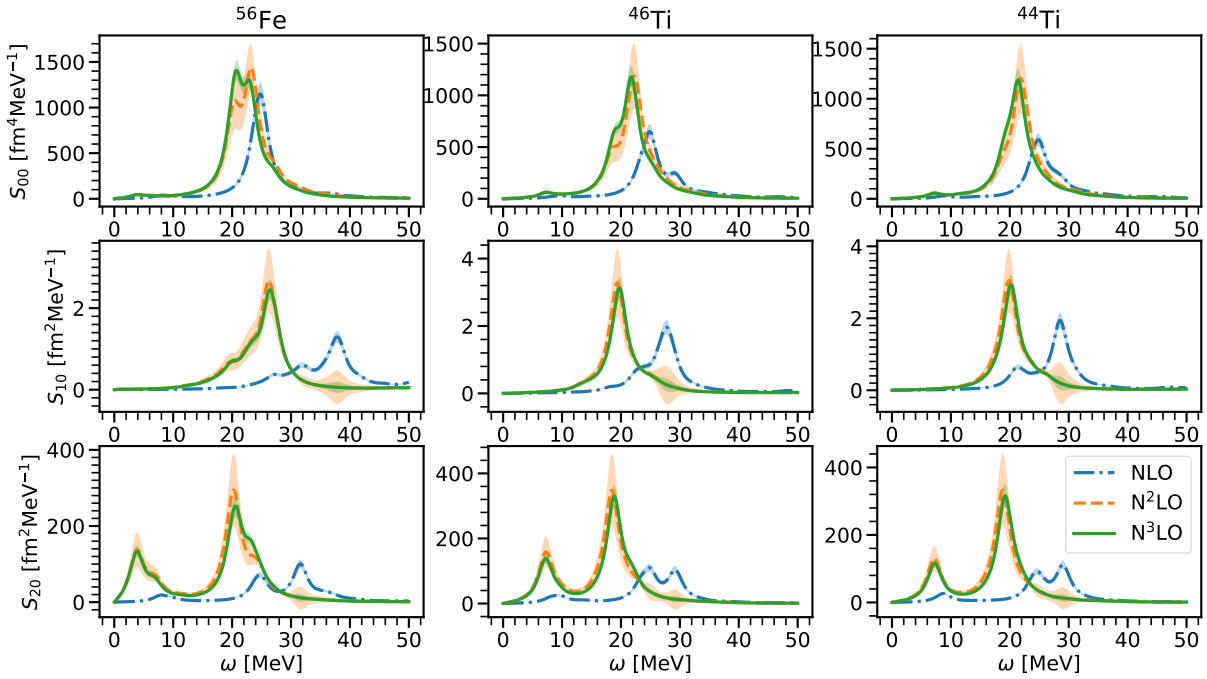

Figure 5.8: Zero-temperature multipolar responses of ^{56}Fe, ^{46}Ti, ^{44}Ti, obtained with the three available orders in the chiral interaction. The error bars are represented as shaded areas. The calculations are carried out at $(e_{max}, e_{3max}) = (10, 14), \hbar\Omega = 16$ MeV and employ a smearing $\gamma = 1.5$ MeV.

similitude of the N^{3}LO and N^{2}LO strengths is present for all three studied nuclei on figure 5.8. Because the moments vary across several orders of magnitude for different values of k, they are normalised with respect to the N^{3}LO ones on figure 5.9. The systematic uncertainties are calculated according to (5.3). Repeating the drills of this section, we find that uncertainty bars associated to the N^{3}LO are within 5-10% relative difference. The NLO moments are systematically far away from the better-quality results, due to the large differences in the strength functions. The NLO peaks always lie at larger energies, a consequence of the single-particle spectrum being more gapped. The corresponding integrated strengths are however always smaller, and both observations explain the accidental result $m_k^{\mathrm{LO}}/m_k^{\mathrm{N^3LO}} \sim 1$ for k around two. For all, the N^{2}LO and N^{3}LO moments differ in at most 10%, and are thus in acceptable (although not excellent) agreement. They only become significant either at small or at large k, owing to small differences in the low- or high-energy strengths.

As mentioned in the beginning of this section, it is also useful and instructing to compare the N^{3}LO strengths and their uncertainty bars for a single frequency. We find that the uncertainty always represent less than 10% of the strength when close to the resonances. The only dramatic increases are found when ω is close to a NLO peak. This good agreement in the results obtained with the two last orders was already observed in the FTHFB calculations. However, the propagators are dressed by the RPA self-energy during the solution of the FTQFAM equation, which can be expected to further magnify differences in the qp spectra between different orders in the chiral expansion. The strong

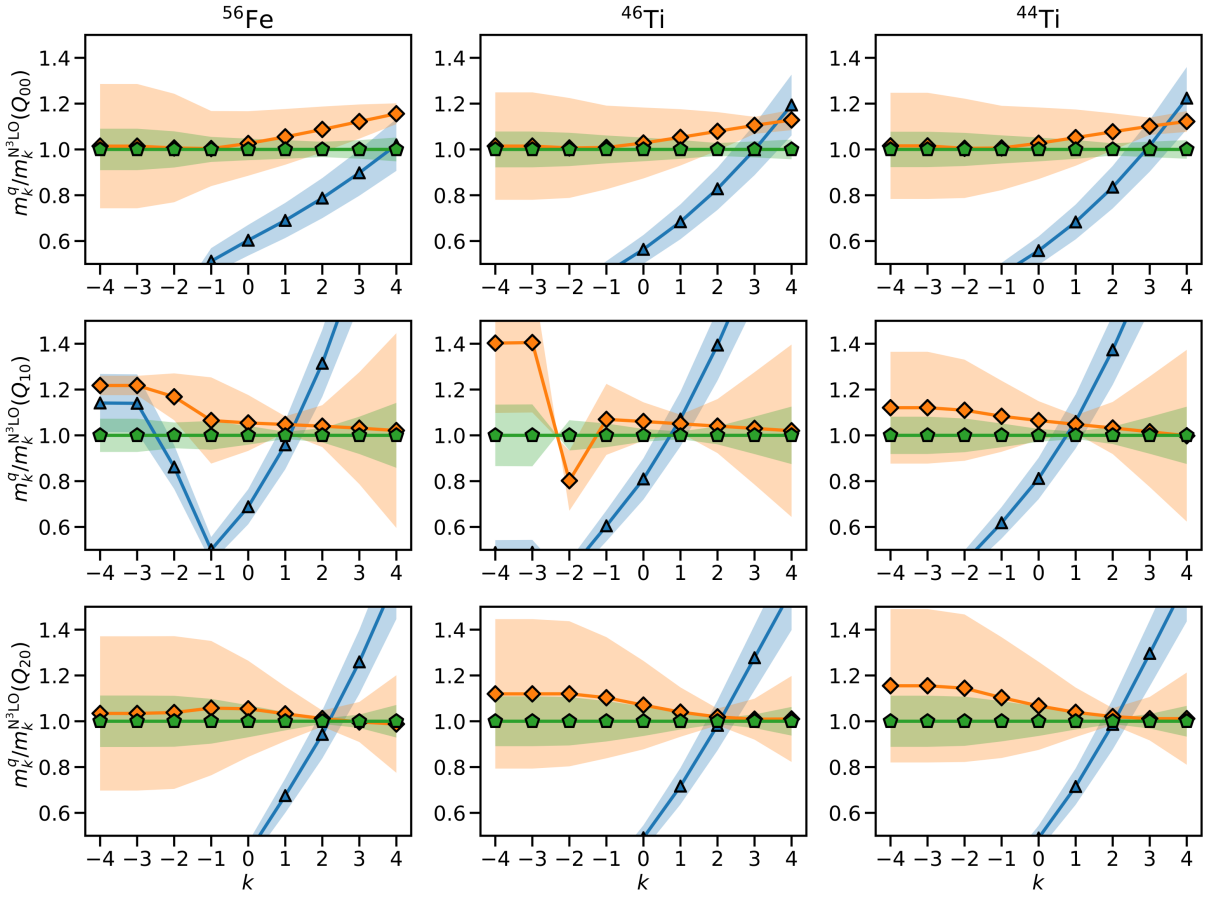

Figure 5.9: Some zero-temperature moments of the strength functions calculated with the NLO (blue triangles), N^{2}LO (orange diamonds) and N^{3}LO (green pentagons), normalised with respect to the N^{3}LO values. The calculations use $(e_{max}, e_{3max}) = (10, 14)$, $\hbar\Omega = 16$ MeV and $\gamma = 1.5$ MeV. The left, centre and right columns correspond to ^{56}Fe, ^{46}Ti and ^{44}Ti, respectively.

resemblance between the N^{2}LO and N^{3}LO strengths functions seems to consolidate that the interaction is well-converged.

5.2.4 Conclusion

All parameters analysed for the convergence of the FTHFB calculations of chapter 4 are found to produce amplified errors at the FTQFAM level. In particular, the choice of the optimal oscillator frequency plays a crucial role within the model spaces studied. The influence of $\hbar\Omega$ on the energy of the GMR shows that tuning this parameter is of great importance for the study of GMR-related quantities, such as the compressibility of nuclear matter.

Regarding the size of the model space, we find already well-converged strength functions (and corresponding moments) at $e_{max} = 6$. The difference with the much larger $e_{max} = 10$ case is of less than 10% at worst for the monopole excitations. We can therefore conclude that these basis sizes are appropriate for a description of giant resonances

with this interaction and for stable nuclei of such masses. The convergence with the size of the three-body space, characterised by e_{3max}, could not be studied in detail. The possibility that sizeable corrections are brought by increasing e_{3max} towards higher values cannot be dismissed. Nonetheless, calculations of ground state properties in $sd-$shell nuclei using the same or close by interactions have been shown to be well converged at $e_{3max} = 14$ [Dik+15; Jan+16; Her20] for shell-model approaches, and the bulk properties of the ground states of stable heavier nuclei ($A \gtrsim 100$) were shown to change in about five percents when increasing e_{3max} from 14 to values yielding convergence [Miy+21]. Although the three present nuclei lie in between in protons and neutrons numbers, we can expect the modifications engendered by lifting e_{3max} to higher values do not change too much the predicted observables.

Lastly, we observe a reasonable convergence of the RPA moments with the number of chiral orders, with roughly 10% relative uncertainty. This stays consistent with the uncertainties obtained for the ground state calculations. While these errors are not large enough to prevent us from extracting meaningful physical information, higher-orders or more evolved interactions would in the future be very relevant, as a back-of-the-enveloppe calculation based on the excellent agreement between N^2LO and N^3LO lets us foresee that each additional chiral order would reduce the uncertainties by a factor $Q = 1/3$.

5.3 Moments of the strength

If one is specifically interested in quantities related to the moments of the strength function $S(F, \omega)$, such as the average excitation energy, the width of the strength, etc, it is possible to use (3.113) around a contour circling all the QRPA poles.

Whenever the cross-section is strongly peaked around one collective frequency, the integrated quantities (5.1a) and (5.1b) can constitute good substitutes to the full strength function. From the theoretical side, it is interesting to study whether the contour integration method can serve as shortcut to obtain the moments m_k with good accuracy. From [Hin+15], we expect a fast convergence of the moments with the number of integration points, so that a couple dozens of nodes should already yield results converged within a few percents.

Tables 5.1-5.2-5.3 give the benchmark results for ^{16}O. The results of the contour integration are compared with the exact results obtained from matrix RPA calculations, and with the appropriate integrals of the FAM strengths on the real ω axis. The contour is composed of four portions (figure 5.10), and is automatically adjusted to enclose all the poles, by imposing a large radius equal to three times the maximum qp energy[2]; the radius of the small semicircle is chosen as the minimum between 500 keV[3] and half the

[2]Without the RPA self-energy, the highest-energy pole lies at two times $\max(E_{qp})$, hence taking a 50% larger radius should certainly enclose all the RPA poles.

[3]If no spurious modes are present, one can let the contour get arbitrarily close to $\omega_\gamma = 0$. A small but finite radius is kept as a middle-ground, to avoid bad surprises in case the removal of the NG suffers from numerical noise.

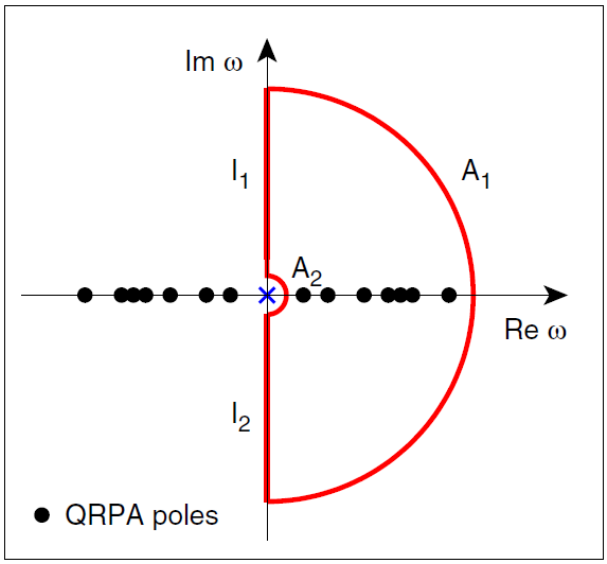

Figure 5.10: Contour in the (ω, γ) plane employed for numerically integrating the m_k moments. The contour is composed of two semicircles A_1 and A_2, and two segments I_1 and I_2. It is oriented counter-clockwise to match the signs of all contour integral formulae given in this thesis. Figure taken from [Hin+15].

smallest qp energy[4].

The spacing between the different integration nodes is adjusted such that each portion contains a number of points proportional to its arc length. The line integrals are calculated by the trapezoid rule. Note that applying Richardson's extrapolation [RG11; RG27] (interestingly, see [Huy54b; Huy54c; Huy54a; Huy54d], and also [Bre09] and references therein) to a series of points whose number grow as 2^k in an attempt to further improve the convergence produces slight but unpredictable instabilities, so that it is safer in practice to keep an eye on the results obtained at each order when carrying it out. Additionally, it can be verified from (2.82) that $S(F, \omega_\gamma)$ possesses the two symmetries

$$\mathrm{Im}\{S(F, \omega + i\gamma)\} = -\,\mathrm{Im}\{S(F, \omega - i\gamma)\}, \tag{5.12}$$
$$\mathrm{Re}\{S(F, \omega + i\gamma)\} = +\,\mathrm{Re}\{S(F, \omega - i\gamma)\}; \tag{5.13}$$

these two can be employed to avoid calculating the strength along either of I_1 or I_2, which provides a $\sim 25\%$ speed-up.

A rather fast convergence is observed for all considered moments and multipolarities, except for the $k = 2$ moment. From the imaginary part of the calculated values, which should be zero in the exact limit, the error due to the integration method and the numerical noise can be estimated to be less than 10^{-5} relative to the values given in tables 5.1, 5.2, 5.3. The source of the important error on m_2 could not be tracked down; it

[4] Again, without the self-consistent rearrangement, the pole is located at twice the smallest qp energy. If the RPA self-energy is large compared with $\min(E_{\mathrm{qp}})$, this contour may miss some poles.

may signal the need for more points as $|k|$ grows. The increase in the error for larger value of $|k|$ is certainly due to the contour extending over a large semicircle, so that the error due to the integration scheme is more important for large $|\omega_\gamma|$ and $|k|$. The same argument can be applied for the negative moments: the frequencies with small $|\omega_\gamma|$ contribute more to the integral, so that more points are required close to the origin of the (ω, γ) plane. Eventually, the convergence should be slightly improved by using a rectangular contour extending up to rather small values of the complex component (figure 5.11).

On the other hand, the moments obtained by integrating a strength function calculated on the real axis yields numerical values roughly 10% off from the exact (QRPA) results. This is due to using a finite number of points, and a non-zero value for γ. Keeping a small but finite smearing width does not improve the results significantly, as a larger number of points is then needed to reach the peaks of $S(F, \omega_\gamma)$. Therefore, the complex plane integration of the strength and the integration along the real axis typically yield results of similar quality when the objective is to determine the moments m_k. This conclusion

	$k=-1$	$k=0$	$k=1$	$k=2$	$k=3$
QRPA	11.37802	303.8041	8198.973	226279.4	6551223.0
FAM (10)	7.24321	907.9113	20882.09	798860.0	4173025.0
FAM (100)	11.35725	301.4375	8184.050	368160.0	6539275.0
FAM (1000)	11.37783	301.3575	8198.825	368115.0	6551100.0
FAM* (100)	11.23504	286.7247	7679.300	212588.3	6085894.2

Table 5.1: Moments of the strength calculated for ^{16}O for an isoscalar monopole excitation. The integration contour is discretised with 10 (top), 100 (middle) and 1000 (bottom) points. The very last line reports the integration of the strength along the real axis for 100 points equally spaced in the $[0; 50]$ MeV interval, with $\gamma = 1.5$ MeV. All calculations are performed at $(\mathrm{e}_{\max}, \mathrm{e}_{3\max}) = (6, 14)$ with $\hbar\Omega = 20$ MeV.

	$k=-1$	$k=0$	$k=1$	$k=2$	$k=3$
QRPA	0.134670	3.627249	101.9405	3071.606	103121.1
FAM (10)	0.088924	11.15050	67.32517	10330.84	68150.04
FAM (100)	0.139408	3.731564	105.5267	5009.105	106745.6
FAM (1000)	0.139661	3.730491	105.7181	5008.888	106942.3
FAM* (100)	0.129732	3.259581	86.86047	2418.481	70549.96

Table 5.2: Same as table 5.1 for the isovector dipole excitation.

	$k=-1$	$k=0$	$k=1$	$k=2$	$k=3$
QRPA	12.31209	319.7424	8319.949	217261.9	5716636
FAM (10)	7.529073	942.9192	5087.849	777409.5	3497214
FAM (100)	11.80407	304.7991	7976.651	347203.7	5480799
FAM (1000)	11.82546	304.6995	7991.106	347137.6	5490692
FAM* (100)	12.18821	303.5510	7922.190	213172.7	5912807

Table 5.3: Same as table 5.1 for the isoscalar quadrupole excitation.

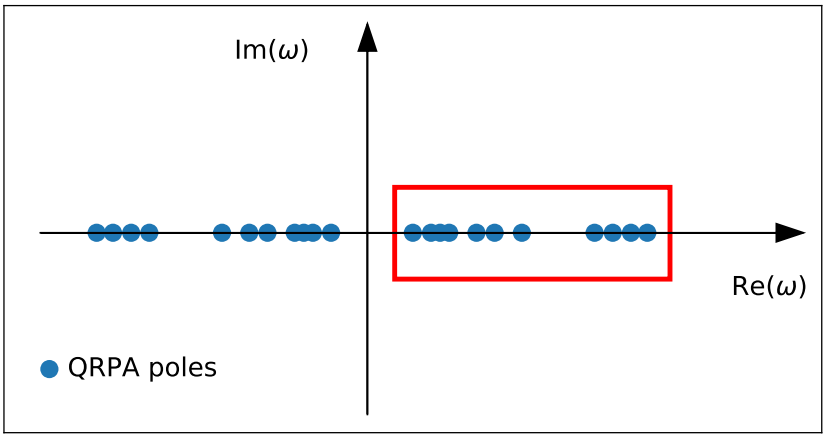

Figure 5.11: Alternative contour for the complex-plane integrations.

is more pessimistic than that of [Hin+15] regarding the efficiency of the complex-plane integration. A thorough study of the different integration schemes and their stability when supplemented by an extrapolation method, along with the potential improvement brought by using a rectangular contour that stays close to the real axis, could be useful to sort this difference of appreciation out.

5.4 Multipolar strengths of selected mid-mass nuclei at finite temperature

In this section, finite temperature strength functions are calculated for ^{56}Fe, ^{46}Ti and ^{44}Ti, as all three show the low-energy $E1 + M1$ enhancement. All calculations are carried out with the parameters $\hbar\Omega = 12$ MeV, $(\mathrm{e}_{\max}, \mathrm{e}_{3\max}) = (10, 14)$ and use the SRG-evolved N^{3}LO interaction, with a three-body part approximated by its normal-ordered form [Rot+14]. Although the present study does not consider all relevant excitation operators, using a panel of three multipole operators applied on top of three deformed systems allows us to grasp the overall effects of temperature on nuclear resonances. The study of astrophysically relevant operators, such as magnetic multipoles and charge-changing excitations, would be highly relevant for further studies. For now, the applications of the FTQFAM are restricted to the subset of electric multipoles with $K = 0$, although the $K \neq 0$ modes, as well as the $M1$ multipole, are also available at zero temperature.

For the sake of setting the stage properly, let us mention that the collective motion in strongly coupled finite systems goes beyond the picture of uncoupled modes: as a consequence of the system being put under motion, its multipole moments may all vary, resulting in an overall coupling of the different multipoles altogether[5]. The pictorial view of this phenomenon suffices in understanding the interplay of the possible excitations[6]:

- The monopole mode corresponds to a spherically symmetric operator, $Q_{00} \propto \sum_i^A \hat{r}_i^2$. It can therefore generate only $SO(3)$-conserving excitations. The only spherical

[5]Naturally, up to the fulfilment of a set of selection rules, detailed for each multipole in what follows.
[6]For clarity, the hats on top of the position operators $\hat{r}$ and $\hat{z}$ are restored for a moment.

harmonic exhibiting this symmetry being Q_{00} itself, monopole excitations do not contain any other modes.

- The isovector dipole corresponds to protons and neutrons vibrating against each other, i.e. $Q_{10}^{\mathrm{IV}} \propto \frac{N}{A}\sum_i^Z \hat{z}_i - \frac{Z}{A}\sum_i^N \hat{z}_i$. This mode a priori modifies the radius of the system, as well as its deformation. It can therefore trigger both monopole and quadrupole motion. Because it breaks both spherical and parity symmetries, it can couple to any other Q_{JK} as well.

- The quadrupole operator $Q_{20} \propto \sum_i^A 3\hat{z}_i^2 - \hat{r}_{\perp,i}^2$, as well as modes of higher multipolarity, induce non-spherical oscillations. The even-J ones do not break the parity symmetry, and therefore they do not contain odd-J oscillations. Conversely, the parity-breaking, odd-J modes may also contain parity-conserving vibrations.

For the modes we restrict this study on, we thus expect to observe an intrusion of monopole modes in dipole and quadrupole oscillations, and a presence of quadrupole modes in the dipole strengths.

Like observed in other studies [Paa+09; Niu+09; Yük+14; Yük+17; LW18; WL19; Yük+19; LW19; LRW20; Yük+20; Rav+20; LR21], the strengths appreciably depend on the temperature in general. These evolutions are explained by two mechanisms. First, the positive energy qp states become occupied, so less energy is required to take the ground state to an excited one. This shifts towards low-ω the large peaks that already exist at $T = 0$. Second, the (positive and negative) low-energy qp states have occupations significantly differing from zero or one, resulting in the W and Z amplitudes becoming of increasing importance. Transitions among qps that do not cross the Fermi energy are now permitted, which causes resonances mainly at low excitation frequencies, without discarding the possibility of important contributions at higher energies.

While these effects do not appear to be very pronounced for the monopole modes, traced in figure 5.12, we note however the disappearing of the low-energy strength in the Ti nuclei. A feeble resonance is visible on the low-energy monopole in Fe as well, but its very weak magnitude with respect to the GMR, and the dependence on $\hbar\Omega$ that is not yet completely washed out within a model space of $(\mathrm{e_{max}}, \mathrm{e_{3max}}) = (10, 14)$, do not allow for unambiguous conclusions. In all cases, the GMR becomes slightly narrower and higher as the temperature increases; this is visibly a consequence of two neighbouring resonances merging. The average excitation energy is globally found to increase with temperature (figure 5.13), due to (i) the collapse of the small resonances below 10 MeV, already complete at $T = 1.5$ MeV, and (ii) the drift of the main peak, and (iii) the enhancement of a secondary peak past the location of the GMR.

A rather similar conclusion is drawn for the isoscalar quadrupole (figure 5.14), in which the energy of the GQR is not so much affected by the temperature. We note however that the strength of the giant resonance in ^{56}Fe becomes quickly doubles, due to different peaks stacking at approximately 20 MeV. For all three nuclei, the effects are more important at low energies ($\omega < 10$ MeV), as usual. In this region, the strengths are quenched by a factor of two. This is tentatively attributed to the diminution of the occupation numbers

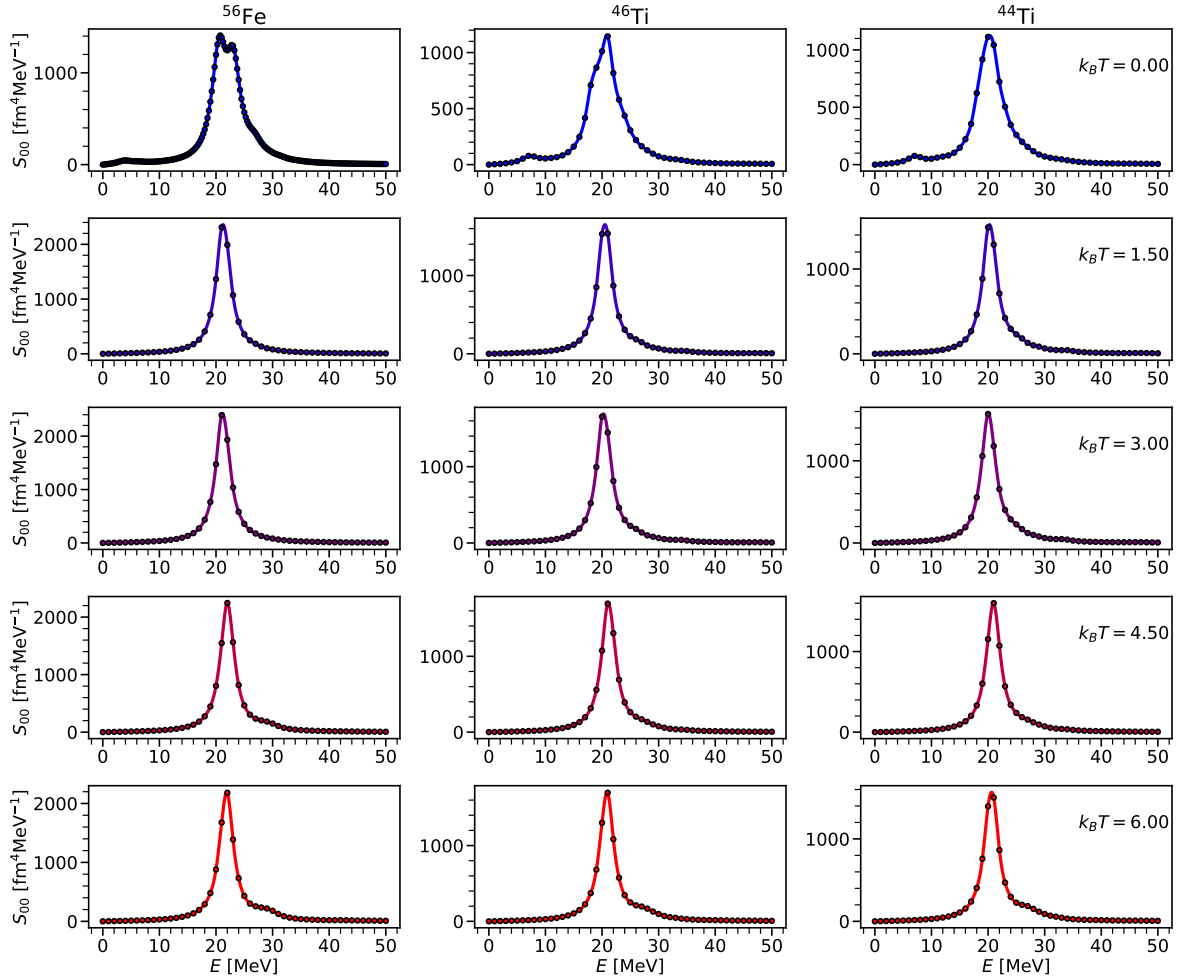

Figure 5.12: Evolution of the S_{00} strength with temperature for ^{56}Fe, ^{46}Ti and ^{44}Ti. All calculations are carried at $(e_{max}, e_{3max}) = (10, 14)$. We use a complex frequency $\gamma = 1.5$ MeV.

of the participant orbitals and the opening of new channels through the W and Z amplitudes as temperature is increased. Such argument is in agreement with the findings of the authors of [Yük+17], who observed an important decrease in the low-energy quadrupole strength. On the opposite, we find in the three systems that the mean excitation energy, represented on figure 5.15, increases in about 2 MeV between $T = 0$ and $T = 6$ MeV. This is due to the sharp diminution of the contribution of the low-energy region. Splitting the strength in two regions located on either side of $\omega = 10$ MeV (figure 5.16), we indeed find that the energy of the GQR is only weakly dependent on T past the critical temperature, showing variations of 400 keV at most in the $T = [1.5, 6]$ MeV range. The low-energy resonances share the same evolution: a sudden diminution of the mean excitation energy is found when heating the systems from $T = 0$ to $T = 1.5$ MeV, followed by a relative stagnation. Operating the separation of the strength into these two regions highlights that for each, the centroid changes in little proportions beyond $T = 1.5$ MeV, while the most sizeable changes occur before the restoration of the spherical symmetry.

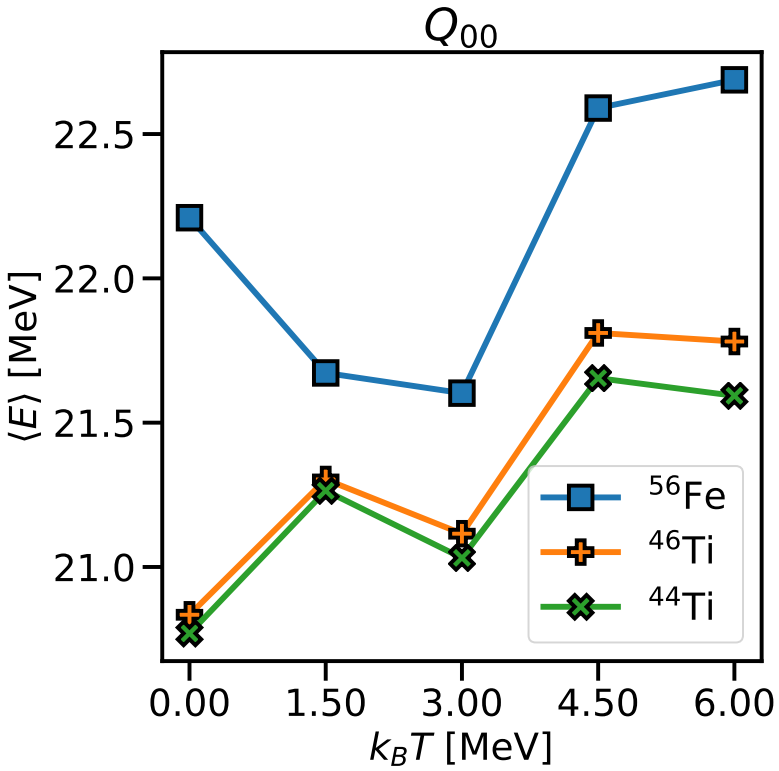

Figure 5.13: Evolution of the mean excitation energy with the temperature, for a isoscalar monopole probe.

Finally, the evolution of the GDR, plotted in figure 5.17 is clearer. Between $T = 0$ and $T = 1.5$ MeV, the maxima of the dipole strengths are shifted of several MeVs. This can be understood from the schematic models of Goldhaber and Teller (GT) [GT48] and Steinwedel, Jensen and Jensen (SJJ) [SJJ50]. The GT model assimilates the GDR as a motion of protons and neutrons fluids against each other, as two spheres attached by a spring whose stiffness is related to the GDR frequency. The model of SJJ implements the GDR as a volume-conserving motion, in which protons and neutrons oscillate between two hemispheres. Both predict a centroid energy decreasing with the radius R, like $R^{-\frac{1}{2}}$ (GT) or R^{-1} (SJJ). The two models were initially derived assuming spherical nuclear shapes; they can however be readily generalised to vibrations of deformed systems along one of their symmetry axis. For axial shapes, we can consider ellipsoids defined by the radial and axial lengths $R_\perp$ and R_z. In the Q_{10} vibrations, motion takes place along the z direction. With respect to the GDR centroids given by the spherical formulae, we can therefore expect the values to be lowered for prolate systems, and raised for oblate ones. These considerations are consistent with the observed evolution of the strength in figure 5.17, where the oblate Fe nucleus sees its mean excitation energy shifted downwards when heated to $T = 1.5$ MeV, where the static deformation is reduced down to approximately 80% of its zero-temperature value. As the shift is essentially absent at higher temperatures -in particular, between $T = 1.5$ and $T = 3$ MeV, where the spherical symmetry is being fully restored-, the decline of β_2 does not seem to entirely explain

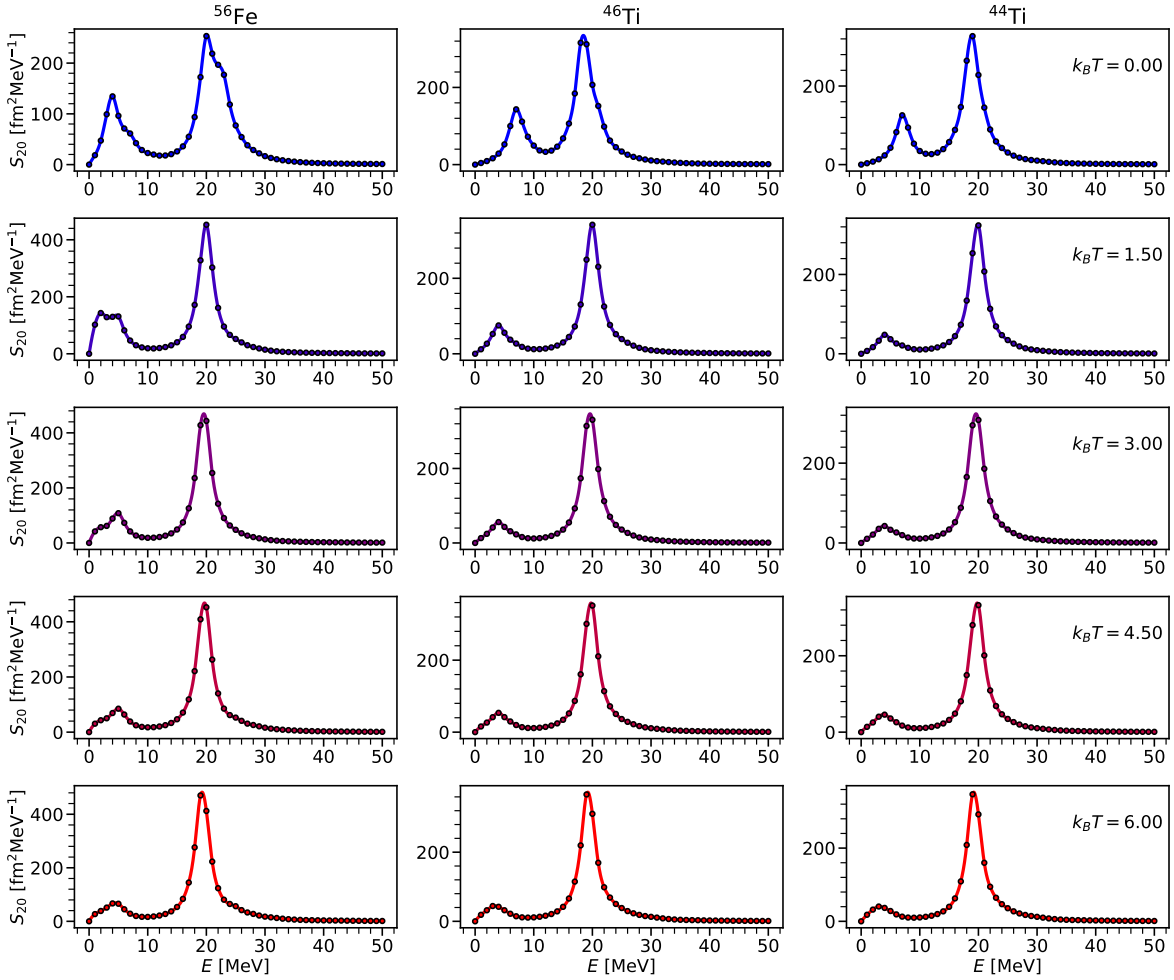

Figure 5.14: Same as figure 5.12 for the S_{20} strength.

the origin of the shift. It can be presumed to be already well-established at ~ 1 MeV below the critical temperature due to the interplay of thermal excitations with the FAM amplitudes, the former allowing the latter to explore configurations that differ from the ground state to a larger extent than what would be permitted at zero temperature. Past $T = 1.5$ MeV, the mean excitation energies always decrease, owing to the amplification of the GDR strength around 15 MeV and the systematic shift of the energy of the maximum. Both terms contribute to comparable extents.

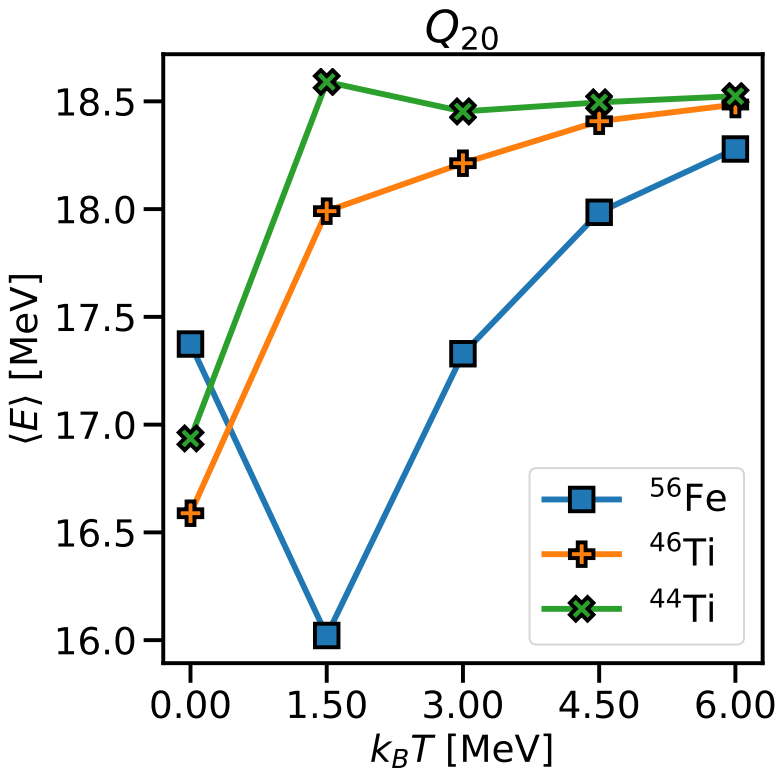

Figure 5.15: Same as figure 5.13 for an isoscalar quadrupole probe.

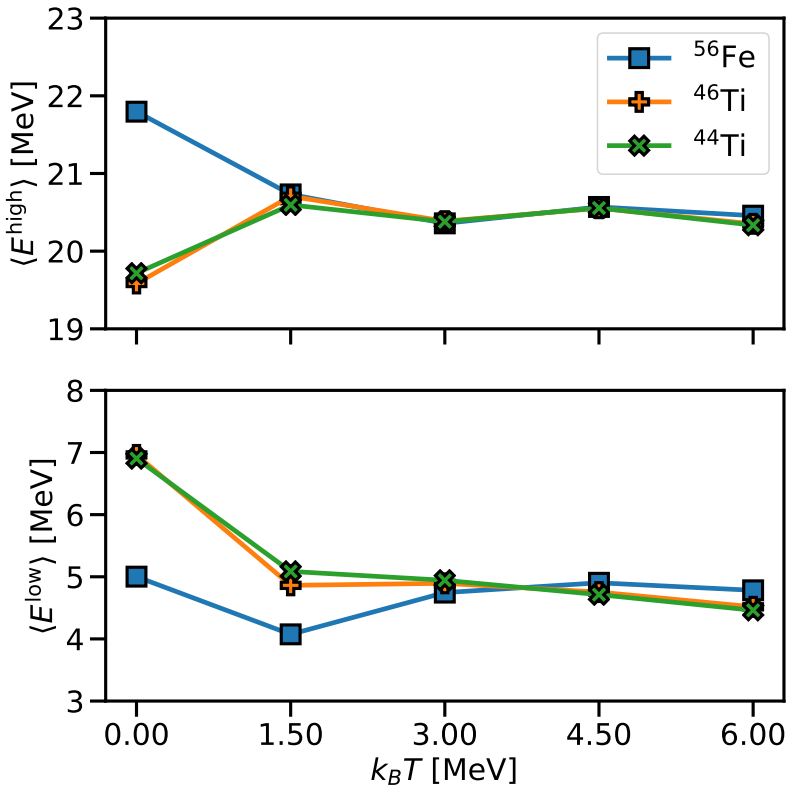

Figure 5.16: Temperature dependence of the high-energy (top) and low-energy (bottom) resonances centroids for the isoscalar quadrupole perturbation. See text for details.

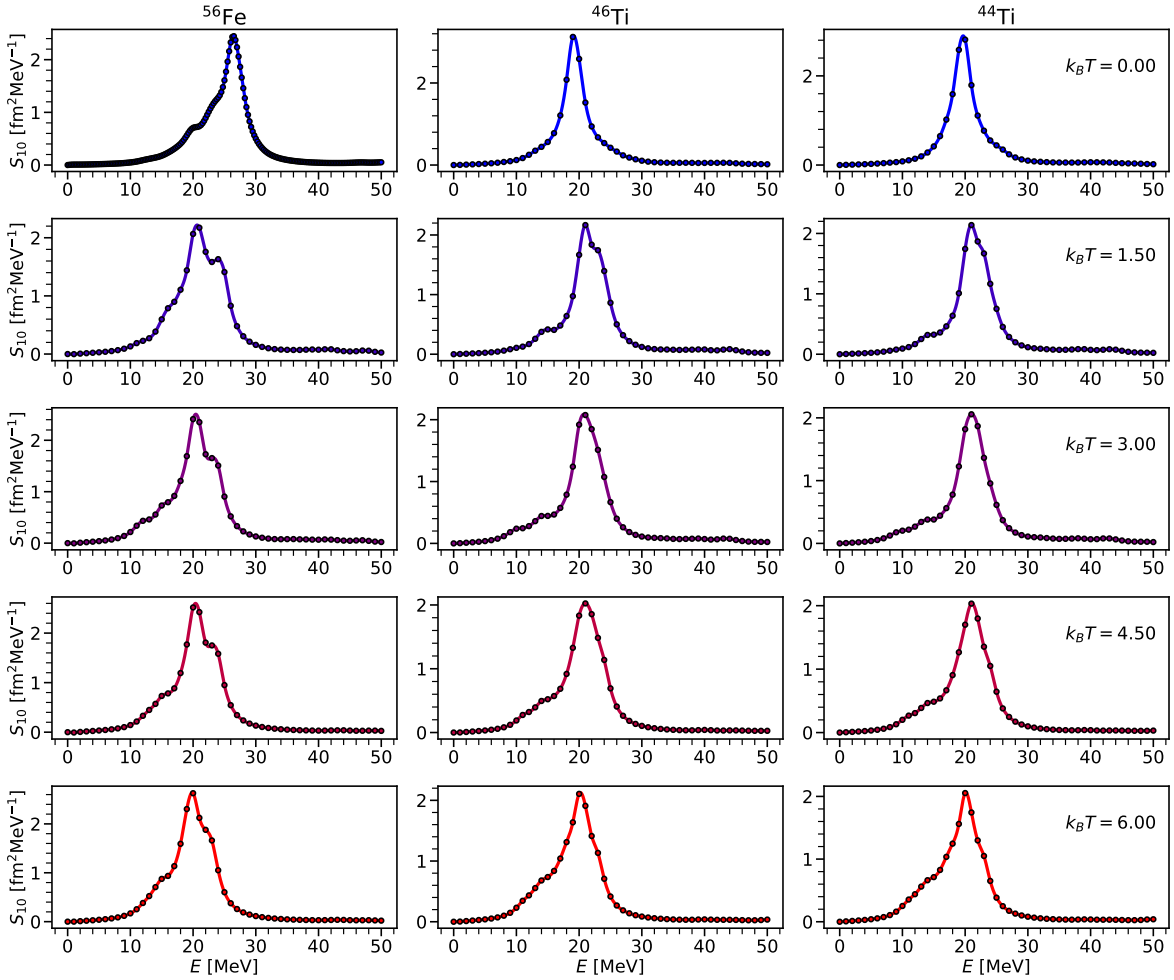

Figure 5.17: Same as figure 5.12 for the S_{10} strength.

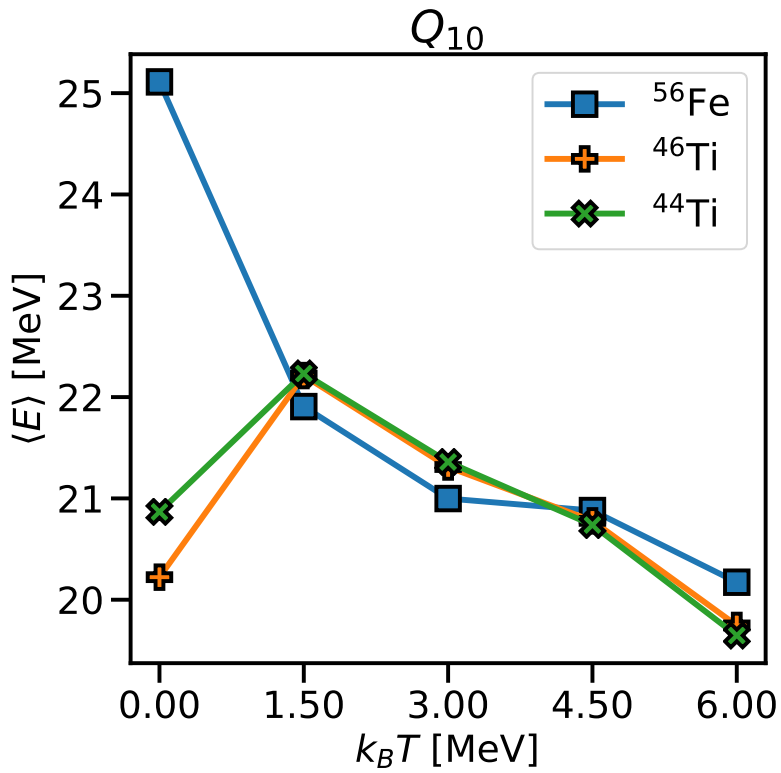

Figure 5.18: Same as figure 5.13 for an isovector dipole probe.

5.5 Conclusion

The thermal evolution of the most frequently studied multipolarities have been analysed for a restricted set of oblate and prolate nuclei, and the qualitative features are in concordance with the ones predicted by schematic models. Although we do not observe the low-energy enhancement of the dipole strength functions, a strong evolution of the IVGDR with temperature is found. This section is concluded by pointing out possible mechanisms that could generate the low-energy up-bend in the studied nuclei. First, the $\propto T^2$ contribution to the width γ could contribute to some extent to producing a wide peak at low energy if the number of RPA eigenstates is very large and located in a small energy window: these several small peaks would overlap, resulting in an amplified strength within a narrow energy interval. The resulting broad resonance however appears rather flat; this mechanism thus cannot by itself explain the increase of the strength function.

Second, although the story is not complete already at the level of the 2qp excitations – the FAM is applied on top of a single-reference, symmetry-unrestored ground state, which may very well possess a spectrum too distant from reality–, we can speculate that higher-order thermal effect play a role. Indeed, four quasi-particle effects should enter the stage by contributing to the 4qp amplitudes as (see appendix D)

$$\mathcal{X}^{4\mathrm{qp}}_{ijkl}(\omega_\gamma) \sim \frac{1}{E_i + E_j + E_k + E_l - \omega_\gamma}, \tag{5.14}$$

and should thus result in eigenstates at energies more or less close to $E_i + E_j + E_k + E_l$[7]. In opposition, thermal excitations mix positive- and negative-energy qps (see the W and Z amplitudes in (3.8)), so that contributions of the form of

$$\mathcal{W}^{4\mathrm{qp}}_{ijkl}(\omega_\gamma) \sim \frac{1}{E_i + E_j - E_k - E_l - \omega_\gamma} \tag{5.15}$$

and the likes are also possible. Now, some of these terms do contribute at low energy, contrarily to amplitudes like (5.14) which should reasonably be located beyond four times the smallest qp energy. A low-energy enhancement of the strength function can therefore be speculated for higher-order RPA and FAM, at non-zero temperature only. Finally, as the present work uses an ab initio interaction and a single HFB vacuum that does break the $SO(3)$ and $U(1)$ symmetries, a significant amount of correlations is not yet included. The extension of the method towards the inclusion of higher-order excitations is an obvious direction. In parallel, the restoration of symmetries, either before or during the FAM step, should improve the quality of the description.

[7] It should be clear that this is only an estimation, as the effects of the self-consistent rearrangement cannot be gauged in this order-of-magnitude calculation.

Chapter 6

Conclusion and perspectives

Incidently, this work presents the first finite temperature calculations for deformed and superfluid nuclei when the interaction derives from an effective theory of quantum chromodynamics at low energy. Prior to this work, ab initio calculations of strength functions had to be restricted to zero-temperature systems and spherical nuclei, while only the superfluid regime could be addressed[1]. Rather than a feat of exceptional intelligence and skill from the author of this thesis, such a fact is entirely a merit of the method's original proponents [NIY07].

In the present work, we have extended the formalism of the FAM to systems writing as statistical mixtures, opening in particular the door to studies of systems in thermal baths. Different aspects of the formalism have been studied in detail, and the connection of the newly developed FTQFAM with the standard FTQRPA has been shown. A first study presented in the thesis concerns the evolution of the HFB ground states with temperature; general features of phase transitions have been observed and analysed. In particular, the critical temperature is within the range of those found in heavier systems with phenomenological interactions. A second study focused on applications of the FTQFAM to axially-symmetric electric transitions. The results coincide with the trends in the evolution of the strength functions that can be expected from schematic models. Both chapters contain a careful analysis of the convergence of the calculation with respect to numerical and physical parameters; and the FAM has been benchmarked scrupulously against existing RPA calculations. Owing to the efficiency and transversality of the method, it should provide a useful tool and a fruitful avenue for previously out-of-reach ab initio studies of multipolar response in strongly coupled quantum systems.

Possible future extensions of the work done in this thesis abound. On a "short" timescale, spectroscopic information on the structure of the resonances could be got by projecting the transition densities on well-defined quantum numbers. Another important perspective would be to open up the study to odd-mass and odd-odd systems, e.g. through the blocking technique mentioned in section 3.1[2] or by treating the last single nucleon(s)

[1] This is only true in the context of an ab initio interaction; full glory calculations using phenomenological interactions have been around for quite a few years.

[2] The explicit treatment of the last nucleon requires the explicit breaking of time-reversal symmetry in the HFB reference state, which is quite some work to implement. Using the equal-filling approximation [PR08] allows one to simplify the problem.

exactly. At the FAM level, the inclusion of more exotic operators can be realised, in order to study charge-changing transitions such as single [Mus+14] or double beta-decay. Although available, the magnetic transitions have not been studied in detailed in this thesis either. On longer terms, the formalism can certainly be adapted to projection techniques, many-particle-many-hole expansions and perhaps a mixing of both. The ground state on top of which the FAM is applied could be further correlated: one could adapt the self-consistent RPA to the FAM (e.g. by recovering the RPA eigenvectors), recasting the correlation obtained through the "vertical" expansion on top of a single reference state. It should also be possible to mix the vertical and horizontal techniques by using a ground state obtained via a multi-reference approach such as the GCM.

Another appealing direction is the possibility to carry out FAM calculations with restored symmetries. It is tempting to say that projecting the reference state before solving the FAM equation identifies with a variation after projection (VAP), while projecting a set of FAM solutions obtained on top of symmetry-breaking ground states constitutes a projection after variation (PAV). The VAP approach requires no formal extension of the FAM formalism, whereas the PAV calls for a procedure of symmetry restoration for the FAM solutions, tentatively entirely analogous to the ones of static HFB solution [SR00; Sim10; SY14; SH17].

Along the line of [Hin15; WHN21], the systematic evolution of inertial masses when calculated over potential energy surfaces according to HFB, cranked RPA (i.e., non-self-consistent QFAM) and self-consistent QFAM[3] could constitute a useful study of the importance of the residual interaction, e.g., along dynamical paths with or without including rotational correlations, which can be addressed in an extension of the FAM to a collective Hamiltonian.

Finally, a more in-depth study of the giant resonances in astrophysically pertinent nuclei could be carried out by adding the Hamiltonian with terms corresponding to electromagnetic fields of magnitude similar to what is speculated to occur in neutron stars and supernovae.

[3]Those last two steps can respectively be understood as including the residual static, then dynamic correlations.

Appendix A

Producing ab initio nuclear interactions

A.1 Quantum chromodynamics and chiral effective field theory

In principle, the description of any nuclear system can be done solely by solving the many-body problem starting from the Lagrangian density of quantum chromodynamics (QCD)[1]. QCD is a non-Abelian gauge theory of interacting fermions (quarks) and bosons (gluons), with a Lagrangian density that writes [MS16]

$$\mathcal{L}_{\text{QCD}} = \mathcal{L} = \bar{q}(i\gamma^\mu D_\mu - M)q - \frac{1}{4}G^a_{\mu\nu}G^{\mu\nu}_a. \tag{A.1}$$

The gauge group of QCD being $SU(N_c)$, there are N_c quarks and $N_c^2 - 1$ gluons. Experimental data on the hadron spectrum indicate that $N_c = 3$, resulting in three quark fields and eight gluons fields. In (A.1):

- q represents the vector of quark fields and $\bar{q}$ its Hermitian conjugate,
- γ^μ the Dirac matrices,
- D_μ the covariant derivative, written in terms of the usual derivative ∂_μ, the gluon fields A^a_μ and the associated generators t_a:

$$D_\mu = \partial_\mu - igA^a_\mu t_a, \tag{A.2}$$

  with g the coupling constant of the theory,

- M is the mass matrix of the quarks:

$$M_{qq'} = m_q\delta_{qq'}, \tag{A.3}$$

[1] Quantum electrodynamics (QED) must be included as well. Being perturbative, it constitutes the "easy" part of the problem, and is therefore omitted from the present appendix.

- $G^a_{\mu\nu}$ is the gluon field tensor, and contains an Abelian term, plus one that depends on the structure constants f_{abc}[2]:

$$G^a_{\mu\nu} = \partial_\mu G^a_\mu - \partial_\nu G^a_\mu + g f_{abc} G^b_\mu G^c_\nu. \tag{A.4}$$

  The last term is, when at play in (A.1), responsible for the three and four gluons vertices.

Owing to the large value of the QCD coupling constant g in the low-energy regime, the spectrum of the theory cannot be determined by perturbative means. This renders any attempt to calculate analytically the properties of nuclear systems extraordinarily difficult, be it in an approximate (but systematically improvable) manner. The alternative path of effective theories exploits chiral perturbation theory, which core ideas are condensed in the following lines.

Following [NJ61; MS16], one can define the left- and right-handed quark fields as

$$q_L \equiv \frac{1-\gamma_5}{2} q, \tag{A.5}$$

$$q_R \equiv \frac{1+\gamma_5}{2} q, \tag{A.6}$$

and obtain that the Lagrangian (A.1) mixes left and right quarks only through the mass term. The massless part of the QCD Lagrangian, $\mathcal{L}^0_{\mathrm{QCD}}$, is on the other hand invariant under rotations of the quark fields (they are identical, up to their colour charge), resulting in the so-called chiral symmetry. This symmetry is however spontaneously broken[3], giving rise to $N_c = 3$ massless Nambu-Goldstone (NG) bosons. In reality, quarks have masses, and the symmetry breaking of $SU(N_c)_{\mathrm{L}} \times SU(N_c)_{\mathrm{R}}$ becomes explicit. The NG modes thus acquire a mass too. Due to these masses vanishing in the chiral limit, the effective Lagrangian of QCD at energies $Q < m_{\mathrm{NG}}$ is essentially driven by $\mathcal{L}^0_{\mathrm{QCD}}$, which can be understood as an interaction occurring at momenta $\sqrt{Q}$ being, at first order, not energetic enough to produce massive NG bosons, and thereby break the chiral symmetry in an explicit manner. Virtual NG modes creation should however be included. The masses of the lightest NG bosons, the pions ($m_\pi \sim 135$ MeV), are small with respect to that of the nucleons ($m_{\mathrm{N}} \sim 939$ MeV). This scale separation $m_\pi/m_{\mathrm{N}} \sim 0.14 < 1$, lets us define an expansion parameter, resulting in the possibility to account for the finite mass of quarks through a perturbative expansion. This yields the possibility to map, at low energy, the full QCD Lagrangian into one containing pion and nucleons only. In other words, starting from $\mathcal{L}^0_{\mathrm{QCD}}$, a hierarchy of interactions in terms of number of participants naturally emerges:

$$\mathcal{L}_{\mathrm{QCD}} \to \mathcal{L}_{\mathrm{EFT}} = \mathcal{L}_{\pi\pi} + \mathcal{L}_{\pi\mathrm{N}} + \mathcal{L}_{\mathrm{NN}} + \dots \tag{A.7}$$

The most intuitive picture of this chiral expansion is to regard above-threshold inter-

[2]Determined such that $[t_a, t_b] = i f_{abc} t_c$.

[3]That is, the vacuum expectation value of the quark condensate $\langle \bar{q} q \rangle$ is non-zero.

actions as multistep mechanisms. Since higher energy phenomena correspond to smaller reaction times, one can see the perturbative expansion as a delving towards faster interactions timescales. Alternatively, it can be interpreted as many one-pion exchanges as needed in order to reach the correct energy. All processes are therefore treated with respect to a timescale $1/\Lambda$, allowing one to classify the interactions. If the time between successive collisions is small, the full process can be treated as a single many-particle collision. Above a certain energy threshold, different processes cannot be distinguished and are treated as a whole. Figure A.1 sketches the emergence of many-body interactions from binary processes, where a series of two-body interactions occurring within a time window $\tau < \Lambda^{-1}$ are not resolved independently, but grouped together and classified as a three-body interaction.

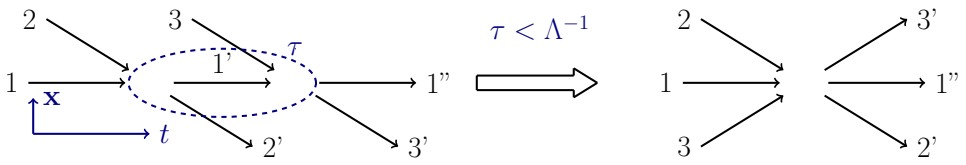

Figure A.1: Schematic interpretation of an effective many-body interaction stemming from two-body interactions.

Nuclear systems being characterised by their number of protons and neutrons, the pions entering (A.7) can in a second step be integrated out, leaving only interactions between nucleons:

$$\mathcal{L}_{\text{EFT}} = \mathcal{L}_{\text{NN}} + \mathcal{L}_{\text{NNN}} + \dots \tag{A.8}$$

The two-, three-, four-nucleons interaction terms appear sequentially through the inclusion of higher orders in the chiral expansion. Figure A.2 illustrates the four first orders and corresponding diagrams, along with the predicted phase shifts at different orders. As the EFT is a low-energy expansion, the agreement is very good at low incident energies, and progressively degrades as the kinetic energy increases.

While it could be expected that the thusly derived and adjusted many-nucleon potentials can be readily employed for any calculation of nuclear structure, it is not so in practice. This is due to these interactions still involving strong couplings between low and high momenta, making the calculated observable strongly sensitive to the size of the model space employed for practical calculations. In addition and loosely speaking, a $k-$body interaction contributes to the energy of a $A-$body system in a combinatorial manner (see appendix B). Both these problems can be circumvented to a large extent by evolving the potentials through a flow equation. A particular flavour of such evolution, the one employed by the Darmstadt group for computing the interaction matrix elements used throughout this thesis, is presented in the next section.

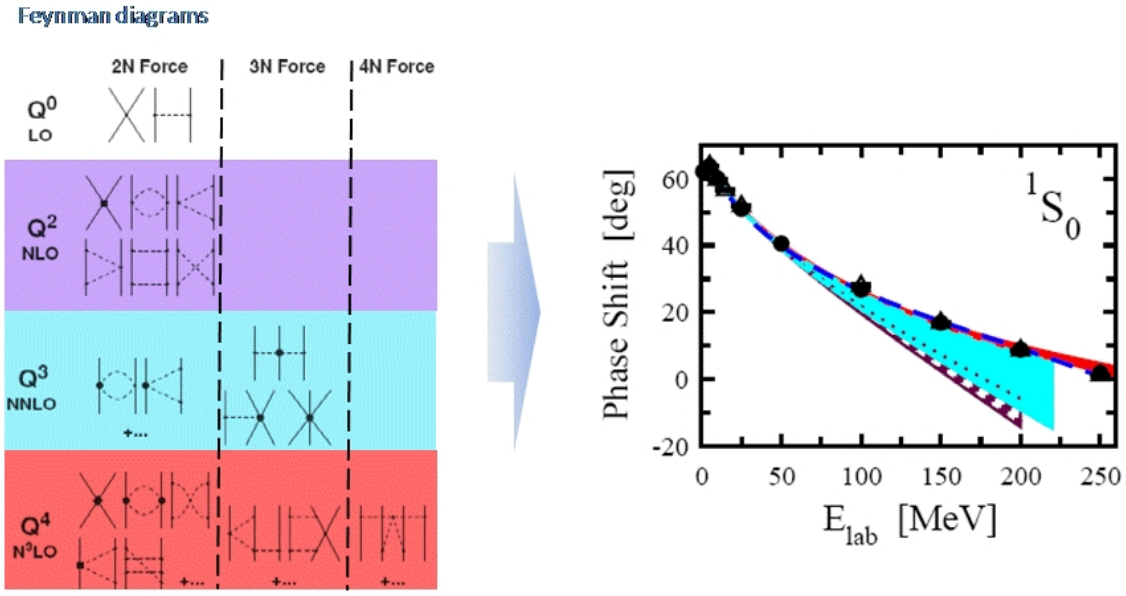

Figure A.2: Left: Diagrammatic representation of the first orders of the expansion. Right: Calculated versus experimental phase-shift in a nucleon-nucleon scattering (from [Epe06]). The convergence of the effective model is clearly visible.

A.2 Similarity renormalisation group treatment of chiral EFT

Although a perturbative series can be defined through the power-counting expansion, it is found to not be straightforwardly suited for the description of systems containing a substantial number of nucleons. Beyond the few-body cases, a direct application of the chiral interactions does not permit calculating observables in a controlled manner, primarily due to strong coupling persisting between low and high momenta. A further refinement of the bare interactions can be realised by taking advantage of the fact that the Hamiltonian is not an observable: it can be transformed at will, provided the expectation values are not affected. This constraint translates into the possibility to carry out unitary ($U^\dagger(s)U(s) = I$) transformations only, that depend on one parameter s:

$$H(s) = U(s)H(0)U^\dagger(s), \tag{A.9}$$

with $H(0)$ the bare Hamiltonian. Taking the derivative with respect to s yields the flow equation

$$\frac{\mathrm{d}}{\mathrm{d}s}H(s) = \left[\frac{\mathrm{d}U(s)}{\mathrm{d}s}U^\dagger, H(s)\right] \equiv [\eta(s), H(s)], \tag{A.10}$$

defining in passing the (anti-Hermitian) generator of the flow, $\eta(s)$. This procedure of transforming an operator by the help of a differential equation is referred to as a similarity

renormalisation group (SRG) approach[4]. The operator U can be any unitary transformation, and it is visible from (A.10) that the flow terminates as soon as $H(s)$ commutes with $\eta(s)$. These two points can be used to pick the generator in a manner that drives the Hamiltonian into a desired structure. For instance, states with different momenta can progressively be decoupled, in order to make the interaction operators diagonal in the momentum representation, see [BFP07; Bog+07], as represented in figure A.3. A common prescription is to take the generator as the commutator of $H(s)$ with its diagonal part, which in momentum basis exponentially suppresses off-diagonal elements.

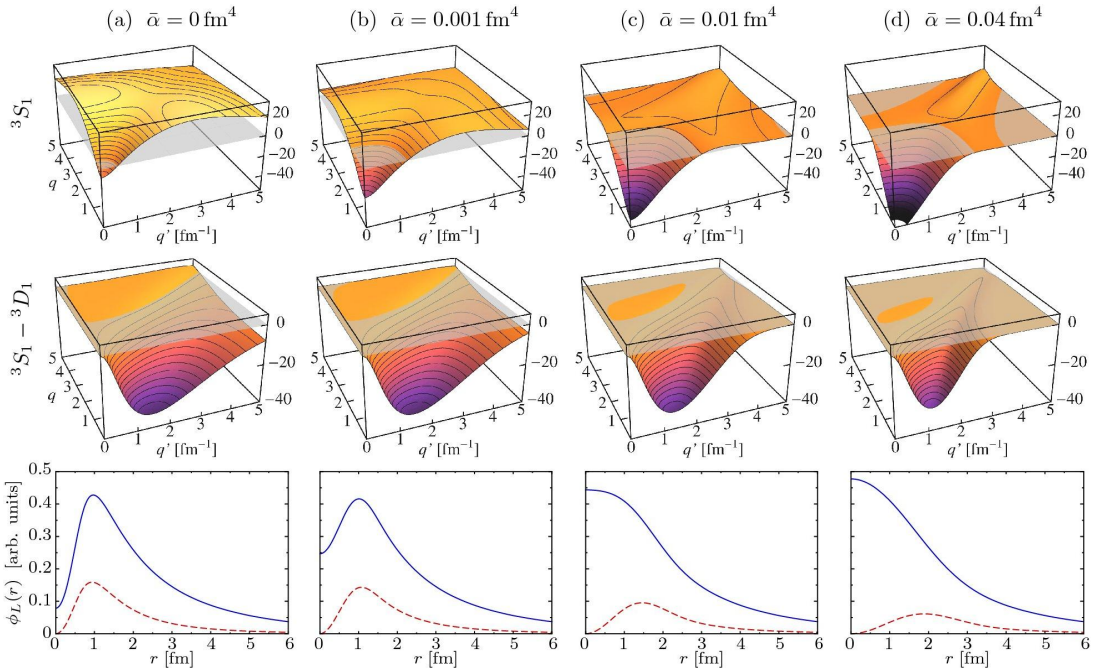

Figure A.3: Matrix elements of a N^{3}LO potential $V_s(k, k')$, through different steps of the SRG flow for the ^{3}S$_1$ (top) and the ^{3}S$_1$–^{3}D$_1$ (middle) partial waves. The bottom rows represent the radial wave functions of the deuteron ground state in the $L = 0$ (solid blue) and $L = 2$ (dashed red) channels at the corresponding SRG steps. The parameter $\bar{\alpha}$ is a different notation for s. Figure taken from [HR07], see this paper for details.

Although the SRG procedure resembles a simple rotation in a high-dimensional space, the fact it involves operators (and not simple matrices) generates additional terms through the evolution. This can be shown directly with the ladder operators: doing the substitution $\eta(s) \to a(s)$ and $H(s) \to b(s)$ for this illustrative purpose,

$$\frac{\mathrm{d}}{\mathrm{d}s} b(s) = [a(s), b(s)] = a(s)b(s) - b(s)a(s). \tag{A.11}$$

[4]One should mention that it is also possible to reduce correlations by an alternative use of unitary transformation, that resorts to a cluster expansion rather than a differential equation [Rot+07]. This defines the Unitary Correlation Operator Method (UCOM); the similarity and differences between SRG and UCOM are discussed in detail in [HR07].

As the flow equation is usually integrated by time-slicing, (A.11) shows that the SRG evolution induces many-body terms regardless of the content of the initial Hamiltonian. Such terms greatly quickly render intractable the numerical integration of (A.10); four-body terms and higher are generally dismissed.

Ab initio nuclear interactions can thus be generated according to the following workflow:

- derive all Feynman diagrams of chiral EFT at a given order,
- adjust the associated low-energy constants to reproduce few-body experimental data,
- calculate the matrix elements of the chiral potentials in a given model space,
- evolve the resulting Hamiltonian through the flow equations (A.10).

The resulting interaction can in a second step used as input ingredients for the solution of the many-body problem, e.g. through in-medium SRG, shell model calculations, or, as done within this document, mean-field calculations. In all numerical calculations of this thesis, we use unless specified otherwise the two- and three-body N^3LO interactions of [EKM15], SRG-evolved up to the final value of the flow parameter $\lambda_{SRG} = s^{-1/4} = 1.88$ fm^{-1} [Hüt+20].

Appendix B

Effective theories ideas applied to an exactly solvable model

The production of the interactions for each order of an effective theory, and the determination of the associated coupling constants, is a greatly arduous task. If the interactions are organised in a sequence of many-body terms, the adjustment of the couplings can however be made in successive steps[1]. The effective approach is nonetheless expected to break down when applied to increasing numbers of particles. This is illustrated in figures B.1-B.4, where a naive effective theory has been designed for a schematic system of two N-fold degenerate shells, known as the Lipkin-Meshkov-Glick [LMG65][2] model. Its simplest version is described by the Hamiltonian

$$H = \frac{\epsilon}{2}\sum_{p\sigma}\sigma a^\dagger_{p\sigma}a_{p\sigma} + \frac{V}{2}\sum_{pp'\sigma} a^\dagger_{p\sigma}a^\dagger_{p'\sigma}a_{p'-\sigma}a_{p-\sigma}; \quad p = \text{shell index}, \sigma = \text{spin}. \tag{B.1}$$

The effective theory allows one to constructively obtain many-body interactions strengths U_k, by matching the sought coupling constants with the exact energies:

$$E(N) = \sum_{k=1}^{N} C_N^k U_k \Rightarrow U_N = E(N) - \sum_{k=1}^{N-1} C_N^k U_k. \tag{B.2}$$

[1] Still, this is no easy game.

[2] To be picky, it should be mentioned that equations (3.4)-(3.5) are half incorrect: one should instead find

$$N=6: \quad \frac{E}{\epsilon} = \pm\left\{5 + 33\left(\frac{V}{\epsilon}\right)^2 \pm 4\left[1 + 6\left(\frac{V}{\epsilon}\right)^2 + 54\left(\frac{V}{\epsilon}\right)^4\right]^{1/2}\right\}^{1/2}, \tag{LGM-3.4 top}$$

$$N=8: \quad \frac{E}{\epsilon} = 0, \pm\left\{10 + 118\left(\frac{V}{\epsilon}\right)^2 \pm 6\left[1 - 2\left(\frac{V}{\epsilon}\right)^2 + 225\left(\frac{V}{\epsilon}\right)^4\right]^{1/2}\right\}^{1/2}. \tag{LGM-3.5 bottom}$$

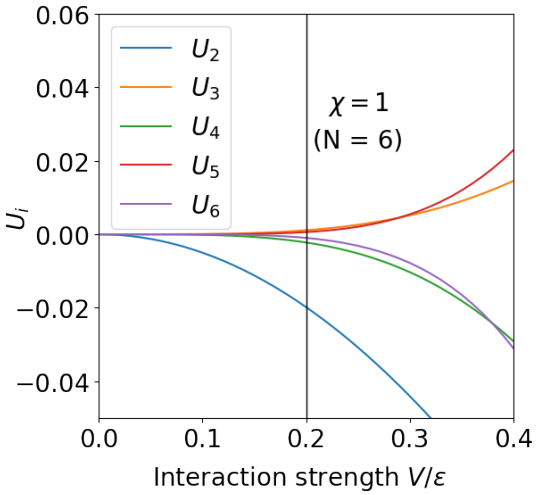

Figure B.1: Multi-body coupling constants as a function of the bare two-body strength V. The vertical line denotes the value of V for which $\chi = 1$.

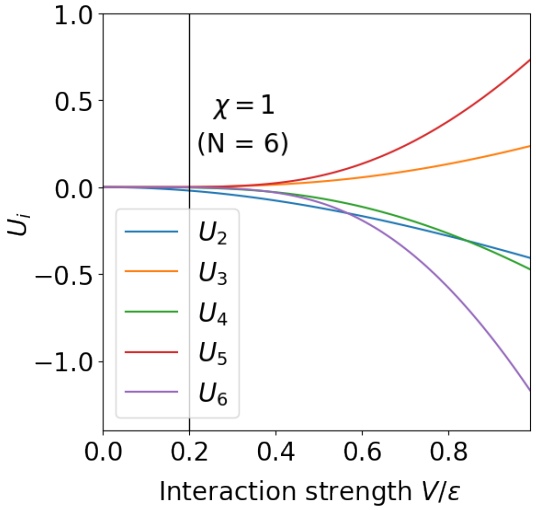

Figure B.2: Same as figure B.1 for a wider range of interaction strengths.

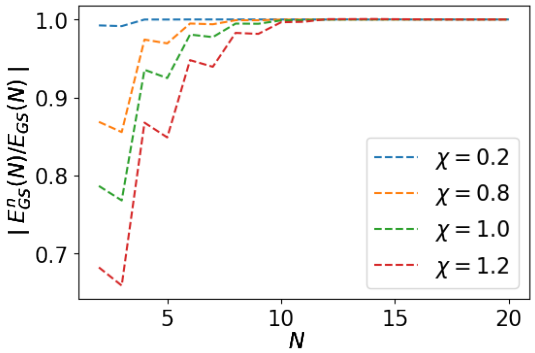

Figure B.3: Contribution of the n-body energies $E^n_{\mathrm{GS}}(N) = C^n_N U_n$ to the total ground state energy.

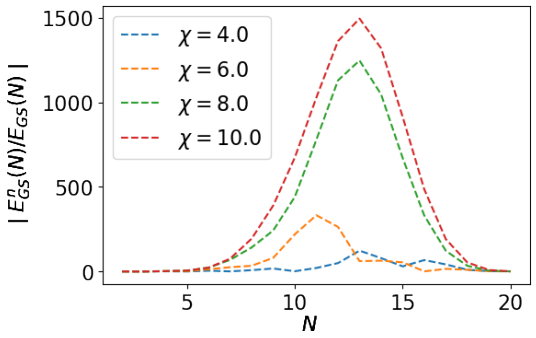

Figure B.4: Same as figure B.3 for a wider range of interaction strengths.

The results shown in figures B.1-B.4 clearly illustrate the breakdown of constructively-designed effective theories. The order parameter $\chi = V(N-1)/\epsilon$, deduced from a mean-field approximation, characterises the perturbative regime $\chi < 1$ in which one has $|U_k| < |U_{k-1}|$. In figure B.1, the breakdown of this regime starts to appear. It is clearly established in figure B.2, especially at very large couplings where U_N dominates. The information on the total energy is represented in figure B.3 for couplings χ within the perturbative regime or close to its limiting value $\chi = 1$. In that case, the different contributions add up rather smoothly towards the exact ground state energy. On figure B.4 however, where the same information is represented for larger strengths, one clearly sees the collapse of the perturbative hypothesis, as the effective couplings U_k do not decrease fast enough to compensate for the combinatorial factors. This very schematic model shows that in practical applications, great care has to be taken not to fall outside the perturbative regime. In the case of many-body systems, this can be translated into a naive way of estimating the number of particles for which the effective theory is no longer valid: the effective theory

is only legitimate for N such that

$$|U_{k+q}|C_N^{k+q} < |U_k|C_N^k \quad \forall k, q > 1. \tag{B.3}$$

Appendix C

Sum rules from the static state

While the sum rules correspond to the different moments of the strength function (2.82), it is possible to obtain some of these from static quantities only. Looking at the quantities we have at hand before starting the RPA calculation, we find that only the Hamiltonian H, the external operator F, the density matrix D and the set of single-particle operators can be used to obtain sum rules expressions. Additionally, we may introduce a parameter λ corresponding to the system constrained as $H + \lambda F$, for which the ground state will be written $|0_\lambda\rangle$. Since we may want to have a general formula, the simplest way is to build the k^{th} commutator on a nested scheme:

$$B^{(k)} = [X_k \dots [X_3[X_1, X_2]]. \tag{C.1}$$

Within this constraint, it is clear that $X_1 \neq X_2$ (otherwise $B^{(k)} = 0$). Additionally, the last term of the $k + 1^{\text{th}}$ commutator must be H in order to obtain the last power of the energy difference. Finally, as we need a second F operator in order to obtain squared matrix elements, we are led to the recurrence relation between the $B^{(k)}$:

$$\begin{aligned} B^{(0)} &\equiv F \\ B^{(1)} &\equiv \left[H, B^{(0)}\right] \\ B^{(k)} &\equiv \left[H, B^{(k-1)}\right] \qquad \text{for } k \geq 1. \end{aligned} \tag{C.2}$$

Then,

$$\begin{aligned} \langle m|B^{(k)}|n\rangle &= \langle m|HB^{(k-1)}|n\rangle - \langle m|B^{(k-1)}H|n\rangle \\ &= (E_m - E_n)\langle m|B^{(k-1)}|n\rangle \\ &= (E_m - E_n)^k \langle m|G|n\rangle\,, \end{aligned} \tag{C.3}$$

hence

$$\langle m|\left[F, B^{(k)}\right]|n\rangle = \sum_l \langle m|F|l\rangle\ \langle l|B^{(k)}|n\rangle - \langle m|B^{(k)}|l\rangle\ \langle l|F|n\rangle$$

$$\text{taking } m = n \rightsquigarrow \sum_l (1-(-1)^k)(E_l - E_n)^k \langle n|F|l\rangle \langle l|F|n\rangle \,. \tag{C.4}$$

For F Hermitian, taking the sum over the n states weighted by their statistical factor leads to the odd-k sum rules:

$$\frac{1}{2}\mathrm{Tr}\big\{\big[G, B^{(k)}\big]\big\} = \begin{cases} 0 & k \text{ even} \\ Z^{-1}\sum_{ln} e^{-\beta E_n}(E_l - E_n)^k |\langle n|F|l\rangle|^2 = m_k(F) & k \text{ odd.} \end{cases} \tag{C.5}$$

A similar derivation can be made for the inverse energy-weighted sum rule (IEWSR): we write a perturbative expansion (the notations are hopefully self-evident)

$$\langle F\rangle_\lambda = \mathrm{Tr}\left\{F\left(D + \lambda\delta D + \frac{1}{2!}\lambda^2\delta^2 D\right) + \mathcal{O}(\lambda^3)\right\}. \tag{C.6}$$

Recalling that $\delta D = RF$ ((2.80)), we can take the derivative and obtain

$$\frac{1}{2}\frac{\mathrm{d}}{\mathrm{d}\lambda}\langle 0_\lambda|F|0_\lambda\rangle\Big|_{\lambda=0} = \mathrm{Tr}\{F\delta D\} = \mathrm{Tr}\{FRF\}. \tag{C.7}$$

From the expression (2.79) of the response function, one identifies the right-hand side term with the IEWSR. This approach unfortunately cannot yield other moments: it would require getting powers of the response function R by taking higher derivative with respect to λ, which'd also make the operator F fall identically many times. Recollecting the different pieces, one sees that the moments are related to expressions involving two times the operator F, whereas each response function must be matched with two of these. Only m_{-1}, involving a first derivative, can be obtained this way.

Appendix D

Higher-order responses

D.1 Linear responses

In this appendix, the linear response of k-body densities is derived. Starting from (2.74), the time-dependent part of the expectation value of an operator O is given as

$$\langle \delta O(t) \rangle = i \,\mathrm{Tr}\Big\{ \int_{t_0}^{t} \mathrm{d}\tau [O_H(t), F_H(\tau)] D_0 \Big\}. \tag{D.1}$$

If both O and F are two-body operators, one ought to introduce closure relations over the two-body Hilbert space in order to replace the propagators by their eigenvalues, that is,

$$\begin{aligned} O_H(t)F_H(\tau) &= \sum_{\mu\nu\lambda\sigma} |\mu\nu\rangle\langle\mu\nu| \, e^{iHt} O_S(t) e^{-iHt} \, |\lambda\sigma\rangle\langle\lambda\sigma| \, e^{iH\tau} F_S(\tau) e^{-iH\tau} \\ &= \sum_{\mu\nu\lambda\sigma} e^{i\Omega^{\mu\nu}_{\lambda\sigma} t} \, |\mu\nu\rangle\langle\mu\nu| \, O_S(t) \, |\lambda\sigma\rangle\langle\lambda\sigma| \, e^{i\Omega^{\lambda\sigma}\tau} F_S(\tau) e^{-iH\tau}, \end{aligned} \tag{D.2}$$

with the notation $\Omega^{ab}_{a'b'} \equiv E_a + E_b - E_{a'} - E_{b'}$. Multiplying by the static density and taking the trace in the two-body Hilbert space yields

$$\begin{aligned} \langle O_H(t)F_H(\tau) \rangle &= \sum_{\kappa\iota} f_\kappa f_\iota \sum_{\mu\nu\lambda\sigma} \langle \kappa\iota|\mu\nu\rangle \, \langle \mu\nu| \, e^{iHt} O_S(t) e^{-iHt} \, |\lambda\sigma\rangle\langle\lambda\sigma| \, e^{iH\tau} F_S(\tau) e^{-iH\tau} \, |\kappa\iota\rangle \\ &= \sum_{\mu\nu\lambda\sigma} f_\mu f_\nu e^{i\Omega^{\mu\nu}_{\lambda\sigma}(t-\tau)} \, \langle \mu\nu|O_S(t)|\lambda\sigma\rangle \, \langle \lambda\sigma|F_S(\tau)|\mu\nu\rangle \, . \end{aligned} \tag{D.3}$$

In this expression, the $\{f_k\}$ are the Fermi-Dirac (or Bose-Einstein in case of bosons) factors. Using individual states rather than many-body eigenstates as done before greatly simplifies the tracing, and is permitted since the trace can be taken in the eigenbasis of the density operator. If O has no explicit time-dependence in the Schrödinger picture ($O_S(t) = O_S$), (D.1) can be written as the sum of two convolutions, as done in (2.76). One obtains the two-body response function

$$\mathfrak{R}^{\rho}_{\substack{\alpha\beta\gamma\delta\\ \epsilon\zeta\eta\theta}}[O] = \sum_{\mu\nu\lambda\sigma} f_\mu f_\nu O_{\alpha\beta\gamma\delta} \times \left[\frac{\langle\mu\nu|a^\dagger_\alpha a^\dagger_\beta a_\gamma a_\delta|\lambda\sigma\rangle \ \langle\lambda\sigma|a^\dagger_\epsilon a^\dagger_\zeta a_\eta a_\theta|\mu\nu\rangle}{\Omega^{\mu\nu}_{\lambda\sigma} - \omega - i\Gamma} - \frac{\langle\mu\nu|a^\dagger_\epsilon a^\dagger_\zeta a_\eta a_\theta|\lambda\sigma\rangle \ \langle\lambda\sigma|a^\dagger_\alpha a^\dagger_\beta a_\gamma a_\delta|\mu\nu\rangle}{\Omega^{\mu\nu}_{\lambda\sigma} + \omega + i\Gamma} \right]. \tag{D.4}$$

Note that the separability of the matrix elements has not been assumed. This procedure generalises clearly to k-body operators (I write $A^{\alpha\beta\ldots}_{\gamma\delta\ldots}$ for $a^\dagger_\alpha a^\dagger_\beta \ldots a_\gamma a_\delta \ldots$ to shorten the expression):

$$\mathfrak{R}^{\rho}_{\substack{\alpha_1\ldots\alpha_k,\beta_1\ldots\beta_k\\ \zeta_1\ldots\zeta_k,\xi_1\ldots\xi_k}}[O] = \sum_{\substack{\mu_1\ldots\mu_k\\ \lambda_1\ldots\lambda_k}} \left(\prod_{j=1}^{k} f_{\mu_j} \right) \langle\alpha_1\ldots\alpha_k|O|\beta_1\ldots\beta_k\rangle \times \left[\frac{\langle\mu_1\ldots\mu_k|A^{\alpha_1\ldots\alpha_k}_{\beta_k\ldots\beta_k}|\lambda_1\ldots\lambda_k\rangle \ \langle\lambda_1\ldots\lambda_k|A^{\zeta_1\ldots\zeta_k}_{\xi_1\ldots\xi_k}|\mu_1\ldots\mu_k\rangle}{\Omega^{\mu_1\ldots\mu_k}_{\lambda_1\ldots\lambda_k} - \omega - i\Gamma} - \frac{\langle\mu_1\ldots\mu_k|A^{\zeta_1\ldots\zeta_k}_{\xi_1\ldots\xi_k}|\lambda_1\ldots\lambda_k\rangle \ \langle\lambda_1\ldots\lambda_k|A^{\alpha_1\ldots\alpha_k}_{\beta_k\ldots\beta_k}|\mu_1\ldots\mu_k\rangle}{\Omega^{\mu_1\ldots\mu_k}_{\lambda_1\ldots\lambda_k} + \omega + i\Gamma} \right]. \tag{D.5}$$

D.2 Non-linear responses

The time-dependent component of the expectation value of an operator O can be written, from (2.72), as a sum of commutators involving nested integrals. Focusing on terms containing N such integrals, one has

$$\langle\delta O(\tau_N)\rangle \sim i^N \,\mathrm{Tr}\left\{ \int_{\tau_{N-1}}^{\tau_N} \mathrm{d}\tau_{N-1} \int_{\tau_{N-2}}^{\tau_{N-1}} \mathrm{d}\tau_{N-2} \cdots \int_{\tau_0}^{\tau_1} \mathrm{d}\tau_0 \, e^{\sum_{q=0}^{N-1} \alpha_q(\tau_{q+1}-\tau_q)} F(\tau_q) O(\tau_N) \right\}. \tag{D.6}$$

One can identify $\tau_N = t$ and $\tau_0 = t_0$ to match the notations employed up to now. Likewise, the α_q identify with the $\Omega^{\mu_1\ldots\mu_k}_{\lambda_1\ldots\lambda_k}$ terms. Eventually, the notation can be made more compact by writing either of

$$\int_{\tau_{N-1}}^{\tau_N} \mathrm{d}\tau_{N-1} \int_{\tau_{N-2}}^{\tau_{N-1}} \mathrm{d}\tau_{N-2} \cdots \int_{\tau_0}^{\tau_1} \mathrm{d}\tau_0 \equiv \prod_{q=0}^{N-1} \int_{\tau_q}^{\tau_{q+1}} \mathrm{d}\tau_q \equiv \int_{\tau_0}^{\tau_N} \mathcal{D}\tau. \tag{D.7}$$

The integrals in (D.6) can be written as a chain of convolutions, after inserting the appropriate step functions to account for the boundaries $\{\tau_q\}$. One can then take the Fourier transform of (D.6), which is now the product of the individual transforms. Prior to this, exponential damping functions of the form $e^{-\sum_{q=0}^{N-1} \Gamma_q \tau_q}$ are introduced, in order

to translate the fact that the probe is switched off and must vanish at infinite times. This has the effect of removing terms that depend on the intermediate times $\tau_{q\neq 0,N}$, which would otherwise make the result a rather messy sum of $2N$ terms[1]. The product of Fourier transforms then becomes a product of two-point functions, with the matrix elements correctly inserted in-between (the factor i^N gets cancelled by the is coming from the integrals, as usual):

$$\mathfrak{R}^{\rho,[N]}_{\substack{\alpha\beta\\ \gamma\delta}}(\omega) \sim Z^{-1} \sum_{\substack{\mu_1\dots\mu_N\\ \nu_1\dots\nu_N}} e^{-\beta\mathcal{E}_\nu} \left[\left(\prod_{q=1}^{N} \frac{\langle \nu_q | a^\dagger_\beta a_\alpha | \mu_q \rangle \ \langle \mu_q | a^\dagger_\gamma a_\delta | \nu_q \rangle}{\Omega^{\nu_q}_{\mu_q} - \omega - i\Gamma} \right) - \left(\prod_{q=1}^{N} \frac{\langle \nu_q | a^\dagger_\gamma a_\delta | \mu_q \rangle \ \langle \mu_q | a^\dagger_\beta a_\alpha | \nu_q \rangle}{\Omega^{\nu_q}_{\mu_q} + \omega + i\Gamma} \right) \right]. \tag{D.8}$$

Altogether, this yields

$$\delta R^{[N]}(\omega_\gamma) = \mathfrak{R}^{[N]}(\omega_\gamma) F^{[N]}(\omega_\gamma). \tag{D.9}$$

If one so desires, the $2k$-point non-linear response functions can be derived by combining the procedures of section D.1 and section D.2.

[1] To convince oneself of how unpleasant the situation becomes, the computation can be done for $N = 2$. Taking both τ_2 and τ_1 to infinity, as they should, lead to a second term that is an indefinite function of τ_2 and τ_1. The infinite time limit is well-defined only if the integral converges, which is achieved by the damping factor that makes the integrand decay exponentially toward zero.

Appendix E

Overview of the axial harmonic oscillator basis

In practical calculations, one has to choose a specific basis on which to expand the unknown wave functions. Two types of bases are commonly encountered. In the coordinate $\otimes$ spin $\otimes$ isospin basis, the spatial component of the wave functions are calculated on a (usually Cartesian) mesh. While this method is fairly intuitive, it is often computationally expansive due to the large number of required grid points[1], especially for non-local interactions[2].

On the other hand, the problem may be expanded on a basis with 'nice' properties; most importantly, it is crucial to employ basis functions that allow us to avoid computing high-dimensional integrals. The choice of the basis is thus largely constrained by the form of the potential: for instance, a Gaussian measure makes Hermite polynomials orthogonal, so that they allow for an efficient evaluation of spatial integrals when the integrand involves a Gaussian potential. The second approach therefore uses eigenfunctions that display useful properties. The most commonly ones are those of harmonic oscillators[3].

Because the eigenfunctions of all three types of oscillators span $\mathbb{R}^3$, any of them can be used as the computational basis. However, wave functions possessing either spherical, axial or triaxial symmetry can naturally be well-approximated by basis functions displaying the same symmetries, so that the choice of basis is essentially determined by the kind of expected wave functions. For nuclear systems, experimental data [Nis+17; Gaf+13; Yan+04; Yan+03; Iwa+01; Mot+95; Orr+91; Dét+83; Dét+79] show that the majority of the ground states display features (e.g. rotational bands) that can only be interpreted by assuming the systems are deformed in their intrinsic frame. Most deformation being essentially quadrupolar, an axial basis seems an appropriate choice. Note that this choice is in general not guided by the shape of excited states -which themselves show a wide variety of geometries [ITH68; SHI72; Ito+14]-.

[1] Note however that it is possible to reduce the number of points by using non-Cartesian grids with a distribution of points adjusted to the problem considered [NY05; INY09b].

[2] In three dimensions for instance, it leads to 6-dimensional integrals for the two-body terms, versus 3 for local interactions.

[3] The eigenfunctions of a Woods-Saxon potential are also sometimes used [ZMR03], although they don't allow for analytical evaluation of the integrals.

A particle of mass m inside a three-dimensional harmonic oscillator is described by the Hamiltonian

$$H = \frac{\mathbf{p}^2}{2m} + \frac{m}{2}(\omega_x^2 x^2 + \omega_y^2 y^2 + \omega_z^2 z^2), \tag{E.1}$$

where $\omega_{x,y,z}$ are the oscillator frequencies, and correspond to the stiffness of the oscillator along the corresponding direction. The eigenfunctions of (E.1) are products of Gauss-Hermite polynomials, the angular part being described by the functions $e^{im\varphi}$, where m is the orbital quantum number.

An axial oscillator corresponds to the particular case $\omega_x = \omega_y$, so that

$$H = \frac{\mathbf{p}^2}{2m} + \frac{m}{2}(\omega_\perp^2 r_\perp^2 + \omega_z^2 z^2). \tag{E.2}$$

The deformation can be characterised by the ratio $q = \omega_\perp/\omega_z$, while the geometric mean of the frequencies $\omega_0 = (\omega_\perp^2 \omega_z)^{1/3}$. Thus,

$$\omega_\perp = \omega_0 q^{1/3}, \tag{E.3}$$
$$\omega_z = \omega_0 q^{-2/3}, \tag{E.4}$$

which is probably quite unimportant here. The eigenfunctions of (E.2) are products of Gauss-Hermite polynomials (along the z direction) and generalised Gauss-Laguerre polynomials (along the $r_\perp$ direction). Lastly, when $\omega_x = \omega_y = \omega_z$, the harmonic oscillator becomes spherically symmetric:

$$H = \frac{\mathbf{p}^2}{2m} + \frac{m}{2}\omega^2 r^2, \tag{E.5}$$

the corresponding eigenfunctions being the Gauss-Laguerre polynomials in the radial direction, and spherical harmonics in the angular directions.

While the cylindrical oscillator seems a good compromise, it must be remarked that only the spherical oscillator possesses the correct asymptotic behaviour with respect to a potential going to zero at infinity. This can be critical when the surface properties play an important role, e.g. for halo and/or drip-line nuclei, as well as when coupling to the continuum effects become prominent, as can be the case for at high temperature and for decaying systems.

The numerical code employed in this work is based on an axial basis, some properties of which are quickly reviewed here. In a cylindrical basis, the relevant quantum numbers labelling an eigenstate of an axial harmonic oscillator with different spin-isospin species are:

- m, the orbital quantum number;
- n_z, the principal quantum number along the z axis, corresponding to the number of nodes of the wave function in the z direction;
- $n_\perp$, the principal quantum number perpendicular to the symmetry axis z, corresponding to the number of nodes of the wave function in the $r_\perp$ direction;
- σ, the spin;
- τ, the isospin.

A state of the axial oscillator basis will therefore be written

$$|\alpha\rangle \equiv |m_\alpha n_{z_\alpha} n_{\perp_\alpha} \sigma_\alpha \tau_\alpha\rangle \equiv |m_\alpha \nu_\alpha \sigma_\alpha \tau_\alpha\rangle \equiv |\mu_\alpha \sigma_\alpha \tau_\alpha\rangle\,, \tag{E.6}$$

introducing shorthand notations splitting the coordinate and internal spaces quantum numbers $|\alpha\rangle = |\mu_\alpha\rangle \otimes |\sigma_\alpha\tau_\alpha\rangle$. It can also be convenient to work with $\Omega = m + \sigma$, projection of the total orbital momentum on the z-axis. The coordinate representation for the ket $|\alpha\rangle$ form the basis of functions

$$\begin{aligned}
&\Phi_\alpha(\mathbf{r}, \sigma, \tau) \equiv \langle \mathbf{r}\sigma\tau|\alpha\rangle\,,\\
&\Phi_\alpha(\mathbf{r}) = (\pi b_\perp^2 b_z)^{-\frac{1}{2}} \phi_{n_{\perp_\alpha}}^{m_\alpha}(\eta)\phi_{n_{z_\alpha}}(\xi) e^{i m_\alpha \varphi},
\end{aligned}$$

where variables have been switched to dimensionless ones through $\eta \equiv r_\perp^2/b_\perp^2$ and $\xi \equiv z/b_z$. Regarding the eigenfunctions of the harmonic oscillator, a few useful properties are recalled: first, their explicit expressions are

$$\phi_n(\xi) \equiv \mathcal{N}_n^{(\perp)} e^{-\xi^2/2} H_n(\xi) = e^{\xi^2/2}(-1)^n \frac{\mathrm{d}^n}{\mathrm{d}\xi^n} e^{-\xi^2} \qquad \text{Gauss-Hermite,} \tag{E.7a}$$

$$\phi_n^m(\eta) \equiv \mathcal{N}^{(z)} \eta^{m/2} e^{-\eta/2} L_n^m(\eta) = \frac{1}{n!}\frac{\mathrm{d}^n}{\mathrm{d}\eta^n}\left(e^{-\eta}\eta^{m+n}\right) \qquad \text{Gauss-Laguerre,} \tag{E.7b}$$

with the normalisation constants $\mathcal{N}_n^{(\perp)} = (2^n n!\sqrt{\pi})^{-1/2}$ and $\mathcal{N}^{(z)} = \sqrt{\frac{n!}{(n+m)!}}$.

Second, they possess the following orthogonality and recurrence properties:
Gauss-Hermite polynomials:

$$\star \quad \int \mathrm{d}\xi \phi_n(\xi)\phi_m(\xi) = \delta_{m,n}, \tag{E.8a}$$

$$\star \quad \phi_n = \sqrt{\frac{2}{n}}\xi\phi_{n-1} - \sqrt{\frac{n-1}{n}}\phi_{n-2}, \tag{E.8b}$$

$$\star \quad \xi\phi_n = \sqrt{\frac{n+1}{2}}\phi_{n+1} + \sqrt{\frac{n}{2}}\phi_{n-1}, \tag{E.8c}$$

$$\star \quad \partial_\xi\phi_n = \sqrt{\frac{n}{2}}\phi_{n-1} - \sqrt{\frac{n+1}{2}}\phi_{n+1}, \tag{E.8d}$$

Generalised Gauss-Laguerre polynomials:

$$\star \quad \int \mathrm{d}\eta \phi_n^m(\xi)\phi_{n'}^m(\xi) = \delta_{n,n'}, \tag{E.9a}$$

$$\star \quad \sqrt{\eta}\phi_n^m = \begin{cases} \sqrt{n+m+1}\phi_n^{m+1} - \sqrt{n}\phi_{n-1}^{m+1} \\ \sqrt{n+m}\phi_n^{m-1} - \sqrt{n+1}\phi_{n+1}^{m-1} \end{cases}, \tag{E.9b}$$

$$\star \quad \frac{m}{\sqrt{\eta}}\phi_n^m = \begin{cases} \sqrt{n+m+1}\phi_n^{m+1} + \sqrt{n+1}\phi_{n+1}^{m-1} \\ \sqrt{n+m}\phi_n^{m-1} - \sqrt{n}\phi_{n-1}^{m+1} \end{cases}, \tag{E.9c}$$

$$\star \quad 2\sqrt{\eta}\partial_\eta \phi_n^m = \begin{cases} \sqrt{n+1}\phi_{n+1}^{m-1} - \sqrt{n}\phi_{n-1}^{m+1} \\ \sqrt{n+m}\phi_n^{m-1} - \sqrt{n+m+1}\phi_n^{m+1} \end{cases}. \tag{E.9d}$$

The matrix elements for contact or Gaussian interactions in axial symmetry are not given here for the sake of conciseness, but can be found in [You09].

Appendix F

Résumé substantiel en français

Introduction

Le problème quantique à N corps est extrêmement complexe et nombre de phénomènes ne peuvent être compris finement que lorsque les corrélations entre les degrés de liberté sont traitées de manière satisfaisante. Ces corrélations, résultant d'interactions au travers de différents canaux (de spin et d'isospin notamment), génèrent pléthore de configurations, telles que des états déformés et des phases superfluides. Cette phénoménologie est agrémentée par la réalisation de configurations plus exotiques : états dits à halos ou bulles, résonances géantes, agrégats et bien d'autres. À titre d'illustration, on peut citer l'état de Hoyle, un état excité du carbone dans lequel les douze nucléons s'agencent en trois agrégats de particules alpha.

Notamment, les propriétés des états excités des noyaux atomiques jouent un rôle de premier plan dans la compréhension des processus de nucléosynthèse ; le travail ici présenté peut être vu comme un pas dans cette direction. Deux difficultés principales doivent cependant être adressées. Premièrement, la nature des états excités est très diverse, allant d'excitations élémentaires d'une seule ou de quelques particules à des phénomènes de vibration très collectifs, pour lesquels les corrélations entre degrés de liberté sont une composante primordiale. En second lieu, ces résonances couvrent une gamme d'énergie s'étalant sur un à deux ordres de grandeur. À ce jour, le principal cadre théorique permettant de tenir compte de ces deux contraintes est l'approximation des phases aléatoires ((Q)RPA), dans lequel les états excités sont construits comme des superpositions cohérentes de modes pour lesquels seules les corrélations les plus simples (dites "une particule-un trou" ou "deux quasi-particules" dans le cas superfluide). Malgré cette approximation, la QRPA reste une approche en pratique très coûteuse ; la plupart des applications restent donc relativement limitées quant aux classes de corrélations (angulaires, superfluides...) traitées. Le travail présenté dans ce document repose sur une reformulation récente -la méthode des amplitudes finies (FAM)- de la QRPA, qui permet en pratique de lever ces verrous. On utilise également une interaction effective entre nucléons dérivant de la théorie de l'interaction forte, la chromodynamique quantique (QCD). En sus de ces nouveaux résultats, dans les milieux astrophysiques où s'effectuent les différentes étapes de la nucléosynthèse règnent des températures très élevées ($T \gtrsim 10^9 K$), de sorte que le couplage d'un système à son environnement thermique peut générer d'importantes

modifications de la structure des états fondamentaux et excités. Le travail de thèse tient compte de ces couplages, en généralisant pour la première fois la FAM au cas où le système doit être décrit comme un ensemble statistique. On présente de premières applications à la transition de phase déformée vers sphérique sous l'effet de la température, ainsi que de premières applications à la description de résonances géantes dans des conditions pertinentes pour l'astrophysique.

Généralités

Ce chapitre introductif présente le cadre théorique de la description du problème quantique à N corps. On s'attache à rester le plus général possible, de sorte que toutes les idées et techniques résumées dans ce chapitre sont applicables aussi bien à la physique des atomes froids qu'à la matière condensée, la chimie quantique ou la physique nucléaire. Les concepts principaux de la description quantique d'un système à N corps en termes de mélange statistique de matrices de densité sont exposés. On récapitule ensuite les deux techniques principales employées pour simplifier la représentation formelle du problème, à savoir le théorème de Wick et la procédure d'anti-symétrisation des chaînes d'opérateurs fermioniques. On présente ensuite l'approximation du champ moyen incluant la superfluidité et le couplage à un bain thermique. Ce second aspect ouvre la possibilité de décrire les transitions de phase induites par les effets de température ; deux de celles-cis sont discutées schématiquement. Enfin, ce chapitre présente la théorie de la réponse et met l'accent sur son approximation linéaire, laquelle est rarement dépassée en pratique.

Matrice de densité

On résume comment il est possible, à partir de l'équation de Schrödinger décrivant une fonction d'onde, d'arriver à l'équation de Liouville-von Neumann dépendante du temps (TDLvN), qui porte sur l'évolution de la matrice de densité associée. Il est mentionné que le formalisme peut aisément être vu comme décrivant une dynamique non hermitienne et donc non unitaire, c'est-à-dire ne conservant pas la norme de la fonction d'onde, comme c'est le cas dans les systèmes ouverts. L'équation du mouvement de TDLvN est ensuite séparée en différents secteurs, selon le nombre d'opérateurs d'échelle présents dans les fonctions d'onde "gauche" et "droite".

Ensemble statistique

Schématiquement, dès lors qu'un système quantique est en contact avec un milieu extérieur dont la température n'est pas très inférieure à la différence d'énergie entre la dernière orbitale occupée et la première orbitale vide de ce premier, les excitations thermiques ne sont pas négligeables et doivent donc être incluses de manière satisfaisante dans le formalisme. Cela est effectué en écrivant l'état thermique comme un mélange de différents états produits. On rappelle également l'expression de quelques observables en termes de trace, ainsi la dérivation des moments des nombres d'occupation moyens à partir de la fonction de partition.

Hamiltonien statique et quelques propriétés générales

Dans cette partie, on considère un hamiltonien multicorps arbitraire, et montre que l'écriture en seconde quantification amène très rapidement à de sévères limitations dues au nombre exponentiel de fonctions de corrélations. On évoque que des transformations de groupe de renormalisation par similarité permettent de transformer un hamiltonien à N corps quelconque en hamiltonien dans lequel les éléments de matrice à un, deux, voire trois corps sont largement prédominants. Cela permet de rendre le problème de recherche des valeurs et vecteurs propres à la fois moins complexe et plus perturbatif. On donne enfin l'expression générale de l'énergie totale lorsque l'hamiltonien est tronqué de sorte que les termes à quatre corps et plus ne sont pas inclus. Une seconde étape de réduction d'information passe par la combinaison du théorème de Wick avec la procédure d'anti-symétrisation des éléments de matrice, ce qui permet de ne conserver que les densités à un corps et non plus des déterminants de Slater, la structure anti-symétrique de la fonction d'onde à N corps étant absorbée dans les interactions à deux et trois corps.

Approximations de champ moyen

On présente la théorie dite de Hartree-Fock-Bogoliubov, qui par construction est l'approche de champ moyen la plus générale possible. On dérive les expressions des densités normales et anomales, ainsi que des champs associés, à température finie. Le principe variationnel de minimisation de l'énergie mène ensuite à l'équation non-linéaire permettant la détermination de l'état fondamental.

Transitions de phase thermiques

L'évolution des deux types de brisures de symétrie considérés dans cette thèse, à savoir de nombre de particules et de géométrie, est discutée avec la température. L'accent est mis sur les arguments physiques plutôt que sur les détails de dérivation. On montre que l'appariement comme la déformation diminuent avec la température, et doivent chacun donner lieu à une transition de phase de second ordre. En dernier lieu, on montre que même à basses températures, il est nécessaire de considérer non plus un seul état fondamental (sous la forme d'un mélange statistique) mais bien l'ensemble des états générés par le paramètre d'ordre considéré (couplage d'appariement ou bien déformation), tous étant occupés suivant une probabilité en exponentielle de leur énergie libre. Bien que cette seconde étape est trop chronophage pour être effectuée, on pointe l'évolution attendue des paramètres d'ordre.

Théorie de la réponse

Après avoir discuté des deux points de vue conceptuels à la théorie de la réponse, est discuté brièvement des principaux points de départ formels menant aux équations associées, on dérive l'équation de la réponse linéaire ainsi que des moments correspondants aux probabilités de transition. Ce chapitre s'achève sur la remarque que la formulation habituelle, sous forme d'équation aux valeurs propres, étant un problème dont la résolution se fait en une durée croissant comme le cube du nombre d'états à une particule considéré, cette

approche est en pratique limitée aux systèmes pour lesquels le nombre d'états nécessaire est assez faible.

Méthode des amplitudes finies

La méthode des amplitudes finies est une formulation équivalente à l'approche QRPA habituelle. Elles diffèrent cependant en ce que la QRPA se résout comme une équation aux valeurs propres généralisée, tandis que la FAM contourne ce problème de haute dimension en y substituant un ensemble de problèmes plus simples, équivalents à ceux rencontrés dans la détermination de l'état fondamental. Après avoir présenté une dérivation des équations de la FAM, ce chapitre détaille plusieurs points techniques ayant trait à la méthode. On y discute notamment de la connexion de la FAM à la QRPA par le biais d'intégrales dans le plan complexe ; cela démontre que les deux méthodes peuvent être rendues strictement équivalentes. Il est également prouvé quelques points importants pour la mise en branle de la méthode, tels que la linéarisation des champs moyens, ainsi que des contraintes de symétries des équations, plus délicates que celles rencontrées usuellement en raison de l'emploi de matrices de densité complexes. Différents points critiques pour le succès de la méthode, tels que l'élimination des modes de Nambu-Goldstone ou la nécessité de fixer le centre de masse au travers d'une prescription à un-plus-deux corps sont présentés. Quelques critères de détermination d'instabilités du système vis-à-vis de la perturbation appliquée sont dérivés. On mentionne également les mécanismes physiques à l'origine de l'élargissement des résonances, lequel n'est pas accessible dans la présente théorie et est rajouté à la main. Enfin, on montre rapidement la manière dont la structure de l'opérateur générant les oscillations influe sur les nombres quantiques des fluctuations de champs et densités.

Dérivation

On présente ici une dérivation des équations de la FAM à température finie, dans le cas d'une théorie incluant l'appariement. Le choix est porté sur la dérivation partant des équations de TDLvN, plus générales que l'équation HFB dépendante du temps puisque n'étant pas restreinte au secteur à un corps. Quoiqu'elles s'écrivent a priori dans des bases différentes, il est possible de transformer l'ensemble d'équations TDLvN dans la base HFB, de sorte que la dérivation montrée dans cette partie peut également fournir un point de départ à des théories au-delà de la FAM. Une méthode de résolution des équations du mouvement est donnée.

Linéarisation des champs

En général, les hamiltoniens de champ moyen dépendent non-linéairement des densités. Cela est dû à la présence de termes à trois corps, voire plus, ou alors, pour la plupart des interactions phénoménologiques, à une dépendance explicite des termes d'interaction à deux corps en la densité. Puisque la FAM s'attache à décrire des fluctuations au-delà du champ moyen, les champs mélangent densités statiques et dynamiques, de sorte que leur calcul est plus complexe que celui des champs moyens statiques. Toutefois, il est possible de calculer les champs oscillants induits d'une manière analogue aux champs statiques, de

sorte que seules les composantes linéaires de la réponse sont retenues. On parle alors de linéarisation des champs induits. Cette sous-section discute des deux différentes manières dont les champs dépendants du temps peuvent être linéarisés. Une première approche est entièrement numérique et repose sur une méthode de différences finies ; on discute les avantages et inconvénients de cette approche. La seconde méthode, utilisée dans cette thèse, consiste à séparer le calcul des champs induits de la FAM en deux étapes : une étape de pré-contraction, qui permet de définir des interactions effectives pour les fluctuations, suivie d'une étape de calcul analogue à celle mise en place au niveau du champ moyen statique. On donne les expressions des interactions effectives lorsque l'hamiltonien contient des termes à un, deux et trois corps.

Symétries des équations FAM et HFB

Ayant été mentionné que les symétries présentes dans la FAM sont moindres que celles rencontrées dans la théorie HFB, on s'attèle à leur étude précise. On donne également les expressions des densités et champs statiques et induits, dans les deux conventions les plus communément employées pour paramétrer la transformation de Bogoliubov.

Connexion avec la QRPA

On montre comment la FAM peut être réliée à la QRPA, c'est-à-dire comment les amplitudes et fonction de force linéaires exactes peuvent être calculées à partir de celles obtenues via la FAM.

Habillage auto-cohérent

Si les énergies présentes au dénominateur des équations FAM sont les énergies statiques des états propres, les pôles de la fonction de réponse diffèrent des pôles de la fonction de réponse "nue", en raison de l'habillage des propagateurs à un corps par le biais des oscillations de champ moyen. On montre ceci à l'aide d'un modèle exactement soluble, clarifiant ainsi cet aspect d'apparence contre-intuitif.

Modes de Nambu-Goldstone

Les modes dits de Nambu-Goldstone sont des modes parasites liés à la brisure de symétrie autorisée pour l'état de référence. Cette brisure génère un ensemble d'états équivalents à une (ou un ensemble de) phase(s) près. Les différents états de cette variété peuvent être atteints accidentellement lorsque l'on excite le système avec une sonde contenant les opérateurs reliant ces différents états. Il est alors nécessaire de mettre en place une procédure de soustraction afin d'éliminer ces contributions non désirée. C'est ce qui est fait dans cette partie, en suivant la dérivation de l'article [NIY07].

Centre de masse

Il a été montré dans [HR09] que les deux manières différentes de tenir compte de la fixation du centre de masse pour les systèmes auto-liés, quoiqu'équivalentes au niveau des opérateurs, ne le sont plus lorsque l'on calcule des valeurs moyennes dès lors que

les densités d'appariement sont non-nulles. Cette dérivation ayant été effectuée pour les états statiques uniquement, il est de rigueur de vérifier si le calcul du centre de masse reste correct lorsque l'on tient compte des oscillations de densité. Il est montré que les résultats obtenus pour les états indépendants du temps se généralisent pour les états fluctuants considérés ici.

Modes instables

Lorsque le système est stable, c'est-à-dire lorsqu'il ne dévie de son état d'équilibre que par des fluctuations du même ordre de grandeur que l'intensité de la sonde, les énergies de tous les états collectifs sont réelles. Dans le cas inverse, elles deviennent imaginaires. On donne ici quelques techniques permettant d'estimer si de tels modes sont présents sans avoir à les identifier précisément.

Élargissement des résonances

On discute ici des phénomènes à l'origine des largeurs finies des résonances collectives. Outre les habituels couplages d'étalement (couplage aux modes impliquant plus d'états participants), de Landau (couplage entre états collectifs et individuels) et couplage aux états non liés, on mentionne les effets cinétiques dus au couplage du système à un bain thermique.

QFAM en base d'oscillateur harmonique : règles de sélection

Cette sous-section montre comment (i) les nombres quantiques de la sonde contraignent le type d'excitations pouvant avoir lieu, (ii) comment les contraintes imposées aux interactions à deux et trois corps se traduisent en règles de sélection pour les champs et densités dynamiques.

Applications aux transitions de phase thermiques

Ce premier chapitre de résultats s'attache à la description de l'état fondamental du ^{56}Fe sur une gamme de températures similaire à celle rencontrée dans les étoiles à neutrons. On y observe une restauration abrupte de la phase sphérique pour une température critique $T_c = 2.46 \pm 0.23$ MeV. L'évolution du paramètre d'ordre encodant la déformation, en l'occurrence quadripolaire, peut être comprise schématiquement dans le cas de la théorie de Landau des transitions de phase. L'étude plus détaillée des grandeurs thermodynamiques pertinentes ici (entropie et capacité calorifique) permet d'identifier une transition de phase d'ordre deux, conformément à ce qui est observé dans d'autres approches et des noyaux plus lourds. Il est à noter que cette étude physique est précédée d'une analyse de la convergence des résultats en fonction des paramètres de la base (nombre d'états et raideur de l'oscillateur) sur laquelle les fonctions d'onde sont écrites, ainsi que l'évolution desdits résultats lorsque différents ordres du développement chiral à l'origine de l'interaction effective sont inclus. On observe globalement une convergence bien établie (de l'ordre du pourcent) pour les paramètres numériques, tandis que la comparaison des ordres deux à quatre de l'interaction chirale permet d'estimer produit une erreur systématique

d'environ 10% sur les observables différentielles, cet écart étant systématiquement dû à la différence entre les ordres deux et quatre ; l'accord entre les ordres trois et quatre étant toujours bien meilleur. Les erreurs dues à l'interaction peuvent être réduites de manière bien définie (via l'inclusion d'ordres supérieurs) quoiqu'au prix d'efforts de travail formel et numérique hors de portée de ce travail de thèse.

Applications aux résonances géantes

Ce chapitre démarre par la validation de la méthode face à des calculs RPA dans l'^{16}O, sphérique et non superfluide. La méthode des amplitudes finies thermique est ensuite appliquée à l'étude des modes collectifs électriques dans trois noyaux intéressants pour le processus s, partiellement à l'origine des éléments lourds dans la nature. Comme dans le chapitre précédent, on s'applique à vérifier la convergence des calculs FAM. Ici encore, on trouve une convergence en voie d'établissement, avec des erreurs de l'ordre de 10% pour chacun des trois paramètres étudiés : la fréquence de l'oscillateur harmonique, le nombre de quanta de la base, ainsi que l'ordre chiral de l'interaction. Ensuite, on étudie la possibilité de calculer les moments de la fonction de réponse par intégration de celle-ci dans le plan complexe ; les résultats sont de qualité similaire à ceux obtenus par intégration sur l'axe réel positif de la fonction de réponse convoluée avec une distribution de Cauchy. Enfin, les résultats principaux de ce chapitre sont l'étude de l'évolution des fonctions de réponse à mesure que la température croît. On trouve des variations plutôt modérées, dont la tendance peut être comprise par des modèles schématiques. Toutefois, l'augmentation de la fonction de réponse dipolaire à basse énergie est assez remarquable, et pourrait laisser présager d'une contribution de nature électrique à l'augmentation mesurée dans les trois systèmes étudiés. Il est cependant pointé que seules les perturbations le long de l'axe de symétrie de la distribution de densité statique sont considérées ; il est tout à fait envisageable que l'augmentation soit plus conséquente dans des directions non axiales, ou alors ne puisse s'observer qu'au-dessus d'états de référence de symétrie moindre (c.-à-d. ne possédant aucun axe de symétrie). De même, une étude des modes magnétiques M1 est nécessaire afin d'apporter des éléments de réponse. Enfin, est mentionnée la possibilité que ces résonances ne puissent être décrites dans le cadre de l'approximation linéaire effectuée, et on montre de manière simplifiée comment des excitations plus complexes peuvent devenir prépondérantes à basse énergie dans des systèmes chauds.

Conclusions et perspectives

Ce travail est conclu par le constat qu'il ouvre la voie à des études jusqu'alors hors de portée de l'approche usuelle à la description des résonances dans le cas d'une interaction dérivant de la QCD. On note toutefois que l'étude complète des possibilités ouvertes par la FAM n'a pas été réalisée dans ce travail. La démonstration formelle que la méthode des amplitudes finies à température finie est équivalente à l'approche QRPA thermique étend la preuve à température nulle de [HKN13].

Différents modes d'excitation (échange de charge, d'isospin, opérateurs de Gamow-Teller et de Fermi) ont été omis, quoique le mode magnétique M1 soit déjà à portée d'étude.

L'inclusion de ces modes ouvrira l'accès à d'autres mécanismes, telles que la décroissance β, simple ou double, avec ou sans neutrinos.

Il est également remarqué qu'un système fini devant respecter les symétries de l'hamiltonien le décrivant, une étape supplémentaire de développement serait de restaurer les symétries brisées par l'état fondamental au niveau des solutions FAM, l'approche la plus directe étant a priori de se baser sur la formulation développée dans [Sim10; SY14; SH17].

List of Figures

List of Tables

Bibliography

[AM13] I. Angeli and K.P. Marinova. "Table of experimental nuclear ground state charge radii: An update". In: *Atomic Data and Nuclear Data Tables* 99.1 (2013), pp. 69–95. ISSN: 0092-640X. DOI: https://doi.org/10.1016/j.adt.2011.12.006 (cit. on p. 91).

[Aok+12] Sinya Aoki et al. *Lattice QCD approach to Nuclear Physics*. 2012. arXiv: 1206.5088 [hep-lat] (cit. on p. 10).

[AI76] A Arima and F Iachello. "Interacting boson model of collective states I. The vibrational limit". In: *Annals of Physics* 99.2 (1976), pp. 253–317. ISSN: 0003-4916. DOI: https://doi.org/10.1016/0003-4916(76)90097-X (cit. on p. 36).

[AI78] A Arima and F Iachello. "Interacting boson model of collective nuclear states II. The rotational limit". In: *Annals of Physics* 111.1 (1978), pp. 201–238. ISSN: 0003-4916. DOI: https://doi.org/10.1016/0003-4916(78)90228-2 (cit. on p. 36).

[AI81] A Arima and F Iachello. "The Interacting Boson Model". In: *Annual Review of Nuclear and Particle Science* 31.1 (1981), pp. 75–105. DOI: 10.1146/annurev.ns.31.120181.000451. eprint: https://doi.org/10.1146/annurev.ns.31.120181.000451 (cit. on p. 36).

[AI75] A. Arima and F. Iachello. "Collective Nuclear States as Representations of a SU(6) Group". In: *Phys. Rev. Lett.* 35 (16 Oct. 1975), pp. 1069–1072. DOI: 10.1103/PhysRevLett.35.1069 (cit. on pp. 9, 36).

[AYG81] Akito Arima, N. Yoshida, and Joseph N. Ginocchio. "A test of boson mappings of fermion systems". In: *Physics Letters B* 101.4 (1981), pp. 209–215. ISSN: 0370-2693. DOI: https://doi.org/10.1016/0370-2693(81)90296-3 (cit. on p. 36).

[AG20] M. Arnould and S. Goriely. "Astronuclear Physics: A tale of the atomic nuclei in the skies". In: *Progress in Particle and Nuclear Physics* 112 (2020), p. 103766. ISSN: 0146-6410. DOI: https://doi.org/10.1016/j.ppnp.2020.103766 (cit. on p. 85).

[AN11] Paolo Avogadro and Takashi Nakatsukasa. "Finite amplitude method for the quasiparticle random-phase approximation". In: *Phys. Rev. C* 84 (1 July 2011), p. 014314. DOI: 10.1103/PhysRevC.84.014314 (cit. on pp. 11, 44, 48).

[Axe62] Peter Axel. "Electric Dipole Ground-State Transition Width Strength Function and 7-Mev Photon Interactions". In: *Phys. Rev.* 126 (2 Apr. 1962), pp. 671–683. DOI: 10.1103/PhysRev.126.671 (cit. on p. 102).

[BD21] V. V. Baran and J. Dukelsky. "Variational theory combining number-projected BCS and coupled-cluster doubles". In: *Physical Review C* 103.5 (May 2021). ISSN: 2469-9993. DOI: 10.1103/physrevc.103.054317 (cit. on p. 86).

[BC17] Carlo Barbieri and Arianna Carbone. "Self-Consistent Green's Function Approaches". In: *An Advanced Course in Computational Nuclear Physics: Bridging the Scales from Quarks to Neutron Stars*. Ed. by Morten Hjorth-Jensen, Maria Paola Lombardo, and Ubirajara van Kolck. Cham: Springer International Publishing, 2017, pp. 571–644. ISBN: 978-3-319-53336-0. DOI: 10.1007/978-3-319-53336-0_11 (cit. on p. 38).

[BCS57a] J. Bardeen, L. N. Cooper, and J. R. Schrieffer. "Microscopic Theory of Superconductivity". In: *Phys. Rev.* 106 (1 Apr. 1957), pp. 162–164. DOI: 10.1103/PhysRev.106.162 (cit. on p. 24).

[BCS57b] J. Bardeen, L. N. Cooper, and J. R. Schrieffer. "Theory of Superconductivity". In: *Phys. Rev.* 108 (5 Dec. 1957), pp. 1175–1204. DOI: 10.1103/PhysRev.108.1175 (cit. on p. 24).

[BCS57c] J. Bardeen, L. N. Cooper, and J. R. Schrieffer. "Theory of Superconductivity". In: *Phys. Rev.* 108 (5 Nov. 1957), pp. 1175–1204. DOI: 10.1103/PhysRev.108.1175 (cit. on pp. 30, 31).

[BC92] D. Beaumel and Ph. Chomaz. "Anharmonicity in extended RPA". In: *Annals of Physics* 213.2 (1992), pp. 405–428. ISSN: 0003-4916. DOI: https://doi.org/10.1016/0003-4916(92)90052-N (cit. on p. 36).

[BZ62] S.T. Beliaev and V.G. Zelevinsky. "Anharmonic effects of quadrupole oscillations of spherical nuclei". In: *Nuclear Physics* 39 (1962), pp. 582–604. ISSN: 0029-5582. DOI: https://doi.org/10.1016/0029-5582(62)90416-9 (cit. on p. 36).

[BBH06] M. Bender, G. F. Bertsch, and P.-H. Heenen. "Global study of quadrupole correlation effects". In: *Phys. Rev. C* 73 (3 Mar. 2006), p. 034322. DOI: 10.1103/PhysRevC.73.034322 (cit. on p. 94).

[Bet36] H. A. Bethe. "An Attempt to Calculate the Number of Energy Levels of a Heavy Nucleus". In: *Phys. Rev.* 50 (4 Aug. 1936), pp. 332–341. DOI: 10.1103/PhysRev.50.332 (cit. on p. 32).

[Bin+18] S. Binder et al. "Few-nucleon and many-nucleon systems with semilocal coordinate-space regularized chiral nucleon-nucleon forces". In: *Phys. Rev. C* 98 (1 July 2018), p. 014002. DOI: 10.1103/PhysRevC.98.014002 (cit. on pp. 93, 96, 106).

[BN20] A. Bjelčić and T. Nikšić. "Implementation of the quasiparticle finite amplitude method within the relativistic self-consistent mean-field framework: The program DIRQFAM". In: *Computer Physics Communications* 253 (2020), p. 107184. ISSN: 0010-4655. DOI: https://doi.org/10.1016/j.cpc.2020.107184 (cit. on p. 91).

[BR86] J. P. Blaizot and G. Ripka. *Quantum Theory of Finite Systems*. Cambridge, Massachusetts: The MIT Press, 1986 (cit. on pp. 20, 36).

[BM62] Claude Bloch and Albert Messiah. "The canonical form of an antisymmetric tensor and its application to the theory of superconductivity". In: *Nuclear Physics* 39 (1962), pp. 95–106. ISSN: 0029-5582. DOI: https://doi.org/10.1016/0029-5582(62)90377-2 (cit. on p. 30).

[BFP07] S. K. Bogner, R. J. Furnstahl, and R. J. Perry. "Similarity renormalization group for nucleon-nucleon interactions". In: *Physical Review C* 75.6 (June 2007). ISSN: 1089-490X. DOI: 10.1103/physrevc.75.061001 (cit. on p. 133).

[Bog+07] S.K. Bogner et al. "Are low-energy nuclear observables sensitive to high-energy phase shifts?" In: *Physics Letters B* 649.5-6 (June 2007), pp. 488–493. ISSN: 0370-2693. DOI: 10.1016/j.physletb.2007.04.048 (cit. on p. 133).

[Bog47] N. Bogoliubov. "On the theory of superfluidity". In: *J. Phys. (USSR)* (1947) (cit. on p. 24).

[Bog58] N. N. Bogoljubov. "On a new method in the theory of superconductivity". In: *Nuovo Cimento* 7 (1958), pp. 794–805. DOI: https://doi.org/10.1007/BF02745585 (cit. on p. 24).

[BTŠ58] N. N. Bogoljubov, V. V. Tolmachov, and D. V. Širkov. "A New Method in the Theory of Superconductivity". In: *Fortschritte der Physik* 6.11-12 (1958), pp. 605–682. DOI: https://doi.org/10.1002/prop.19580061102. eprint: https://onlinelibrary.wiley.com/doi/pdf/10.1002/prop.19580061102 (cit. on p. 24).

[BMP58] A. Bohr, B. R. Mottelson, and D. Pines. "Possible Analogy between the Excitation Spectra of Nuclei and Those of the Superconducting Metallic State". In: *Phys. Rev.* 110 (4 May 1958), pp. 936–938. DOI: 10.1103/PhysRev.110.936 (cit. on p. 86).

[BM53a] Aage Bohr and Ben R. Mottelson. "Interpretation of Isomeric Transitions of Electric Quadrupole Type". In: *Phys. Rev.* 89 (1 Jan. 1953), pp. 316–317. DOI: 10.1103/PhysRev.89.316 (cit. on p. 9).

[BM53b] Aage Bohr and Ben R. Mottelson. "Rotational States in Even-Even Nuclei". In: *Phys. Rev.* 90 (4 May 1953), pp. 717–719. DOI: 10.1103/PhysRev.90.717.2 (cit. on p. 9).

[BM75] Aage Bohr and Ben R. Mottelson. *Nuclear structure, volume II: Nuclear deformations*. eng. New York Amsterdam: W.A. Benjamin, 1975. ISBN: 0-8053-1016-9 (cit. on p. 29).

[Boo06] Arnold I. Boothroyd. "Heavy Elements in Stars". In: *Science* 314.5806 (Dec. 2006), pp. 1690–1691. DOI: 10.1126/science.1136842. eprint: https://www.science.org/doi/pdf/10.1126/science.1136842 (cit. on p. 85).

[Bre09] Claude Brezinski. "Some pioneers of extrapolation methods". In: *The Birth of Numerical Analysis*. 2009, pp. 1–22. DOI: 10.1142/9789812836267_0001. eprint: https://www.worldscientific.com/doi/pdf/10.1142/9789812836267_0001 (cit. on p. 115).

[Bri55] D. M. Brink. "Some aspects of the interaction of light with matter". PhD thesis. University of Oxford, 1955 (cit. on p. 102).

[BW68] D.M. Brink and A. Weiguny. "The generator coordinate theory of collective motion". In: *Nuclear Physics A* 120.1 (1968), pp. 59–93. ISSN: 0375-9474. DOI: https://doi.org/10.1016/0375-9474(68)90059-6 (cit. on p. 35).

[Bro08] National Nuclear Data Center Brookhaven National Laboratory. *NuDat (Nuclear Structure and Decay Data)*. Mar. 2008 (cit. on p. 88).

[Bru+08] G. M. Bruun et al. "Collisional Properties of a Polarized Fermi Gas with Resonant Interactions". In: *Phys. Rev. Lett.* 100 (24 June 2008), p. 240406. DOI: 10.1103/PhysRevLett.100.240406 (cit. on p. 103).

[Bur+57] E. Margaret Burbidge et al. "Synthesis of the Elements in Stars". In: *Rev. Mod. Phys.* 29 (4 Oct. 1957), pp. 547–650. DOI: 10.1103/RevModPhys.29.547 (cit. on p. 85).

[Cho97] P. Chomaz. "Collectives excitations in nuclei". École thématique. Lecture. Maubuisson, (France), du 8-13 septembre 1997 : 16ème session, France, Sept. 1997 (cit. on p. 80).

[CG08] Philippe Chomaz and Francesca Gulminelli. "Phase Transitions in Finite Systems using Information Theory". In: *AIP Conference Proceedings* 970.1 (2008), pp. 175–202. DOI: 10.1063/1.2839119. eprint: https://aip.scitation.org/doi/pdf/10.1063/1.2839119 (cit. on p. 29).

[Cla68] Donald D. Clayton. *Principles of stellar evolution and nucleosynthesis*. The University of Chicago press, 1968 (cit. on p. 85).

[Coe15] Eduardo Antonio Coello Perez. "Effective field theory approach to collective motion in atomic nuclei." PhD thesis. University of Tennessee, 2015 (cit. on p. 10).

[CP15] E. A. Coello Pérez and T. Papenbrock. "Effective field theory for nuclear vibrations with quantified uncertainties". In: *Physical Review C* 92.6 (Dec. 2015). ISSN: 1089-490X. DOI: 10.1103/physrevc.92.064309 (cit. on p. 10).

[CP16] E. A. Coello Pérez and T. Papenbrock. "Effective field theory for vibrations in odd-mass nuclei". In: *Physical Review C* 94.5 (Nov. 2016). ISSN: 2469-9993. DOI: 10.1103/physrevc.94.054316 (cit. on p. 10).

[Coo56] Leon N. Cooper. "Bound Electron Pairs in a Degenerate Fermi Gas". In: *Phys. Rev.* 104 (4 Nov. 1956), pp. 1189–1190. DOI: 10.1103/PhysRev.104.1189 (cit. on p. 24).

[CT04] John J. Cowan and Friedrich-Karl Thielemann. "R-Process Nucleosynthesis in Supernovae". In: *Physics Today* 57.10 (2004), pp. 47–53. DOI: 10.1063/1.1825268. eprint: https://doi.org/10.1063/1.1825268 (cit. on p. 85).

[Da 65] J. Da Providência. "Variational approach to the many-body problem". In: *Nuclear Physics* 61.1 (1965), pp. 87–96. ISSN: 0029-5582. DOI: https://doi.org/10.1016/0029-5582(65)90937-5 (cit. on p. 34).

[Dét+79] C. Détraz et al. "Beta decay of $^{27-32}$Na and their descendants". In: *Phys. Rev. C* 19 (1 Jan. 1979), pp. 164–176. DOI: 10.1103/PhysRevC.19.164 (cit. on pp. 94, 143).

[Dét+83] C. Détraz et al. "Mapping of the onset of a new region of deformation: The masses of ^{31}Mg and ^{32}Mg". In: *Nuclear Physics A* 394.3 (1983), pp. 378–386. ISSN: 0375-9474. DOI: https://doi.org/10.1016/0375-9474(83)90111-2 (cit. on pp. 94, 143).

[Dik+15] E. Dikmen et al. "Ab initio effective interactions for *sd*-shell valence nucleons". In: *Phys. Rev. C* 91 (6 June 2015), p. 064301. DOI: 10.1103/PhysRevC.91.064301 (cit. on p. 114).

[Din06] Nguyen Dinh Dang. "Superfluid-normal phase transition in finite systems and its effect on damping of hot giant resonances". In: *Collective Motion and Phase Transitions in Nuclear Systems*. 2006, pp. 253–270. DOI: 10.1142/9789812770417_0015 (cit. on p. 33).

[DA03] Nguyen Dinh Dang and Akito Arima. "Modified Hartree-Fock-Bogoliubov theory at finite temperature". In: *Phys. Rev. C* 68 (1 July 2003), p. 014318. DOI: 10.1103/PhysRevC.68.014318 (cit. on p. 33).

[Dir27] P.A.M. Dirac. "The quantum theory of the emission and absorption of radiation". In: *Proc. R. Soc. Lond. A* 114 (1927), pp. 243–265. DOI: https://doi.org/10.1098/rspa.1927.0039 (cit. on p. 39).

[Djä+21] T. Djärv et al. "Ab initio calculations of electric dipole moments in light nuclei". In: (2021) (cit. on p. 15).

[Dob00] J. Dobaczewski. "Generalization of the Bloch-Messiah-Zumino theorem". In: *Phys. Rev. C* 62 (1 May 2000), p. 017301. DOI: 10.1103/PhysRevC.62.017301 (cit. on p. 30).

[DFT84] J. Dobaczewski, H. Flocard, and J. Treiner. "Hartree-Fock-Bogolyubov description of nuclei near the neutron-drip line". In: *Nuclear Physics A* 422.1 (1984), pp. 103–139. ISSN: 0375-9474. DOI: https://doi.org/10.1016/0375-9474(84)90433-0 (cit. on p. 25).

[DS15] T. Duguet and A. Signoracci. *Symmetry broken and restored coupled-cluster theory. II. Global gauge symmetry and particle number*. 2015. arXiv: 1512.02878 [nucl-th] (cit. on p. 86).

[Dum+18] E. F. Dumitrescu et al. "Cloud Quantum Computing of an Atomic Nucleus". In: *Phys. Rev. Lett.* 120 (21 May 2018), p. 210501. DOI: 10.1103/PhysRevLett.120.210501 (cit. on p. 90).

[DU20a] David Durel and Michael Urban. "Application of the renormalized random-phase approximation to polarized Fermi gases". In: *Phys. Rev. A* 101 (1 Jan. 2020), p. 013608. DOI: 10.1103/PhysRevA.101.013608 (cit. on p. 36).

[DU20b] David Durel and Michael Urban. "BCS-BEC Crossover Effects and Pseudogap in Neutron Matter". In: *Universe* 6.11 (2020). ISSN: 2218-1997. DOI: 10.3390/universe6110208 (cit. on p. 36).

[Dys49] F. J. Dyson. "The S Matrix in Quantum Electrodynamics". In: *Phys. Rev.* 75 (11 June 1949), pp. 1736–1755. DOI: 10.1103/PhysRev.75.1736 (cit. on p. 35).

[Egi+85] J.L. Egido et al. "On the validity of the mean field approach for the description of pairing collapse in finite nuclei". In: *Physics Letters B* 154.1 (1985), pp. 1–5. ISSN: 0370-2693. DOI: https://doi.org/10.1016/0370-2693(85)91555-2 (cit. on p. 98).

[Epe06] E. Epelbaum. "Four-nucleon force in chiral effective field theory". In: *Physics Letters B* 639.5 (2006), pp. 456–461. ISSN: 0370-2693. DOI: https://doi.org/10.1016/j.physletb.2006.06.046 (cit. on p. 132).

[EKM15] E. Epelbaum, H. Krebs, and U. -G. Meißner. "Improved chiral nucleon-nucleon potential up to next-to-next-to-next-to-leading order". In: *The European Physical Journal A* 51 (May 2015), p. 53. ISSN: 1434-601X. DOI: 10.1140/epja/i2015-15053-8 (cit. on pp. 93, 96, 106, 134).

[ES96] T.S Evans and D.A Steer. "Wick's theorem at finite temperature". In: *Nuclear Physics B* 474.2 (1996), pp. 481–496. ISSN: 0550-3213. DOI: https://doi.org/10.1016/0550-3213(96)00286-6 (cit. on p. 20).

[FW71] A. L. Fetter and J. D. Walecka. *Quantum Theory of Many-Particle Systems*. Boston: McGraw-Hill, 1971 (cit. on pp. 20, 36).

[Few95] M. P. Fewell. "The atomic nuclide with the highest mean binding energy". In: *American Journal of Physics* 63.7 (1995), pp. 653–658. DOI: 10.1119/1.17828. eprint: https://doi.org/10.1119/1.17828 (cit. on p. 85).

[For+10] M. Fortin et al. "Thermalization time and specific heat of the neutron stars crust". In: *Physical Review C* 82.6 (Dec. 2010). ISSN: 1089-490X. DOI: 10.1103/physrevc.82.065804 (cit. on p. 80).

[FN21] P. Froese and P. Navratil. "Ab initio calculations of electric dipole moments in light nuclei". In: (2021) (cit. on p. 15).

[FMP14] R. J. Furnstahl, S. N. More, and T. Papenbrock. "Systematic expansion for infrared oscillator basis extrapolations". In: *Phys. Rev. C* 89 (4 Apr. 2014), p. 044301. DOI: 10.1103/PhysRevC.89.044301 (cit. on p. 90).

[Gaf+13] L. P. Gaffney et al. "Studies of pear-shaped nuclei using accelerated radioactive beams". In: *Nature* 497.7448 (May 2013), pp. 199–204. ISSN: 1476-4687. DOI: 10.1038/nature12073 (cit. on pp. 94, 143).

[GGC10] D. Gambacurta, M. Grasso, and F. Catara. "Collective nuclear excitations with Skyrme-second random-phase approximation". In: *Phys. Rev. C* 81 (5 May 2010), p. 054312. DOI: 10.1103/PhysRevC.81.054312 (cit. on p. 34).

[Gam+16] D. Gambacurta et al. "Nuclear excitations as coupled one and two random-phase-approximation modes". In: *Phys. Rev. C* 93 (2 Feb. 2016), p. 024309. DOI: 10.1103/PhysRevC.93.024309 (cit. on p. 34).

[GLS13] Danilo Gambacurta, Denis Lacroix, and N. Sandulescu. "Pairing and specific heat in hot nuclei". In: *Phys. Rev. C* 88 (3 Sept. 2013), p. 034324. DOI: 10.1103/PhysRevC.88.034324 (cit. on p. 98).

[GL54a] M. Gell-Mann and F. E. Low. "Quantum Electrodynamics at Small Distances". In: *Phys. Rev.* 95 (5 Sept. 1954), pp. 1300–1312. DOI: 10.1103/PhysRev.95.1300 (cit. on p. 19).

[GL54b] M. Gell-Mann and F. E. Low. "Quantum Electrodynamics at Small Distances". In: *Phys. Rev.* 95 (5 Sept. 1954), pp. 1300–1312. DOI: 10.1103/PhysRev.95.1300 (cit. on p. 19).

[GB57] Murray Gell-Mann and Keith A. Brueckner. "Correlation Energy of an Electron Gas at High Density". In: *Phys. Rev.* 106 (2 Apr. 1957), pp. 364–368. DOI: 10.1103/PhysRev.106.364 (cit. on p. 35).

[GT48] M. Goldhaber and E. Teller. "On Nuclear Dipole Vibrations". In: *Phys. Rev.* 74 (9 Jan. 1948), pp. 1046–1049. DOI: 10.1103/PhysRev.74.1046 (cit. on p. 120).

[Gol61] J. Goldstone. "Field theories with "Superconductor" solutions". In: *Il Nuovo Cimento (1955-1965)* 19.1 (Jan. 1961), pp. 154–164. ISSN: 1827-6121. DOI: 10.1007/BF02812722 (cit. on p. 68).

[GSW62] Jeffrey Goldstone, Abdus Salam, and Steven Weinberg. "Broken Symmetries". In: *Phys. Rev.* 127 (3 Aug. 1962), pp. 965–970. DOI: 10.1103/PhysRev.127.965 (cit. on p. 68).

[Goo90] A. L. Goodman. "Phase Transitions in Nuclei at Low Temperatures". In: *Phase Structure of Strongly Interacting Matter*. Ed. by Jean Cleymans. Berlin, Heidelberg: Springer Berlin Heidelberg, 1990, pp. 26–52. ISBN: 978-3-642-87821-3 (cit. on p. 94).

[Goo86] Alan L. Goodman. "Finite-temperature Hartree-Fock-Bogoliubov calculations in rare earth nuclei". In: *Phys. Rev. C* 34 (5 Nov. 1986), pp. 1942–1949. DOI: 10.1103/PhysRevC.34.1942 (cit. on p. 94).

[Gor96] S. Goriely. "A new nuclear level density formula including shell and pairing correction in the light of a microscopic model calculation". In: *Nuclear Physics A* 605.1 (1996), pp. 28–60. ISSN: 0375-9474. DOI: https://doi.org/10.1016/0375-9474(96)00162-5 (cit. on p. 31).

[Gor+19] S. Goriely et al. "Reference database for photon strength functions". In: *The European Physical Journal A* 55.10 (Oct. 2019), p. 172. ISSN: 1434-601X. DOI: 10.1140/epja/i2019-12840-1 (cit. on p. 103).

[Gut+11] M. Guttormsen et al. "Fermi's golden rule applied to the γ decay in the quasicontinuum of ^{46}Ti". In: *Physical Review C* 83.1 (Jan. 2011). ISSN: 1089-490X. DOI: 10.1103/physrevc.83.014312 (cit. on p. 103).

[HW01] Muhsin N. Harakeh and Adriaan van der Woude. *Giant Resonances: Fundamental High-Frequency Modes of Nuclear Excitation*. Ed. by P. E. Hodgson. 2001. ISBN: 0-19-851733-5 (cit. on p. 78).

[HM52] Chushiro Hayashi and Yasuo Munakata. "On a Relativistic Integral Equation for Bound States". In: *Progress of Theoretical Physics* 7.5-6 (May 1952), pp. 481–516. ISSN: 0033-068X. DOI: 10.1143/PTP.7.5.481. eprint: https://academic.oup.com/ptp/article-pdf/7/5-6/481/24072334/7-5-481.pdf (cit. on p. 35).

[HPR11] H. Hergert, P. Papakonstantinou, and R. Roth. "Quasiparticle random-phase approximation with interactions from the Similarity Renormalization Group". In: *Phys. Rev. C* 83 (6 June 2011), p. 064317. DOI: 10.1103/PhysRevC.83.064317 (cit. on p. 11).

[HR07] H. Hergert and R. Roth. "Unitary correlation operator method from a similarity renormalization group perspective". In: *Physical Review C* 75.5 (May 2007). ISSN: 1089-490X. DOI: 10.1103/physrevc.75.051001 (cit. on p. 133).

[HR09] H. Hergert and R. Roth. "Treatment of the intrinsic Hamiltonian in particle-number nonconserving theories". In: *Physics Letters B* 682.1 (2009), pp. 27–32. ISSN: 0370-2693. DOI: https://doi.org/10.1016/j.physletb.2009.10.100 (cit. on pp. 72, 73, 75, 151).

[Her+13] H. Hergert et al. "In-medium similarity renormalization group with chiral two- plus three-nucleon interactions". In: *Physical Review C* 87.3 (Mar. 2013). ISSN: 1089-490X. DOI: 10.1103/physrevc.87.034307 (cit. on p. 86).

[Her+18] H. Hergert et al. "Nuclear Structure from the In-Medium Similarity Renormalization Group". In: *Journal of Physics: Conference Series* 1041 (June 2018), p. 012007. DOI: 10.1088/1742-6596/1041/1/012007 (cit. on p. 19).

[Her20] Heiko Hergert. "A Guided Tour of ab initio Nuclear Many-Body Theory". In: *Frontiers in Physics* 8 (2020), p. 379. ISSN: 2296-424X. DOI: 10.3389/fphy.2020.00379 (cit. on pp. 19, 86, 114).

[Her+17] Heiko Hergert et al. "In-Medium Similarity Renormalization Group Approach to the Nuclear Many-Body Problem". In: *An Advanced Course in Computational Nuclear Physics: Bridging the Scales from Quarks to Neutron Stars*. Ed. by Morten Hjorth-Jensen, Maria Paola Lombardo, and Ubirajara van Kolck. Cham: Springer International Publishing, 2017, pp. 477–570. ISBN: 978-3-319-53336-0. DOI: 10.1007/978-3-319-53336-0_10 (cit. on p. 19).

[HG07] S. Hilaire and M. Girod. "The AMEDEE nuclear structure database". In: EDP Sciences, 2007. DOI: 10.1051/ndata:07709 (cit. on pp. 91, 94).

[Hil+12] S. Hilaire et al. "Temperature-dependent combinatorial level densities with the D1M Gogny force". In: *Phys. Rev. C* 86 (6 Dec. 2012), p. 064317. DOI: 10.1103/PhysRevC.86.064317 (cit. on p. 94).

[Hil78] Wolfgang Hillebrandt. "The rapid neutron-capture process and the synthesis of heavy and neutron-rich elements". In: *Space Science Reviews* 21.6 (Apr. 1978), pp. 639–702. ISSN: 1572-9672. DOI: 10.1007/BF00186236 (cit. on p. 85).

[Hin15] Nobuo Hinohara. "Collective inertia of the Nambu-Goldstone mode from linear response theory". In: *Phys. Rev. C* 92 (3 Sept. 2015), p. 034321. DOI: 10.1103/PhysRevC.92.034321 (cit. on p. 128).

[HKN13] Nobuo Hinohara, Markus Kortelainen, and Witold Nazarewicz. "Low-energy collective modes of deformed superfluid nuclei within the finite-amplitude method". In: *Phys. Rev. C* 87 (6 June 2013), p. 064309. DOI: 10.1103/PhysRevC.87.064309 (cit. on pp. 56, 58, 61, 65, 67, 153).

[Hin+15] Nobuo Hinohara et al. "Complex-energy approach to sum rules within nuclear density functional theory". In: *Phys. Rev. C* 91 (4 Apr. 2015), p. 044323. DOI: 10.1103/PhysRevC.91.044323 (cit. on pp. 40, 76, 114, 115, 117).

[Hop+21] J. Hoppe et al. "Natural orbitals for many-body expansion methods". In: *Phys. Rev. C* 103 (1 Jan. 2021), p. 014321. DOI: 10.1103/PhysRevC.103.014321 (cit. on p. 92).

[Hoy54] F. Hoyle. "On Nuclear Reactions Occuring in Very Hot STARS.I. the Synthesis of Elements from Carbon to Nickel." In: *The Astrophysical Journal Supplement Series* 1 (Sept. 1954), p. 121. DOI: 10.1086/190005 (cit. on p. 9).

[Hup+13] Guillaume Hupin et al. "Ab initiomany-body calculations of nucleon-4He scattering with three-nucleon forces". In: *Physical Review C* 88.5 (Nov. 2013). ISSN: 1089-490X. DOI: 10.1103/physrevc.88.054622 (cit. on p. 86).

[Hüt+20] Thomas Hüther et al. "Family of chiral two- plus three-nucleon interactions for accurate nuclear structure studies". In: *Physics Letters B* 808 (2020), p. 135651. ISSN: 0370-2693. DOI: https://doi.org/10.1016/j.physletb.2020.135651 (cit. on pp. 93, 96, 106, 134).

[Huy54a] Christiaan Huygens. "De Circuli Magnitudine Inventa". In: *De Circuli Magnitudine Inventa*. Ed. by Christiaan Huygens. San Diego: Elsevier, 1654, pp. 1–44. ISBN: 978-1-4933-0403-5. DOI: https://doi.org/10.1016/B978-1-4933-0403-5.50003-9 (cit. on p. 115).

[Huy54b] "Front Matter". In: *De Circuli Magnitudine Inventa*. Ed. by Christiaan Huygens. San Diego: Elsevier, 1654, p. ii. ISBN: 978-1-4933-0403-5. DOI: https://doi.org/10.1016/B978-1-4933-0403-5.50001-5 (cit. on p. 115).

[Huy54c] Christiaan Huygens. "Illustrium Quorundam Problematum Constructiones". In: *De Circuli Magnitudine Inventa*. Ed. by Christiaan Huygens. San Diego: Elsevier, 1654, pp. 45–72. ISBN: 978-1-4933-0403-5. DOI: https://doi.org/10.1016/B978-1-4933-0403-5.50023-4 (cit. on p. 115).

[Huy54d] "PRÆFATIO". In: *De Circuli Magnitudine Inventa*. Ed. by Christiaan Huygens. San Diego: Elsevier, 1654, pp. iv–ix. ISBN: 978-1-4933-0403-5. DOI: https://doi.org/10.1016/B978-1-4933-0403-5.50002-7 (cit. on p. 115).

[ITH68] Kiyomi Ikeda, Noboru Takigawa, and Hisashi Horiuchi. "The Systematic Structure-Change into the Molecule-like Structures in the Self-Conjugate 4n Nuclei". In: *Progress of Theoretical Physics Supplement* E68 (July 1968), pp. 464–475. ISSN: 0375-9687. DOI: 10.1143/PTPS.E68.464. eprint: https://academic.oup.com/ptps/article-pdf/doi/10.1143/PTPS.E68.464/5216547/E68-464.pdf (cit. on pp. 102, 143).

[INY09a] Tsunenori Inakura, Takashi Nakatsukasa, and Kazuhiro Yabana. "Self-consistent calculation of nuclear photoabsorption cross sections: Finite amplitude method with Skyrme functionals in the three-dimensional real space". In: *Phys. Rev. C* 80 (4 Oct. 2009), p. 044301. DOI: 10.1103/PhysRevC.80.044301 (cit. on pp. 44, 48).

[INY09b] Tsunenori Inakura, Takashi Nakatsukasa, and Kazuhiro Yabana. "Self-consistent calculation of nuclear photoabsorption cross sections: Finite amplitude method with Skyrme functionals in the three-dimensional real space". In: *Physical Review C* 80.4 (Aug. 2009). ISSN: 1089-490X. DOI: 10.1103/physrevc.80.044301 (cit. on p. 143).

[IAH07] N. Ishii, S. Aoki, and T. Hatsuda. "Nuclear Force from Lattice QCD". In: *Physical Review Letters* 99.2 (July 2007). ISSN: 1079-7114. DOI: 10.1103/physrevlett.99.022001 (cit. on p. 10).

[Ito+14] M Itoh et al. "Cluster structure of broad resonances near threshold in12C and16O". In: *Journal of Physics: Conference Series* 569 (Dec. 2014), p. 012009. DOI: 10.1088/1742-6596/569/1/012009 (cit. on pp. 102, 143).

[Iwa+01] H. Iwasaki et al. "Large collectivity of 34Mg". In: *Physics Letters B* 522.3 (2001), pp. 227–232. ISSN: 0370-2693. DOI: https://doi.org/10.1016/S0370-2693(01)01244-8 (cit. on pp. 94, 143).

[JS64] B. Jancovici and D.H. Schiff. "The collective vibrations of a many-fermion system". In: *Nuclear Physics* 58 (1964), pp. 678–686. ISSN: 0029-5582. DOI: https://doi.org/10.1016/0029-5582(64)90578-4 (cit. on pp. 35, 36).

[Jan+16] G. R. Jansen et al. "Open *sd*-shell nuclei from first principles". In: *Phys. Rev. C* 94 (1 July 2016), p. 011301. DOI: 10.1103/PhysRevC.94.011301 (cit. on p. 114).

[Jon+18] M. D. Jones et al. "Examination of the low-energy enhancement of the γ-ray strength function of ^{56}Fe". In: *Physical Review C* 97.2 (Feb. 2018). ISSN: 2469-9993. DOI: 10.1103/physrevc.97.024327 (cit. on p. 103).

[Käl52] Gunnar Källén. "On the Definition of the Renormalization Constants in Quantum Electrodynamics". In: *Helvetica Physica Acta* 25 (1952), pp. 417–434. DOI: https://dx.doi.org/10.5169/seals-112316. eprint: https://www.e-periodica.ch/digbib/view?pid=hpa-001:1952:25::814 (cit. on p. 38).

[KG06] Joseph I Kapusta and Charles Gale. *Finite-temperature field theory: principles and applications; 2nd ed.* Cambridge monographs on mathematical physics. Cambridge: Cambridge Univ. Press, 2006. DOI: 10.1017/CBO9780511535130 (cit. on p. 16).

[KN20] Yu Kashiwaba and Takashi Nakatsukasa. "Coordinate-space solver for finite-temperature Hartree-Fock-Bogoliubov calculations using the shifted Krylov method". In: *Phys. Rev. C* 101 (4 Apr. 2020), p. 045804. DOI: 10.1103/PhysRevC.101.045804 (cit. on pp. 94, 98).

[Kol15] U. van Kolck. *Few-Nucleon Systems in a Quirky World: Lattice Nuclei in Effective Field Theory*. 2015. arXiv: 1505.06323 [nucl-th] (cit. on p. 10).

[KMC00] V. N. Kondratyev, T. Maruyama, and S. Chiba. "Shell Structure of Nuclei in Strong Magnetic Fields in Neutron Star Crusts". In: *Phys. Rev. Lett.* 84 (6 Feb. 2000), pp. 1086–1089. DOI: 10.1103/PhysRevLett.84.1086 (cit. on p. 80).

[KMC01] V. N. Kondratyev, Toshiki Maruyama, and Satoshi Chiba. "Magnetic Field Effect on Masses of Atomic Nuclei". In: *The Astrophysical Journal* 546.2 (Jan. 2001), pp. 1137–1148. DOI: 10.1086/318276 (cit. on p. 80).

[KHN15] M. Kortelainen, N. Hinohara, and W. Nazarewicz. "Multipole modes in deformed nuclei within the finite amplitude method". In: *Phys. Rev. C* 92 (5 Nov. 2015), p. 051302. DOI: 10.1103/PhysRevC.92.051302 (cit. on p. 48).

[LCA98] Denis Lacroix, Philippe Chomaz, and Sakir Ayik. "Finite temperature nuclear response in the extended random phase approximation". In: *Phys. Rev. C* 58 (4 Oct. 1998), pp. 2154–2160. DOI: 10.1103/PhysRevC.58.2154 (cit. on p. 34).

[LCA99] Denis Lacroix, Philippe Chomaz, and Sakir Ayik. "On the simulation of extended TDHF theory". In: *Nuclear Physics A* 651.4 (1999), pp. 369–378. ISSN: 0375-9474. DOI: https://doi.org/10.1016/S0375-9474(99)00136-0 (cit. on p. 34).

[Lan37] L. D. Landau. "On the theory of phase transitions". In: *Zh. Eksp. Teor. Fiz.* 7 (1937), pp. 19–32 (cit. on pp. 84, 95).

[LL67a] L.D. Landau and E.M. Lifshitz. *Quantum Mechanics. 2nd edition.* Moscow: MIR Editions, 1967 (cit. on p. 16).

[LL67b] L.D. Landau and E.M. Lifshitz. *Statistical Physics, Part I. 2nd Edition.* Moscow: MIR Editions, 1967 (cit. on pp. 15, 16, 84, 94).

[Lar+17] A C Larsen et al. "Low-energy enhancement and fluctuations of γ-ray strength functions in ^{56,57}Fe: test of the Brink–Axel hypothesis". In: *Journal of Physics G: Nuclear and Particle Physics* 44.6 (Apr. 2017), p. 064005. ISSN: 1361-6471. DOI: 10.1088/1361-6471/aa644a (cit. on p. 103).

[Lar+12] A. C. Larsen et al. "Primary γ-ray spectra in ^{44}Ti of astrophysical interest". In: *Physical Review C* 85.1 (Jan. 2012). ISSN: 1089-490X. DOI: 10.1103/physrevc.85.014320 (cit. on p. 103).

[Lat15] James M. Lattimer. "Introduction to neutron stars". In: *AIP Conference Proceedings* 1645.1 (2015), pp. 61–78. DOI: 10.1063/1.4909560. eprint: https://aip.scitation.org/doi/pdf/10.1063/1.4909560 (cit. on pp. 79, 80).

[LY52] T. D. Lee and C. N. Yang. "Statistical Theory of Equations of State and Phase Transitions. II. Lattice Gas and Ising Model". In: *Phys. Rev.* 87 (3 Aug. 1952), pp. 410–419. DOI: 10.1103/PhysRev.87.410 (cit. on p. 29).

[Leh54] H. Lehmann. "Über Eigenschaften von Ausbreitungsfunktionen und Renormierungskonstanten quantisierter Felder". In: *Il Nuovo Cimento* 11 (Apr. 1954), pp. 342–357. DOI: https://doi.org/10.1007/BF02783624 (cit. on p. 38).

[Li+15] Jia Jie Li et al. "Pairing phase transition: A finite-temperature relativistic Hartree-Fock-Bogoliubov study". In: *Phys. Rev. C* 92 (1 July 2015), p. 014302. DOI: 10.1103/PhysRevC.92.014302 (cit. on p. 98).

[Lia+13] Haozhao Liang et al. "Feasibility of the finite-amplitude method in covariant density functional theory". In: *Phys. Rev. C* 87 (5 May 2013), p. 054310. DOI: 10.1103/PhysRevC.87.054310 (cit. on pp. 44, 48).

[LMG65] H.J. Lipkin, N. Meshkov, and A.J. Glick. "Validity of many-body approximation methods for a solvable model: (I). Exact solutions and perturbation theory". In: *Nuclear Physics* 62.2 (1965), pp. 188–198. ISSN: 0029-5582. DOI: https://doi.org/10.1016/0029-5582(65)90862-X (cit. on p. 135).

[LS50] B. A. Lippmann and Julian Schwinger. "Variational Principles for Scattering Processes. I". In: *Phys. Rev.* 79 (3 Aug. 1950), pp. 469–480. DOI: 10.1103/PhysRev.79.469 (cit. on p. 35).

[LR21] Elena Litvinova and Caroline Robin. "Impact of complex many-body correlations on electron capture in thermally excited nuclei around Ni78". In: *Physical Review C* 103.2 (Feb. 2021). ISSN: 2469-9993. DOI: 10.1103/physrevc.103.024326 (cit. on pp. 103, 118).

[LRW20] Elena Litvinova, Caroline Robin, and Herlik Wibowo. "Temperature dependence of nuclear spin-isospin response and beta decay in hot astrophysical environments". In: *Physics Letters B* 800 (Jan. 2020), p. 135134. ISSN: 0370-2693. DOI: 10.1016/j.physletb.2019.135134 (cit. on pp. 103, 118).

[LW18] Elena Litvinova and Herlik Wibowo. "Finite-Temperature Relativistic Nuclear Field Theory: An Application to the Dipole Response". In: *Physical Review Letters* 121.8 (Aug. 2018). ISSN: 1079-7114. DOI: 10.1103/physrevlett.121.082501 (cit. on pp. 103, 118).

[LW19] Elena Litvinova and Herlik Wibowo. "Nuclear response in a finite-temperature relativistic framework". In: *The European Physical Journal A* 55.12 (Dec. 2019). ISSN: 1434-601X. DOI: 10.1140/epja/i2019-12771-9 (cit. on pp. 103, 118).

[LPG09] K. Lodders, H. Palme, and H.-P. Gail. *4.4 Abundances of the elements in the Solar System: Data sheet from Landolt-Börnstein - Group VI Astronomy and Astrophysics · Volume 4B: "Solar System" in Springer Materials (https://doi.org/10.1007/978-3-540-88055-4_34)*. Ed. by J.E. Trümper. accessed 2021-08-05. 2009. DOI: 10.1007/978-3-540-88055-4_34 (cit. on p. 85).

[Lüs86] M. Lüscher. "Volume dependence of the energy spectrum in massive quantum field theories". In: *Communications in Mathematical Physics* 104 (2 June 1986), pp. 177–206. DOI: 10.1007/BF01211589 (cit. on p. 90).

[MS16] R Machleidt and F Sammarruca. "Chiral EFT based nuclear forces: achievements and challenges". In: *Physica Scripta* 91.8 (July 2016), p. 083007. DOI: 10.1088/0031-8949/91/8/083007 (cit. on pp. 10, 93, 129, 130).

[Mai05] Paul Mainwood. *Phase Transitions in Finite Systems*. 2005. eprint: http://philsci-archive.pitt.edu/8340/1/Phase_transitions_in_finite_systems.pdf (cit. on p. 29).

[MVS09] P. Maris, J. P. Vary, and A. M. Shirokov. "Ab initio no-core full configuration calculations of light nuclei". In: *Phys. Rev. C* 79 (1 Jan. 2009), p. 014308. DOI: 10.1103/PhysRevC.79.014308 (cit. on p. 90).

[MER03a] V. Martin, J. L. Egido, and L. M. Robledo. "Publisher's Note: Thermal shape fluctuation effects in the description of hot nuclei [Phys. Rev. C 68, 034327 (2003)]". In: *Phys. Rev. C* 68 (5 Nov. 2003), p. 059902. DOI: 10.1103/PhysRevC.68.059902 (cit. on pp. 33, 94, 96, 98).

[MER03b] V. Martin, J. L. Egido, and L. M. Robledo. "Thermal shape fluctuation effects in the description of hot nuclei". In: *Phys. Rev. C* 68 (3 Sept. 2003), p. 034327. DOI: 10.1103/PhysRevC.68.034327 (cit. on pp. 33, 94, 96, 98).

[MYT64] Toshio Marumori, Masatoshi Yamamura, and Akira Tokunaga. "On the "Anharmonic Effects" on the Collective Oscillations in Spherical Even Nuclei. I". In: *Progress of Theoretical Physics* 31.6 (June 1964), pp. 1009–1025. ISSN: 0033-068X. DOI: 10.1143/PTP.31.1009. eprint: https://academic.oup.com/ptp/article-pdf/31/6/1009/5270097/31-6-1009.pdf (cit. on p. 36).

[MC90] G. J. Mathews and J. J. Cowan. "New insights into the astrophysical r-process". In: *Nature* 345.6275 (June 1990), pp. 491–494. ISSN: 1476-4687. DOI: 10.1038/345491a0 (cit. on p. 85).

[Miy+21] T. Miyagi et al. *Converged ab initio calculations of heavy nuclei*. 2021. arXiv: 2104.04688 [nucl-th] (cit. on p. 114).

[Möl+95] P. Möller et al. "Nuclear Ground-State Masses and Deformations". In: *Atomic Data and Nuclear Data Tables* 59.2 (1995), pp. 185–381. ISSN: 0092-640X. DOI: https://doi.org/10.1006/adnd.1995.1002 (cit. on p. 94).

[Möl+16] P. Möller et al. "Nuclear ground-state masses and deformations: FRDM(2012)". In: *Atomic Data and Nuclear Data Tables* 109-110 (2016), pp. 1–204. ISSN: 0092-640X. DOI: https://doi.org/10.1016/j.adt.2015.10.002 (cit. on p. 94).

[Mor73] L.G. Moretto. "Finite temperature calculation of angular velocities and moments of inertia in rotating nuclei". In: *Physics Letters B* 44.6 (1973), pp. 494–496. ISSN: 0370-2693. DOI: https://doi.org/10.1016/0370-2693(73)90006-3 (cit. on p. 94).

[Mot+95] T. Motobayashi et al. "Large deformation of the very neutron-rich nucleus ^{32}Mg from intermediate-energy Coulomb excitation". In: *Physics Letters B* 346.1 (1995), pp. 9–14. ISSN: 0370-2693. DOI: https://doi.org/10.1016/0370-2693(95)00012-A (cit. on pp. 94, 143).

[Mus+14] M. T. Mustonen et al. "Finite-amplitude method for charge-changing transitions in axially deformed nuclei". In: *Phys. Rev. C* 90 (2 Aug. 2014), p. 024308. DOI: 10.1103/PhysRevC.90.024308 (cit. on p. 128).

[NY05] T. Nakatsukasa and K. Yabana. "Unrestricted TDHF studies of nuclear response in the continuum". In: *The European Physical Journal A - Hadrons and Nuclei* 25.1 (Sept. 2005), pp. 527–529. ISSN: 1434-601X. DOI: 10.1140/epjad/i2005-06-052-x (cit. on p. 143).

[NIY07] Takashi Nakatsukasa, Tsunenori Inakura, and Kazuhiro Yabana. "Finite amplitude method for the solution of the random-phase approximation". In: *Phys. Rev. C* 76 (2 Aug. 2007), p. 024318. DOI: 10.1103/PhysRevC.76.024318 (cit. on pp. 11, 44, 47, 48, 127, 151).

[NJ61] Y. Nambu and G. Jona-Lasinio. "Dynamical Model of Elementary Particles Based on an Analogy with Superconductivity. II". In: *Phys. Rev.* 124 (1 Oct. 1961), pp. 246–254. DOI: 10.1103/PhysRev.124.246 (cit. on p. 130).

[Nam50] Yoichiro Nambu. "Force Potentials in Quantum Field Theory". In: *Progress of Theoretical Physics* 5.4 (July 1950), pp. 614–633. ISSN: 0033-068X. DOI: 10.1143/ptp/5.4.614. eprint: https://academic.oup.com/ptp/article-pdf/5/4/614/5430503/5-4-614.pdf (cit. on p. 35).

[Nam60] Yoichiro Nambu. "Quasi-Particles and Gauge Invariance in the Theory of Superconductivity". In: *Phys. Rev.* 117 (3 Feb. 1960), pp. 648–663. DOI: 10.1103/PhysRev.117.648 (cit. on p. 68).

[Ney+20] E. M. Ney et al. "Global description of β^- decay with the axially deformed Skyrme finite-amplitude method: Extension to odd-mass and odd-odd nuclei". In: *Phys. Rev. C* 102 (3 Sept. 2020), p. 034326. DOI: 10.1103/PhysRevC.102.034326 (cit. on pp. 44, 45).

[Nik+13] T. Nikšić et al. "Implementation of the finite amplitude method for the relativistic quasiparticle random-phase approximation". In: *Phys. Rev. C* 88 (4 Oct. 2013), p. 044327. DOI: 10.1103/PhysRevC.88.044327 (cit. on pp. 44, 48).

[Nis+17] H. Nishibata et al. "Shape coexistence in the N=19 neutron-rich nucleus ^{31}Mg explored by $\beta-\gamma$ spectroscopy of spin-polarized ^{31}Na". In: *Physics Letters B* 767 (2017), pp. 81–85. ISSN: 0370-2693. DOI: https://doi.org/10.1016/j.physletb.2017.01.049 (cit. on pp. 94, 143).

[Niu+09] Y.F. Niu et al. "Low-energy monopole and dipole response in nuclei at finite temperature". In: *Physics Letters B* 681.4 (Nov. 2009), pp. 315–319. ISSN: 0370-2693. DOI: 10.1016/j.physletb.2009.10.046 (cit. on p. 118).

[Noz64] P. Nozières. *Theory of interacting Fermi systems*. New York: W.A. Benjamin, 1964 (cit. on p. 35).

[OKH16] Tomohiro Oishi, Markus Kortelainen, and Nobuo Hinohara. "Finite amplitude method applied to the giant dipole resonance in heavy rare-earth nuclei". In: *Phys. Rev. C* 93 (3 Mar. 2016), p. 034329. DOI: 10.1103/PhysRevC.93.034329 (cit. on p. 48).

[Okn14] Andrzej Okniński. "On the Mechanism of Fermion-Boson Transformation". In: *International Journal of Theoretical Physics* 53 (2014), pp. 2662–2667. DOI: 10.1007/s10773-014-2062-4 (cit. on p. 33).

[Orr+91] N.A. Orr et al. "New mass measurements of neutron-rich nuclei near N=20". In: *Physics Letters B* 258.1 (1991), pp. 29–34. ISSN: 0370-2693. DOI: https://doi.org/10.1016/0370-2693(91)91203-8 (cit. on pp. 94, 143).

[Paa+06] N. Paar et al. “Collective multipole excitations based on correlated realistic nucleon-nucleon interactions”. In: *Phys. Rev. C* 74 (1 July 2006), p. 014318. DOI: 10.1103/PhysRevC.74.014318 (cit. on p. 11).

[Paa+09] N. Paar et al. “Calculation of stellar electron-capture cross sections on nuclei based on microscopic Skyrme functionals”. In: *Phys. Rev. C* 80 (5 Nov. 2009), p. 055801. DOI: 10.1103/PhysRevC.80.055801 (cit. on pp. 103, 118).

[PW16] T Papenbrock and H A Weidenmüller. “Effective field theory for deformed atomic nuclei”. In: *Physica Scripta* 91.5 (Apr. 2016), p. 053004. ISSN: 1402-4896. DOI: 10.1088/0031-8949/91/5/053004 (cit. on p. 10).

[PW14] T. Papenbrock and H. A. Weidenmüller. “Effective field theory for finite systems with spontaneously broken symmetry”. In: *Physical Review C* 89.1 (Jan. 2014). ISSN: 1089-490X. DOI: 10.1103/physrevc.89.014334 (cit. on p. 10).

[Peñ+11] D. Peña Arteaga et al. “Nuclear structure in strong magnetic fields: Nuclei in the crust of a magnetar”. In: *Phys. Rev. C* 84 (4 Oct. 2011), p. 045806. DOI: 10.1103/PhysRevC.84.045806 (cit. on p. 80).

[PR08] Sara Perez-Martin and L. M. Robledo. “Microscopic justification of the equal filling approximation”. In: *Phys. Rev. C* 78 (1 July 2008), p. 014304. DOI: 10.1103/PhysRevC.78.014304 (cit. on p. 127).

[PN66] David Pines and Philippe Nozières. *The theory of quantum liquids, volume I: Normal Fermi liquids*. eng. New York Amsterdam: W.A. Benjamin, 1966 (cit. on pp. 34, 39).

[Pol88] A.M. Polyakov. “Fermi-Bose transmutations induced by gauge fields”. In: *Modern Physics Letters A* 03.03 (1988), pp. 325–328. DOI: 10.1142/S0217732388000398. eprint: https://doi.org/10.1142/S0217732388000398 (cit. on p. 33).

[Pot10] Aleksandr Y Potekhin. “The physics of neutron stars”. In: *Physics-Uspekhi* 53.12 (Dec. 2010), pp. 1235–1256. DOI: 10.3367/ufne.0180.201012c.1279 (cit. on pp. 79, 80).

[Qiu+19] Y. Qiu et al. “Particle-number projected Bogoliubov-coupled-cluster theory: Application to the pairing Hamiltonian”. In: *Physical Review C* 99.4 (Apr. 2019). ISSN: 2469-9993. DOI: 10.1103/physrevc.99.044301 (cit. on p. 86).

[Rai50] James Rainwater. “Nuclear Energy Level Argument for a Spheroidal Nuclear Model”. In: *Phys. Rev.* 79 (3 Aug. 1950), pp. 432–434. DOI: 10.1103/PhysRev.79.432 (cit. on p. 9).

[Rav+20] A. Ravli ć et al. “Stellar electron-capture rates based on finite-temperature relativistic quasiparticle random-phase approximation”. In: *Phys. Rev. C* 102 (6 Dec. 2020), p. 065804. DOI: 10.1103/PhysRevC.102.065804 (cit. on pp. 103, 118).

[RA15] A. K. Rhine Kumar and P. Arumugam. “Thermal shape fluctuation model study of the giant dipole resonance in ^{152}Gd”. In: *Phys. Rev. C* 92 (4 Oct. 2015), p. 044314. DOI: 10.1103/PhysRevC.92.044314 (cit. on pp. 94, 98).

[RG27] Lewis Fry Richardson and J. Arthur Gaunt. "VIII. The deferred approach to the limit". In: *Philosophical Transactions of the Royal Society of London. Series A, Containing Papers of a Mathematical or Physical Character* 226.636-646 (1927), pp. 299–361. DOI: 10.1098/rsta.1927.0008. eprint: https://royalsocietypublishing.org/doi/pdf/10.1098/rsta.1927.0008 (cit. on p. 115).

[RG11] Lewis Fry Richardson and Richard Tetley Glazebrook. "IX. The approximate arithmetical solution by finite differences of physical problems involving differential equations, with an application to the stresses in a masonry dam". In: *Philosophical Transactions of the Royal Society of London. Series A, Containing Papers of a Mathematical or Physical Character* 210.459-470 (1911), pp. 307–357. DOI: 10.1098/rsta.1911.0009. eprint: https://royalsocietypublishing.org/doi/pdf/10.1098/rsta.1911.0009 (cit. on p. 115).

[RS80] P. Ring and P. Schuck. *The nuclear many-body problem*. New York: Springer-Verlag, 1980 (cit. on pp. 9, 30, 34, 35, 36).

[RB11] L. M. Robledo and G. F. Bertsch. "Global systematics of octupole excitations in even-even nuclei". In: *Phys. Rev. C* 84 (5 Nov. 2011), p. 054302. DOI: 10.1103/PhysRevC.84.054302 (cit. on p. 94).

[Rot+07] R. Roth et al. "Nuclear Structure in the UCOM Framework: From Realistic Interactions to Collective Excitations". In: *Nuclear Physics A* 788.1-4 (May 2007), pp. 12–19. ISSN: 0375-9474. DOI: 10.1016/j.nuclphysa.2007.01.008 (cit. on p. 133).

[Rot+14] Robert Roth et al. "Evolved chiral NN+3N Hamiltonians for ab initio nuclear structure calculations". In: *Physical Review C* 90.2 (Aug. 2014). ISSN: 1089-490X. DOI: 10.1103/physrevc.90.024325 (cit. on pp. 86, 117).

[Row68] D. J. Rowe. "Equations-of-Motion Method and the Extended Shell Model". In: *Rev. Mod. Phys.* 40 (1 Jan. 1968), pp. 153–166. DOI: 10.1103/RevModPhys.40.153 (cit. on p. 35).

[Sak85] J. J. Sakurai. *Modern Quantum Mechanics*. 3rd ed. Cambridge University Press, 1985. ISBN: 0-8053-7501-5 (cit. on pp. 36, 39).

[SB51] E. E. Salpeter and H. A. Bethe. "A Relativistic Equation for Bound-State Problems". In: *Phys. Rev.* 84 (6 Dec. 1951), pp. 1232–1242. DOI: 10.1103/PhysRev.84.1232 (cit. on p. 35).

[Sán+20] M. Sánchez Sánchez et al. "Improved description of light nuclei through chiral effective field theory at leading order". In: *Phys. Rev. C* 102 (2 Aug. 2020), p. 024324. DOI: 10.1103/PhysRevC.102.024324 (cit. on p. 90).

[SH17] Guillaume Scamps and Yukio Hashimoto. "Transfer probabilities for the reactions ^{14,20}O $+^{20}$ O in terms of multiple time-dependent Hartree-Fock-Bogoliubov trajectories". In: *Phys. Rev. C* 96 (3 Sept. 2017), p. 031602. DOI: 10.1103/PhysRevC.96.031602 (cit. on pp. 128, 154).

[Sch26] E. Schrödinger. "An Undulatory Theory of the Mechanics of Atoms and Molecules". In: *Phys. Rev.* 28 (6 Dec. 1926), pp. 1049–1070. DOI: 10.1103/PhysRev.28.1049 (cit. on p. 14).

[Sch+20] P. Schuck et al. "Equation of Motion Method to strongly correlated Fermi systems and Extended RPA approaches". In: (Sept. 2020). DOI: arXiv:2009.00591 (cit. on pp. 34, 35, 36).

[Sch19] Nicolas Schunck, ed. *Energy Density Functional Methods for Atomic Nuclei*. 2053-2563. IOP Publishing, 2019. ISBN: 978-0-7503-1422-0. DOI: 10.1088/2053-2563/aae0ed (cit. on p. 40).

[Sch51] Julian Schwinger. "On the Green's functions of quantized fields. I". In: *Proceedings of the National Academy of Sciences* 37.7 (July 1951), pp. 452–455. ISSN: 0027-8424. DOI: 10.1073/pnas.37.7.452. eprint: https://www.pnas.org/content/37/7/452.full.pdf (cit. on p. 35).

[SHB13] Gustavo E. Scuseria, Thomas M. Henderson, and Ireneusz W. Bulik. "Particle-particle and quasiparticle random phase approximations: Connections to coupled cluster theory". In: *The Journal of Chemical Physics* 139.10 (2013), p. 104113. DOI: 10.1063/1.4820557. eprint: https://doi.org/10.1063/1.4820557 (cit. on p. 35).

[SHS08] Gustavo E. Scuseria, Thomas M. Henderson, and Danny C. Sorensen. "The ground state correlation energy of the random phase approximation from a ring coupled cluster doubles approach". In: *The Journal of Chemical Physics* 129.23 (2008), p. 231101. DOI: 10.1063/1.3043729. eprint: https://doi.org/10.1063/1.3043729 (cit. on p. 35).

[SY14] Kazuyuki Sekizawa and Kazuhiro Yabana. "Particle-number projection method in time-dependent Hartree-Fock theory: Properties of reaction products". In: *Phys. Rev. C* 90 (6 Dec. 2014), p. 064614. DOI: 10.1103/PhysRevC.90.064614 (cit. on pp. 128, 154).

[SR00] Javid A. Sheikh and Peter Ring. "Symmetry-projected Hartree–Fock–Bogoliubov equations". In: *Nuclear Physics A* 665.1 (2000), pp. 71–91. ISSN: 0375-9474. DOI: https://doi.org/10.1016/S0375-9474(99)00424-8 (cit. on p. 128).

[Sim10] Cédric Simenel. "Particle Transfer Reactions with the Time-Dependent Hartree-Fock Theory Using a Particle Number Projection Technique". In: *Phys. Rev. Lett.* 105 (19 Nov. 2010), p. 192701. DOI: 10.1103/PhysRevLett.105.192701 (cit. on pp. 128, 154).

[Som+14] V. Somà et al. "Chiral two- and three-nucleon forces along medium-mass isotope chains". In: *Physical Review C* 89.6 (June 2014). ISSN: 1089-490X. DOI: 10.1103/physrevc.89.061301 (cit. on p. 86).

[Som20] Vittorio Somà. "Self-Consistent Green's Function Theory for Atomic Nuclei". In: *Frontiers in Physics* 8 (2020), p. 340. ISSN: 2296-424X. DOI: 10.3389/fphy.2020.00340 (cit. on p. 38).

[Som83] H. Michael Sommermann. "Microscopic description of giant resonances in highly excited nuclei". In: *Annals of Physics* 151.1 (1983), pp. 163–203. ISSN: 0003-4916. DOI: https://doi.org/10.1016/0003-4916(83)90318-4 (cit. on pp. 34, 35, 40, 56, 57, 58).

[SJJ50] Helmut Steinwedel, J. Hans D. Jensen, and Peter Jensen. "Nuclear Dipole Vibrations". In: *Phys. Rev.* 79 (6 Sept. 1950), pp. 1019–1019. DOI: 10.1103/PhysRev.79.1019 (cit. on p. 120).

[Sto+11] M. Stoitsov et al. "Monopole strength function of deformed superfluid nuclei". In: *Phys. Rev. C* 84 (4 Oct. 2011), p. 041305. DOI: 10.1103/PhysRevC.84.041305 (cit. on pp. 44, 48).

[SL17] Xuwei Sun and Dinghui Lu. "Implementation of a finite-amplitude method in a relativistic meson-exchange model". In: *Phys. Rev. C* 96 (2 Aug. 2017), p. 024614. DOI: 10.1103/PhysRevC.96.024614 (cit. on p. 48).

[SHI72] Yasuyuki Suzuki, Hisashi Horiuchi, and Kiyomi Ikeda. "Study of α Chain States through Their Decay Widths". In: *Progress of Theoretical Physics* 47.5 (May 1972), pp. 1517–1536. ISSN: 0033-068X. DOI: 10.1143/PTP.47.1517. eprint: https://academic.oup.com/ptp/article-pdf/47/5/1517/5304507/47-5-1517.pdf (cit. on pp. 102, 143).

[Tic+18] A. Tichai et al. "Bogoliubov many-body perturbation theory for open-shell nuclei". In: *Physics Letters B* 786 (Nov. 2018), pp. 195–200. ISSN: 0370-2693. DOI: 10.1016/j.physletb.2018.09.044 (cit. on p. 86).

[TRD20] Alexander Tichai, Robert Roth, and Thomas Duguet. *Many-body perturbation theories for finite nuclei*. 2020. arXiv: 2001.10433 [nucl-th] (cit. on p. 86).

[Tic+16] Alexander Tichai et al. "Hartree–Fock many-body perturbation theory for nuclear ground-states". In: *Physics Letters B* 756 (May 2016), pp. 283–288. ISSN: 0370-2693. DOI: 10.1016/j.physletb.2016.03.029 (cit. on p. 86).

[Tic+19] Alexander Tichai et al. "Natural orbitals for ab initio no-core shell model calculations". In: *Phys. Rev. C* 99 (3 Mar. 2019), p. 034321. DOI: 10.1103/PhysRevC.99.034321 (cit. on pp. 90, 92).

[Tse13] V. I. Tselyaev. "Subtraction method and stability condition in extended random-phase approximation theories". In: *Phys. Rev. C* 88 (5 Nov. 2013), p. 054301. DOI: 10.1103/PhysRevC.88.054301 (cit. on p. 34).

[UK51] Hiroomi Umezawa and Susumu Kamefuchi. "The Vacuum in Quantum Electrodynamics". In: *Progress of Theoretical Physics* 6.4 (Aug. 1951), pp. 543–558. ISSN: 0033-068X. DOI: 10.1143/ptp/6.4.543. eprint: https://academic.oup.com/ptp/article-pdf/6/4/543/5418774/6-4-543.pdf (cit. on p. 38).

[VBG09] Sergey Vaintraub, Nir Barnea, and Doron Gazit. "^{6}He β-decay rate and the suppression of the axial constant in nuclear matter". In: *Phys. Rev. C* 79 (6 June 2009), p. 065501. DOI: 10.1103/PhysRevC.79.065501 (cit. on p. 90).

[VGG18] O. Vasseur, D. Gambacurta, and M. Grasso. "Systematic study of giant quadrupole resonances with the subtracted second random-phase approximation: Beyond-mean-field centroids and fragmentation". In: *Phys. Rev. C* 98 (4 Oct. 2018), p. 044313. DOI: 10.1103/PhysRevC.98.044313 (cit. on p. 34).

[VM84] D. Vautherin and N.Vinh Mau. "Temperature dependence of collective states in the random-phase approximation". In: *Nuclear Physics A* 422.1 (1984), pp. 140–156. ISSN: 0375-9474. DOI: https://doi.org/10.1016/0375-9474(84)90434-2 (cit. on p. 40).

[Voi+04] A. Voinov et al. "Large Enhancement of Radiative Strength for Soft Transitions in the Quasicontinuum". In: *Phys. Rev. Lett.* 93 (14 Sept. 2004), p. 142504. DOI: 10.1103/PhysRevLett.93.142504 (cit. on p. 102).

[Voi+06] A. V. Voinov et al. "Level density of ^{56}Fe and low-energy enhancement of γ-strength function". In: *Phys. Rev. C* 74 (1 July 2006), p. 014314. DOI: 10.1103/PhysRevC.74.014314 (cit. on pp. 102, 103).

[WHN21] Kouhei Washiyama, Nobuo Hinohara, and Takashi Nakatsukasa. "Finite-amplitude method for collective inertia in spontaneous fission". In: *Phys. Rev. C* 103 (1 Jan. 2021), p. 014306. DOI: 10.1103/PhysRevC.103.014306 (cit. on p. 128).

[Wei79] Steven Weinberg. "Phenomenological Lagrangians". In: *Physica A: Statistical Mechanics and its Applications* 96.1 (1979), pp. 327–340. ISSN: 0378-4371. DOI: https://doi.org/10.1016/0378-4371(79)90223-1 (cit. on p. 10).

[WL19] Herlik Wibowo and Elena Litvinova. "Nuclear dipole response in the finite-temperature relativistic time-blocking approximation". In: *Physical Review C* 100.2 (Aug. 2019). ISSN: 2469-9993. DOI: 10.1103/physrevc.100.024307 (cit. on pp. 103, 118).

[Wic50] G. C. Wick. "The Evaluation of the Collision Matrix". In: *Phys. Rev.* 80 (2 Oct. 1950), pp. 268–272. DOI: 10.1103/PhysRev.80.268 (cit. on p. 20).

[WK74] Kenneth G. Wilson and J. Kogut. "The renormalization group and the ϵ expansion". In: *Physics Reports* 12.2 (1974), pp. 75–199. ISSN: 0370-1573. DOI: https://doi.org/10.1016/0370-1573(74)90023-4 (cit. on p. 19).

[Yan+19] Zhenjie Yan et al. "Boiling a Unitary Fermi Liquid". In: *Phys. Rev. Lett.* 122 (9 Mar. 2019), p. 093401. DOI: 10.1103/PhysRevLett.122.093401 (cit. on p. 103).

[Yan+03] Y. Yanagisawa et al. "The first excited state of ^{30}Ne studied by proton inelastic scattering in reversed kinematics". In: *Physics Letters B* 566.1 (2003), pp. 84–89. ISSN: 0370-2693. DOI: https://doi.org/10.1016/S0370-2693(03)00802-5 (cit. on pp. 94, 143).

[Yan+04] Y. Yanagisawa et al. "The first excited state of ^{30}Ne studied by proton inelastic scattering in reversed kinematics". In: *Nuclear Physics A* 734 (2004), pp. 374–377. ISSN: 0375-9474. DOI: https://doi.org/10.1016/j.nuclphysa.2004.01.071 (cit. on pp. 94, 143).

[YL52] C. N. Yang and T. D. Lee. "Statistical Theory of Equations of State and Phase Transitions. I. Theory of Condensation". In: *Phys. Rev.* 87 (3 Aug. 1952), pp. 404–409. DOI: 10.1103/PhysRev.87.404 (cit. on p. 29).

[Yan87] Constantine Yannouleas. "Zero-temperature second random phase approximation and its formal properties". In: *Phys. Rev. C* 35 (3 Mar. 1987), pp. 1159–1161. DOI: 10.1103/PhysRevC.35.1159 (cit. on pp. 34, 35).

[You09] W. Younes. "Gaussian matrix elements in a cylindrical harmonic oscillator basis". In: *Computer Physics Communications* 180.7 (July 2009), pp. 1013–1040. ISSN: 0010-4655. DOI: 10.1016/j.cpc.2008.12.021 (cit. on p. 146).

[Yük+14] E. Yüksel et al. "Effect of temperature on the effective mass and the neutron skin of nuclei". In: *The European Physical Journal A* 50.10 (Oct. 2014), p. 160. ISSN: 1434-601X. DOI: 10.1140/epja/i2014-14160-4 (cit. on pp. 103, 118).

[Yük+17] E. Yüksel et al. "Multipole excitations in hot nuclei within the finite temperature quasiparticle random phase approximation framework". In: *Phys. Rev. C* 96 (2 Aug. 2017), p. 024303. DOI: 10.1103/PhysRevC.96.024303 (cit. on pp. 103, 118, 119).

[Yük+19] E. Yüksel et al. "Nuclear excitations within microscopic EDF approaches: Pairing and temperature effects on the dipole response". In: *The European Physical Journal A* 55.12 (Dec. 2019), p. 230. ISSN: 1434-601X. DOI: 10.1140/epja/i2019-12918-8 (cit. on pp. 103, 118).

[Yük+20] E. Yüksel et al. "Gamow-Teller excitations at finite temperature: Competition between pairing and temperature effects". In: *Phys. Rev. C* 101 (4 Apr. 2020), p. 044305. DOI: 10.1103/PhysRevC.101.044305 (cit. on pp. 103, 118).

[Zee10] A. Zee. *Quantum field theory in a nutshell (2nd edn)*. 2010. ISBN: 978-0-691-14034-6. DOI: 10.1088/0264-9381/28/8/089003 (cit. on p. 20).

[ZN17] W. Zhang and Y. F. Niu. "Shape transition with temperature of the pear-shaped nuclei in covariant density functional theory". In: *Phys. Rev. C* 96 (5 Nov. 2017), p. 054308. DOI: 10.1103/PhysRevC.96.054308 (cit. on pp. 94, 98).

[ZMR03] Shan-Gui Zhou, Jie Meng, and P. Ring. "Spherical relativistic Hartree theory in a Woods-Saxon basis". In: *Physical Review C* 68.3 (Sept. 2003). ISSN: 1089-490X. DOI: 10.1103/physrevc.68.034323 (cit. on p. 143).

[Zum62] Bruno Zumino. "Normal Forms of Complex Matrices". In: *Journal of Mathematical Physics* 3.5 (1962), pp. 1055–1057. DOI: 10.1063/1.1724294. eprint: https://doi.org/10.1063/1.1724294 (cit. on p. 30).